Spring 2020

Research and Design of a Two-Stage Supersonic Rocket

Ryan Hannaford
rmh111@zips.uakron.edu

James Gase
jrg111@zips.uakron.edu

Matthew Reppa
mmr77@zips.uakron.edu

Harrison Lewis
hdl6@zips.uakron.edu

Project BOGO: Research and Design of a Two-Stage Supersonic Rocket

ME Senior Design/Honors Project
4600:497-001
Group 59

Group Members:
Matthew Reppa
Harrison Lewis
James Gase
Ryan Hannaford

1.1

This report documents the design process for a supersonic two-stage rocket and highlights the team's research, design, testing, and construction of key elements of the rocket. Most major systems of the launch vehicle, including motors, electronics systems, interior and exterior structures, and recovery, will be analyzed and assessed during the design process. The launch vehicle is set was intended to compete at the 2020 Spaceport America Cup in Las Cruces, New Mexico prior to the shutdown of the competition due to the COVID-19 epidemic. Undergoing this project allowed the team members to further develop the skills learned throughout the Mechanical Engineering and Aerospace Systems Engineering curriculums at the University of Akron. Additionally, the findings of this report will provide a basis for future innovation within the University of Akron's Akronauts Rocket Design Team.

Table of Contents

Project BOGO will be a culmination of The University of Akron's Mechanical and Aerospace Systems Engineering programs. The group will be entering the design into the Spaceport America Cup under the 30,000 feet altitude division with the goal of having the most successful and accurate design, based on the actual versus the predicted maximum altitude of the rocket. The development process of the two-stage rocket will be submitted as the capstone project for the four seniors working on it for The University of Akron's College of Engineering senior design course and competition.

The team is developing a multistage launch vehicle capable of flying at supersonic speed. The vehicle will be reusable and robust as to sustain the entirety of the flight and recovery without significant damage. The team's research will focus on identifying the best structural design options for supersonic flight, optimizing the event sequences and timings to provide a safe and stable flight through launch and recovery, and developing a reliable stage separation system. The team will compare fin retention systems and conduct finite element analysis on the airframe, determine the ideal airframe design for the fins through research, FEA and CFD, and research and plot key flight parameters to assess the best motor choices, separation delay, and sustainer ignition delay, under the constraints of launch day conditions and competition requirements. The remaining components required to round out the launch vehicle design, including parachutes, payload(s), altimeters, GPS, and electronics bays, will be selected or have their location(s) identified, but they will not be the focus of the senior design project. The senior design team has developed detailed team requirements specific to the recovery and payload systems that must be met for integration with the current rocket design.

2.1. Background

The Akronauts Rocket Design Team is a University of Akron student-led design team focusing on the design and development of vertical launch vehicles and creative payloads with real world applications. To further the understanding of rocketry and capabilities of the Rocket Design Team, the research, design, and construction of a two-stage rocket was undertaken.

A vertical launch vehicle, or rocket, is a system comprised of exterior structural elements such as body tubes, fins, and a nose cone, interior structural elements, including bulkheads and centering rings, at least one propulsion system, at least one recovery system, and at least one electronics system to communicate with the recovery system(s). The addition of a second stage, referred to as "staging", adds to the complexity of the design, essentially adding an extra rocket to the architectural layout.

There are two primary methods to stage a rocket, including tandem staging and parallel staging. The type of staging utilized is dependent upon the mission objective and the desired performance of the vehicle. Tandem staging is common among amateur rocketeers, where the additional vehicle stages are located directly on top of the first, or booster, stage, and are active one at a time. Parallel staging, seen in amateur rocketry as well as larger vehicles meant to reach or surpass orbit (e.g. Saturn V), is the use of several stages that are active at the same time. For the purposes of this design project, the team focused on tandem staging, which will be further discussed in the Rocket Staging Techniques section.

The two stages of the rocket are referred to as the booster and sustainer. The booster, or first stage, has a motor ignited on the launch pad, while the sustainer, or second stage, has a motor ignited mid-flight.

2.2. Spaceport America Cup

The Spaceport America Cup is an international collegiate rocketry competition located at Spaceport America in Las Cruces, New Mexico, and governed by the Experimental Sounding Rocket Association (ESRA). Over 110 teams participate annually, representing 10+ countries. The competition categories are broken down by projected altitude (10,000 ft or 30,000 ft) and type of propulsion system (Commercial Off The Shelf or Student Researched And Designed). Awards are given based on vehicle and payload designs, as well as actual altitude reached versus predicted altitude. The team will be competing in the 30,000 ft COTS competition.

Scoring for the competition is broken into several components including three project update reports, a final technical report, a poster presentation outlining the design, and the overall flight and recovery of the rocket. There are also points allotted for payload scoring, which is not the focus of the senior design project. For the flight scoring, the team will select a target altitude within 30% above or below the 30,000 feet competition category (i.e. between 21,000 feet and 39,000 feet). This altitude will be selected on the day of the flight, so an accurate prediction based on launch day conditions can be selected. This helps the team through the design process because the overall altitude is not as critical of a criterion to design for as the overall flight and recovery, along with payload performance.

2.3. Requirements

The team is expected to meet requirements set forth by the University of Akron Mechanical Engineering Department, the University of Akron Williams Honors College, and ESRA. Additionally, the team has self-imposed requirements. All requirements can be seen below in Table 1.

2.3.1. University of Akron ME Department Requirements

The team's research project must follow all guidelines set by the University of Akron Mechanical Engineering Department. The research project must be an open-ended design problem, with a clear objective and design strategy specified. Each team member should spend approximately 400 hours on the research project. The research project should conclude with a manufactured and tested prototype, if possible.

2.3.2. University of Akron Honors College Requirements

The team's research project must meet or exceed all expectations of the Williams Honors College, as each team member is a Williams Honors Scholar. The research project should meet the high standards of scholarship within the Williams Honors College, as well as all requirements of the Mechanical Engineering Department. Further, the research project should prove to be a culmination of the team members' undergraduate studies. Finally, the team members' interests and exemplary academic achievement developed throughout their undergraduate studies should be reflected.

Rules and requirements set forth by ESRA for the Spaceport America Cup can be found at the website listed in *citation [27]*.

These requirements are referenced throughout the report. Based on project updates, more information has been released regarding the requirements of the project and the team's design must change to accommodate their requirements. This is an important aspect in designing a product because even in industry, the requirements are not always clear from the outset of the project and could be constantly changing.

2.3.4. Experimental Modeling Rocket Derivation Requirements

The following requirements are self-imposed by the team to help achieve the overall goals of the project. They are broken up into requirements for the launch vehicle, recovery systems, and payload system. Some of these requirements will be referenced throughout the senior design report, specifically for the launch vehicle since it is the focus of the project. Others were created by the senior design team as specifications for the rest of the rocket design, mainly the parachutes and payload design. A brief justification is listed along with each requirement. Overall, the team gained experience with requirements derivation which is a common aspect of aerospace systems projects and almost all contract work in industry.

2.3.4.1. Team Derived Rocket Requirements

Team Derived Vehicle Requirements

Requirement	Justification	Verification Plan	Status
The team will utilize a stability ballast system in the launch vehicle design.	A stability ballast increases the team's ability to adjust the stability margin to maintain a safe flight and to meet the predicted apogee.	The launch vehicle design at the final progress report will incorporate a stability ballast.	Will be verified with submission of IREC project report.
The team will make use of commercial components throughout the launch vehicle and attempt to limit custom designed components.	Utilizing commercial components will allow for quick replacement of parts in case of broken airframe, fins, or nose cone.	The launch vehicle design will verify commercial component use.	Will be verified with submission of IREC project report.
Flight profile predictions will be validated with redundant simulation software.	The redundant simulations and calculations will be used to accurately predict the flight performance and apogee of the rocket, which will help improve the flight score at competition.	OpenRocket, RASAero II, and RockSim will be utilized to simulate the flight of the launch vehicle.	Will be verified with submission of IREC project report.
Fin flutter factor of safety will be at least 1.3 pre-manufacturing.	A factor of safety on fin flutter will leave a margin of error to adjust the fin dimensions to accommodate stability of the launch vehicle based on weight changes through the manufacturing process.	Fin flutter calculations will prove the factor of safety.	Will be verified with submission of IREC project report.
The launch vehicle will be assembled utilizing standardized hardware.	Standardized launch vehicle hardware will reduce assembly and disassembly time by limiting the types of hardware items needed.	The launch vehicle assembly checklist will verify the use of standard hardware for assembly of components.	Will be verified with submission of IREC project report.

Fin attachment system will allow for changing out fin designs.	Fin modularity allows for replacement of fins for improved flight performance on launch day or to adjust the stability margin post-manufacturing.	The final launch vehicle assembly procedure will demonstrate the modularity of the fin attachment design.	Will be verified with submission of IREC project report.
Launch vehicle static stability margin and the stability margin of each stage will be at most 3.50.	A maximum stability margin will reduce the chance of the launch vehicle steering into the wind which could hinder the ability to meet the predicted apogee.	Mission performance predictions for the final launch vehicle will verify the launch vehicle stability margin meets the team's requirement.	Will be verified with submission of IREC project report.
Launch vehicle static stability margin and the stability margin of each stage will be at least 1.75.	A minimum stability margin will reduce the chance of the launch vehicle having an unstable flight, specifically at rail exit, which could hinder the ability to meet the predicted apogee.	Mission performance predictions for the final launch vehicle will verify the launch vehicle stability margin meets the team's requirement.	Will be verified with submission of IREC project report.
All electronics bay wires will be braided.	Braided wires allow for easier wire management in complex electrical systems such as the team's electronics bays. It can also reduce assembly and troubleshooting time.	The electronics bay assembly checklist will verify the braiding of all wires.	Will be verified with submission of IREC project report.
Electronics bay solder connections will be protected or covered where possible.	Heat shrink wrapping or covering will add security to connections which reduces the likelihood the connections will fail mid-flight and cause a non-nominal flight.	The electronics bay assembly checklist will verify the heat shrink wrapping of solder connections.	Will be verified with submission of IREC project report.
All batteries in the electronics bay will be securely fastened with redundant fastening methods.	Losing power to electronics in flight can result in catastrophic failure, especially if the rocket does not separate.	The electronics bay assembly procedure will verify the redundant fastening methods including zip ties.	Will be verified with submission of IREC project report.
The sustainer stage will have a separation angle less than or equal to 20°.	Igniting a second stage at an angle greater than 20° could result in a potentially dangerous flight angle or send the rocket on a path excessively far from the launch pad.	The tiltmeter will feature a requirement of at most +/- 20° for second stage ignition	Will be verified with submission of IREC project report.
The upper stage motor will be protected from FOD through second stage ignition.	Utilizing a black powder stage separation system prior to 2nd stage ignition could cause damage to the propellant in the 2nd stage motor. Protecting the motor until ignition could reduce the possibility of poor 2nd stage motor performance.	Separation tests will be done to verify that the expelled black powder will not get through the FOD cover on the motor.	Will be verified with submission of IREC project report.
Upper stage fins will not interfere with the separation system.	The upper stage of the launch vehicle requires fins near the aft end to maintain stability. Retaining these to the body tube without interfering with separation nor contacting the coupler section is essential to the success of the separation mechanism.	A fin retention system will be designed for the upper stage that will not contact the stage connecting coupler.	Will be verified with submission of IREC project report.

Rail exit velocity will be at least 70 ft/s.	A rail exit velocity below 70 ft/s could cause instability off the rail, which could cause a poor flight.	Mission performance predictions for the final launch vehicle will verify the rocket's rail exit velocity meets the team's requirement.	Will be verified with submission of IREC project report.

Table 1 - Team Derived Launch Vehicle Requirements

Team Derived Recovery Requirements

Requirement	Justification	Verification Plan	Status
The main parachute will be a maximum of 200" in diameter.	A parachute with larger diameter could cause the rocket to drift excessively far from the launch site.	Parachute sizing calculations will verify the need for a smaller diameter parachute. The final diameter will be detailed in the IREC project report.	Will be verified with submission of IREC project report.
Shock cords will be five times the length of the section to which they are connected.	Longer shock cords allow the energy associated with separating the rocket to dissipate and places the shock force from the parachute opening onto the attachment points.	The final shock cord lengths will be detailed in the IREC project report.	Will be verified with submission of IREC project report.
Protective Kevlar sheathing will be used to protect the parachutes and ropes.	Without this heat-resistant barrier of protection, the black powder ejection charges could potentially damage the ropes, resulting in tearing or breaking. This could cause the parachute to detach from the rocket.	The recovery preparation procedure will detail the placement of protective Kevlar sheathing to protect parachutes and ropes.	Will be verified with submission of IREC project report.
All recovery hardware and ropes will be tensile tested to prove load capacity.	Some commercial components have built in factors of safety, so a tensile test can verify that all components have a load capacity above expected loads during rocket recovery.	The team will conduct tensile tests during the testing phase of the project.	Will be verified with submission of IREC progress report.
The rocket will have terminal descent velocity of less than 30 ft/s which will be controlled by the main parachute's diameter.	Exceeding this velocity could cause damage to the rocket's airframe or structure upon landing.	Kinetic Energy at landing calculations will verify the descent velocity meets the team requirement.	Will be verified with submission of IREC project report.

2.3.4.2. Team Derived Payload Requirements

2.3.4.3. Team Derived Payload Requirements

Table 2 - Team Derived Vehicle Recovery Requirements

Team Derived Payload Requirements

Requirement	Justification	Verification Plan	Status

The payload will be completely modular and stand-alone from the launch vehicle.	Having a modular payload system will decrease complexity of both the payload system and electronics systems and allow for easy assembly.	Payload electronics and vehicle electronics will be kept in separate bays and all wiring will be internal for each bay.	Will be verified with submission of IREC project report.
The payload electronics and wiring will not interfere with other vehicle electronics or wiring.	Having payload electronics wiring separate from launch vehicle electronics wiring will simplify the assembly of the launch vehicle and decrease failure modes for each system, particularly during parachute deployment.	Payload electronics and vehicle electronics will be kept in separate bays and all wiring will be internal for each bay.	Will be verified with submission of IREC project report.
The payload will include an adjustable stability ballast.	The stability of both stages is important to the success of the flight. Any difference in payload weight could affect the stability margin. Therefore, a ballast system can help adjust for differences post-manufacturing.	The payload design at the final progress report will incorporate a stability ballast.	Will be verified with submission of IREC project report.
The payload will be housed in the nose cone.	Having the payload in the nose cone will help the launch vehicle remain stable through flight.	The payload system will be designed to mount in the nose cone.	Will be verified with submission of IREC project report.

Table 3 - Team Derived Payload Requirements

2.4. Objectives

The goal of this research project is to design, manufacture, test, and launch a two-stage supersonic rocket at the Spaceport America Cup, with the intention to further the research and design capabilities of the University of Akron Rocket Design Team. The primary design objectives include developing a safe and easy-to-assemble stage separation system to effectively separate the two stages of the launch vehicle, understanding and optimizing stage separation and sustainer ignition timing and sequences, and integrating a reliable vehicle recovery system layout with the separation system. Secondary objectives include composing a fin retention system capable of withstanding expected aerodynamic forces, identifying key structural design options for supersonic flight, and selecting necessary components that round out the entire rocket architecture to ensure it is a complete design. The team hopes to test several components and subsystems as well as manufacturing a subscale rocket to flush out manufacturing and assembly issues prior to building the full-scale version for the competition in mid-June.

2.5. Solution

To accomplish the objectives set forth above, as well as satisfy all requirements laid out by the University of Akron Mechanical Engineering Department, University of Akron Williams Honors College, Experimental Sounding Rocket Association, and those self-imposed, the team has designed a two-stage launch vehicle that will be capable of reaching supersonic speeds and an altitude of approximately 30,000 feet. It is important to note that a team of four undertaking a project of this scale is quite challenging, leading the team to utilize COTS options

for simple components when possible. By doing so, the team was able to spend valuable time on key design aspects, such as airframe optimization, fin retention, and staging delay timings and sequences. The layout of the final launch vehicle design can be seen below.

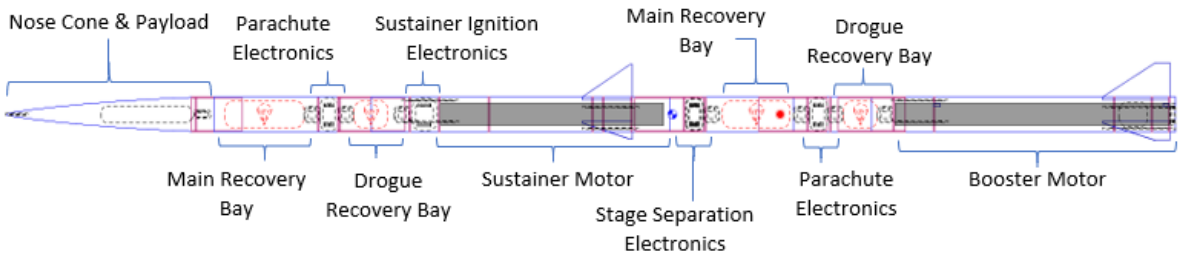

Figure 1 – Two-Stage Launch Vehicle Layout

The launch vehicle will utilize a 6” diameter fiberglass airframe and a fiberglass Von Karman nose cone. The booster and sustainer stages will both utilize a set of three aluminum clipped delta fins. For both stages, the fins will be retained by two or three slotted centering rings and L-brackets. The rocket will be propelled by a CTI (Cesaroni Technology Incorporated) N-5800 motor in the booster stage, with a CTI N-1100 motor in the sustainer stage. The booster stage will retain the motor with an Aeropack retainer cap at the aft end, while the sustainer stage will utilize the forward closure of the motor, an aluminum bulkhead, and an eyebolt to retain the motor. There will be four separate electronics bays to house the GPS units, altimeters, timers, and tiltmeter. All these components are discussed in more depth in the following sections.

2.6. Reasoning

Throughout the design of the launch vehicle, the team had to consider several factors when making decisions. These include performance, time, available COTS (commercial off the shelf) resources, financial resources, previous knowledge, and commonly cited issues with two-stage rockets. While performance of the launch vehicle and the overall success of the project were the primary concerns, several aspects of the design were not necessarily optimal in terms of flight performance. This could have been due to time constraints, lack of manufacturing ability, or simply ensuring the safety of the overall flight and recovery. Further, when simulating the flight of the rocket, the team relied upon the use of OpenRocket and RASAero II software to provide accurate and reliable data. The team has used both software packages in the past, contributing to their use with high confidence in the results. RockSim software will be analyzed as a third software for future development and to establish a wider range for potential flight results. Financial resources were not a key driving factor since the rocket design team will be using this rocket for the Spaceport America Cup competition and has the resources to purchase any components in the team’s design scope. Some decisions considered cost, but it was relatively negligible in the overall decision making process. Finally, the team relied on commonly known issues that other teams or individuals have had when launching two-stage rockets. For example, areas where issues often arise include fin retention, stage separation, the proper use of a tiltmeter, and the structural integrity of the rocket when traveling at supersonic speeds. To ensure the mitigation of issues the team faces in those areas of common failure, the team paid

close attention to them and learned how to avoid making the same mistakes past teams or individuals have made.

The team has two rocketry mentors, Chris Pearson and Steve Eves, who are local rocket hobbyists in the northeast Ohio area with certifications in rocketry. Both have worked with the rocket design team in the past and are level three members certified through either the National Association of Rocketry (NAR) or Tripoli Rocketry Association (TRA) to handle rocket motors and conduct launches. These two organizations are the prominent rocketry organizations in the United States, and they impose strict guidelines on conducting launches and even acquiring rocket motors of all categories. The help and experience of these two individuals will be cited frequently throughout the report in areas of concern.

Using these ideas, the team developed a hierarchy chart that reflects the decision making process for most of the designs the team considered. The hierarchy chart, shown in Figure 2, includes three levels. The first level details the three most important aspects which the team determined were Quality, Manufacturing, and Safety. Quality refers to the ability of the rocket to perform as expected, manufacturing ensures the ability to produce the intended design, and safety covers the requirements set forth from the outset of the project, as well as additional concerns raised through the design process.

The second level is broken into categories that indicate what the team valued within each aspect. Quality includes the functionality, or reliability, that the design will work as intended as well as the optimization of the design to perform as well as possible under given constraints. Manufacturing includes the manufacturability of the design and the ease of assembly. Both manufacturing categories were driving factors for key multistage elements. The team learned more through the manufacturing of a subscale two-stage rocket, which can be implemented for the full-scale competition rocket. Safety includes the team and competition requirements put in place to facilitate a safe and successful flight and recovery.

The third level identifies where the reasoning will be or has been derived for each category. Some of these areas include the seniors', mentors', or IREC judges' experience with previous projects, research the seniors conducted, simulations and analysis, and rocket design needs. The hierarchy chart was not strictly used for all design considerations, but it provides a baseline of the team's mindset for the project. It can be seen in the figure below.

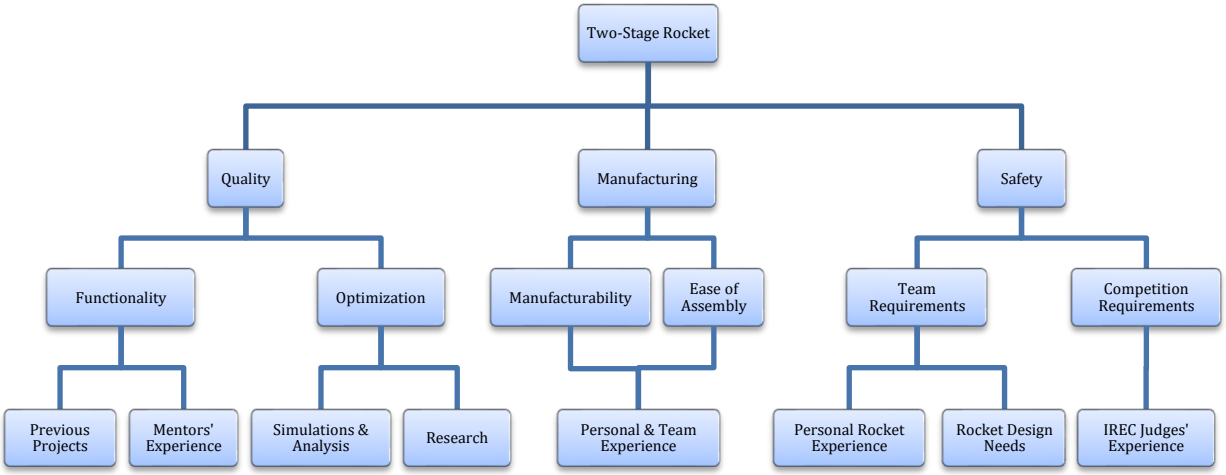

Figure 2 - Project Hierarchy Chart Breakdown

3. Structural Design

The team's main focus for the structural design of the two-stage rocket is on nose cone design, fin design, and fin retention. The team also investigated some other aspects such as motor retention and rail buttons, as well as explaining the team's use of bulkheads and centering rings. The team's methodology in these sections was not to "reinvent the wheel," so to speak, as far as structural design in several areas, but to investigate options used by the team, while designing or identifying alternatives that could be better than what is currently in use. The team used research, flight simulations, FEA and CFD analysis, CAD software, rocket hobbyists' experiences, and the team members' own manufacturing experience to justify the chosen designs for the structure of the two-stage rocket.

The airframe selection, bulkhead design, and motor design were not the focus of the design project. The team is utilizing flight-proven options in these areas such as 6" diameter fiberglass COTS airframe, 0.25" thick aluminum 6061 for bulkheads, and COTS motors. These components have been flown successfully by the team, with physical testing to back up the designs. The senior design team members were large contributors to the implementation of designs currently in use by the team, but they will not be analyzed in detail in this report.

3.1. Nose Cone Design

The nose cone is one of the main components of the overall airframe of a rocket. Proper nose cone selection is integral to achieving a successful flight. Several factors need to be considered, such as the drag force applied to the vehicle, the weight of the nose cone, commercial availability, and the manufacturability of the nose cone. For a multistage supersonic vehicle, minimizing drag force and weight is critical due to the nature of the altitude-based competition. Further, commercial availability and manufacturability of the nose cone are important to consider due to the team's resources and time constraints, as well as quality of the final product. The team researched multiple nose cone characteristics to find the optimal design for this project, including shape and fineness ratio, while keeping the above factors in mind. These characteristics are explored in more depth below.

3.1.1. Nose Cone Shape

The shape of the nose cone is necessary to consider, as it can have a significant impact on the overall drag applied to the launch vehicle and the weight of the launch vehicle. The shape is used to develop the boundary layer for the rocket, and, in the case of supersonic flight, this is extremely important as the drag induced in a compressible flow is much more impactful at Mach speed. Additionally, certain nose cone shapes are more readily available than others and more easily prepared for assembly.

Several nose cone shapes were reviewed and analyzed based on the primary factors being considered, including conical, parabolic, L-V HAACK, Von Karman, $X^{1/2}$, and $X^{3/4}$. The graph below was obtained from a 1954 National Advisory Committee for Aeronautics (NACA) report [28] regarding nose cone shape optimization. Much of the scientific data the team obtained regarding nose cone and fin geometry comes from this research. NACA tested the previously mentioned nose cone shapes on equivalent rocket designs in Wallops Island, Virginia, using a Langley helium gun.

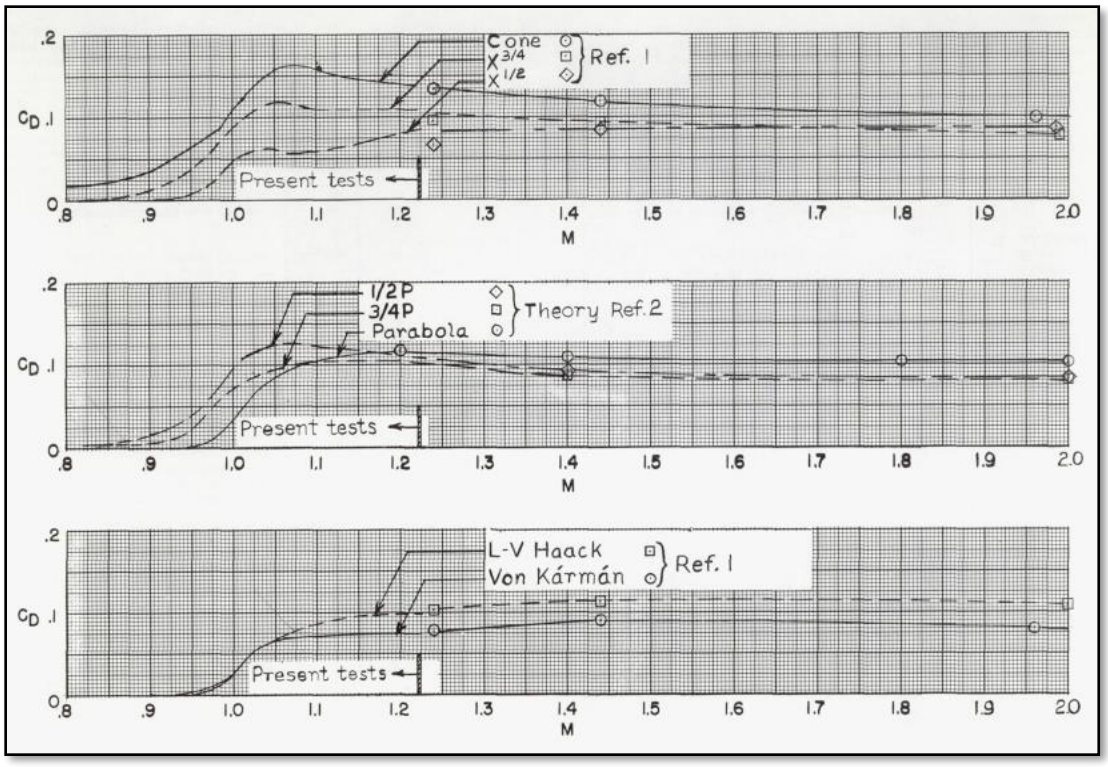

Figure 3 – 1954 NACA nose cone testing results

The above graph indicates that the $X^{1/2}$ nose cone has the lowest drag coefficient from Mach 1.0-1.2, the predicted speed of the rocket. The Von Karman shape shows a similarly low drag coefficient and is widely available for purchase as a COTS option. Although the $X^{1/2}$ shape presents a potentially lower drag option, the team would prefer the best commercial option rather than manufacturing a nose cone in-house, as that would require significant time that could be better spent elsewhere, as well as increase the potential for error during the manufacturing process.

Some of the nose shapes are shown below with pressure-drag coefficient plots at various Mach numbers for clarity. The fineness ratio, which is examined next, was 3:1 for these tests.

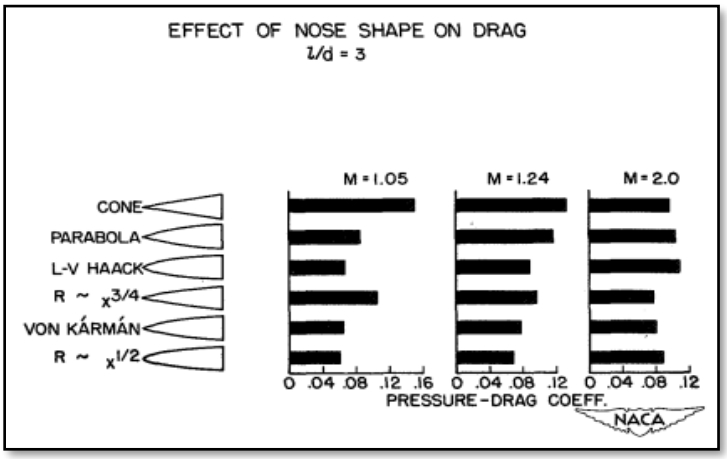

Figure 4 - NACA nose cone pressure-drag coefficient chart

The fineness ratio, commonly referred to as the aspect ratio of the nose cone, is important to reducing wave drag coefficient, the drag experienced when the vehicle reaches the critical Mach number, for the rocket. Further NACA testing goes on to detail the fineness ratio, which is the ratio of the length to diameter of the nose cone. The report mentions that a ratio of about 5:1 is good for supersonic speeds. Test data shown below for a LD Haack or Von Karman cone, shows that increasing fineness ratio decreases wave drag coefficient, but the effects are reduced at higher fineness ratios. Past a certain fineness ratio, the nose cone's additional weight and length will be more of a factor than the reduced wave drag coefficient. This is around the 5:1 value previously mentioned [23].

3.1.2. Fineness Ratio

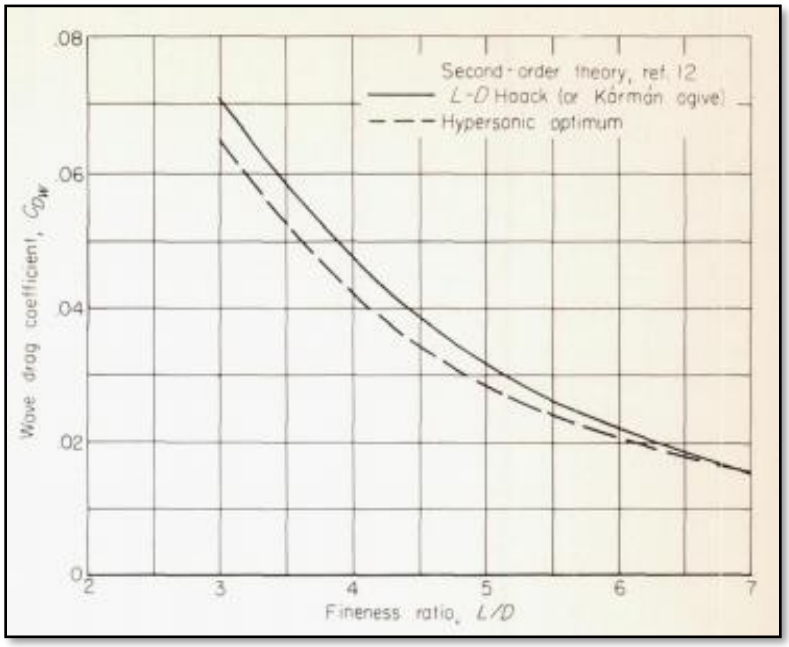

Figure 5 - NACA fineness ratio testing results

3.1.3. Manufacturability

The rocket design team has manufactured their own nose cones in the past, which involved the use of a filament winder at NASA Glenn Research Center along with a 3D printed mandrel that cost the team roughly $550 to print in five pieces. Additionally, the material cost is approximately $80. Commercial nose cone options were almost half of this overall cost. Additionally, it would sink multiple weeks of design into the mandrel layout and printing, along with finding an available time with the rocket team contact at NASA Glenn to even see if such a project could proceed as it had in the past when the filament winder at the Glenn Research Center was not busy. For these reasons, the senior design team decided to focus on the COTS nose cone options for this design project. After reviewing commercially available nose cones, there were options for 5:1 and 5.5:1 fineness ratios of the Von Karman design from Madcow Rocketry and Wildman Rocketry, respectively. The team purchased both cones to review them in person to determine which would be best. A photo of the two cones next to each other is shown below.

Figure 6 - 5:1 (top) and 5.5:1 (bottom) fiberglass Von Karman nose cones

Both cones are fiberglass material, which the team has experience with from previous rockets. After reviewing the cones, the team found that the longer cone (5:1 black nose cone) was lighter weight. However, the team foresaw manufacturing issues with the black-colored nose cone. Normally, the team can shine a phone light or flashlight from within the airframe to locate holes with a locator since the light green color is slightly translucent. However, the dark cone is not translucent enough to shine light through. The team developed another method of using a paper towel wrapped around the rocket and using the circumference of the airframe divided by six to locate six equally-spaced holes on the airframe in which the team can drill six holes to mount a bulkhead. After testing the method on another nose cone when a locating tool was unavailable, the team was able to successfully place the holes. A photo of the manufacturing layout is below.

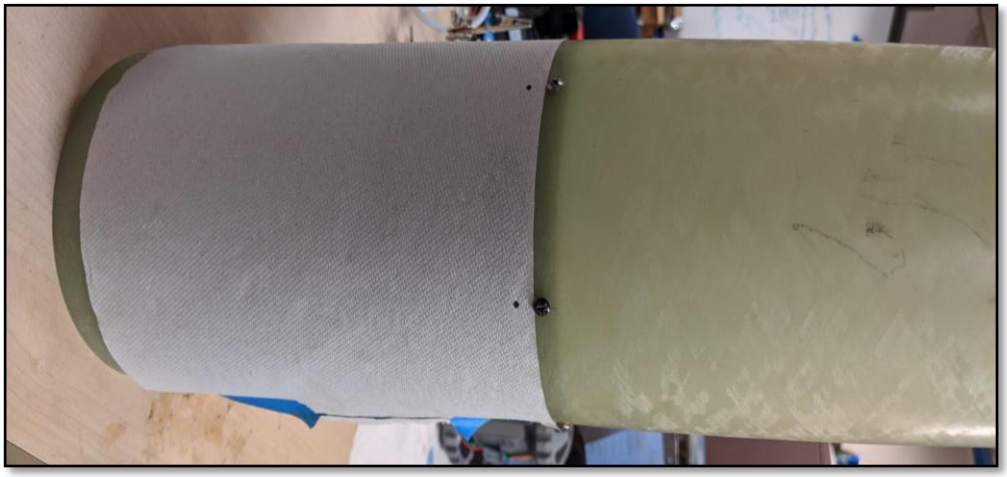

Figure 7 - Nose cone airframe hole manufacturing layout

After reviewing the two nose cones and identifying another method for manufacturing the mounting hole locations, the team decided the 5:1 black Madcow Rocketry nose cone was the best option. Below is a pro-con chart comparing the commercially available nose cones.

Commercial Von Karman Nose Cone Pros & Cons

	Pros	Cons
Von Karman 5.5:1	• Simplifies manufacturability (translucent material)	• Longer • Heavier
Von Karman 5:1	• More ideal geometry	• Complicates manufacturability (opaque material)

Table 4 - Commercial Von Karman nose cone pros and cons

3.1.4. Simulation Analysis

The team further explored these options using both OpenRocket. OpenRocket was used to provide an in-depth aerodynamic analysis of the launch vehicle's flight profile. OpenRocket is able to provide accurate data by considering the total weight of the rocket throughout flight (i.e. as fuel is being burned off, when the stages separate, etc.), as well as the center of pressure and center of gravity of the vehicle, based on the location of each individual component within the rocket. The program then takes geographic location and launch conditions into account, giving the team valuable insight into the potential flight profile. The key information gathered from these simulations include maximum altitude reached, maximum drag force experienced by the launch vehicle, and the maximum velocity of the launch vehicle. By changing the nose cone style and dimensions, effects of the shape and fineness ratio were observed. The results of the simulations can be seen below. Note that these simulations were taken using a preliminary design, as the goal of this was to understand the nose cone shape effect on the flight and to determine the most ideal shape.

OpenRocket Nose Cone Flight Results Comparison

Nose Cone Design	Altitude (ft)	Max Drag (lbf)	Max Velocity (ft/s)
Conical	26,829	192.1	1,233
Ogive	28,251	180.3	1,270
Ellipsoid	27,856	174	1,263
Power Series	28,855	169.1	1,288
Parabolic Series	28,516	174.2	1,279
Haack Series (Von Karman)	28,869	169.3	1,289

Table 5 - OpenRocket nose cone flight results comparison

While the NACA research stated that the Haack Series profiles are the most efficient for speeds at Mach 1.2, the entirety of the flight is not at this speed. Therefore, the team used OpenRocket to simulate the entire flight and determine the most ideal design. As shown above, the resulting flights, while keeping all rocket components and launch characteristics the same, state that the Haack Series design reaches the highest altitude, with the lowest maximum drag and highest maximum velocity. It should be noted that there are two primary types of Haack Series: the LD (Von Karman), and the LV. Both designs have a variable C that differentiates their curvature. As the Von Karman design is commercially available, this is the one that was used in the simulations [25].

$$\theta = \cos^{-1}(1 - \frac{2x}{L})$$

Equation 1 - Von Karman Constant

$$Y = \frac{R}{\sqrt{\pi}}\sqrt{\theta - \frac{\sin(2\theta)}{2} + C\sin^3(\theta)}$$

Equation 2 - Von Karman Equation

The LV iteration had a maximum drag of 172 lbf, a maximum velocity of 1,282 ft/s, and an apogee of 28,599 feet which proves the Von Karman version is better because it has less drag and reaches a higher maximum altitude.

The point at which the launch vehicle will experience the highest temperature is the stagnation point, or nose cone tip. Through research, the team discovered that some rockets surpassing supersonic speeds have experienced temperatures high enough to raise concern over potentially damaging or melting the nose cone tip. The team calculated the stagnation temperature using the equation below, found from a North Atlantic Treaty Organization article regarding in-flight temperature measurements. It assumes an isentropic flow. To ensure the aluminum tip would not be compromised during flight, the team assumed a worst-case scenario.

$M_a = 1.2$
$\gamma = 1.4$
$T_s = 100°F$

$$T_{nc} = T_s\left(1 + \frac{\gamma - 1}{2}{M_a}^2\right)^{-1}$$

Equation 3 - Stagnation temperature

Plugging in the variables above, it was determined the maximum stagnation temperature the aluminum nose cone tip would face is 77.64°F, which is well below the 1,220.67°F melting point of aluminum, offering a 15.72 FOS [31].

3.2. Fin Design

The fins of the launch vehicle are a significant structural component and are used to provide stability for the rocket. Fin design covers aspects such as the number of fins, the leading-edge design, and the trailing-edge design. To find the best design for this rocket, the team considered factors including weight, the applied drag force, the effect on rocket stability, structural integrity, and manufacturability. For the design of a launch vehicle traveling at supersonic speeds, the structural integrity of the design and the stability of the rocket were of the utmost importance, leading to the decision to use aluminum as the fin material. The flutter analysis section provides calculations and simulation analysis of the structural integrity. Beyond this, the team's decision was heavily influenced by the weight and the applied drag force, as the Spaceport America Cup

competition is altitude-based. This led the team to investigate an airfoiled leading-edge. These design considerations will be detailed further in the following sections.

One of the initial design decisions was the number of fins per stage. The number of fins can affect the stability of the rocket, the weight of the rocket, and the applied drag force. The team considered the following pros and cons in the analysis.

3.2.1. Number of Fins

Number of Fins Pros & Cons

Number of Fins	Pros	Cons
3	• Less drag • Less weight • Less material (cheaper) • Easiest to manufacture	• Least stable • Most force on one component
4	• More stability • More force distribution	• More drag • More expensive • Heavier
5	• Best force distribution	• Insignificant stability increases from 4 fins • Most costly • Least symmetrical • Most difficult to manufacture • Most drag

Table 6 - Number of fins pros and cons

Three fins is fairly standard in model rocketry. Testing results from the Pilotless Aircraft Research Division of the Langley Memorial Aeronautical Laboratory show the drag coefficient for rockets with 3, 4, and 5 fin arrangements for various Mach numbers [19]. Based on the results, the drag coefficient increases with each additional fin. The fin designs used in this testing were clipped delta design and could help the team predict the expected fin arrangement drag coefficient for the final launch vehicle.

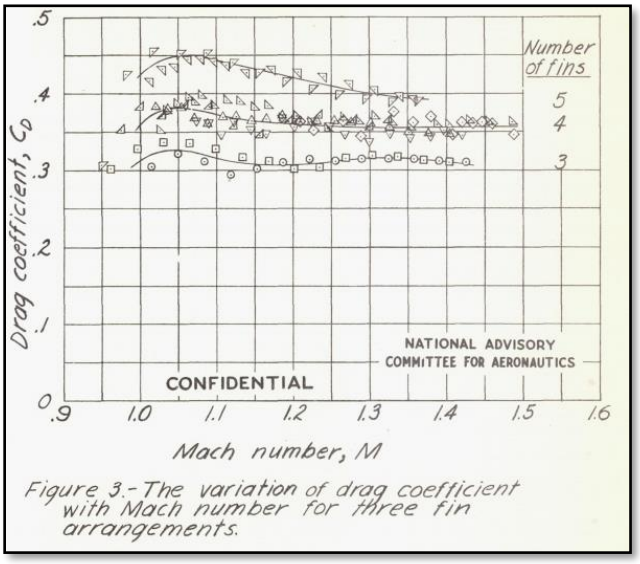

Figure 8 - Pilotless Aircraft Research Division fin testing results

Additionally, the team is familiar with the flight characteristics associated with a vehicle using three fins. For these reasons, and the desire to maintain a simpler design where possible, the rocket will use three fins. The team will keep both sets of fins aligned radially to reduce drag and to promote more uniform airflow over the airframe.

The leading-edge of the fins plays a major role in the drag and stability of the launch vehicle, with the sweep angle being the primary design consideration. The sweep angle is the angle between the line from the leading point of the root and tip chords and a perpendicular line from the body of the rocket starting at the lead point of the root chord. Typically, as sweep angle increases, the drag of the launch vehicle decreases, though the stability decreases as well. For this reason, a range of sweep angles must be considered to ensure a sufficient stability margin is maintained while decreasing the drag as much as possible.

The 1952 NACA report [25] also included some valuable information on fin design to improve aerodynamic performance. Based on testing several arrangements with varying fin sweep angles, a sweep angle of 70-degrees was best for all speeds tested. The graph below shows the test results for drag coefficient vs Mach number for three and four wing arrangements using the same fin shape for each. The plot seems to indicate that a larger sweep angle is best, not necessarily that a 70-degree angle is optimal. Beyond 70-degree sweep angles were not included in the testing. However, the OpenRocket and RockSim simulation software both showed a drop in stability margin for the overall rocket design on sweep angles above 70 degrees. For this reason, the team hopes to utilize a leading-edge sweep angle as steep as possible, but below 70-degrees for both stages. Final sweep angle values may vary based on stability needs for the overall rocket design.

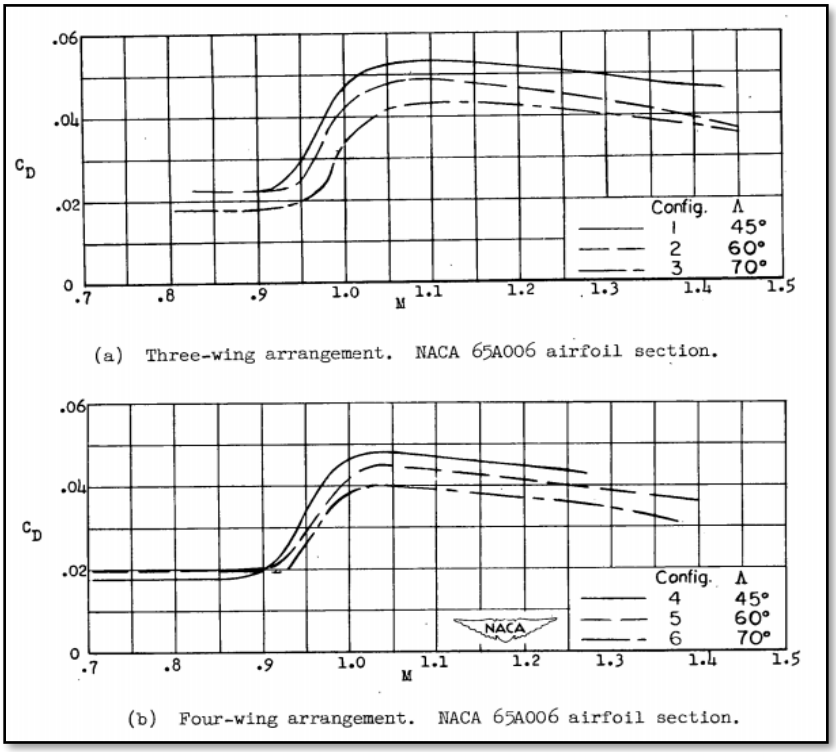

Figure 9 - 1952 NACA testing results for leading-edge sweep angle

The team ran OpenRocket simulations while only adjusting the leading-edge sweep angle of the 2nd stage fins in increments of one degree to analyze the impact on stability margin of each stage and the altitude achieved. This same simulation was conducted on the RockSim software, but the results (while showing an upward slope) showed very little impact and did not offer any further validation. Although the 1st stage fins were kept constant throughout the analysis, the results can be applied to the 1st stage fins to produce similar improvements to the rocket design. Below is a plot of OpenRocket altitude versus leading-edge sweep angle which shows that altitude varies fairly linearly with an increasing sweep angle.

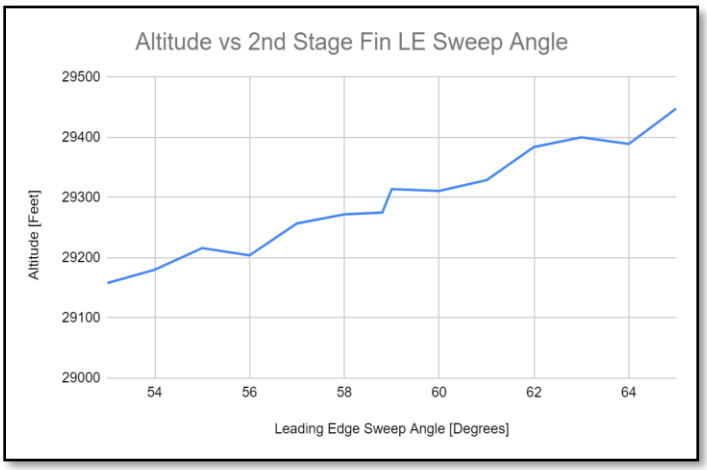

Figure 10 - OpenRocket Altitude vs 2nd Stage Fin LE Sweep Angle

The team also checked the stability margins for the rocket for each leading-edge sweep angle using both OpenRocket and RockSim. The plot below shows that the stability margin of both stages increases linearly while the stability margin of the second stage drops off fairly linearly. The team stopped running simulations around 65 degrees since the second stage stability margin dropped under 2.0. The team would like to keep the stability margin for each stage at or above 1.75 if possible, so some margin for error was included here. Details regarding stability margin are covered in the Stability section of the report. Overall, the OpenRocket and RockSim results are similar, with RockSim stability margin being offset slightly lower for both stages of the rocket design.

Figure 11 - Stability Margin vs 2nd Stage Fin LE Sweep Angle

Based on the results of the simulations, a steeper leading-edge sweep correlated to a higher overall altitude. Using this, the team determined that they should increase the sweep angle as much as possible, while remaining within competition and team stability requirements. The final sweep angles selected will depend on the final weight distribution of the rocket, since the fin design is the easiest method of adjusting the stability margin post-manufacturing. These simulations will be re-analyzed after the full-scale rocket has been manufactured with actual weights recorded, but the current plots provide valuable insight for the current design estimates.

The team analyzed the trailing-edge fin design for similar characteristics as the leading-edge design, including altitude variation and stability margin of each stage. Brief online research revealed that a tapered swept trailing-edge design could be the most effective. However, additional NACA testing [17] revealed the swept design is not optimal for supersonic speeds. The graph below depicts testing of various airfoil shapes at supersonic speeds. The plots are for drag coefficient vs Mach number, again. The results show that a delta fin (5) or trapezoidal fin with no tip chord (6) have the lowest drag coefficients at supersonic speeds.

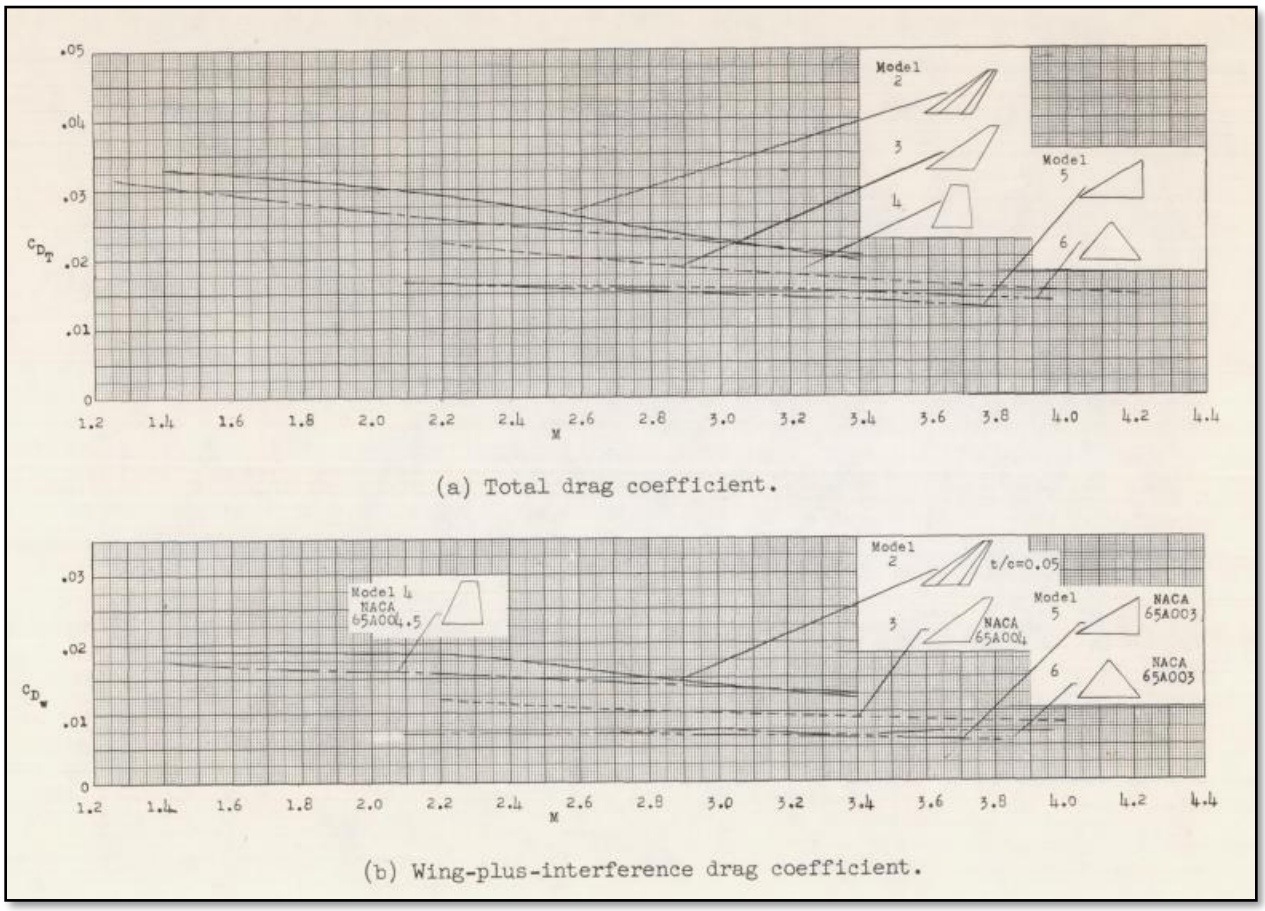

Figure 12 - NACA fin testing results for supersonic speeds

Although data is not shown for the highest speeds of the current launch vehicle design (Mach 1.0-1.2), the data is fairly consistent for the supersonic speeds recorded. Using OpenRocket, the team again adjusted the 2nd stage fins to compare stability margin values and

apogee. OpenRocket showed continuous improvement as the trailing edge increased, dissimilar to what would be expected from the increase in drag shown in the chart. RockSim was also used, with the initial trend of the sweep distance increasing raising the altitude, but once the root chord was reduced to zero, the altitude decreased. For the sake of the trailing edge, the software both match up. For these simulations, the trailing-edge was the only variable adjusted between simulations. OpenRocket, nor RockSim have an adjustable input of “trailing sweep angle,” however the input of tip chord can be adjusted which corresponds to trailing-edge sweep distance. Trailing sweep distance is the length the fins are swept back from a perpendicular position to the airframe. For these simulations, it was adjusted in increments of 0.5”. A negative trailing sweep distance corresponds to a tapered swept fin. A trailing sweep distance of zero corresponds to a clipped delta fin. A positive trailing sweep distance corresponds to a forward swept trailing-edge like a trapezoidal fin. All three fin orientations are shown below for clarity.

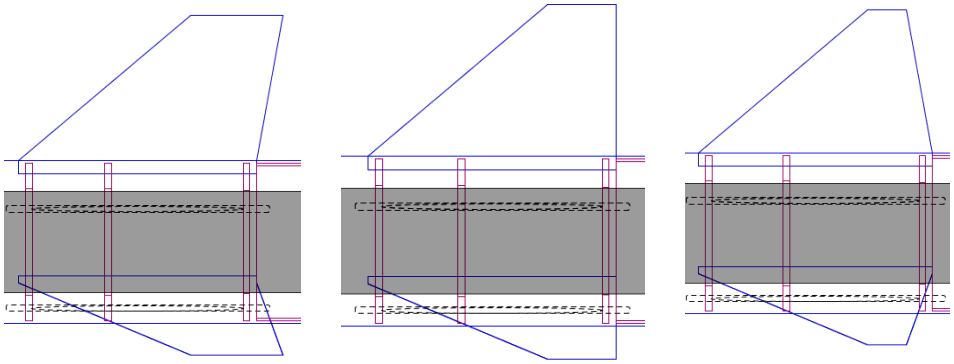

Figure 13 - Fin trailing sweep distance orientations

The results for altitude in OpenRocket shown below display that the trailing-edge has minimal effect on altitude even though there is a linear increase as the trailing-edge sweep moves forward. The team believes the altitude increase can be attributed to the weight lost in material on the three fins since the max drag was relatively constant for all sweep distances.

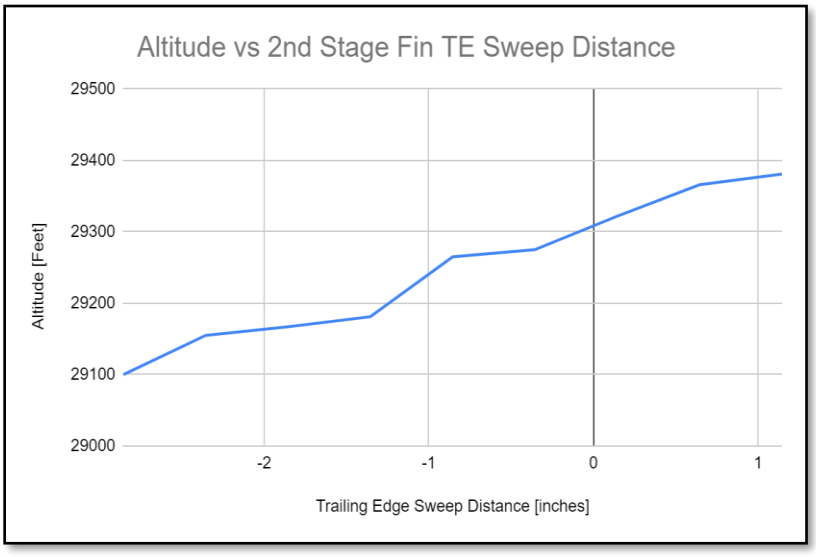

Figure 14 - OpenRocket Altitude vs 2nd Stage Fin TE Sweep Distance

Again, the trend results are the same for RockSim, with the only difference being the final plot point. The team theorizes this is due to the tip chord of this simulation being reduced to zero to adapt a changing trailing edge. This plot point will not be regarded for the case of the trailing-edge impact but will be recalled for any instance the team considers using a triangular fin set.

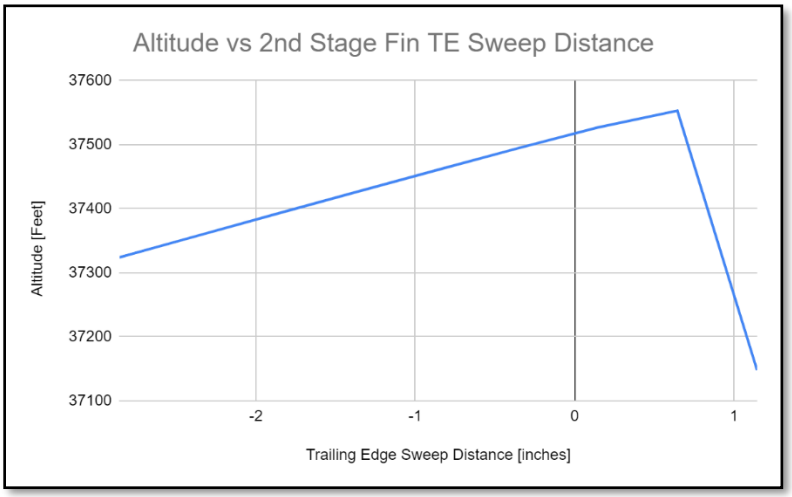

Figure 15 - RockSim Altitude vs 2nd Stage Fin TE Sweep Distance

The results for stability margin in OpenRocket are shown below. They indicate that the trailing-edge design has minimal effect on stability of both stages together but have a larger impact on the 2nd stage stability, which begins to drop below 2.0 once the fins are swept 1" forward.

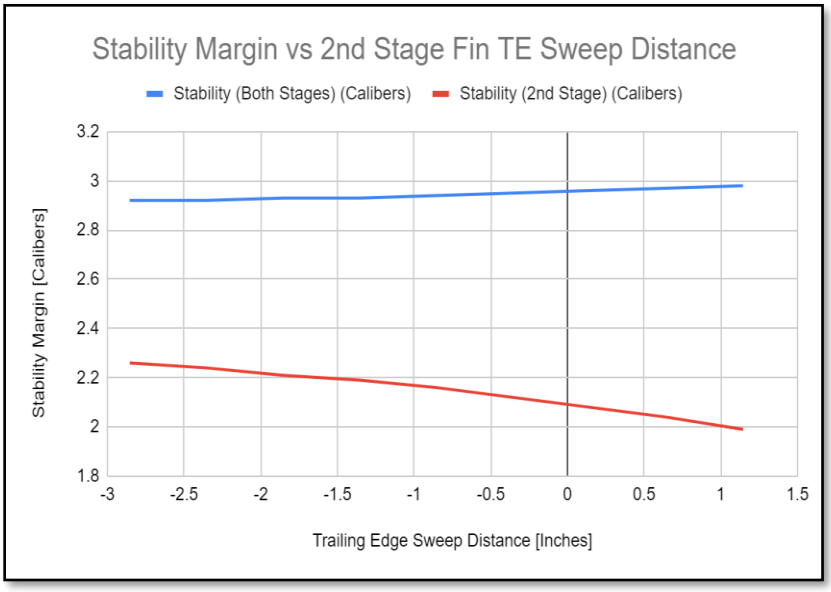

Figure 16 - OpenRocket Stability Margin vs 2nd Stage Fin TE Sweep Distance

Based on this research and the flight simulations primarily in OpenRocket, the team believes that the trailing-edge sweep does not have a significant effect on altitude or drag, but it will affect stability. For this reason, the team is leaning more toward a clipped delta fin design for the

second stage for manufacturing simplicity and stability. However, final weight distributions and the results from the critical Mach analysis will have an influence on the design.

The team suggests future readers investigate a forward swept trailing-edge for reduced weight and less concern for the fins breaking upon impact with the ground. A forward swept trailing-edge will have a lower stability margin, as shown above, but it could reduce the chance of the fins impacting the ground when the rocket lands. They also caution the use of triangular tipped fins as these will have significant impact on altitude.

An airfoil cross-section is best for aerodynamic performance, but difficult to manufacture symmetrically. Sharp leading edges are also more common at supersonic speeds, as opposed to a round leading-edge, as the effect of drag is decreased significantly. However, sharp leading edges are difficult to manufacture with symmetry. Due to the team's manufacturing and financial limitations, an airfoil cross-section will not be utilized for the fins unless a local company can support manufacturing.

The rocket team received a service donation of airfoiled fins from NMG Aerospace in the past and this opportunity was investigated again for this project. Around January 2020, the team found out that NMG Aerospace did not have the capabilities to support the manufacturing of the team's airfoiled fins this year.

The team also reached out to Fredon, a company that had worked with Tomahawk and Patriot missile manufacturing, in February 2020. The team submitted a preliminary fin design to get a cost estimate. The following design was quoted for $2,000 to $3,000 by the Vice President of Operations per fin, which is outside the budget allocated for the project and a sponsorship opportunity was not available.

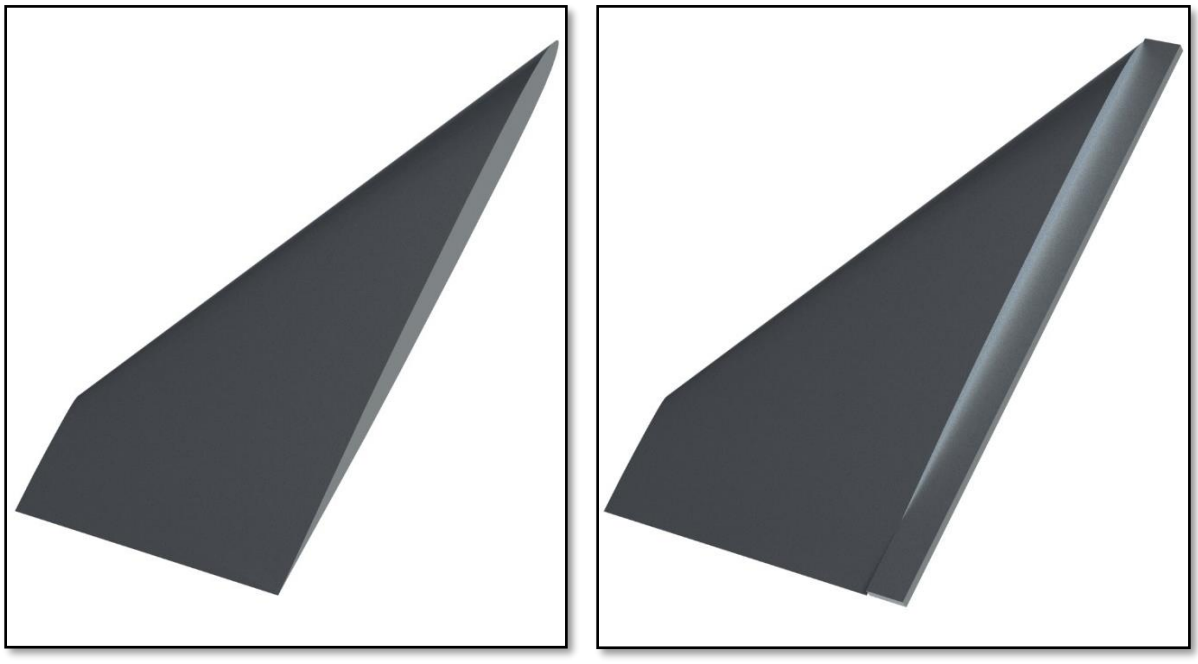

Figure 17 - Airfoiled fin design with and without attachment plate

The team utilized their primary research in fin design to direct them toward optimizing the flight profile. The primary goal of the CFD analysis was to determine the Critical Mach value of the flight profile. Project BOGO will be experiencing flight forces at Mach speed, drastically increasing the amount of drag that the airframe will incur. The Critical Mach value is the speed at which the airflow over the body of the rocket will reach Mach speed. This is due to the local flow needing to travel further than the freestream outside the airframe's boundary of influence.

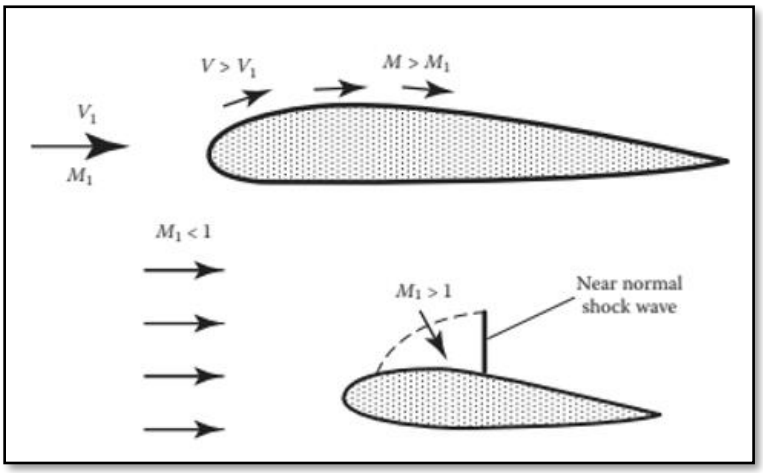

Figure 18 - Visual flow over an airfoil

When this local velocity reaches the speed of sound, it will induce a significant amount of drag. This is due to the formation of a near normal shock wave. Thus, the higher the value of the critical Mach number, or the faster the vehicle can go prior to its local flow reaching Mach speed, the less drag the rocket will face.

To determine this, the team set up two flight profiles into ANSYS Workbench and Fluent and found the point at which the local flow reaches the speed of sound. The team built a rocket profile with a swept edge design and a clipped delta design.

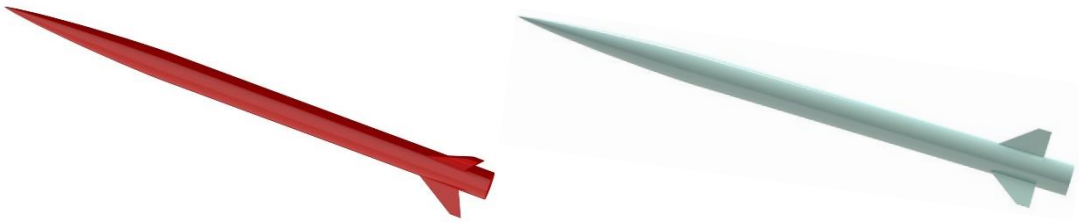

Figure 19 - Swept Fin Profile (left) and Clipped Fin Profile (right)

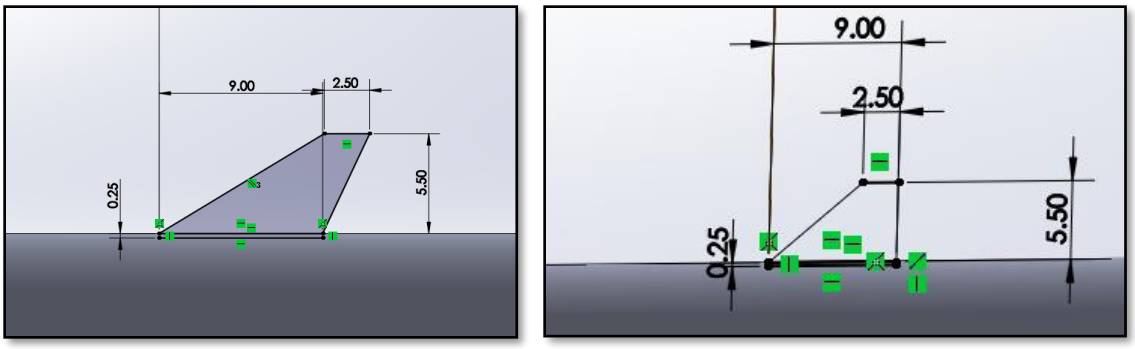

Figure 20 - Swept fin dimensions (left) Clipped Delta fin dimensions (right)

By saving the models as Parasolids, they are made to be compatible with Siemens's ANSYS software. The file format also allows easy integration with Boolean operations, which is ideal for a flow simulation requiring a boundary setup. To emulate the flow of air, the vehicle models were put into boxed enclosures. The boxes were made out to be much larger than the models. The distance from each wall to the vehicle is approximately five times the length of the rocket. The wake of the rocket is the area most affected by the fins and where any eddies or other vortices will develop. This will potentially take up a large are between the back wall (the outlet) and the aft end of the rocket, so this distance was expanded to ten times the length of the enclosure (10 meters).

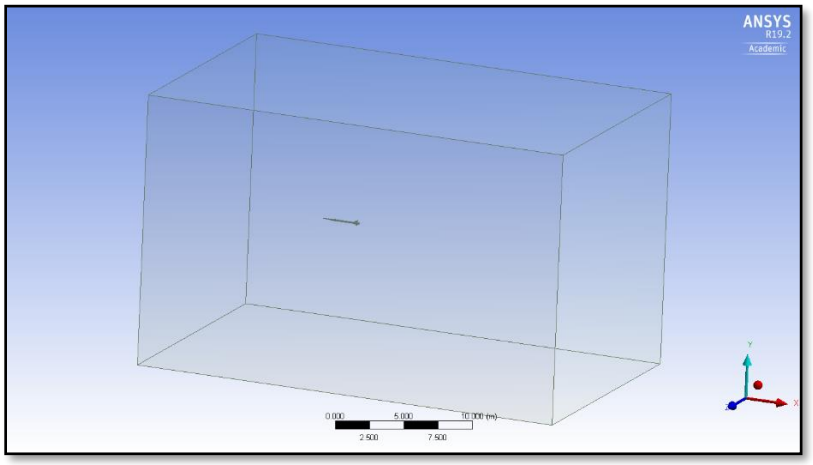

Figure 21 - Fluid Boundary Box

The model layout was then transferred to an ICEM CFD application in the ANSYS Workbench. This allows the model to be meshed for the Fluent software. In the ICEM, the major components of the model can be called out. The left-most face as the Inlet (where the air will enter), the right-most face as the Outlet (where the air will exit), the surrounding walls as the SYS (for simple reference), and the rocket's fins and body both labeled as such for future callouts. The meshing software can set element size based on labeled bodies so the user can apply more focus on parts of interest. As the team is mostly concerned with the velocity of the air flowing over the rocket, the body and fins will be set to smaller meshes. To compare, the global maximum element size was set to 2 meters while the body mesh was set to 0.0325 and

the fin mesh to 0.0156 meters. Note, that these dimensions limit the maximum size of the mesh, and the contours and curves of the designs are much smaller.

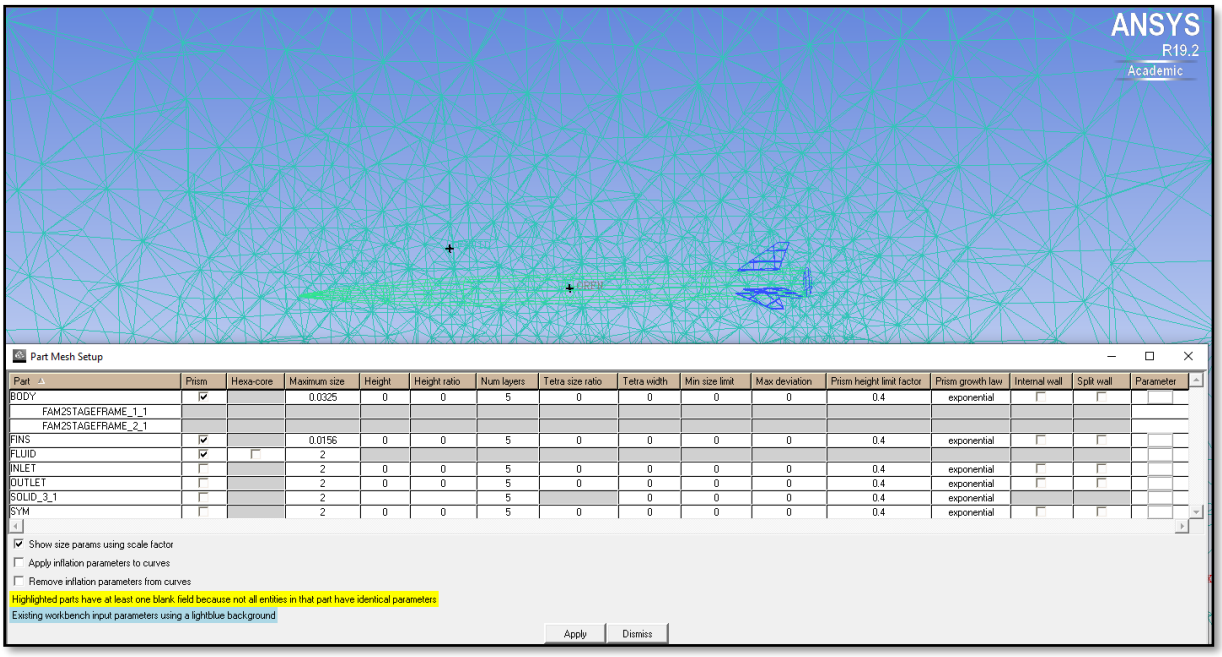

Figure 22 – Vehicle Wire Mesh Layout

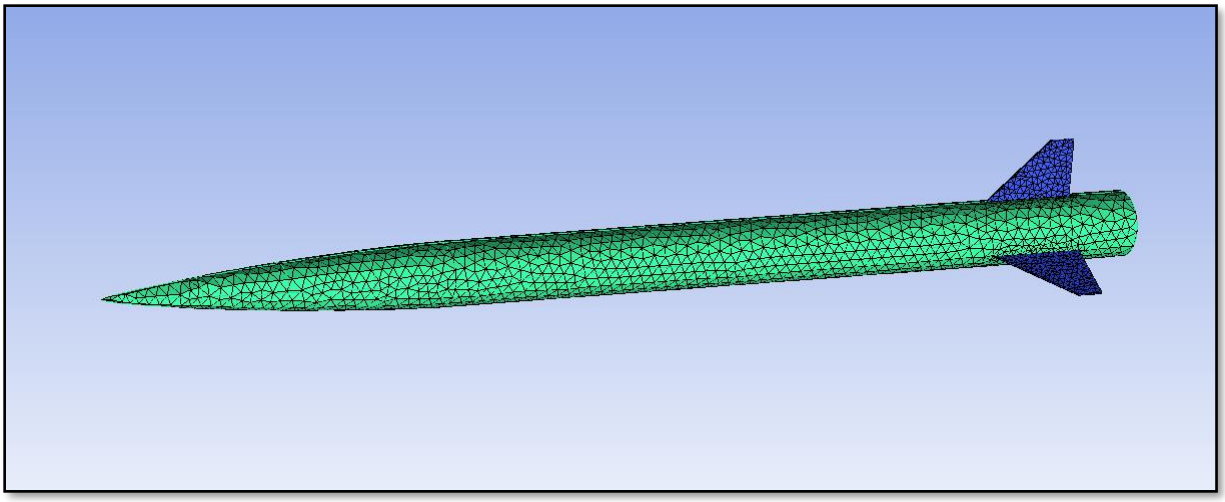

Figure 23 - Isolated Vehicle Mesh

To speed up the solution solving time, the volume of the rocket can be removed. By selecting two diametrical points of the rocket and titling it ORFN, the program will delete and not mesh the volume of the selected body. While that volume is unnecessary, the volume of the enclosure is necessary as to emulate the flow of air over the rocket. By selecting the edge of the rocket body and an arbitrary point inside the enclosure, a fluid was volume was defined for the entire volume of the enclosure. This part is named Fluid for the solve. To further improve the quality of the mesh, the team re-established the meshing for the Fluid, the Fins, and the Body as prisms. Prism features require more resources to solve, however get more detailed results

from meshes. The prism heights limiting factors are set of 0.4 meters and their growth law is set to be exponential. Furthermore, the layering was increased to five to better detail flow near the rocket body. From there, the mesh was computed using a prism mesh solve and recorded using the replay control.

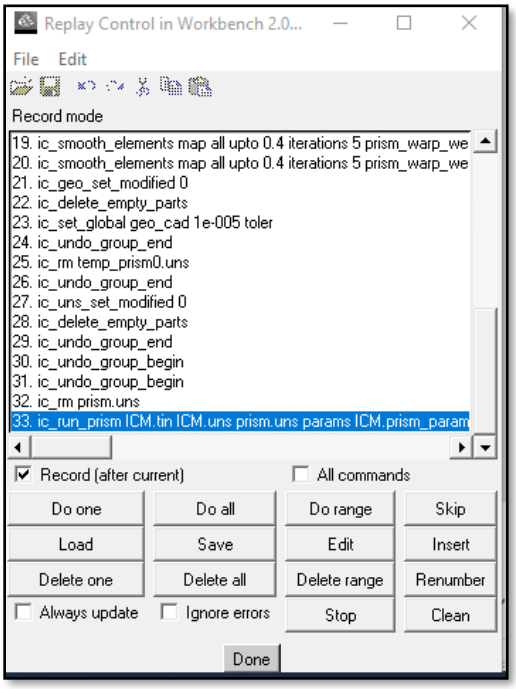

Figure 24 - Replay control playout for meshing

Once the mesh completed, the data was transferred to the Fluent application.

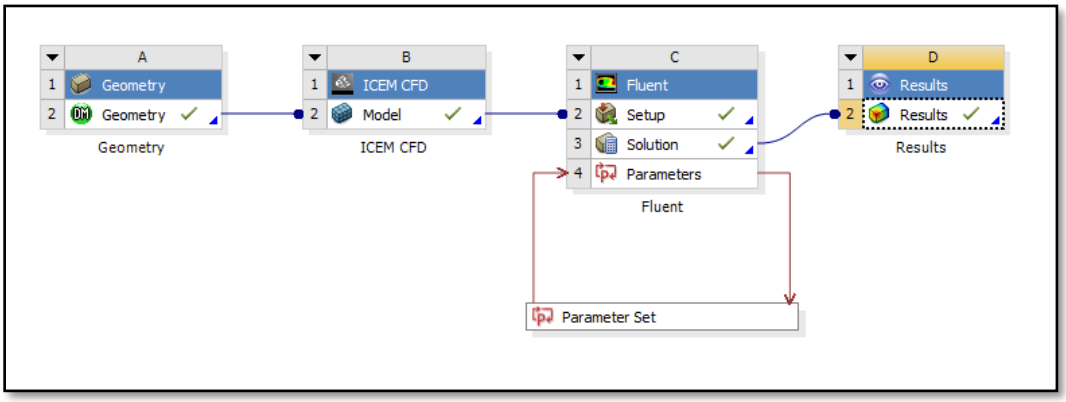

Figure 25 - Workbench layout

The experiment was solved under density-based parameters using the Spalart-Allmaras singular equation, which is generally used for aerospace related flow simulations for finding kinematic eddy turbulent viscosity. This setup is used for walled in flows and specializes in simulations that might have boundary layer development on the model within the enclosure.

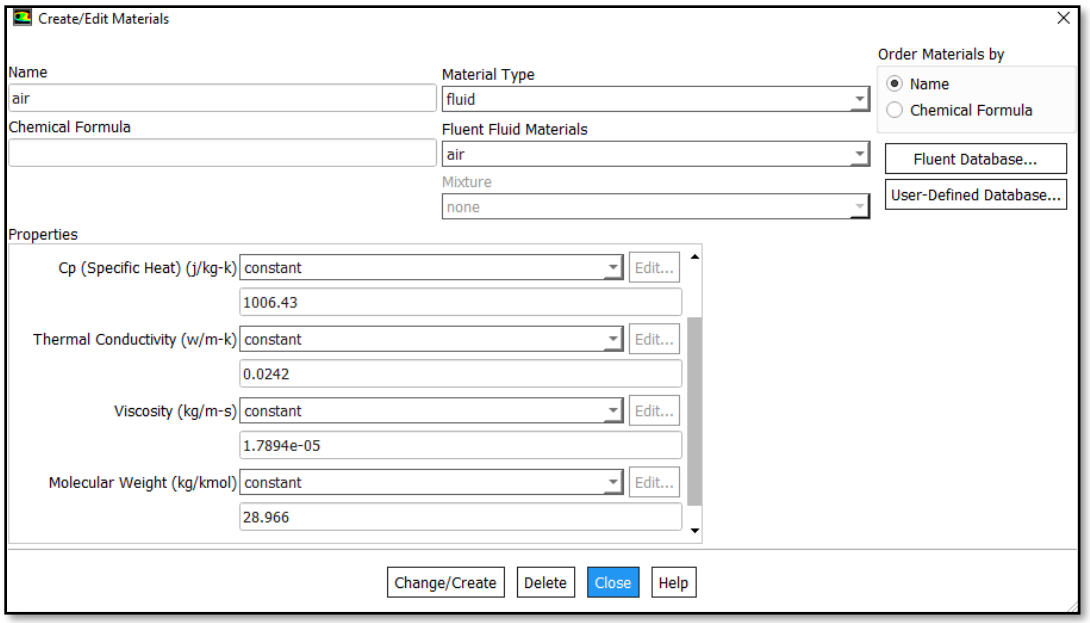

Figure 26 - Fluid "Air" Definition

The fluid for the simulation was stated as air with an ideal gas density definition. The Inlet of the airflow was set to start at a 300 m/s velocity magnitude. The report definitions were set for finding the velocity and velocity magnitude of the fluid on the rocket fins and body. To maximize results, the continuity was set to 1e-12 so it would never converge. The initialization setup was set to external aero favorable settings and the iterations were solve for 1000 results. In the parameter layout, the requested fluid inlet speeds were from 300 m/s to 280 m/s in increments of 1 m/s. The results were then visualized to get an early prediction of which design was more optimal.

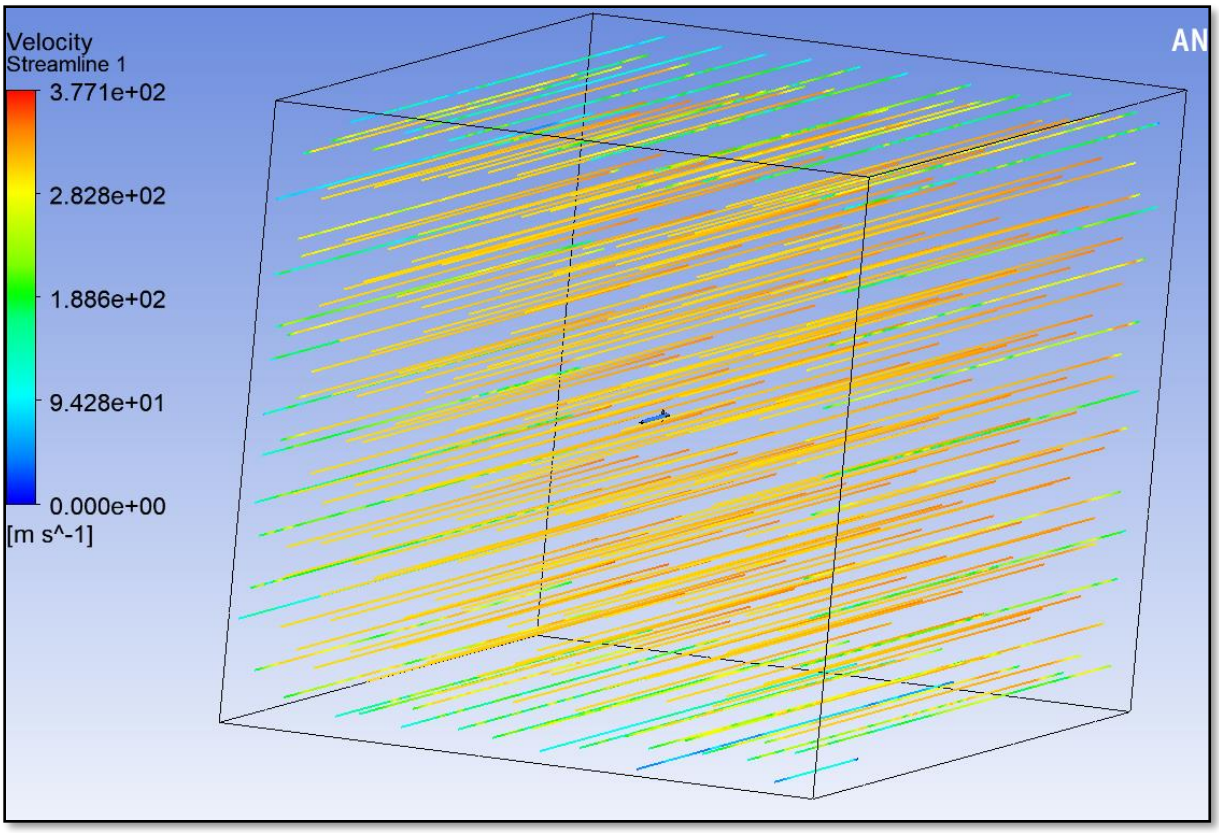

Figure 27 - Critical Mach Streamlines over a Swept Fin Design

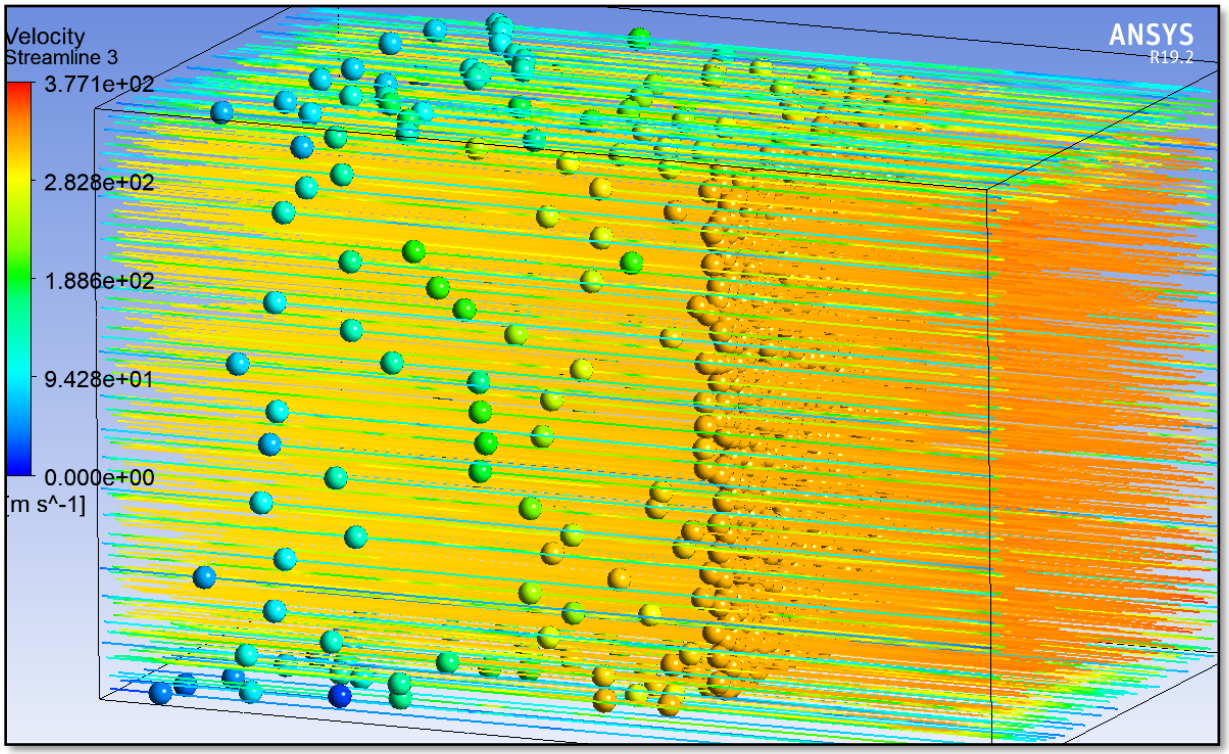

Figure 28 - Critical Mach Particles over a Swept Fin Design

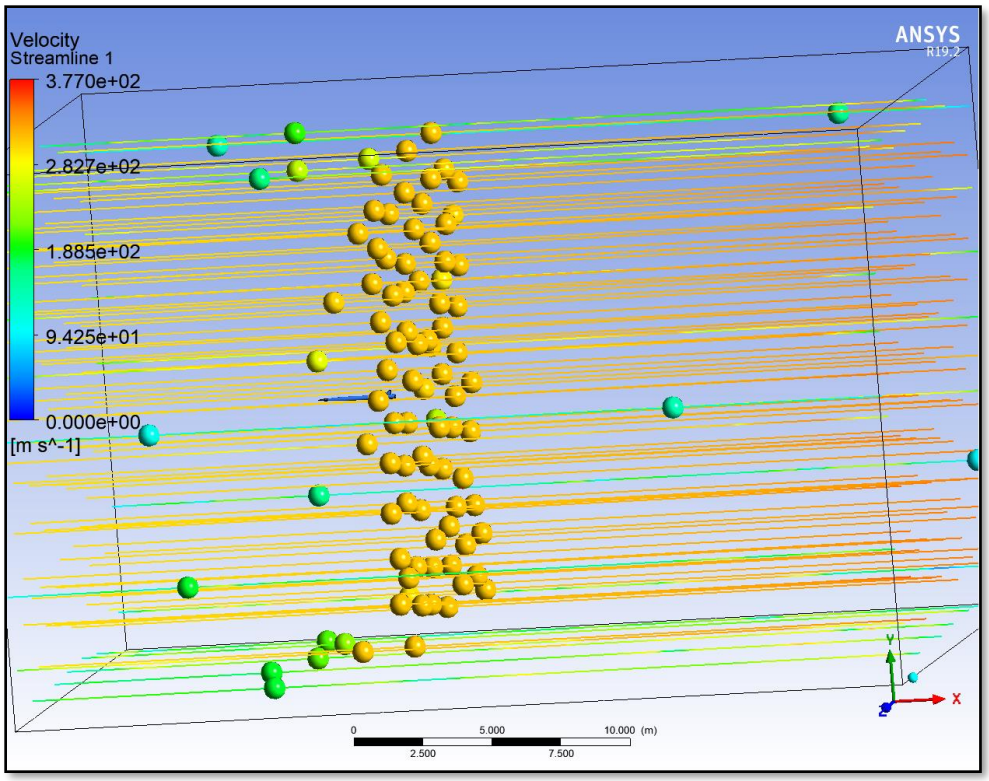

Figure 29 - Critical Mach Streamlines and Particles over a Clipped Delta Fin Design

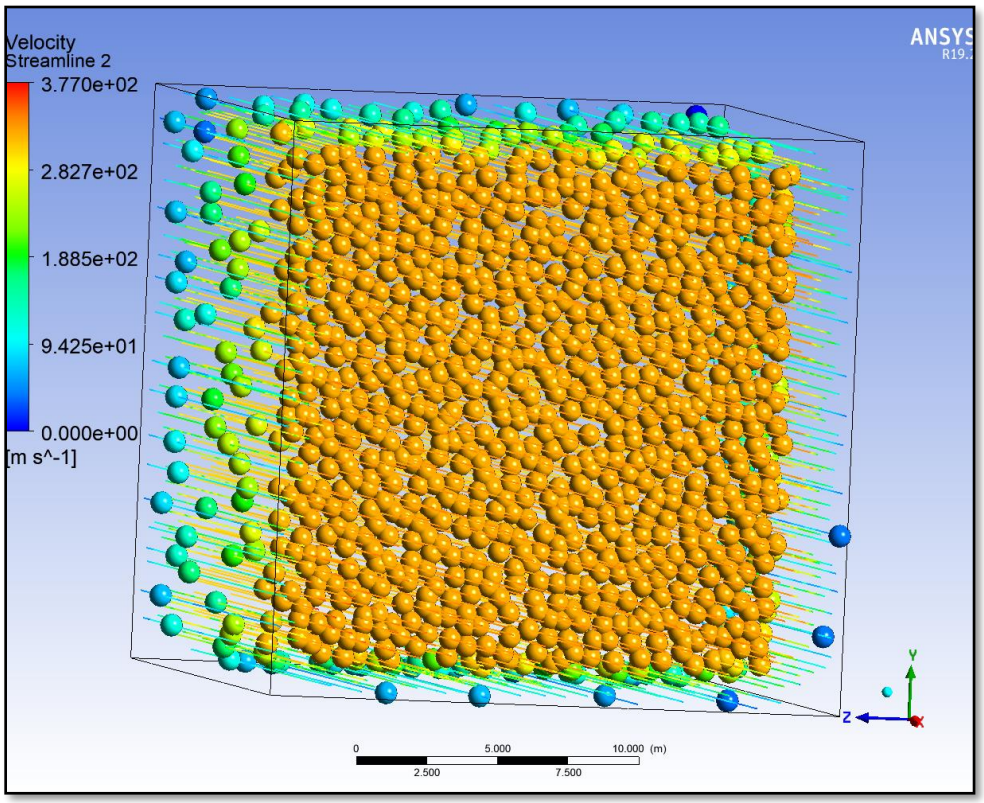

Figure 30 - Critical Mach Particles over a Clipped Delta Fin Design

The figures illustrate that the closer the airflow is to the rocket body, the fast the air travels. Under close examination, it maximized directly over the rocket body. The colorization of the streamlines is too broad to show this, so the particles were input to show the slight increase in speeds right on top of the rocket body. However, the visualization regards no obvious choice as to which design is more optimal, so the team had to investigate the numeric results coming from the inlet velocities in comparison to the rocket surface velocities. The resulting speeds for inlet and body are shown below.

CFD Inlet and Body Velocities Comparison

Inlet Velocity (m/s)	Swept Fin Velocity (m/s)	Clipped Fin Velocity (m/s)
300	391.74	468.40
299	351.78	464.57
298	350.12	459.70
297	348.84	454.85
296	347.57	402.01
295	346.15	349.06
294	344.55	347.60
293	342.23	345.59
292	338.23	342.04
291	331.59	335.29
290	329.00	329.48
289	328.08	329.46
288	325.50	330.09
287	318.89	324.96
286	321.21	313.99
285	319.03	310.57
284	312.92	316.22
283	309.94	316.65
282	309.35	315.66
281	310.41	316.45
280	310.38	316.43

Table 7 - CFD inlet and body velocities comparison

The results are fairly consistent and were conducted under separate workbenches, which helps validate the proper mesh sizing for the results. It is worth noting the major local velocity shift that the fluids undergo and are detailed in the results. This is likely due to the inconsistencies of transonic flow as well as the impact of the velocities overcoming the speed of sound and the Mach drag ensuing from it. Along with this, it shows that it requires higher velocities for the swept fins reach this major shift than it does for the clipped fins. This can be used to support the use of the swept fins so that the rocket experiences less drag and stress on the body.

By taking the velocities over the bodies that are at approximately the speed of sound and taking the dividend between them and the inlet velocity, the critical Mach value is determined by the ratio. The speed of sound is determined by the following equation.

$$a = \sqrt{\lambda RT}$$

Equation 4 - Speed of Sound

Using 1.4 for the ratio of specific heats, λ, for air, a general temperature of 20°C, and the gas constant of 286 m2/s2K, the resulting speed of sound is 343 m/s. Thus, the extrapolated velocities for the surfaces are 293.33 m/s for the swept body and 292.27 for the clipped body. The critical Mach value for the swept body is 0.855 and the clipped delta body is 0.852. The swept fin design is more ideal for the reduction of Mach drag; however, these values are extremely close, showing that they are fairly inconsequential regarding the activation of Mach drag. Both designs state that the flow over the rocket body will not reach Mach speed until the rocket is moving at approximately Mach 0.85. Anything above Mach 0.8 is acceptable, being within transonic speeds. It is theorized that the lack of thickness (3/16”), the minute sweep angle differences, and the small proportional size of the fins (approximately 1 caliper), that the change in fin design does not diverge the critical Mach values. Large fins would result in more varied values.

Given more time and resources, the team would have made the boundary larger and the meshing of higher quality to create a model of higher fidelity. Then, they would analyze designs with more drastic dimensions and then optimize the best with minor changes so that they could determine an ideal design.

By utilizing the information provided by the NACA research along with the flight simulations and CFD analysis, the team was able to justify a clipped delta fin design for both stages. The fins will have a steep leading-edge sweep that will not exceed 70-degrees to maintain stability. There will be no trailing-edge sweep, which the team proved was a minor factor in stability and altitude. There will be three fins for simplicity and reduced drag and the fins will not be airfoiled due to manufacturing constraints. This design will not incur sub-optimal drag forces and it will provide a high critical Mach value of 0.85. Final fin dimensions will be adjusted based on manufacturing of the full-scale two-stage rocket to adjust the stability margin as needed.

3.2.7. Flutter Analysis

Fin flutter and fin retention are two of the most common points of failure with supersonic rockets. Therefore, the team has put a heavy focus on both aspects in the two-stage rocket design. For fin flutter, NASA uses a 15% safety margin on flutter velocity, which is the maximum velocity a rocket can experience before the fins begin to experience flutter. Considering it is the team’s first time flying a supersonic rocket, a much higher safety margin will be utilized. The team created a fin flutter calculator based on an article from Apogee Components to help predict the flutter velocity [15].

Fin flutter is an aerodynamic instability of the fins due to geometry, material, and fluid properties. It is like bending and torsion modes of a bridge. The fins are typically secured on one side only near the base of the rocket, leaving them cantilevered and capable of bending at the tip chord. Smaller fins and stronger materials can be incorporated for a tradeoff of less rocket stability and additional weight. The fin design is typically the last component to be finalized after all component weights are recorded to achieve an adequate stability margin for the rocket while maintaining a sufficient altitude. For calculation purposes, a worst-case scenario of the second stage fin design will be used to verify fin flutter safety. It should be noted that the key assumptions in the equations below are that the air is modeled as an ideal gas and the temperature and pressure equations are only valid within the Troposphere, which is below

36,152 ft. Below is the equation for flutter velocity along with accompanying equations and fin dimensions used for each variable.

$$V_f = \alpha \sqrt{\frac{G}{\frac{1.337(AR)^3(P)(\lambda+1)}{2(AR+2)\left(\frac{t}{C_r}\right)^3}}}$$

Equation 5 - Fin Flutter Boundary Velocity

Sustainer stage fin dimensions are shown below.

$$C_r\,(Root\ Chord) = 9"$$
$$C_t\,(Tip\ Chord) = 0.5"$$
$$t\,(Thickness) = 0.1875"$$
$$b\,(Semi-Span) = 5.75"$$
$$G\,(Shear\ Modulus\ \text{of Aluminum}) = 3{,}625{,}950\ psi$$
$$h\,(Height\ of\ Maximum\ Velocity) = 9{,}380\ ft$$

The equations used to find the flutter velocity are followed in sequence below.

$$S = \frac{(C_r + C_t)}{2} b = \frac{9+0.5}{2}\ 5.75 = 27.3125\ in^2$$

Equation 6 - Surface area for fin

$$AR = \frac{b^2}{S} = \frac{5.75^2}{27.3125} = 1.210$$

Equation 7 - Aspect ratio for fin

$$\lambda = \frac{C_t}{C_r} = \frac{0.5}{9} = 0.0556$$

Equation 8 - Ratio of tip to root chord

$$T = 59 - 0.00356(h) = 59 - 0.00356(9{,}380) = 25.607°F$$

Equation 9 - Temperature of fluid

$$\alpha = \sqrt{1.4(1{,}716.59)(T+459.7)} = \sqrt{1.4(1{,}716.59)(25.607+459.7)} = 1{,}079.95\ ft/s$$

Equation 10 - Speed of sound

$$P = \frac{2116}{144}\left(\frac{T+459.7}{518.6}\right)^{5.256} = \frac{2116}{144}\left(\frac{25.607+459.7}{518.6}\right)^{5.256} = 10.37\ \frac{lb}{in^2}$$

Equation 11 - Pressure acting on fin

Finally, the flutter velocity can be calculated below.

$$V_f = \alpha \sqrt{\frac{G}{\frac{1.337(AR)^3(P)(\lambda+1)}{2(AR+2)\left(\frac{t}{C_r}\right)^3}}} = 1{,}079.95 \sqrt{\frac{3{,}625{,}950}{\left(\frac{1.337(1.210)^3(10.37)(0.0556+1)}{2(1.210+2)\left(\frac{0.1875}{9}\right)^3}\right)}} = 3{,}075.46\ ft/s$$

The estimated flutter velocity gives a factor of safety of 2.32 against fin flutter considering the maximum velocity of the rocket of 1,325 ft/s utilizing up-to-date simulations with zero stage separation and sustainer ignition times. The delay times will be analyzed in more detail later, but the lowest delay times produced a worst-case scenario.

3.2.8. Modal Analysis

The team conducted modal analysis on the fin designs to determine the natural frequency of the fins and verify that they will not match the forcing frequencies of the flight. A common concern is in flight is the aeroelasticity of an external component. Aeroelastic flutter, as described in the previous section, is the occurrence when aerodynamic forces overcome the structural dampening of a component. While airspeed overcoming a flutter velocity is one example of how vibrations may occur, an object experiencing its natural frequency is another less likely example. If an object's natural frequency were to meet the forced frequency (in this case, the airflow) it will begin to resonate and potentially break during flight. Using modal analysis, the team determined the eigenfrequency of the fin sets to ensure they would not be the same as the frequency of the sonic boom, which is commonly ranging from 0.1 to 100 Hz based on a US Air Force research article [26].

The team uploaded the two models of their fin sections into ANSYS Workbench for a modal analysis. Due to the simplicity of the designs, the solver did not require high fidelity meshing. The following chart compares the similarities of the results of the same structure with difference qualities of meshing and then displays the second structure's results.

Fin Natural Frequencies

Iteration	Frequency (Hz)						Fidelity		
Lower Fins	**Mode 1 Fin A**	**Mode 1 Fin B**	**Mode 1 Fin C**	**Mode 2 Fin A**	**Mode 2 Fin B**	**Mode 2 Fin C**	**Smoothing**	**Transition**	**Span Angle**
1	210.94	211	211.02	576.3	576.35	576.43	Medium	Fast	Course
2	210.25	210.25	210.28	577.03	577.11	577.18	High	Fast	Fine
Upper Fins									
Lower settings	182.76	182.77	182.79	592.74	592.78	592.81	Medium	Fast	Course

Table 8 - Fin Natural Frequencies

The chart shows the resulting natural frequencies of the first and second mode of each fin for the upper and lower fins. After testing the consistency of the meshing results by increasing their quality for the first solution of the aft set, the results were shown to be similar enough to use the lower quality sets to save solving time for the upper fins. Furthermore, the analysis showed that each fin has the same natural frequency as the others in its set. Below are some

visual results of the deformation that the fins would face when experiencing their first and second mode.

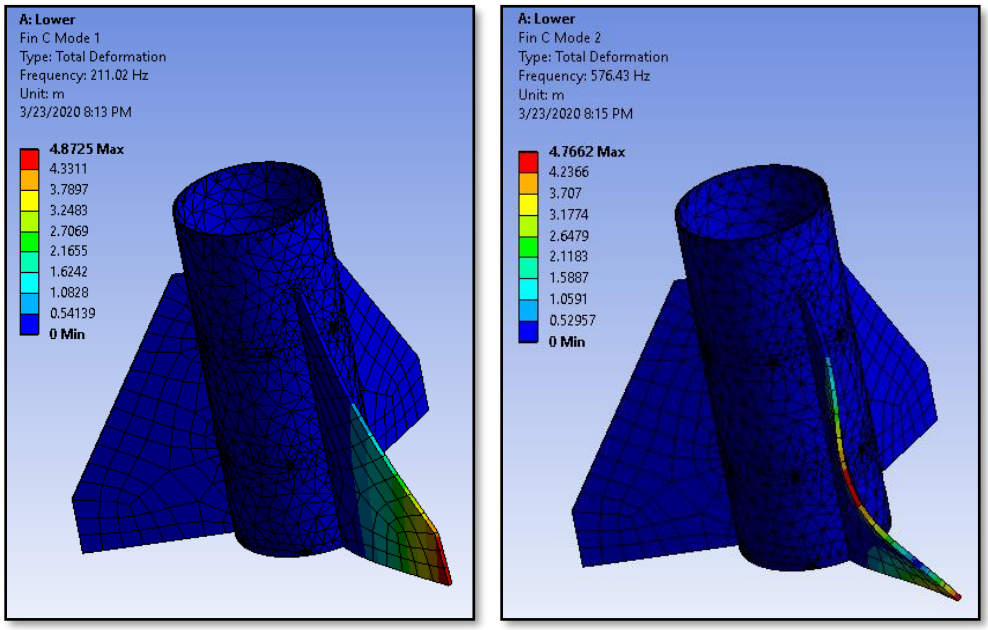

Figure 31 - Booster Fin Set Deformation at Mode 1 (left) and Mode 2 (right)

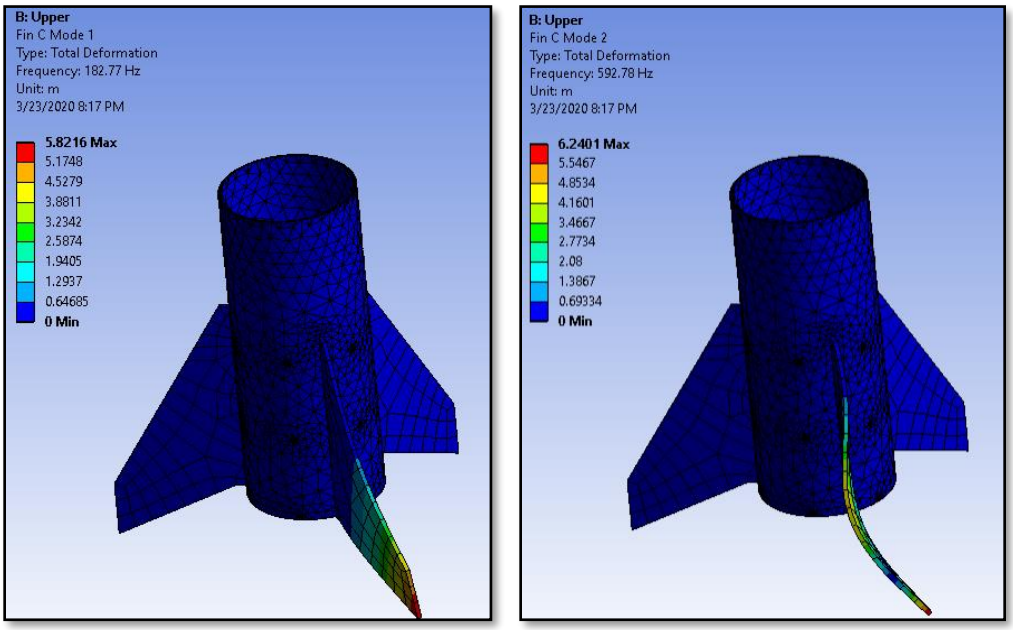

Figure 32 - Sustainer Fin Set Deformation at Mode 1 (left) and Mode 2 (right)

The eigenfrequencies are symmetrical per set, with the sustainer fins having a value of 182.8 Hz for the first mode and 592.8 Hz for the second mode. The booster fins have mode 1 at 211.0 Hz and mode 2 at 576.35 Hz. All these natural frequencies are well above and more than twice the maximum range of a sonic booms forced frequency. Therefore, the boom will not cause these structures to resonate due to the frequency. This further establishes the team's confidence in their fin designs.

Fin retention is a critical element with regards to vehicle safety and performance. Fin failure is a very common failure mode for launch vehicles, especially when flying at supersonic speeds or flying multistage rockets. Several factors must be considered when designing a fin retention system, such as structural rigidity, ease of assembly, machinability, and weight. For all launch vehicles, reducing fin flutter and ensuring the fins will be retained is critical to achieve a successful flight. Further, weight, ease of assembly and machinability of the fin retention system are important to consider due to altitude concerns, the team's resources, and time constraints, as well as quality of the final product. System weight will be considered to achieve altitude requirements. However, creating a structurally sound retention system is the main objective, even if weight or stability are not ideal. Multiple retention methods will be designed and considered to find the best design for this project. These methods and characteristics are explored in more depth below.

To determine the requirements of the fin retention system and later validate the decision, the team needed to perform strength calculations to prove that the fins will be retained successfully. This requires knowing what the rocket's acceleration is throughout the flight so the team can apply G-forces to the fins. The team must also know the drag force that the fins will experience, which requires the team to have an approximation of the coefficient of drag for the fins at different speeds. Below is the plotted flight from OpenRocket that the team used to determine their acceleration and velocity values at certain altitudes and flight times. The plot was created with a 0 second stage separation and sustainer ignition delay as it would have the highest velocity and acceleration based on previously found information.

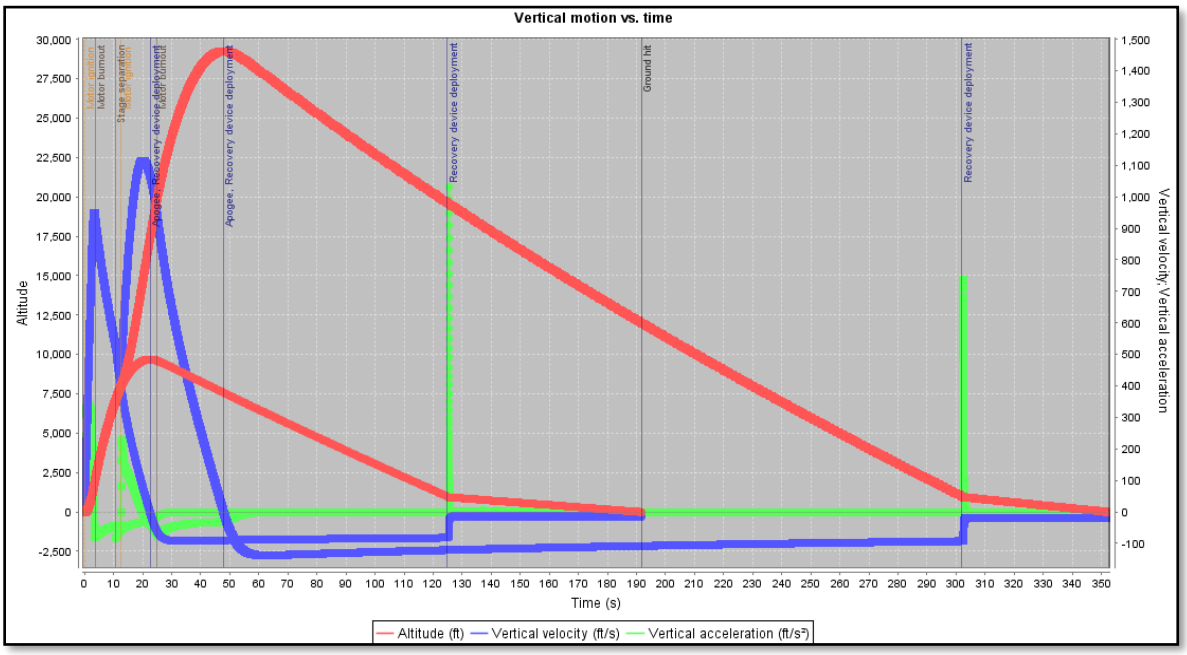

Figure 33 – OpenRocket Altitude, Velocity, and Acceleration vs Time

Using the OpenRocket simulations, the team developed an array for the acceleration of the rocket at key points in flight, including the first and second stage ignitions, the motor burnouts, the stage separation, and the recovery deployments. Using these points and a few other high velocity and acceleration areas, the team determined the maximum G-force applied to the three fins by using the equations. By dividing the acceleration of the rocket by the acceleration due to gravity, the G-Force ratio was developed. This value was multiplied by the combined estimated weight of the three fins (1.97 lb) to get the new active force in the G-Force column.

Gravitational Forces on Rocket through Flight Events

Height (ft)	Acceleration (ft/s^2)	G-Force (lbf)	Stages
0	58.84	3.60274756	1st Motor Ignition
0	240	14.69509542	-
0	312	19.10362404	-
1	312	19.10362404	-
180	312	19.10362404	-
825	310	18.98116492	-
1,240	210	12.85820849	-
2,030	55	3.367626033	1st Motor burnout/2nd ignition
9,250	255	15.61353888	Stage Separation
14,150	72	4.408528626	2nd Motor Burnout
7,000	32.1740	1.97	Lower Main Recovery Deployment
1,000	1040	63.67874681	Lower Active Chute
1,000	32.1740	1.97	Upper Main Recovery Deployment
1,000	738	45.18741841	Upper Active Chute

Table 9 - Gravitational forces on rocket through flight events

Using ANSYS Fluent, the team developed a model of the fin to approximate the coefficient of drag. This layout was built based on the Supersonic Flow Over a Wedge Cornell Experiment [6].

The FLUENT process utilizes 2D inviscid compressible flow equations. However, the team used 1D inviscid flow equations to initialize their understanding of the Navier Stokes equations. The FLUENT output can be set to find the coefficient of drag once the mesh is completed.

$$\frac{\partial e}{\partial t} + \mathbf{u} \cdot \nabla e + \frac{p}{\rho} \nabla \cdot \mathbf{u} = 0$$

$$\frac{\partial \rho}{\partial t} + \mathbf{u} \cdot \nabla \rho + \rho \nabla \cdot \mathbf{u} = 0$$

$$\frac{\partial \mathbf{u}}{\partial t} + \mathbf{u} \cdot \nabla \mathbf{u} = -\frac{\nabla p}{\rho}$$

Equation 12 - Navier Stokes: Conservation of Energy, Mass, and Momentum

With this, multiple iterations were run with higher and higher fidelity until grid independence was established as shown in Table 10. The mesh quality was enhanced by adding body sizing, edge sizing, and inflation parameters to isolate more crucial dimensions about the fin.

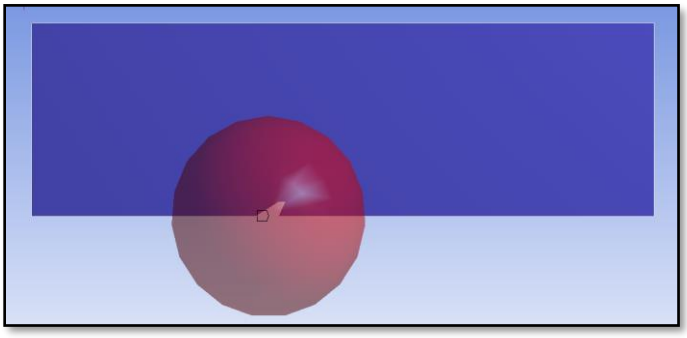

Figure 34 - Body Sizing used to define area for more resource application.

The Body Sizing application allows the user to add a sphere of influence to the meshing. This results in the ability to control a general location's mesh quality. In the case above, the mesh around the fin was improved.

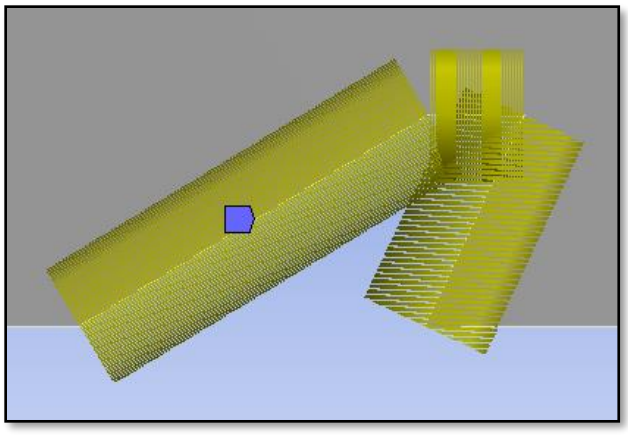

Figure 35 - Edge Sizing used to refine edges of meshed component

The Edge Sizing application allows the user to divide the elements into a certain amount per edge space. By forcing the model to create 750 divisions, the mesh was highly refined for the edges of the fins.

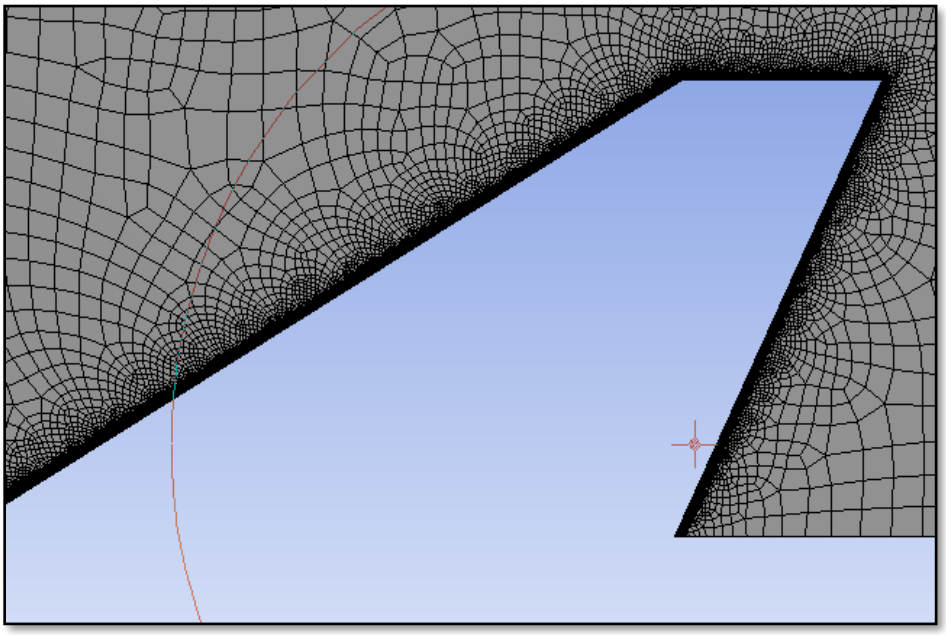

Figure 36 - Impact of Inflation parameters on meshing areas desiring higher quality resource devotion

The Inflation application allows the user to self-define the growth rate of elements for a determined number of layers. In this case, for 20 layers, the growth rate was limited to only 120%, ensuring the solver did not immediately increase the size of the elements to the limit at the default rate.

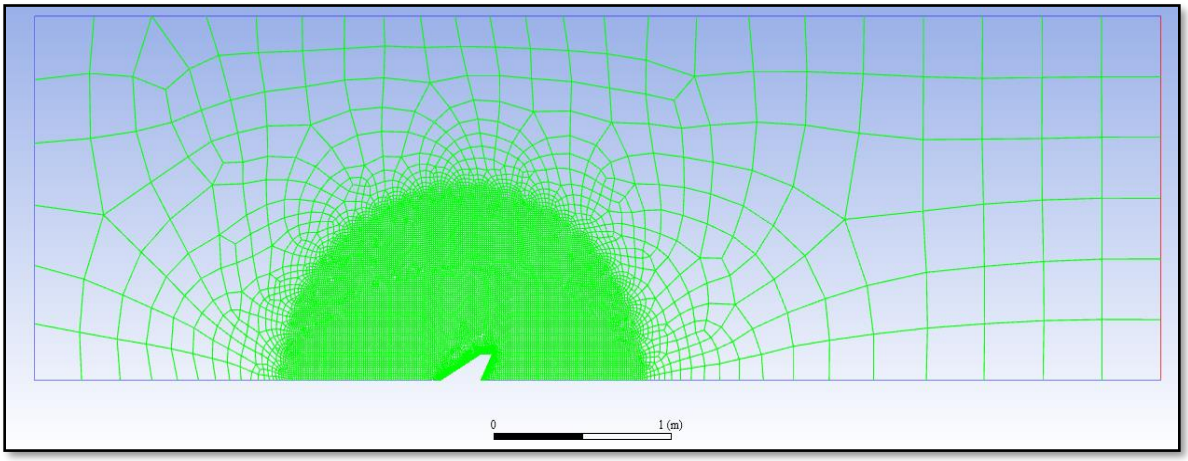

Figure 37 - Resulting Mesh Quality to compare low importance areas to high importance areas.

By looking at the mesh quality around the fin and comparing it to the inlet and outlet, there is a vast size difference. This allows more solving resources to be focused on the fin and not wasted on the simple fluid space without any complex shapes. This minimizes the time used to solve the overall file. The final, highlighted iteration was the one chosen to run for the simulations.

Meshing Grid Independence Results

Iteration	Forces	Fidelity		
	Coefficient of Drag (Mach 1.2)	Body Sizing	Edge Sizing	Inflation
1	0.078362	.25m, 5e-2	150 divisions	5 layers, 1.2 growth, 5e-2
2	0.086794605	0.5m rad, 1e-2m size	250 divisions	10 layers, 1.2 growth rate, 1e-2m max thick
3	0.074151422	1m, 7.5e-3m size	500 divisions	15 layers, 1.2 growth, 5e-3 max thick
4	0.07082005	1m, 7.5e-3m size	750 divisions	20 layers, 1.2 growth, 2.5e-3 max thick

Table 10 - Meshing Grid Independence Results

Using the highlighted meshing layout above, the team then analyzed the fin's coefficient of drag at different speeds at the available velocities that were occurring at the same time as the acceleration data points. These values were used in the ANSYS Fluent Simulation with an individual fin from the upper stage of the vehicle. By establishing the inlet velocity to the desired value, the team was able to have their coefficient of drag converge to a constant value for each wind speed.

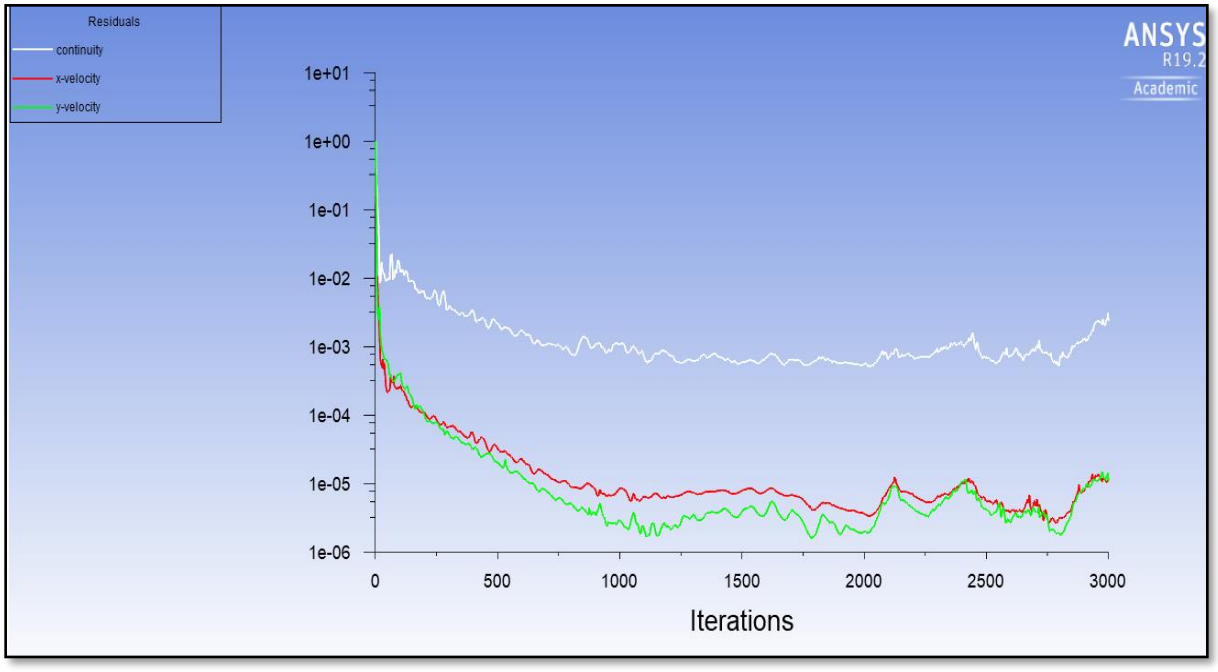

Figure 38 - Iteration Readout showing resulting Coefficients of Drag and Continuity

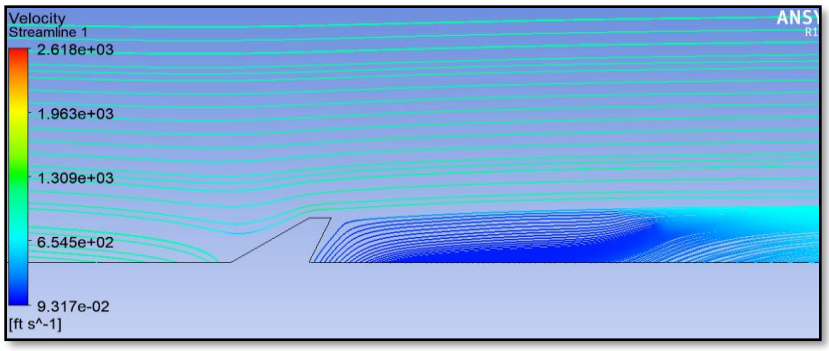

Figure 39 - Velocity Streamlines over the rocket fin

The swept fin was used for the simulation as the lower stage's coefficient of drag would be comparable. By using the drag equation below, the team determined the amount of resistive force acting against fins.

$$D = \frac{C_d \rho V^2 A}{2}$$

Equation 13 - Drag Equation

Drag is the air resistance or friction that a body in motion induces. It is equal to half the product of the coefficient of drag (determined in the simulation), the density of the medium (air), the velocity of the body, and the cross-sectional area of the body.

Drag Force on Rocket Fin through Flight Events

Height (ft)	Air Density (slug/ft^3)	Velocity (ft/s)	Coefficient of Drag	Drag Force (lbf)
0	0.0020809	0	0	0
0	0.0020809	1	0.066166987	0.00001774869979
0	0.0020809	3	0.071622733	0.0001729093918
1	0.0020808	15	0.069460426	0.004192028961
180	0.002069056	312	0.065772854	1.70766271
825	0.002026615	750	0.072052373	10.58805144
1,240	0.001999308	850	0.069344466	12.91229198
2,030	0.002243426	950	0.072483568	17.65456315
9,250	0.00151766667	1040	0.071530611	15.1359256
14,150	0.0013843625	875	0.067643184	9.241957116
7,000	0.0015566667	100	x	0
1,000	0.0018901	100	x	0
1,000	0.0018901	100	x	0
1,000	0.0018901	100	x	0

Table 11 - Drag force on rocket fin through flight events

The bottom four rows were not completed as the rocket would be in downward descent under drogue and the cross-sectional area of the fin would be inconsistent. By adding the total G-Force and Drag force together, the team found the maximum amount of force that the fin retention system would have to endure.

Total Force on Rocket Fins through Flight Events

Height (ft)	Total Force Acting (lbf)
0	3.60274756
0	14.69511317
0	19.10379695
1	19.10781607
180	20.81128675
825	29.56921636
1,240	25.77050047
2,030	21.02218919
9,250	30.74946449
14,150	13.65048574
7,000	1.97
1,000	**63.67874681**
1,000	1.97
1,000	45.18741841

Table 12 - Total force on rocket fins through flight events

Based on the results, the shock force experienced by the ejecting parachute would result in the highest amount of stress on the fin retention system. Had the fins been thicker or lighter, this may not have been the case. The team used the determined force to simulate the maximum amount of stress the fins would endure in an ANSYS Static Structural test for some of the considered designs. The described example is for the L-Bracket retention system, since this is the design that the team chose in the end.

By applying the maximum resistive forces onto the fins (an acceleration of 255 ft/s^2 and a drag force of 15.61 lbf) the team was able to set up a workbench that could determine the maximum stress, strain, and deformation for each assessed model. The team developed grid independence by conducting higher fidelity simulations (going from an element target size of 0.01 meters to 0.001 meters) and gained the same exact results. The forces were applied to the fins' sides that are cross-directional to the flight path. The assembly was fixed in position of the 12 screw holes for the fin retention rings.

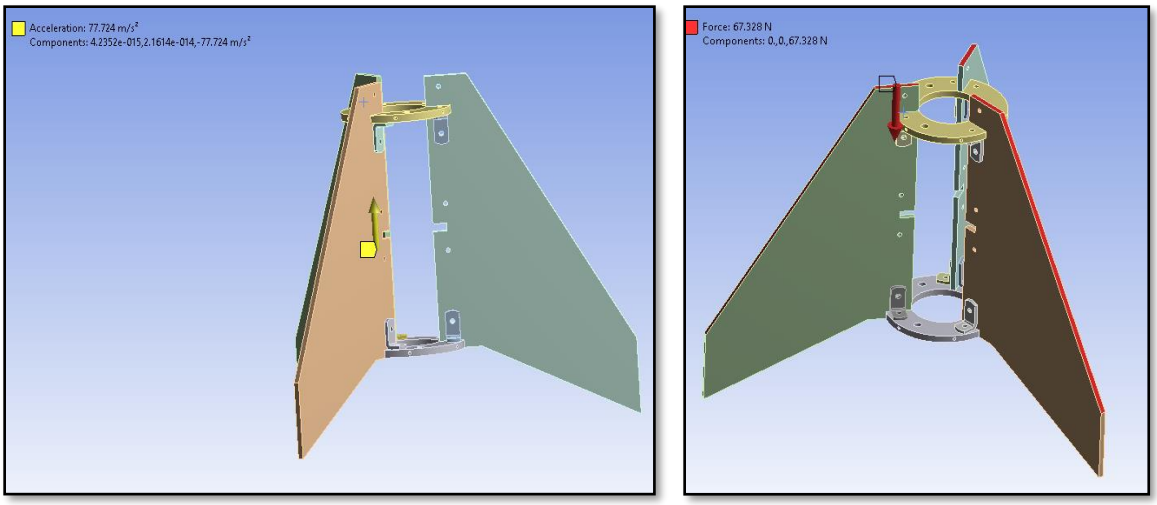

Figure 40 - Acceleration (left) and Drag Force (right) being applied to the fin retention system

Note that the team removed some of the L-brackets due to their sense of security and its strength for the final design. This reduced the complexity of the design while maintaining sufficient strength.

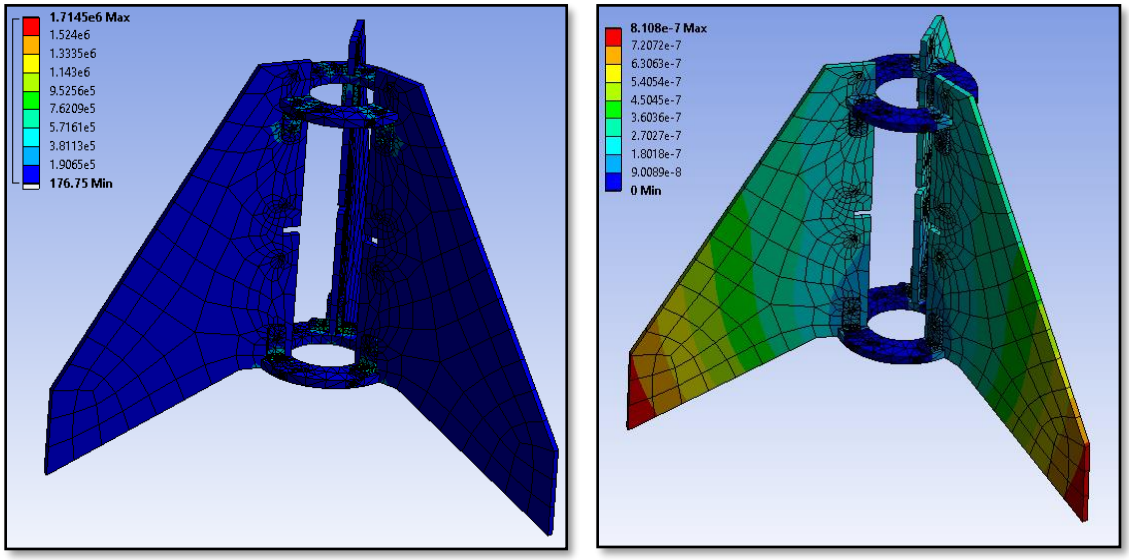

Figure 41 - Fin Retention Stress (left) and Deformation (right)

Using the stress result photos, the team can determine that the highest points of stress are found in the L-Brackets and the screw holes in the aluminum rings. The results of this simulation are detailed in the Internal Hardware Section.

The team then needed to simulate the shock force of the main parachute deployment. Due to the ejection method of the parachute, the team determined that the immediate deacceleration of the rocket would be in the opposite direction of gravity.

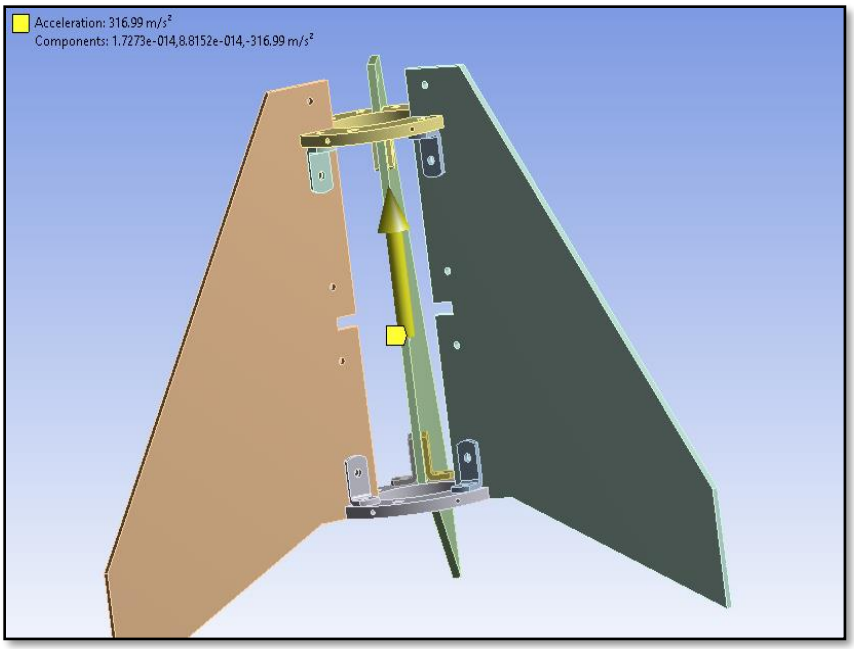

Figure 42 - Deceleration due to Shock Force from parachute

The analysis showed that the system would experience a maximum stress of 3.6669e6 Pa and a maximum deformation of 1.553e-6 m. Due to the layout of the design and distributed forces, the fins were retained better than expected through the shock force of the parachute.

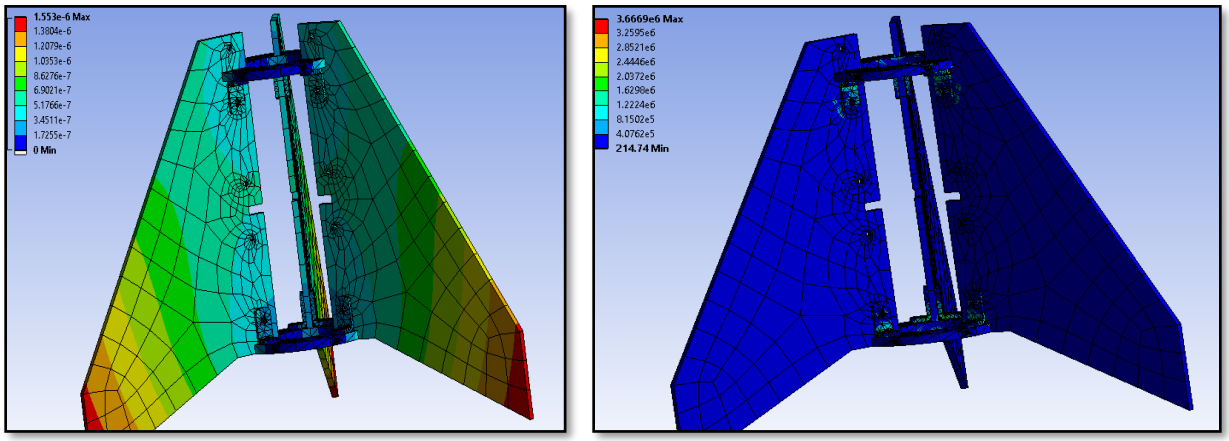

Figure 43 - Fin Retention Stress (left) and Deformation (right)

3.3.2. Printed Canister

The team performed these analyses for other designs that were considered for flight to determine their most optimal design.

The team is very familiar with using a 3D printed canister. The design is a proven concept after flying successfully on at least four other Akronauts' rockets and is adaptable to a multitude of designs.

Figure 44 - Akronauts' previous 3D printed fin retention canisters

The team developed a computer aided design of an assembly and simulated expected forces that the cannisters would face during flight (acceleration of 255 ft/s^2 and drag force of 15.61 lbf). With a maximum equivalent stress of 232 psi, a maximum equivalent strain of 1.34e-3 ft/ft, and a maximum deformation of 1.23e4 ft, the fin can had promising integrity. ABS has a tensile strength ranging from 4,000-8,000 psi and a yield strength of 2,683-7,397 psi.

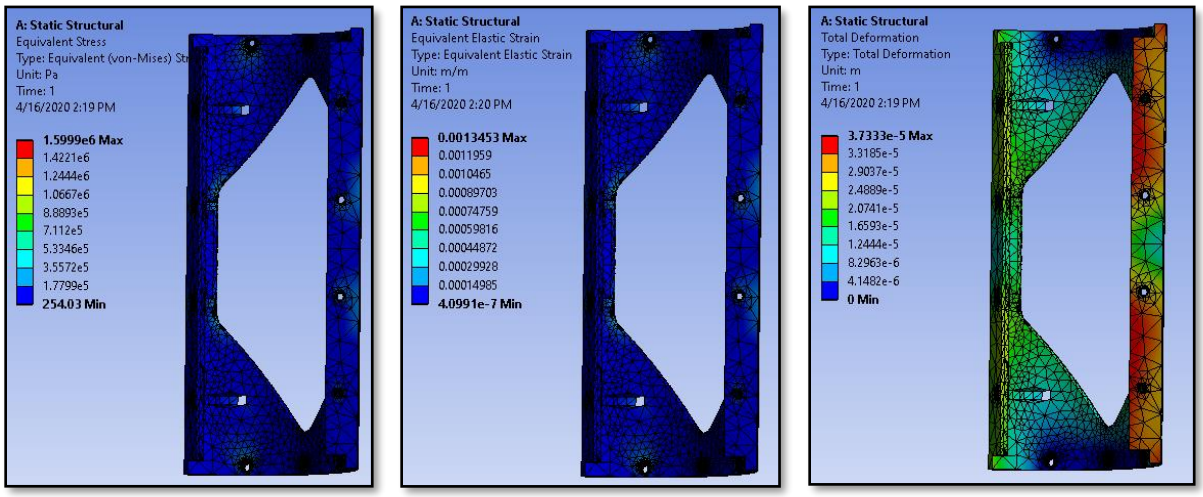

Figure 45 - ABS Fin Can Equivalent Stress (left), Equivalent Strain (middle), and Total Deformation (right)

This leaves the fin can without any major structural concerns at first glance. Since the system is fairly light, the shock force from the parachute did not exceed the flight forces. This would have been different had the team included the fins or emulated their mass with a mass point. Though only approximately 2 lb for all three fins, this could have compromised the design. In hindsight, the metal hardware retention system had a safety factor of 40.9, the plastic design would have been much lower. However, at the time of the decision, the team still did not feel safe with using the plastic retention system for fear of forces being higher than expected or additional unaccounted factors [8].

Although 3D printed canisters have been successful in the past, there is one other concern with using a similar design: the assembly of the system. While the fin canister can secure the fins to it, getting the assembled retention system into the upper stage airframe is a difficult task due to the stage separation mechanism in place. The current stage separation mechanism includes a coupler that must reach 6” into the sustainer stage. The fin attachment must reach beyond this point without interference. The stage separation system selection will be discussed in more detail in a later section. As can be seen below, the fins will need to secure to the fin canister without obstructing the movement of the coupler during stage separation.

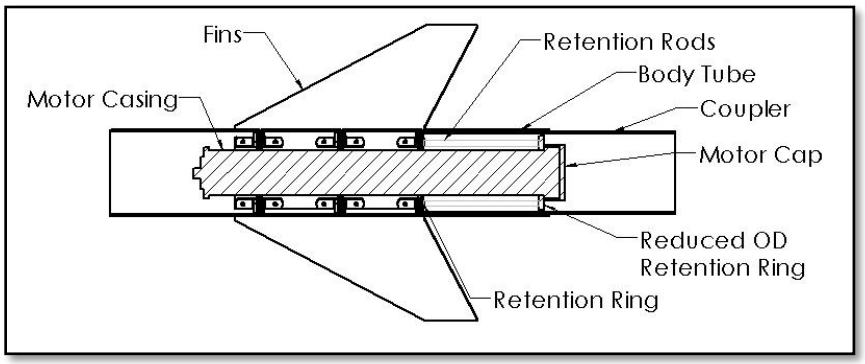

Figure 46 – Potential Stage Separation Layout

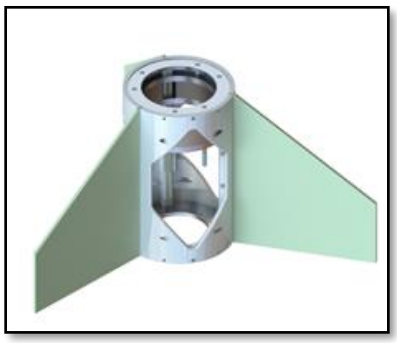

Figure 47 - 3D Printed Fin Canister

3.3.3 External Fin Retainer

Due to the strength and assembly concerns, the 3D printed canister was not selected for the team’s two-stage fin retention system.

The senior design team has attended several rocketry competitions and has made note of the recurring use of external fin retention systems. The use of these devices ensures easy assembly, as the internals of the vehicle can be set up without any concern for the fins that will be retained solely outside of the rocket. While this setup is very easy, it is inefficient with respect to drag. External fin retention systems increase the amount of surface area exposed in the cross-section of the rocket. The maximum additional drag applied is calculated below. The maximum drag occurs at maximum velocity, which is during the sustainer stage flight. An example flange geometry would extend approximately 0.75” from the airframe and increase the width by 0.5625”. The equations below outline the added drag force to the rocket. Drag force, *D* is the force applied on one retainer assembly, so *D* is multiplied by three to account for the total additional drag.

$$D = \frac{C_d \rho V^2 A}{2}$$

$$\rho = 0.0018\ Slugs/ft\text{^}3$$

$$A = \frac{0.5625 * 0.75}{144} = 0.00293\ ft\text{^}2$$

$$V = 1{,}191\ ft/s$$

$$c_D = 0.625$$

$$D = 2.33\ lbf$$

$$D_{Total} = 7.00\ lbf$$

Although the additional 7 lbf of drag force applied is relatively low, an external fin retention system could cause additional flight stability issues if manufactured poorly. Additionally, an internal retention system would be optimal to reduce drag. For these reasons, an external fin retention system was not selected.

The team has investigated other methods of internal retention and have forgone using the fin canister. Instead, they considered slotting the rings used to center the motor and then incorporating L-brackets to secure the fins to the rings. This method was explored further as it offered the potential of a high safety factor for retention strength. One issue that the team must consider is the assembly of the device. It is very simple to assemble externally. However, the group must have the ability to insert screws through the airframe to secure the fins to the L-brackets.

The team has had assembly issues with a fin attachment system involving L-brackets in the past, although not entirely due to the L-brackets. Concerns with the parts fitting snug are of no concern as a CNC lathe could manufacture any of the ring options. To make the assembly work for the upper stage, with an area that must be pressure-sealed below the fins, the team will have to cut hole slots into the rocket airframe and insert the fins to attach them to the bracket system. There must also be a hole to insert the final screw for each fin hole to clamp the aluminum fin between the two L-brackets. An example SolidWorks model the team created is shown below.

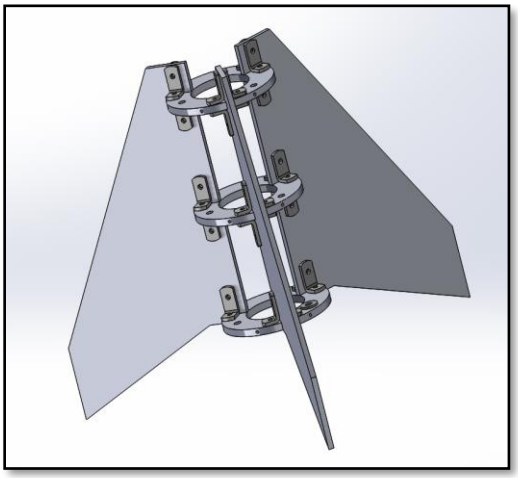

Figure 48 - Internal Hardware Fin Retention System

Based on the structural opportunities and ease of assembly, the team chose to manufacture this option for consideration.

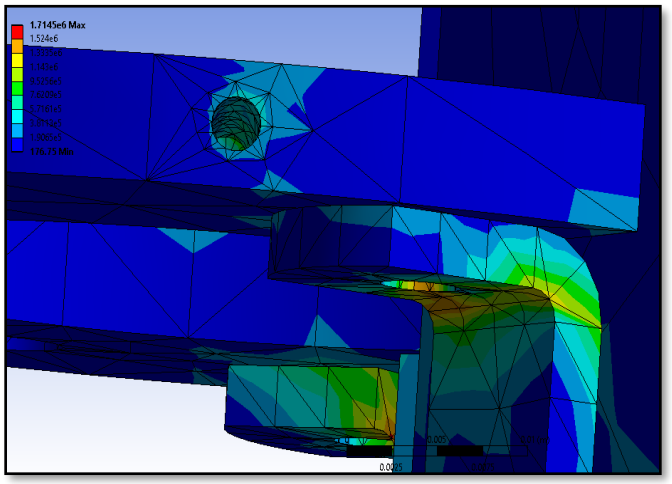

Figure 49 - Close up of Fin Retention system's weakest points

As shown in the Design Factors section, the team found that the worst case forces on the system. The system will experience a maximum stress of 3.6669e6 Pa and a maximum deformation of 1.553e-6 m at its weakest points. The stainless-steel brackets have a theoretical strength of 5.05e8 Pa, giving the team a safety factor of over 136. The aluminum rings have a strength of approximately 1.50e8 Pa, giving them a safety factor of 40.9. This proves the design is worthy of final consideration.

3.3.5. Tapered Inserts

The team noted that their primary reasoning with designing a new fin retention system is ease of assembly for the upper stage system. The ideal situation is being able to assemble the rocket's airframe and then attach the fins afterward. Considering this, a tapered insert was proposed. By adding holes into the centering rings and decreasing their area towards the bottom face, the team can add tapered slots to the fins so that they may have an interference fit with the rings. This would allow for the fins to be inserted into slots in the airframe post-assembly. After discussing this idea, the concern for the aluminum wearing down and reducing the interference was raised. This was alleviated after discussing the hardness of components and developing a confidence that they would not wear down, as the team has had ample experience with Aluminum 6061 and it not showing any signs of deformation.

While easy assembly was solved, the team still faced the requirement that the fins must be retained and remain stationary during the flight mission. The design proposed may keep the fins rigid, however it does not guarantee that the part is locked into place. The force due to drag will keep the fins pressed into the slots, yet this force will not actively be holding the fins in place through the recovery phase. Thus, the team proposed adding in a screw hole at the base of the fin to try to secure it. A prototype was made to test this model and was still easy to assemble. Still uncertain of it being allowed to use in competition, the team reached out the judges of the IREC competition. After discussion with the IREC judge, it was determined this mode of fin retention would not be eligible for flight and the fins would need to be fastened or epoxied in addition to the proposed retention system. Given the fins will need to be removed for sustainer

motor ignitor assembly, the fins cannot be epoxied. A model of the proposed retention system is shown below.

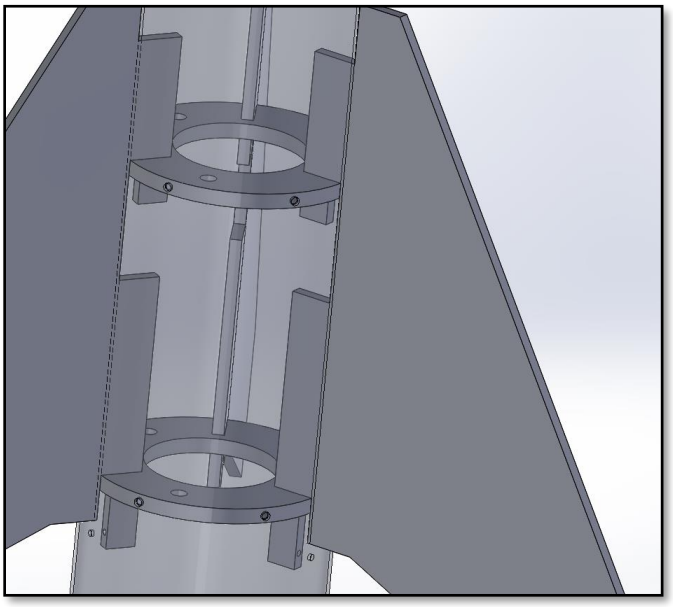

Figure 50 - Tapered Fin Design with Single Screw Retention

3.3.6. Tangential Screw Alignment

The tangential screw ring design is another structurally sound option the team considered, as the aluminum flanges are rigid and would allow for a fastener to clamp the fin. Assembly of the rings into the airframe would be like standard bulkheads and centering rings are fastened into the airframe. Assembly of the fins to the retaining ring would require through holes concentric to the tangent holes to be drilled into the airframe to fasten the fin. Manufacturing the rings would be challenging since all tangential holes must be have the correct tolerance to ensure the fins are properly aligned and fastened. A CNC mill could be utilized to enhance consistency between all rings.

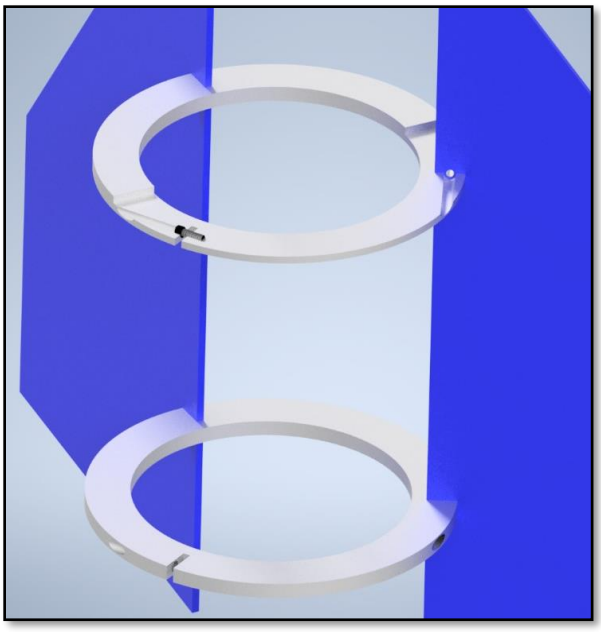

Figure 51 - Cutout of Screw Insertion for Fin Retention

The team considered a second version of this design as shown below. The fins would be aligned and clamped using the protruding flanges and would fasten similarly to the tangential screw alignment shown above. Assembly of this layout would be very similar to the L-bracket design. Since the clamp force applied to the fin will be similar for both this design and the L-bracket design, and given the L-Bracket design has more contact area with the fin, the L-bracket design will apply less stress to the fin.

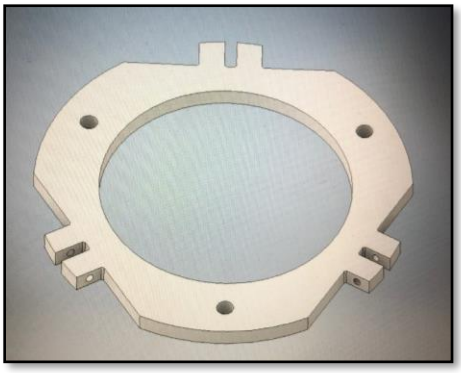

Figure 52 - Fin Retention Ring for Tangential Screw Concept

3.3.7. Final Design

The main fear with this design is like the tapered fin retention design. There is very little surface area to hold the fins in place. Fin flutter has the potential to occur due to this and the team does not feel that this is the safest option.

After considering the strength and assembly requirements, the team found that the L-Bracket design would be the most favorable. Being comprised of steel and aluminum, the team had no reservations for the structural integrity of the design. Its weakest points are the aluminum rings, having a strength of approximately 1.50e8 Pa. The resulting strength safety

factor when the parachute deploys is approximately 40.9 when the maximum stress is 3.6669e6 Pa. Regarding structural integrity, this design is sufficient.

Regarding assembly, using a prototype model, the team found that they could put together the fin retention system externally. By drilling small holes into the airframe to insert and then fasten the screws with a magnetic screwdriver, the components could be fully retained. The model for the final fin retention system design is shown below.

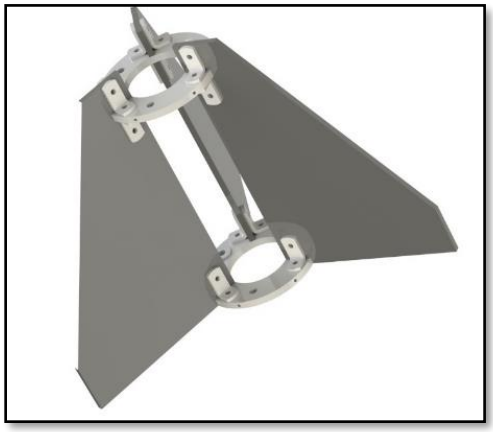

Figure 53 - Final Design for Fin Retention

3.4. Bulkheads & Centering Rings

The team will use 0.25” plates of 6061 Aluminum for all bulkheads and centering rings in the rocket. This has been a standard practice for the rocket design team and has proved capable of withstanding all flight forces on previous rockets. The senior design team will conduct shear tests and compression tests to verify the strength of the bulkheads and centering rings can handle expected loads. All the bulkheads and centering rings are manufactured by the senior design team in the University of Akron’s machine shop. The team is familiar with operating the lathe and end mill, the two primary machines necessary to manufacture these components. The CNC was used to manufacture the fin retention centering rings, though, as the fin retention design requires a tight tolerance to be assembled properly. The sections below will briefly describe the bulkheads and centering rings and the components that attach to them. The team attempted to keep the designs standard throughout the rocket layout to avoid complexity and for ease of assembly. The components that attach to the bulkheads are all standard components used on the rocket team and were not part of the design process that the team focused on.

The bulkheads, which are fastened to the body tube radially in six places with 6-32 screws, separate the vehicle into separate areas of the rocket, commonly referred to as bays. In some cases, a U-bolt is fastened to one or both faces of the bulkheads, which attach the shock cords, allowing the rocket to remain tethered to a parachute after separation occurs. PVC ejection charge cups and terminal blocks can also be attached for wiring the black powder separation charges. A subscale bulkhead is pictured below showing all hole locations for common components. The assembled bulkhead is shown to the right of it.

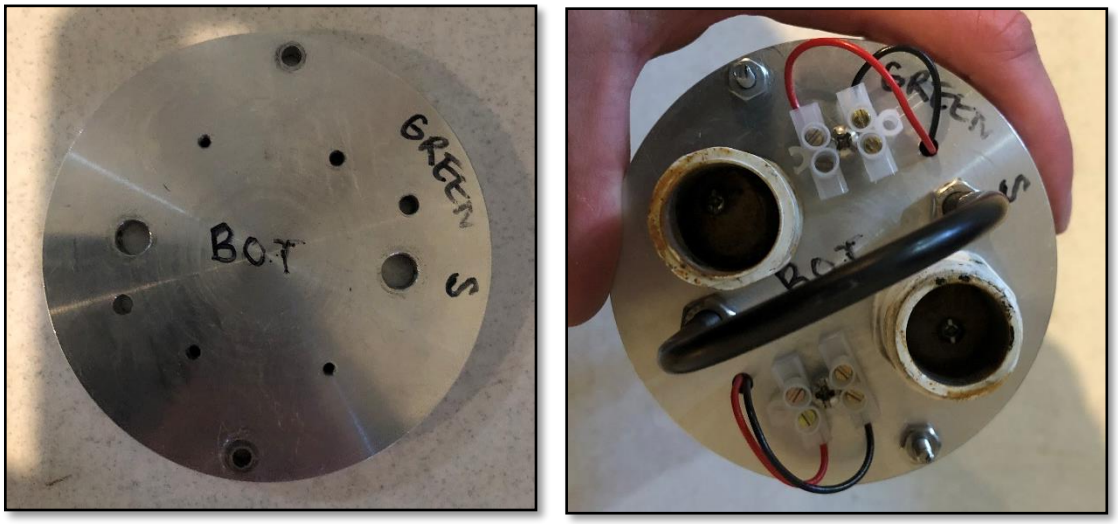

Figure 54 - Example subscale bulkhead (left) with assembled components (right)

The centering rings are used to keep the motor centered within the rocket. However, in this launch vehicle, they will also be used to retain the fins for the booster and sustainer stages. An example subscale centering ring can be seen below followed by an assembled centering ring set with hardware to show how the fins will be attached.

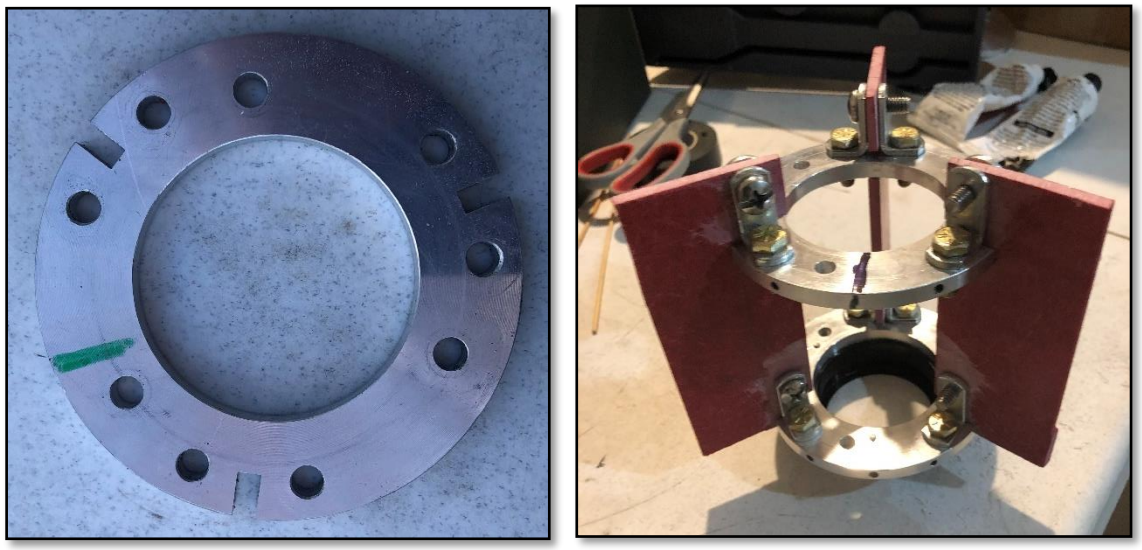

Figure 55 - Example subscale centering ring (left) with assembled components (right)

3.5.

Motor retention is a critical design consideration to avoid losing the motor in flight or recovery as well as absorbing the thrust at takeoff. The addition of the second stage with an additional motor adds complexity to the retention system, specifically for the second stage. The team analyzed several retention options to find the simplest assembly option that would provide sufficient strength while also investigating two potential concerns for the full-scale rocket retention: thread engagement and the Krushnic Effect.

The team has used Aeropack retainer caps at the aft end of the rocket in the past to retain the motor and absorb the thrust. They hardware fasten to a centering ring at the base of the rocket and provide sufficient strength to survive the maximum thrust and hold onto the motor through the shock forces of parachute deployment. A photo is shown below of the retention cap.

3.5.1. Retention Options

Figure 56 - Aeropack aluminum retention cap

Due to the complexity of the 2nd stage area and separation space available for deployment, the team would have major difficulty placing a centering ring around the aft end of the 2nd stage motor for motor retention and thrust.

With the coupler reaching 6” into the 2nd stage, the centering ring could not be fixed to the airframe on the diameter, since it would need to allow the coupler to slide past. Another option considered was using axial threaded rods to connect the motor retention centering ring to the lower fin centering ring that can be fixed into the airframe. This would be complex to manufacture, but it is a potential option to still include an Aeropack retainer on the sustainer. A sketch of this option is shown below.

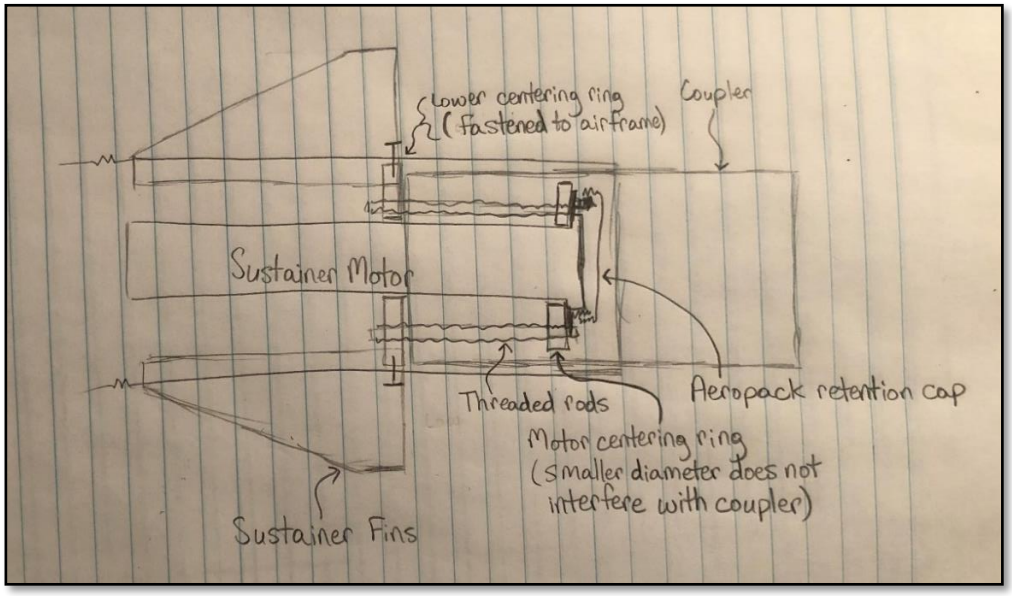

Figure 57 - Concept sketch for Aeropack motor retention on sustainer stage

Another COTS option is forward retention of the motor through the threaded forward closure. Typically used for minimum diameter rocket motor retainers, a similar design could be

implemented with a thrust plate the rocket team commonly uses [7]. A simplified assembly step plan is shown below including the motor.

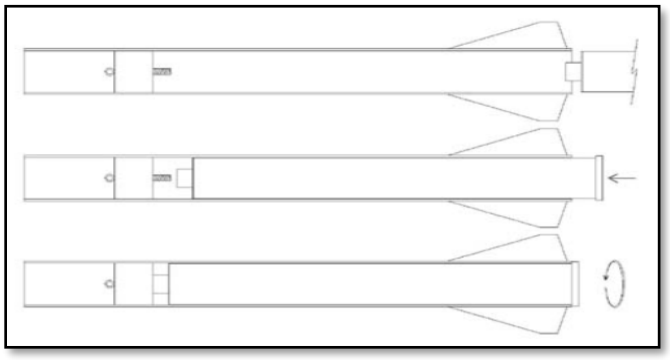

Figure 58 - Forward closure motor retention assembly step process

The team consulted both team mentors, Chris and Steve, who verified this mounting method and its thrust bearing capabilities. Other rocket hobbyists with experience launching two-stage rockets have confirmed this method of motor retention. Richard, a rocket hobbyist in the Mojave, California area, flew a two-stage rocket at FAR (Friends of Amateur Rocketry) launch site. He utilizes forward retention with an eyebolt in the forward closure and says it is strong enough to support the thrust of the motor as well. Based on this information, the team will utilize forward retention with the eyebolt for the sustainer motor and an Aeropack retainer for the booster motor.

3.5.2. Thread Engagement

Since the team has not utilized the forward closure mounting in the past, tensile strength and minimum thread engagement calculations were conducted to verify the eye bolt is strong enough to retain the motor when the parachutes deploy to produce the shock force. The shock force for the sustainer stage was not calculated by the senior design team, but by rocket design team members and found to be around 1,000 lbf. This can vary based on weight changes in certain areas, but it will be used as a baseline for calculations.

The forward closure for the 98mm full-scale motor utilizes a 3/8”-16 thread. 3/8” steel eye bolts from McMaster-Carr have a vertical capacity of around 1,300 lbf, but the rocket design team has shown through previous testing of similar components that the actual maximum capacity could be at least twice this loading without any visible effects. This would indicate a manufacturer built-in factor of safety. Still, the vertical capacity has a 1.3 factor of safety. The team will proceed with the calculations for verification.

Assuming the 3/8” eye bolt is equivalent to a McMaster-Carr low strength 3/8” threaded rod for a worst-case scenario, it would have a tensile strength around 50,000 psi. The tensile stress area for a 3/8”-16 thread was obtained from Table 8-2 in Shigley’s Mechanical Engineering Design textbook [4] shown below indicating an area of 0.0775 in^2.

Diameters and Areas for Unified Screw Threads

Table 8–2

Size Designation	Nominal Major Diameter in	Coarse Series—UNC Threads per Inch N	Coarse Series—UNC Tensile-Stress Area A_t, in²	Coarse Series—UNC Minor-Diameter Area A_r, in²	Fine Series—UNF Threads per Inch N	Fine Series—UNF Tensile-Stress Area A_t, in²	Fine Series—UNF Minor-Diameter Area A_r, in²
0	0.0600				80	0.001 80	0.001 51
1	0.0730	64	0.002 63	0.002 18	72	0.002 78	0.002 37
2	0.0860	56	0.003 70	0.003 10	64	0.003 94	0.003 39
3	0.0990	48	0.004 87	0.004 06	56	0.005 23	0.004 51
4	0.1120	40	0.006 04	0.004 96	48	0.006 61	0.005 66
5	0.1250	40	0.007 96	0.006 72	44	0.008 80	0.007 16
6	0.1380	32	0.009 09	0.007 45	40	0.010 15	0.008 74
8	0.1640	32	0.014 0	0.011 96	36	0.014 74	0.012 85
10	0.1900	24	0.017 5	0.014 50	32	0.020 0	0.017 5
12	0.2160	24	0.024 2	0.020 6	28	0.025 8	0.022 6
1/4	0.2500	20	0.031 8	0.026 9	28	0.036 4	0.032 6
5/16	0.3125	18	0.052 4	0.045 4	24	0.058 0	0.052 4
3/8	0.3750	16	0.077 5	0.067 8	24	0.087 8	0.080 9
7/16	0.4375	14	0.106 3	0.093 3	20	0.118 7	0.109 0
1/2	0.5000	13	0.141 9	0.125 7	20	0.159 9	0.148 6
9/16	0.5625	12	0.182	0.162	18	0.203	0.189
5/8	0.6250	11	0.226	0.202	18	0.256	0.240
3/4	0.7500	10	0.334	0.302	16	0.373	0.351
7/8	0.8750	9	0.462	0.419	14	0.509	0.480
1	1.0000	8	0.606	0.551	12	0.663	0.625
1 1/4	1.2500	7	0.969	0.890	12	1.073	1.024
1 1/2	1.5000	6	1.405	1.294	12	1.581	1.521

Figure 59 – Diameters and Areas for Unified Screw Threads from Shigley's Mechanical Engineering Design textbook

The resulting maximum tensile force is 3,875 lbf which yields a 3.875 factor of safety. The reason the shock force was used in this case instead of the motor thrust is because the six 6-32 screws in the outside diameter of the airframe assist with absorbing the thrust rather than the eye bolt. This is only the case if the forward closure is interfacing with the thrust plate bulkhead, which is shown in the section above and will be detailed on the subscale rocket model. Shear testing will be conducted to verify the six 6-32 screws will sufficiently absorb the maximum thrust of both motors independently.

In addition to the tensile strength calculation, a minimum thread engagement calculation was conducted to verify that the rod would fail before the thread strips. ISO (International Organization for Standardization) uses the following equation for minimum thread engagement of a screw in a tapped hole for metric threads. It will be used as a baseline, although the 3/8"-16 thread in the motor has English units.

$$L_e = \frac{2A_t}{0.5\pi(D - 0.64952p)}$$

Equation 14 - ISO minimum screw thread engagement

Inputting the tensile area of 0.0775 in^2, the major diameter of 0.3750", and the pitch of 0.04167 inches which is the inverse of threads per inch, the minimum thread engagement length is 0.2836". All values for the calculation above were obtained from Table 8-2 from the mechanical engineering design textbook referenced above. It should be noted that this is only the minimum thread engagement to ensure that the rod will fail before the threads strip. The calculation method was also a reference for metric standards and does not factor in the material strength of either component, the screw or the tapped hole. However, the following ISO equation accounts for a difference in material strengths between the screw and hole. The variable *J* is the ratio of tensile strengths between the screw and hole.

$$L_{e2} = JL_e$$

Equation 15 - ISO minimum thread engagement for different materials

The eye bolt is steel with an assumed tensile strength of about 50,000 psi. The forward closure of the motor is aluminum, but the alloy is unknown. For calculations, the tensile strength for aluminum 6061 of 42,000 psi will be used. This results in a minimum thread engagement of 0.3376” for the forward closure [13].

Finally, the team reviewed the full-scale motor forward closure to verify the thread engagement was feasible. The drawing below from Cesaroni Technology Inc. details a 1” tapped hole for the forward closure which results in a factor of safety of about 3 for thread engagement if the eye bolt is fully engaged [24].

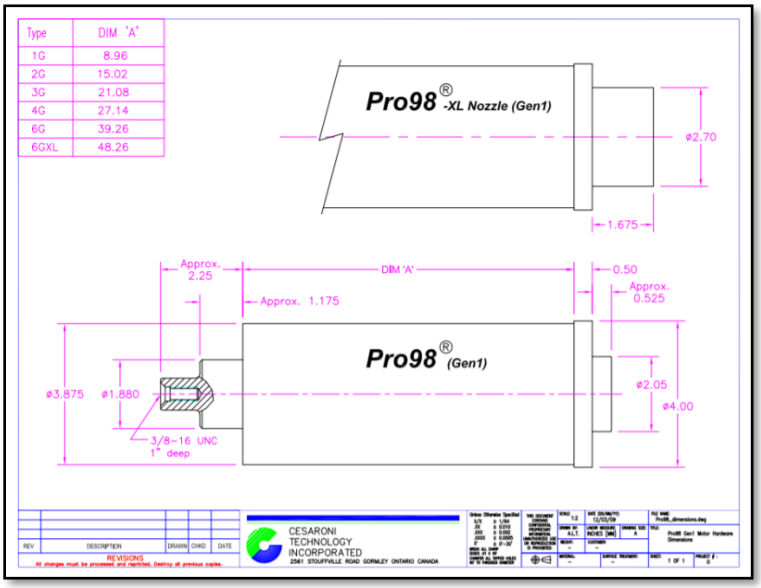

Figure 60 - CTI 98mm motor drawing

3.5.3. Krushnic Effect

The Krushnic Effect occurs when an engine nozzle has its exit flow within the body tube. Motors are made with the intent to ignite and have the exhaust flow immediately into an open area where they can expand at atmospheric pressure. The rapid expansion and exhaust cause vortices to build up around the outside of the motor, as shown below [18].

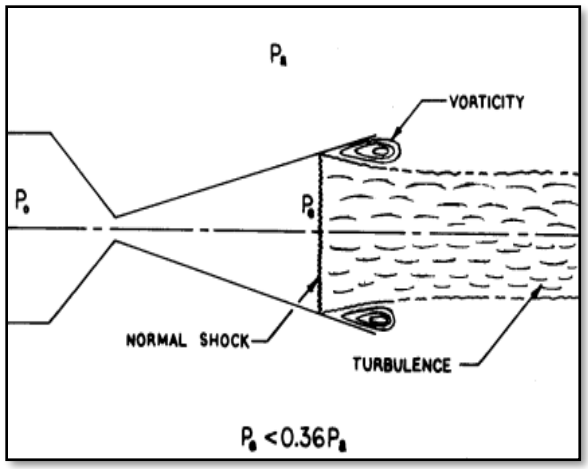

Figure 61 – Normal motor exhaust flow

However, when this flow is released within the body tube, it cannot fully expand. Shown in the figure below, the trapped exhaust results in an increase in pressure at the exit of the nozzle. This results in a loss of thrust from the motor since the pressure difference is lower than if the exhaust was expanding to atmospheric pressure.

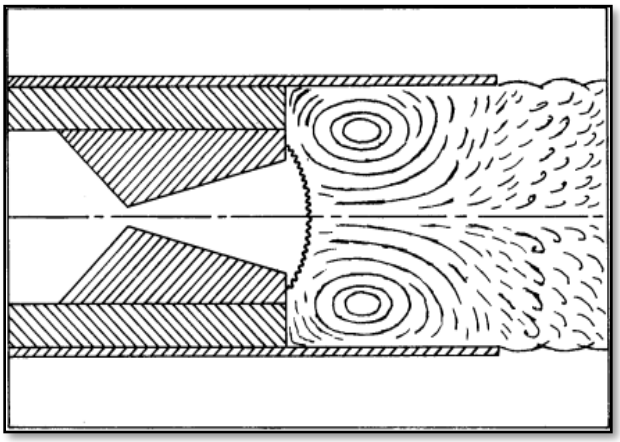

Figure 62 – Motor exhaust flow within the airframe

A potential issue with mounting the 2nd stage motor is the motor being placed too far up into the body tube. This is normally done to provide better stability for the rocket or to aid in securing or retaining the motor. The team must account for the Krushnic effect as they design the layout of their vehicle to ensure that it will not hinder their motor's performance. Similar articles indicate that the Krushnic Effect will not occur if the motor recession is less than half of a body caliber within the body tube, or 3" for the team's 6" airframe. The current motor recession for both the 1st and 2nd stage motors is about 1", which should be sufficient to avoid a loss of thrust [3 & 11].

The rail buttons or launch lugs are devices that are used to keep the rocket attached to the launch rail during takeoff. The placement of these components primarily affects the rail exit velocity, which can determine the stability of the rocket off the launch rail. It is also important to keep them secured to the rocket mechanically throughout flight, so they do not detach from the rocket while it is on the launch rail and cause an unstable flight. These two characteristics, the placement and attachment, are analyzed in detail in the following sections. The commercial rail buttons the team uses commonly are shown below for clarity, but the rail button design or selection is not the focus of the team's research. The rail buttons typically slide onto 1515 aluminum rail which is the launch rail available at competition and they can be mounted with an 8-32 or 10-24 screw.

Figure 63 - Commercial rail button mounted to airframe

3.6.1. Rail Button Placement

The team has developed a general understanding of the rail button placement through previous rocket constructions. The lower button must be placed as close to the bottom of the rocket as possible to keep it attached to the rail as long as possible and increase the rail exit velocity. The upper button's ideal placement is less clear, although the team has placed them around or just above the Center of Pressure in the past. The CP is the point at which all aerodynamic forces act on the rocket and is identified in the photo above with the brown circle.

The team spoke with team mentors and IREC judges about the ideal placement of the rail buttons for two-stage rockets. Chris Pearson and Steve Eves both recommended placing them on the second stage of the rocket since that is what they have seen on two-stage rocket kits. The team did not believe this was best since rail exit velocity would likely be hindered. The reason for kit placement on the second stage could be due to varying diameter between the booster and sustainer sections of the kit rockets. If the booster section has a smaller diameter airframe, the rail button would need to be placed on the sustainer stage.

The team tried to study the effects of the rail button placement using their simulation software, but none of them showed the exit rail velocity being impacted. RASAero II does not even offer an option to change their placement. However, after some critical thinking, the team theorized that the ideal position for the upper rail button must be to aft of the Center of Gravity (CG). This is the point at which the rocket body will rotate around and in the case of a launch error where the lower rail button does not retain the vehicle, the rocket will not flip. Being as close to the CG is also important, as this allow for the least amount of torque on the button while the rocket is on the launch rail.

After reviewing with IREC judges, it was suggested to place the lower rail button as low as possible, like the team hypothesized, to maximize rail exit velocity. It was also suggested to place the upper rail button about two to three feet up from the first rail button. The judges noted that this suggestion was based on the size of the team's rocket as well as the 17-foot launch rail available at IREC but did not include specific details on how they came to their conclusion. The team believes it was most likely an experience suggestion. They also mentioned that a third rail button could be added if desired, but the alignment of the three would be much more critical since they would all need to be straight to slide on the rail. The team will move forward with two rail buttons for simplicity and keep them about two to three feet apart per the judges' suggestions for the current design.

As far as rail button attachment, there are two methods the team has used and an additional method the team investigated for better attachment to the airframe. The goals of investigating rail button attachment were to improve the strength of the attachment point while maintaining ease of assembly.

The first method utilizes a hex nut on the inside of the airframe to tighten the screw and secure the rail button to the body tube. This requires being able to access the nut within the airframe when assembling the rail button, which could be difficult depending on surrounding components. It has also been difficult in the past to tighten the nut to a curved surface such as the cylindrical body tube, but it does provide sufficient rigidity if assembled correctly. A photo of this attachment method is shown below.

Figure 64 - Rail Button Hex Nut attachment method

Due to assembly difficulty, the team moved to a threaded rubber insert attachment method. Once the screw is tightened into the insert, it expands to provide a tight fit in the hole for the rail button. It is easier to assemble from the exterior of the airframe. The issue with this method is that the friction fit is not as sturdy for heavier rockets and the hole tolerance is critical. A drawing of the rubber insert is shown below along with a photo of the rail buttons and inserts.

Figure 65 - Rail Button Threaded Insert

Since this is the heaviest rocket the rocket team has ever worked on, the team investigated an alternative mounting solution for more structural rigidity. The idea developed was to mount the rail button into one of the 0.25” thick aluminum centering rings or bulkheads with an 8-32 tapped hole on the outside diameter of the ring or bulkhead. The team machined their own bulkheads and centering rings and is well-versed in tapping holes on the diameter of the airframe with an end mill. An attachment into metal would provide much more strength to attach to the launch rail without issues. The design was manufactured for the subscale rocket and provides simple assembly and much more rigidity than the previous two methods. The only downside is the location of the bulkheads and centering rings restricts the potential locations for the rail buttons. This can be somewhat mitigated by putting additional 8-32 tapped holes in nearby bulkheads or centering rings to be able to switch out the location easily. A photo of this attachment method is shown below for the subscale two-stage rocket.

Figure 66 - Rail Button Ring Attachment Method

Overall, the team is satisfied with the new rail button attachment method due to its rigidity and ease of assembly in comparison to previous methods. A pro-con chart is shown below to summarize the three methods investigated.

Rail Button Fastening Pros & Cons

	Hex Nut Fastening	Threaded Rubber Insert	8-32 Tap in Aluminum
Pros	• Sufficient rigidity	• Easy to assemble	• Easy to assemble • Most rigid option
Cons	• Most difficult to assemble	• Least rigid • Friction fit could be pulled out with enough force	• Potential locations somewhat restricted

Table 13 - Rail button fastening pros and cons

The team reviewed several aspects specific to two-stage rocket development including rocket layout, stage separation, motor selection, sustainer separation & ignition timing, maximum dynamic forces on the rocket, parachute deployment methods, and sustainer ignition avionics. Several rocket hobbyists and online articles, along with IREC rules and the team's knowledge of rocket manufacturing, were used to determine the two-stage rocket architecture. OpenRocket, RASAero II, and RockSim simulations were conducted to validate motor choices and delay timing methodology. The following sections outline the team's decision making process for each section along with information discovered to help reach these conclusions.

4.1

There are a few different multistage layouts commonly used in amateur rocketry. The most prevalent options are a varying diameter rocket (with a booster stage larger diameter than the sustainer stage), a constant diameter rocket (with equivalent diameter airframes between both stages), and cluster motors on either or both stages [22]. For simplification, the team decided not to pursue cluster motors for either stage of the rocket. The team can reach the competition altitude range with one motor on each stage and trying to wire multiple motors in parallel to ignite at the same time could complicate the system beyond the team's scope.

4.2. Stage Separation

With regards to stage separation, the team investigated using either constant or varying diameter airframe and either passive or forced separation. Additionally, the team reviewed known methods of stage separation and potential issues to form a design for the best stage separation system possible under the given constraints. The team considered ease of assembly to be the most important factor in considering stage separation mechanisms, while also taking into account both the team's experience with given systems and the accuracy of simulating the flight. The following sections outline the team's thought process in designing the separation system.

4.2.1. Constant vs Varying Diameter

Between the two options of varying or constant diameter staging, both are plausible. Varying diameter rockets typically involve a transition section which acts as an assembly piece to couple the two varying diameter sections of the rocket. A photo of a small cardboard kit rocket showing several key components including a transition section can be seen below. The transition to a smaller diameter airframe reduces weight on the upper stage, allowing the rocket to fly higher on the same size motors. The tradeoff with regards to a smaller diameter rocket is the lack of space inside the airframe to fit or mount components, which could result in a longer rocket that adds back to the lost weight.

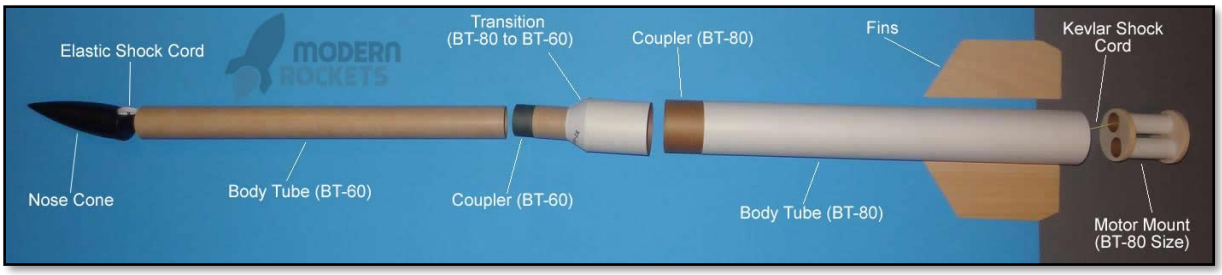

Figure 67 - Rocket kit components

The photo above indicates a single stage rocket. However, transitions are used commonly in multistage rockets as well, including at the amateur and industry levels. One such example is the Saturn V, whose layout is depicted below. The photo shows the three stages of the rocket and the transition section between the second and third stages.

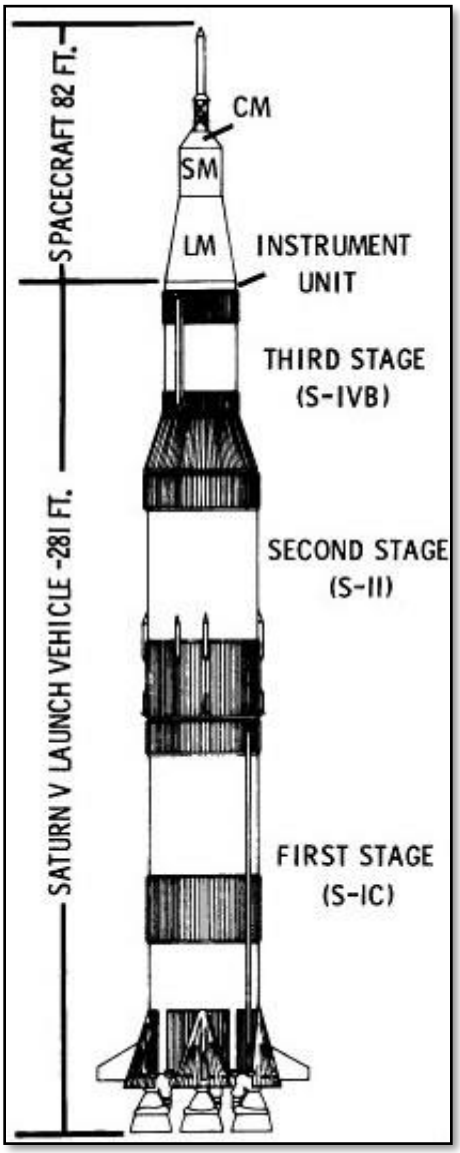

Figure 68 - Saturn V rocket layout

As shown, it is typical for a transition section to be placed between stages of the rocket, if one is used. However, the first and second stages of the Saturn V do not include a transition section and instead use a constant diameter airframe coupling. This is the typical coupling between two sections that the senior design team is familiar with through previous rocket construction. The team has never worked with a varying diameter rocket though, let alone one with multiple stages, so the team would be inexperienced using or manufacturing one.

The team investigated commercial options for transition sections and found that they are only available for smaller scale rockets. It is common for a rocket of this size to have a custom-built transition section, if one is to be used, for stage separation. At this point, the team reviewed the first-year rocket design team's stage separation mechanism from its failed two-stage rocket to determine the causes and hopefully adapt a better solution. The first-year design team utilized a custom-built stage separation mechanism with a varying diameter rocket. After reviewing their senior design report and discussing with alumni team members, it was determined that the custom-machined, tight-tolerance stage separation system for their rocket would have provided too much friction and locked up in flight if any moment were applied to it. The stage separation layout, coupled and decoupled, is shown in both orientations below.

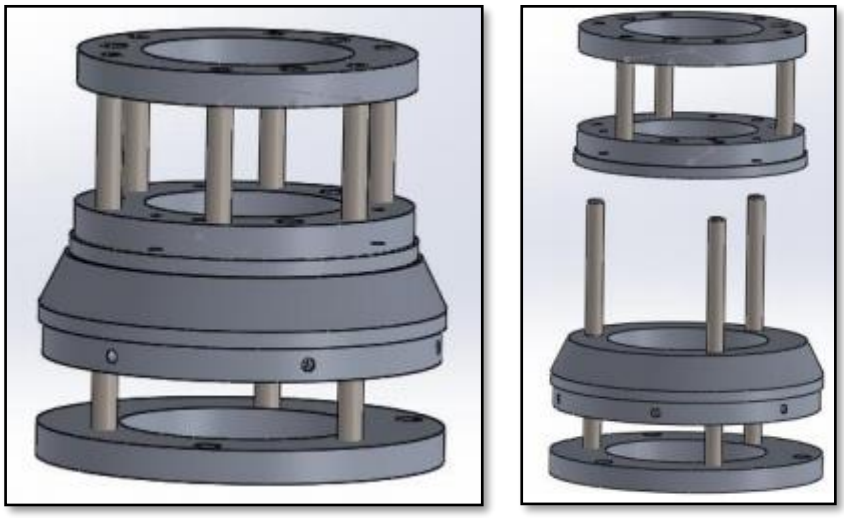

Figure 69 - First-year Akronauts two-stage separation layout coupled (left) and decoupled (right)

4.2.2. Passive vs Forced Separation

It is believed that the simplest method for stage separation would help the team avoid issues with custom components like this. For these reasons, it was decided the best solution for building a functional stage separation would be a constant diameter rocket.

Passive and forced stage separation are both common in model rocketry. Passive stage separation involves allowing the rocket to separate on its own without any event, typically due to the increased drag on the lower stage. Through research, it was determined that passive stage separations commonly involve varying diameter rockets, since the transition to a smaller airframe section reduces the drag on the second stage. Passive stage separation, or drag separation, would mean that the booster stage would fall off the sustainer stage after first stage motor burnout due to additional drag on the first stage, which commonly has the larger diameter

airframe. This would allow the second stage motor to ignite following the separation event. It is typically the simplest form of stage separation, but it would be difficult to test without a test flight.

A senior design team member had the opportunity to witness a two-stage rocket flown at FAR (Friends of Amateur Rocketry) launch site in Mojave, California, which had a black powder stage separation with a varying diameter rocket and it succeeded in reaching 18,000 feet. Richard, the owner of the two-stage rocket, said he typically has a black powder stage separation for all his two-stage rockets, even if it may drag separate prior to the ejection charge igniting. He has no way of verifying which method provided the stage separation, but the ejection charges provide a redundant and controlled method for separation. A photo of his two-stage rocket is shown below, which includes a commercial transition section due to the smaller size of the rocket.

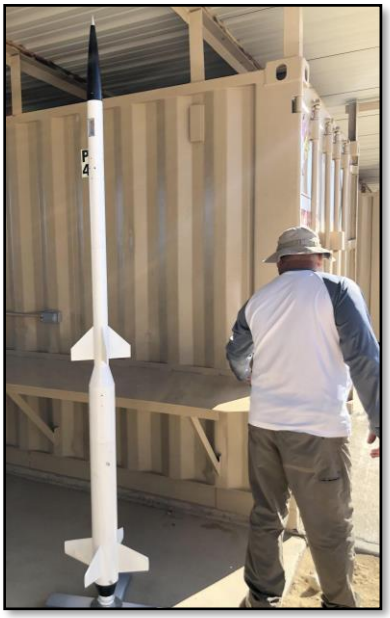

Figure 70 - Two-stage rocket flown at FAR in fall 2019

After reviewing the competition rules, a requirement for redundant recovery electronics was found, which cannot be satisfied by drag separation alone. The requirement states that a redundant method must be utilized for all rocket recovery events, which includes stage separation for multistage rockets. Additionally, the team investigated the effect of varying stage separation delay times on the final altitude achieved, which will be shown in a future section. If the rocket is passively separated, there would be no way to accurately determine or control the stage separation time. This could lead to inaccurate simulations for the rocket's flight.

Black powder ejection with a coupler attachment to a constant diameter is the separation method for all other separating sections of the rocket to deploy the parachutes. The team witnessed Georgia Tech's rocket design team use an identical black powder forced stage separation method for a constant diameter two-stage rocket at the Spaceport America Cup competition in June 2019, with a successful stage separation and flight to around 29,000 feet. For all these reasons, two black powder charges will be used to separate the stages at a predetermined time, rather than relying on a drag separation. The team has high confidence in this method because of the team's experience with it through all other rocket constructions.

The team identified a potential fin attachment issue prior to manufacturing the two-stage rocket. The team typically uses an end mill to cut the fin slots down to the end of the tube to slide the retained fins in through the bottom of the rocket body. If this is done for the stage separation side, the team will not be able to seal the slots to hold the pressure of the ejection. A test piece was manufactured using scrap components to illustrate this, as shown in the photo below. As the tubes begin to separate, the fin slot gap will increase and allow the pressure to escape without separating the two tubes. Even if the ejection was nearly instantaneous, the lowest centering ring on the second stage cannot be sealed without a small gap between the ring and the coupler.

Figure 71 – Assembled fin slot stage separation test piece

With the fin slots cut through the end of the airframe, the tube sections can bend inward, causing more friction holding the coupler onto the second stage. This could also cause stage separation issues, increasing the force required to separate the systems.

These issues were identified prior to manufacturing, allowing the team to devise a back-up plan of cutting the fin slots up to the lower centering ring and not all the way to the end of the airframe. This method was implemented on the subscale two-stage rocket with success, as the coupling section could still be pressure-sealed, and the coupler could slide into the airframe without the increased friction. A drawing of the fin slots for the second stage of the subscale two-stage rocket is shown below. This fin slot method was used on the first stage fin slots as well, although they were cut lower on the airframe since the fins are mounted at the base of the first stage.

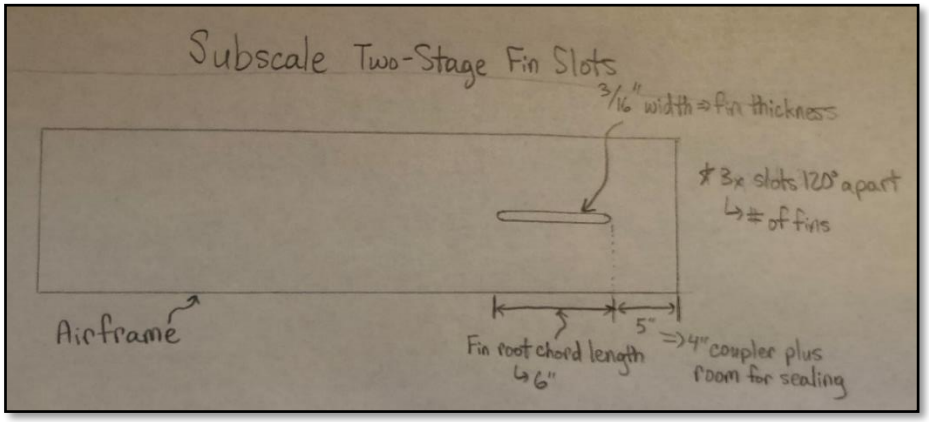

Figure 72 - Subscale 2nd stage fin slot drawing

The two-stage rocket needs to incorporate two carefully selected motors to meet the Spaceport America Cup and team expectations. The initial thrust to weight ratio and launch rail exit velocity are key contributors to booster stage motor selection. If the thrust to weight ratio or launch rail exit velocity is too low, the rocket will be unstable at takeoff and it could cause a poor or catastrophic flight. Even if the rocket can weather cock into a more stable flight off the rail, the maximum altitude will be hindered, preventing the launch vehicle from reaching the team's projected altitude. Further, the sustainer motor might not ignite if the trajectory angle is more than the maximum angle the tiltmeter allows. The tiltmeter will be covered in more detail in the Sustainer Ignition Avionics section.

Based on previous team research and discussing with Chris and Steve, a 5:1 thrust to weight ratio is typically sufficient for adequate liftoff and rail exit velocity for single stage rockets. The typical method the team has used to review motor performance for a given rocket construction is to estimate all rocket component weights and simulate the flight in OpenRocket. Initially, the team reviewed potential Aerotech and Cesaroni Technology motors for performance. Research showed that a fast burning booster motor is optimal since it would provide an adequate thrust to weight ratio and the rail exit velocity required to stabilize the weight of the two-stage rocket at takeoff [20]. A sustainer motor is a bit more open in terms of selection, so the team listed the pros and cons between a fast- and slow-burning sustainer motor below.

Sustainer Motor Pros & Cons

	Fast-Burning Sustainer	Slow-Burning Sustainer
Pros	• Easier to ignite • Higher altitude	• More stable flight • Maintains high velocity for longer time
Cons	• Instability at 2nd stage ignition could occur	• More difficult to ignite

Table 14 - Sustainer motor pros and cons

Based on the pros and cons, the team believes a slow-burning sustainer motor would be best. The con of difficulty to ignite can be mitigated by dipping the electric match igniter in pyrogen or some other material to improve ignition performance. More details on the 2nd stage igniters can be found in the Sustainer Avionics and Wiring section. For the team, flight stability was determined to be the most important factor in selecting a 2nd stage motor. Simulations showed that the rocket could reach competition altitude requirements of between 21,000' and 39,000' with either type of motor, and the higher potential altitude was not a key factor in the team's decision process.

Due to the team's familiarity and past success with Cesaroni motors, the team began researching them as the primary motor supplier. Based on some brief simulations to identify motor options, the CTI N3180 and CTI O3400 were identified as potential booster motors and the N1100 was selected as the best sustainer motor option. The burn times are relatively low for both the N3180 and the O3400 at 4.5s and 6.1s, respectively. Both achieve over a 5:1 thrust to

weight ratio and a sufficient rail exit velocity, while keeping the team within the target altitude range. The N3180 motor resulted in a final altitude around 24,000' which is close to the bottom of the acceptable competition range of 21,000'. Any off-nominal flight occurrences or underestimates on weight could result in an altitude below competition requirements, which would result in a loss of 70% (350 points) of the team's flight performance score. The team was hesitant to move forward with the O3400 motor due to its additional length. Longer motors are more likely to experience issues such as cracked grains or grains that are too long which could cause performance issues. After further research, it was determined that commercially manufactured motors are reliable. After talking to alumni about a previous senior design motor that did not perform as expected due to the length of the grains being too long, they reiterated what research had suggested: the commercial motors should not be an issue and the team could be confident that they are manufactured well. Team mentors also confirmed that the commercial options should perform well even at the extra-large length.

The N1100 has a 12 second burn time which is classified as a longer burning motor in comparison to the booster motors above. It produces a max thrust of 609 lbf and an average thrust of 262 lbf over the burn time. The thrust curve is shown below.

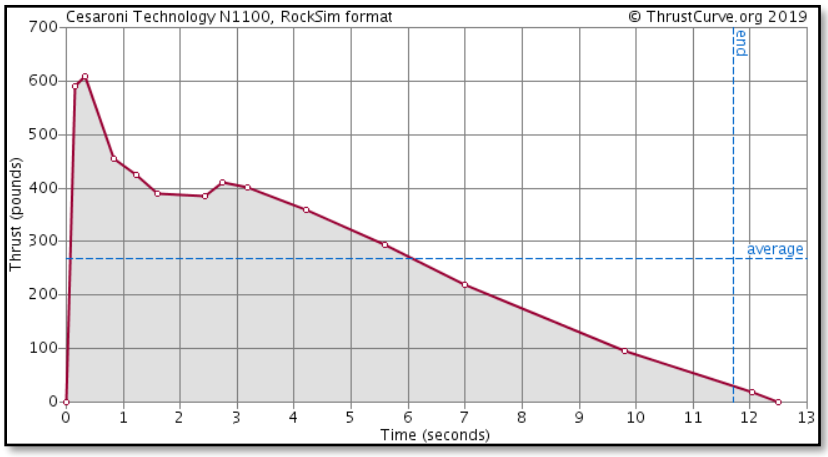

Figure 73 - CTI N1100 thrust curve

The O3400 produces a max thrust of 1,056 lbf and an average thrust of 769 lbf over 6.1s. After reviewing competition rules, the team identified several requirements relating to rail exit velocity and thrust to weight ratio for multistage rockets. The IREC competition requirement for minimum rail exit velocity is 50 ft/s with detailed analysis such as flight simulations, but the team will look to keep the rail exit velocity above 70 ft/s as a team requirement. The competition requirement for thrust to weight ratio of multistage rockets is 8:1 on the booster stage and 3:1 on the sustainer stage.

Utilizing weight estimates for all components, the team can predict the maximum wet weight of the two-stage rocket to be about 138 lb and the sustainer stage alone to be about 71.8 lb. This can vary significantly with motor changes and throughout the manufacturing process, so a factor of safety on rail exit velocity and thrust to weight ratio will benefit the team greatly. The wet weight includes the propellant in the motors while the dry weight includes only the casing weight. With this weight estimate, the team can calculate the thrust to weight ratio for each stage with the equation below.

$$R = \frac{T}{W}$$

Equation 16 - Thrust to weight ratio

$$T = Max\ Thrust$$
$$W = Wet\ Weight$$
$$R = Thrust\ to\ Weight\ Ratio$$

Using the equation above with each stage's wet weight, the O3400 resulted in a thrust to weight ratio of 7.65 while the N1100 has a ratio of 8.48. The rail exit velocity with the O3400 motor was around 80 ft/s. Based on this data, the team determined the CTI O3400 was insufficient due to the thrust to weight ratio below competition requirements even prior to manufacturing. The N1100 was validated with this data and the requirements.

The team faced two options to reach the desired thrust to weight ratio at this point: cut out at least 6 lb of weight from the rocket post-manufacturing or select another motor that would achieve an adequate ratio and still maintain a sufficient altitude. The easier of these two options was to select another motor, which the team was able to find in the CTI N5800. It is another 6G XL motor like the O3400, but it has a 3.5s burn time, which is much quicker than the 6.1s of the O3400. The N5800 has a max thrust of 1,564 lbf and an average thrust of 1,296.5 lbf. The thrust to weight ratio for this booster motor is 11.33 which meets competition requirements. The N5800 thrust curve is shown below.

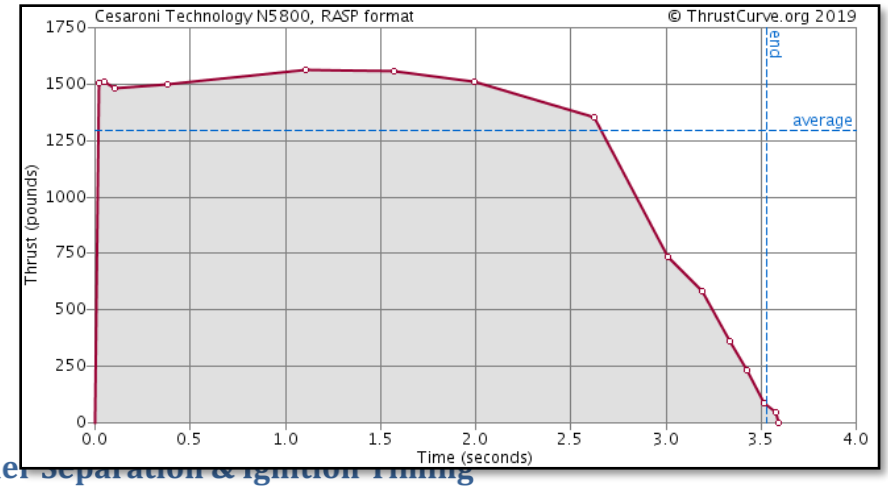

Figure 74 - CTI N5800 thrust curve

4.4. Sustainer Separation & Ignition Timing

One of the primary challenges when designing a multistage launch vehicle is determining when to separate the two stages and ignite the sustainer stage. This decision can have an enormous impact on the overall flight of the rocket, changing maximum altitude by thousands of feet or potentially not igniting the sustainer motor if the angle of attack is too far from vertical, both of which drastically affect the competition score. For this reason, the team must find the best delay times that will optimize altitude and ensure a successful flight.

While researching this topic, the team initially utilized OpenRocket to simulate stage separation and sustainer ignition delay times ranging from 0-15 seconds. For understanding the following analysis, the following two important terms must be properly defined. *Stage separation delay* is the time after the 1st stage motor burns out at which the 1st and 2nd stages will separate. *Sustainer ignition delay* is the time after the 1st stage motor burns out at which the 2nd stage motor should ignite. Based on this understanding, one can reasonably assume that the stage separation must be set to occur at the same time or before the sustainer motor ignites. If the sustainer motor ignites before the stages separate, it will separate the stages anyways, which might not be taken into account correctly in the flight simulations themselves, leading to bad data. For this reason, the team ran all simulations by varying both delays up to 10 seconds in one second intervals while keeping the separation delay at or less than the sustainer ignition delay.

While analyzing the data, the team focused on the effect of stage separation and ignition delay times on altitude, the vehicle's angle off the vertical axis, maximum velocity, and drift distance. The figures below depict the results obtained from the simulations. It should also be noted that the results depend largely on the rocket design and motors used in the simulations. For this reason, the team waited to have a fairly final rocket layout design and motors finalized as the CTI N5800 and N1100 before proceeding with the simulations. After manufacturing the full-scale rocket, the simulations should be reanalyzed in a smaller window of delay times to verify that the optimal delays have not changed based on differences between the design and the manufactured versions of the rocket. However, the initial simulations will provide the team with a general idea of the trend that the different ignition times will incur. RASAero II and RockSim were used later for a comparison of the results. Each individual plot required 1-3 hours of simulation time by the senior design team members, depending on the flight characteristic and software program. A smaller window of time delays with more computers to run the simulations at the same time will help reduce this extensive simulation time in the future.

The team had two reviews with IREC judges. In the second review, a judge pointed out that the CTI N1100 typically takes about two seconds to come up to pressure and actually produce the initial thrust. This is not factored into the delay times in the simulation software and should be accounted for in the team's tiltmeter settings. It should be noted that this two second pressure buildup can vary based on the quality of motor manufacturing and any changes to the 2nd stage motor choice. It is also very difficult to predict without expensive testing since these motors cost over $1,000 each. The best data the team has available to use is the experience of other rocket hobbyists or the manufacturers at this point. Flying this motor and recovering the rocket should yield valuable data for future flights.

4.4.1 Altitude and Velocity Analysis

The team began by simulating altitude for various wind speeds with only a sustainer ignition delay change. The separation delay was kept constant at zero seconds. As can be seen from the graph below, the predicted altitudes all fall within a range of 25,000 ft to 31,000. According to the Spaceport America Cup competition rules, this range is acceptable for the launch vehicle to be scored. After simulating up to a 15 second sustainer ignition delay, the team noticed that altitude dropped off significantly and cut back the max sustainer ignition delay to 10 seconds for further analysis. Overall, the altitude dropped with wind speed for all delay values simulated.

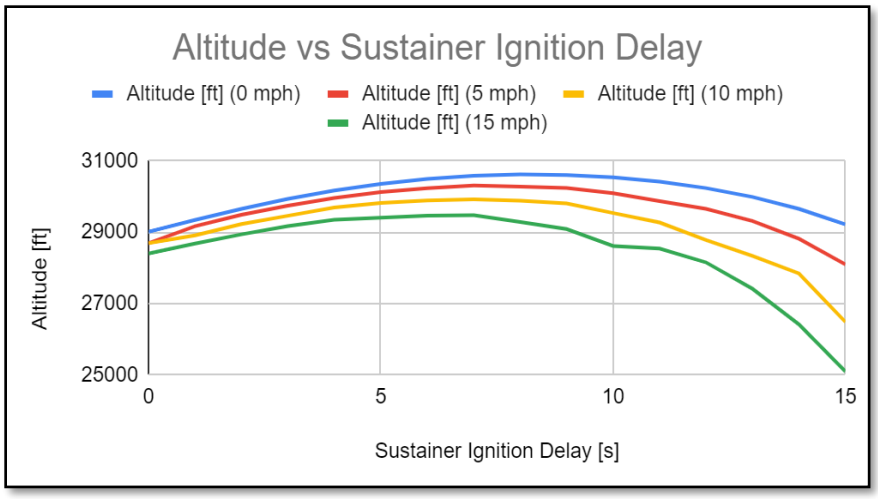

Figure 75 - OpenRocket Altitude vs Sustainer Ignition Delay

The figure below shows the maximum Mach number reached versus the sustainer ignition delay for the same wind speeds and sustainer ignition delays with the separation delay kept constant at zero seconds. The team wants to ensure the rocket reaches a speed above Mach 1.0 to fully test the launch vehicle's structural capabilities. As seen below, the maximum Mach number reached will remain above Mach 1.0 for all sustainer ignition delays and wind speeds within the team's range. The Mach number did not vary much with wind speed.

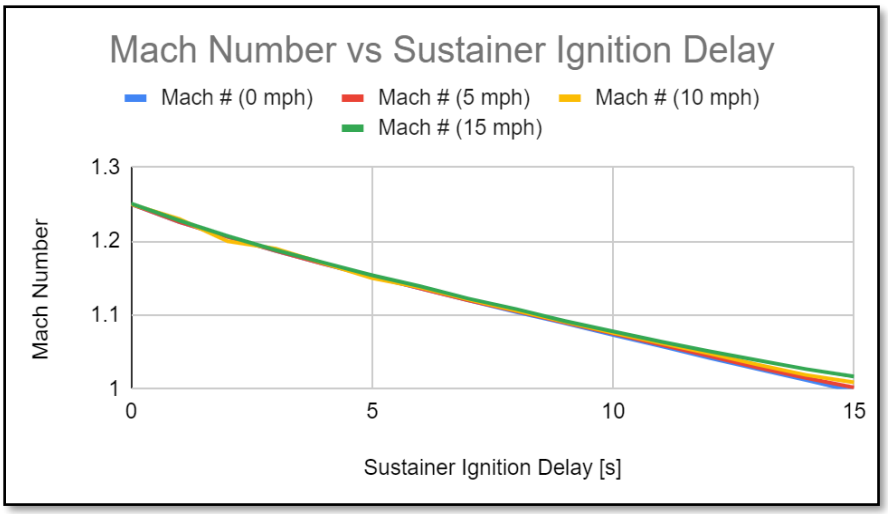

Figure 76 - OpenRocket Mach Number vs Sustainer Ignition Delay

Next, the team analyzed altitude at a constant wind speed of 10 mph while varying stage separation and sustainer ignition delays up to 10 seconds. The results are shown below with each colored line representing a different stage separation delay time. These lines start at different points because the stage separation delay must be at or less than the sustainer ignition delay. Overall, the results show that the altitude can vary by nearly 2,500 feet simply by adjusting the delay times. The maximum altitude of 30,249 feet occurred for a stage separation delay of 6 seconds and a sustainer ignition delay of 8 seconds.

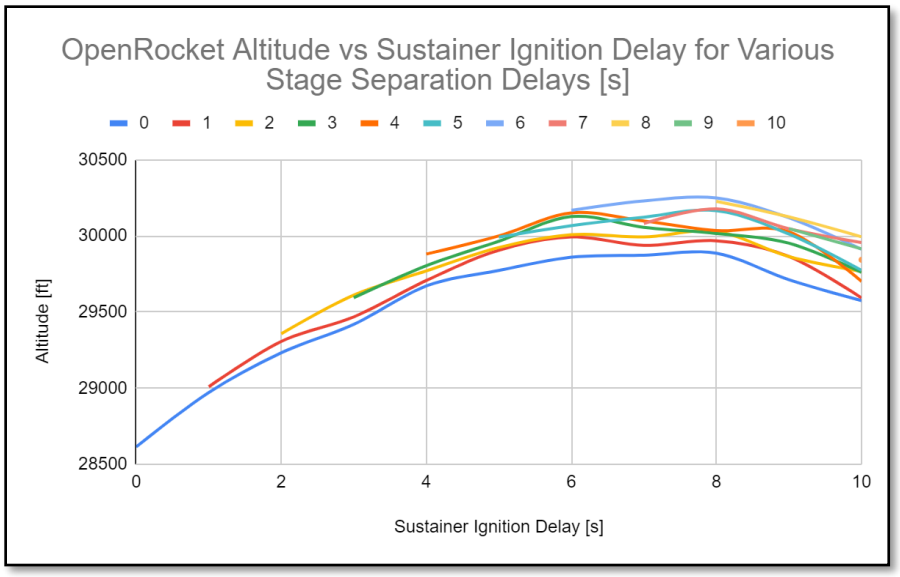

Figure 77 - OpenRocket Altitude vs Sustainer Ignition Delay for Various Stage Separation Delays

After growing comfortable with the simulation methodology, the team wanted to check the OpenRocket simulations against another commonly used simulation software, RASAero II. The altitude predictions for the same delay times were plotted below using RASAero II. The results are relatively similar to OpenRocket. The maximum altitude of 30,924 feet occurs at 9 second stage separation delay and 9 sustainer ignition delay. RASAero II also shows that the altitude increases with a delayed sustainer ignition, and the stage separation appears to be a smaller factor. Overall, the team is pretty equally trusting of both software packages based on previous experience, although OpenRocket has a much more in-depth and user-friendly interface. The team will consider these plots in more detail after analyzing vertical orientation and drift analysis plots.

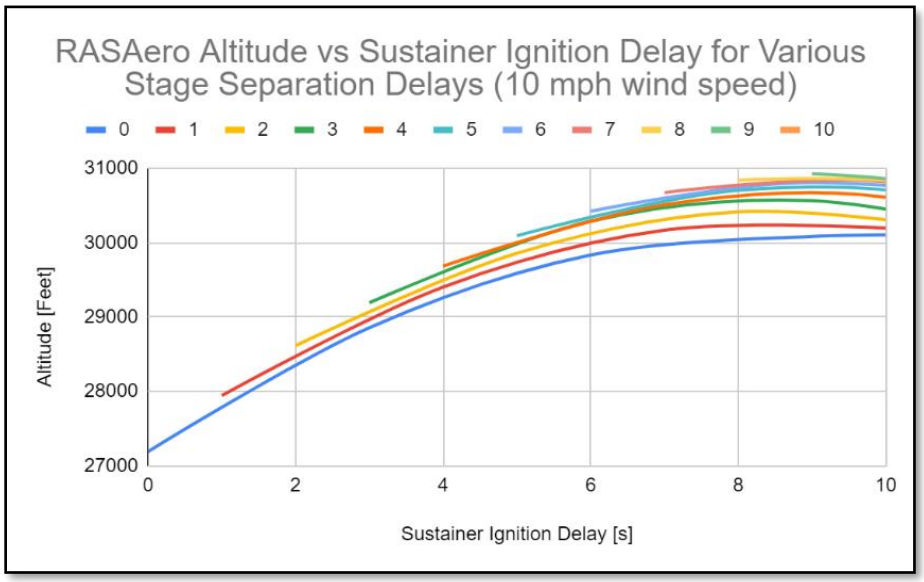

Figure 78 – RASAero II Altitude vs Sustainer Ignition Delay for Various Stage Separation Delays

Later in the development stages, the team became more capable with the RockSim software. They used the same model, motors, and launch settings in their simulations. While the trend for sustainer delay time is the same, the resulting altitudes were much higher, ranging from 33,000 to 39,000 ft. As the team has never launched a multistage rocket, nor broken the sound barrier, the team is not sure if their opensource software (RASAero II and OpenRocket) is accurate for their simulations. These results, while establishing an understanding of the ignition and separation delay trends, do raise concerns of the altitude of the rocket launch. The team does not wish to overshoot for competition scoring reasons, so a method to help validate the simulations is needed. Actual flight testing on multistage and supersonic launches will be the best method for validating which software is more accurate for the mission. However, given the team's experience and accuracy with the previous two software, the team is more confident in them at this time.

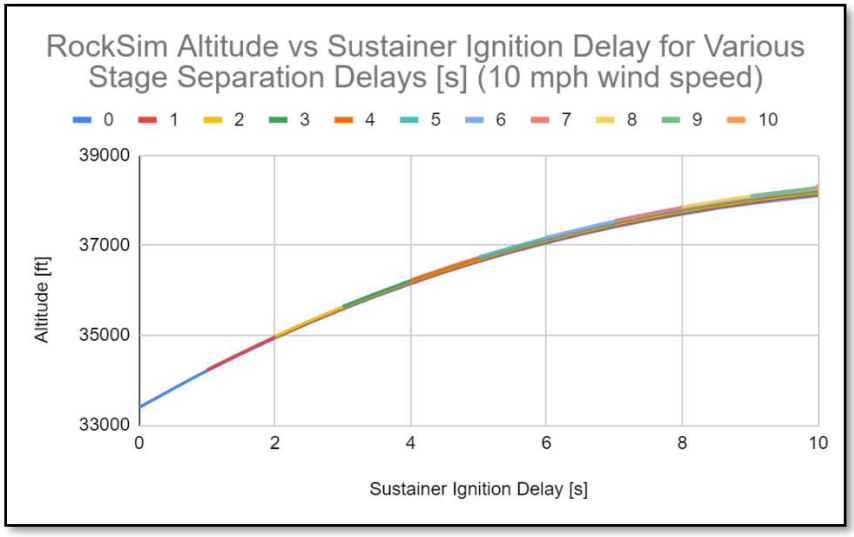

Figure 79 - RockSim Altitude vs Sustainer Ignition Delay for Various Stage Separation Delays

4.4.2. Vertical Orientation Analysis

Following the altitude plot developments, the team wanted to analyze the vertical orientation for the same delay times to verify that it is not too far off from the vertical axis to inhibit igniting the sustainer motor. If the angle from vertical is too large, the rocket will fly much farther from the launch site and be difficult to recover before the GPS batteries die. It should be understood that the simulations cannot take into account all factors in flight and a factor of safety should be developed to ensure a safe flight. For this reason, the team has a self-imposed requirement that the sustainer motor should not ignite if the rocket's angle from vertical is greater than 20-degrees. The team will likely select delay times that produce a vertical orientation angle well-within this range for even the highest wind speeds the team may see on launch day.

The team developed vertical orientation plots for wind speeds of 0, 5, 10, 15, and 20 mph by varying only the stage separation delay and sustainer motor ignition delay like the simulations above. Below is the plot for 10 mph wind speeds. In this case, 90 degrees is vertical, and the competition requirements permit multistage rockets to launch at an angle of 3 degrees off the vertical axis (87 degrees). The plot shows that the vertical orientation varies linearly with sustainer ignition delay without stage separation delay having much of a factor. Even at a 10

second delay, the simulations predict that the rocket will be between 10-12 degrees off the vertical axis, which meets the team's requirement.

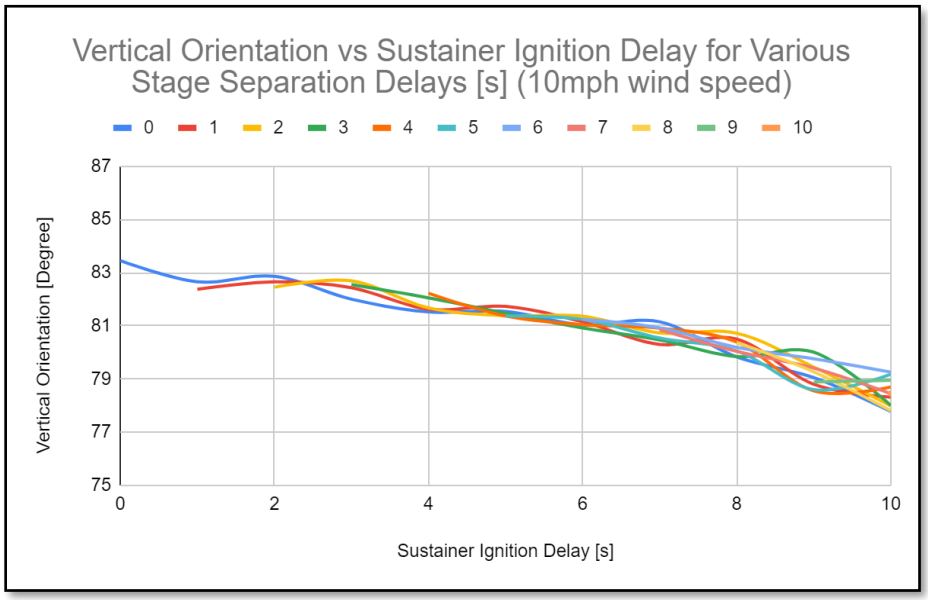

Figure 80 - OpenRocket Vertical Orientation vs Sustainer Ignition Delay for Various Stage Separation Delays (10 mph wind speed)

As a worst-case scenario, the team analyzed 20 mph wind speed plots, since the Range Safety Officer (RSO) will not permit a launch if wind speeds exceed 20 mph. The plot for 20 mph wind speeds is shown below which also shows a linear correlation between vertical orientation and sustainer ignition delay, regardless of stage separation delay. As the delays increase, the deviation grows for potential sustainer ignition angles, like the previous plot. Overall, the 10 second delay values all fall around 15-18 degrees from vertical, which meets team requirements. However, these values are much closer to the 20-degree requirement, so the team will consider decreasing the delays to ensure a safe flight in higher wind speeds.

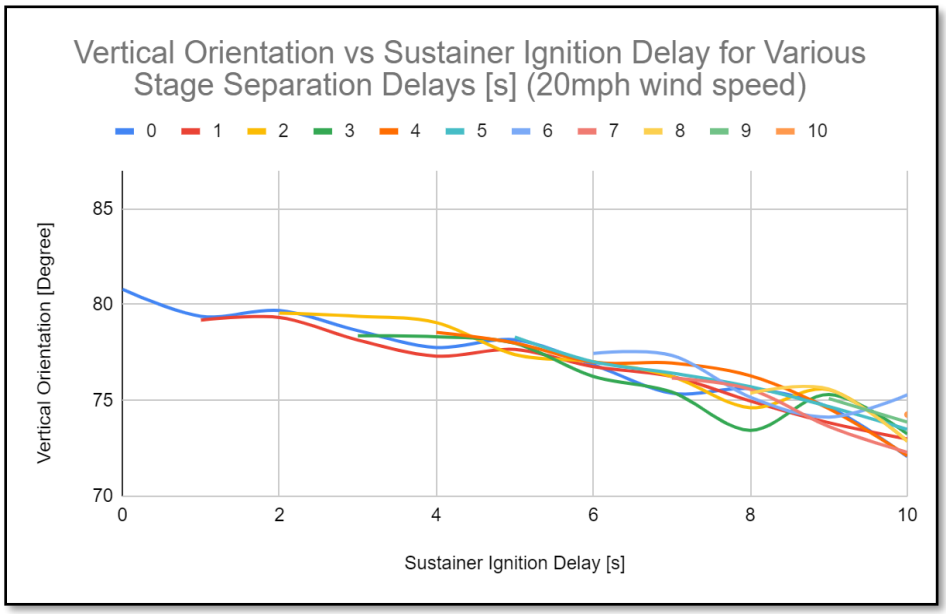

Figure 81 - OpenRocket Vertical Orientation vs Sustainer Ignition Delay for Various Stage Separation Delays (20 mph wind speed)

Below is the plot for 10 mph wind speeds using RASAero II. Again, 90 degrees is vertical, and the competition requirements permit multistage rockets to launch at an angle of 3 degrees off the vertical axis (87 degrees). The plot shows that the vertical orientation results are comparable to the output given by OpenRocket. The worst-case condition of a 10 second delay results in the rocket orientation 11-12 degrees off the vertical axis, which still satisfies the team's requirement.

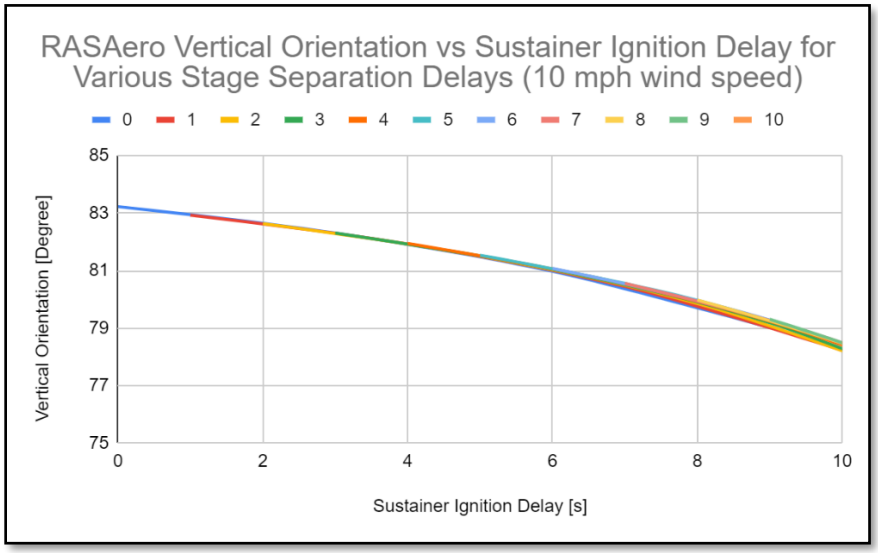

Figure 82 – RASAero II Vertical Orientation vs Sustainer Ignition Delay for Various Stage Separation Delays (10 mph wind speed)

Lastly, the team utilized the RockSim software. While this simulation predicts the rocket to go to a much higher altitude than the other software, the vertical orientation is much less drastic than the previous simulation arrays. At 10 mph wind speeds, a 10 second ignition delay results in a vertical angle of close to 90 degrees. The flight path shows that the rocket returned from the 3 degree launch angle to an almost vertical flight by stage separation. Based on the RockSim simulations, the flight would require stronger winds or longer delays to go beyond the 20 degree safety margin. At 10 mph, a 10 second separation delay with a 9 second ejection delay afterwards would result in a 69 degree second stage ignition angle. At 20 mph, this is reduced to a 7 second separation delay with a 6 second ignition delay. Due to these safer predictions, the team will have to abide by OpenRocket or RASAero II as worst-case situations.

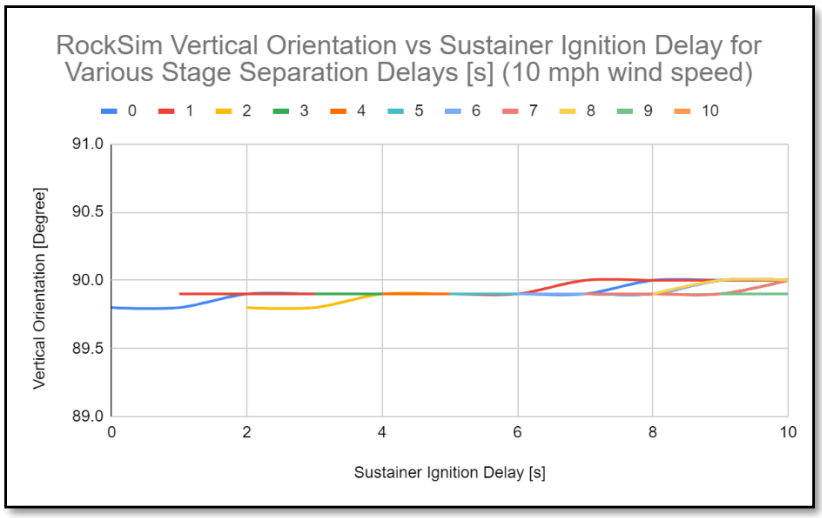

Figure 83 - RockSim Vertical Orientation vs Sustainer Ignition Delay for Various Stage Separation Delays (10 mph wind speed)

Overall, the plots above show once again that OpenRocket and RASAero II are more similar than the RockSim simulations. All three software show that delay times in the 5-8 second range are all within the 20-degree threshold and should be sufficiently safe for flight. These delay times will keep the rocket within the team's vertical angle criteria while maximizing altitude.

4.4.3 Drift Analysis

The team used OpenRocket, RASAero II, and RockSim to analyze the potential drift of the launch vehicle once parachutes are deployed. This analysis gave the team a better idea of the amount of drift likely to be seen for any of the cases being considered and will assist in the final determination of the optimal delays to use during flight. The drift distance was plotted against the sustainer ignition delay for several stage separation delays and wind speeds. The OpenRocket results can be seen below for 10 and 20 mph wind speeds.

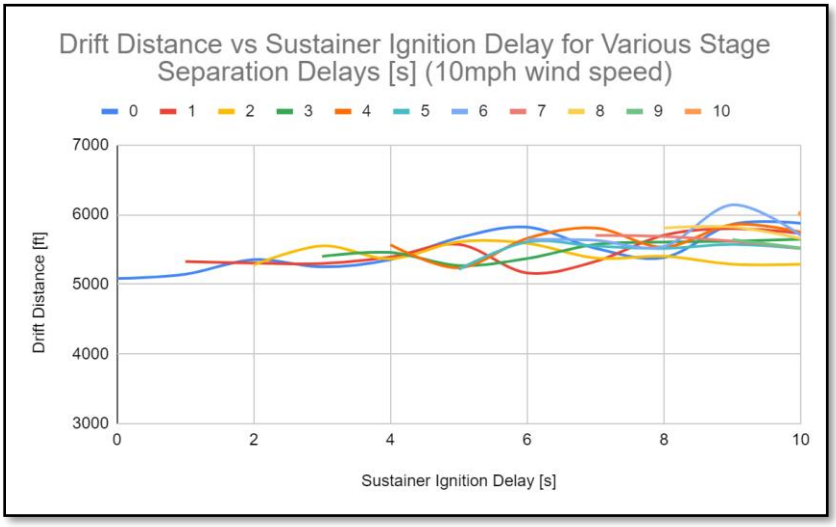

Figure 84 - OpenRocket Drift Distance vs Sustainer Ignition Delay for Various Stage Separation Delays (10 mph wind speed)

The maximum drift distance for the launch vehicle, at a wind speed of 10 mph, is expected to be approximately 5,900 feet. The minimum drift distance is just over 5,000 feet.

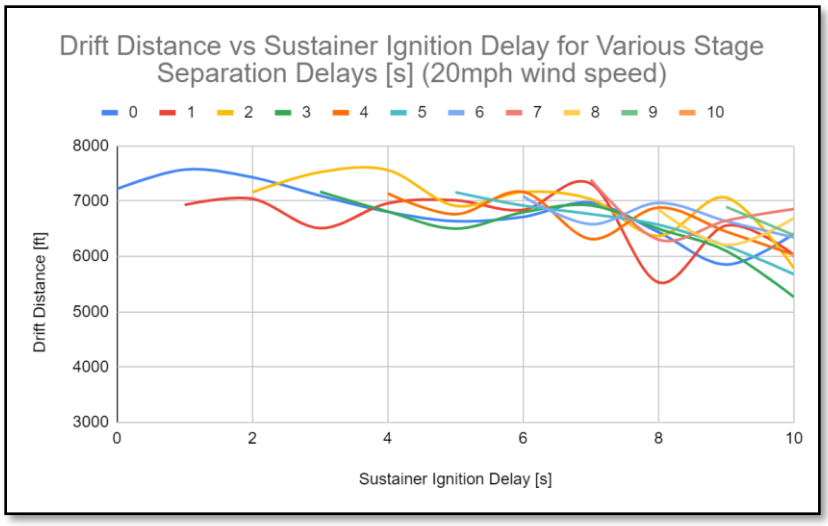

Figure 85 - OpenRocket Drift Distance vs Sustainer Ignition Delay for Various Stage Separation Delays (20 mph wind speed)

The drift distance at 20 mph shows significant variability and decreases with a longer sustainer ignition delay. The team expects the variability is caused by the deviations incorporated into OpenRocket's code at such high wind speeds. Additionally, the decrease in drift distance can be attributed to a lower angle of flight and lower flight time in general since the rocket cannot reach as high of an altitude. The maximum drift would be around 7,500 feet and would occur for lower delay times. Overall, the parachutes will have a much larger contribution to the rocket's drift distance, but the delay times can have a small effect as well.

For a quick comparison using RASAero II, the team plotted drift distance for 10 mph wind speeds. The plot shown below expects a drift distance of 3,800 feet to 4,300 feet for most separation and ignition delay cases. All drift distances are less than what was calculated using OpenRocket under the same wind speed condition. The RASAero II plot is much more consistent since it does not include a standard deviation for wind speed like OpenRocket.

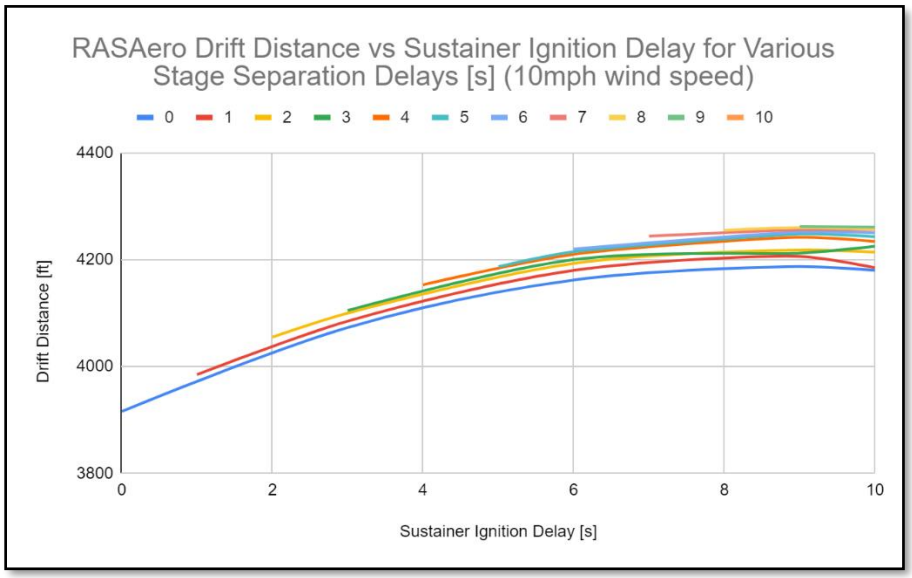

Figure 86 – RASAero II Drift Distance vs Sustainer Ignition Delay for Various Stage Separation Delays (10 mph wind speed)

The same array for drift at 10 mph winds was plotted using RockSim as well, which is shown below. These results showed the same trend as the previous software in regards to impact of stage separation and sustainer ignition over drift distance. At 10 mph, all drift values are between 4,900 and 5,600 feet. The team is fairly content with the results found with the software as it shares the same drifting trends as the previous ones, and in this case, ranging between the two for the drift results.

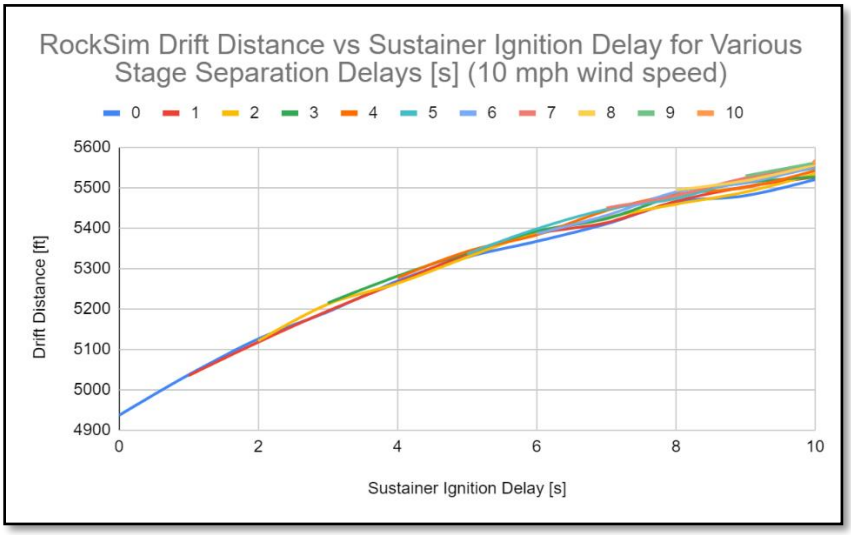

Figure 87 - RockSim Drift Distance vs Sustainer Ignition Delay for Various Stage Separation Delays (10 mph wind speed)

Overall, the team is expecting to see a maximum drift distance between 3,000 feet and 7,000 feet, which is sufficiently low for a rocket achieving 30,000 feet altitude. For wind speeds 10 mph and below, it seems that the sustainer ignition delay is directly proportional to the drift distance. At wind speeds greater than 10 mph, the drift distance is not greatly influenced by the sustainer ignition delay, but rather the wind speed. It should be noted that the drift distance increases nearly linearly until a sustainer ignition delay of approximately 7 seconds. At this point, the maximum altitude of the launch vehicle actually begins to decrease, resulting in lower drift distances. This is evident in comparing the OpenRocket plots for altitude, vertical orientation, and drift. Further, the team noticed that as the wind speeds increased, the data became less consistent. These inconsistencies are most likely caused by the OpenRocket software introducing a level of uncertainty into the calculations.

In conclusion, the team successfully analyzed altitude, velocity, vertical orientation, and drift distances for the various stage separation and sustainer ignition delay times. The team found that the optimal delay times vary between OpenRocket, RASAero II, and RockSim and that launch day conditions can be a major factor. For now, the team is considering a stage separation delay time of 4-6 seconds and a sustainer ignition delay time of 5-8 seconds since these values produce the highest altitude while remaining within sufficient boundaries of vertical orientation and drift distance for all three software. The team will reanalyze the delay times in a smaller window after the manufactured version of the rocket is produced. Finally, the team will consider the two second pressure build up for the CTI N1100, per the IREC judge's recommendation. Due to the team's experience with OpenRocket and RASAero II, the team elected to focus on these two software until RockSim could be validated.

“Max Q” is referred to as the maximum dynamic pressure the rocket will endure through flight. If the rocket cannot handle the maximum dynamic force or pressure in flight, it will tear the rocket apart or the fins off the rocket when it occurs. In space flights, the point of maximum dynamic pressure is well-calculated, and it is a good thing if nothing happens out of the ordinary at this time. The team hopes for the same with this rocket. It does not correlate directly to speed or Mach 1 conditions. The defining equation for dynamic pressure is shown below.

$$q = \frac{1}{2}\rho v^2$$

Equation 17 - Max Dynamic Pressure

Based on this defining equation, dynamic force increases with either an increase in velocity or density. For all nominal rocket flights, density is highest initially and decreases through flight as the rocket reaches higher altitudes. Velocity is the lowest prior to ignition and at apogee, and its maximum is at motor burnout of the final stage of the rocket. There is nothing to suggest the maximum dynamic force will occur at any specific rocket event. The only way to know for sure when it will occur is to have every density and corresponding velocity value through flight, or to be able to predict it within close proximity.

Through research, three methods were found for calculating maximum dynamic force with varying difficulties and confidence levels. Beginning with the easiest method and working up, the simplest method for calculating it would be to plot drag force during flight in OpenRocket and find the point of maximum drag force, which is the point of max Q. The two are related through the drag coefficient equation and the drag coefficient can be plotted over time as well to yield the drag coefficient at the point of max drag force. Below is the drag coefficient equation replaced with dynamic pressure.

$$C_d = \frac{F_d}{(\frac{1}{2}\rho v^2)A} = \frac{F_d}{(q)A}$$

Equation 18 - Drag Coefficient in terms of dynamic pressure

Utilizing the frontal area of the rocket and rearranging to solve for maximum dynamic pressure, and the resulting maximum dynamic force by multiplying by planform area of the rocket, the team was able to plot the dynamic force on the rocket through flight. The maximum dynamic force by this method was around 217 lbf, which is easily surmountable with the structure systems in place. The maximum dynamic force occurred at 2nd stage motor burnout in this case. The shear strength of the six 6-32 screws holding the bulkheads in place is around 4,500 lbf, which is the limiting structural item in the rocket. For more details regarding the shear test that validated this information, see the Testing section of the report. As a reference, the maximum thrust of the first stage CTI N-5800 motor is 1,564 lbf.

The second method for determining max dynamic pressure is using known density values at given altitudes from a density-altitude table [32]. The density values were plotted with a best fit 2nd degree polynomial equation between points on the chart to develop density values at corresponding velocity points. These density values can be plugged into the max dynamic pressure equation above with velocity values from OpenRocket or from a custom flight simulation which produces velocity values through flight. By multiplying by planform area of the

rocket, the dynamic force can be found throughout flight. For the team's purposes, OpenRocket velocity values were used. However, given a longer timeline and more focus time specifically on dynamic force calculations, RASAero II, RockSim, or a custom simulation program could be developed in MATLAB [9]. This second method resulted in a very similar plot, with a slightly lower max dynamic force of around 189 lbf. Both max dynamic force curves are plotted on the same graph below.

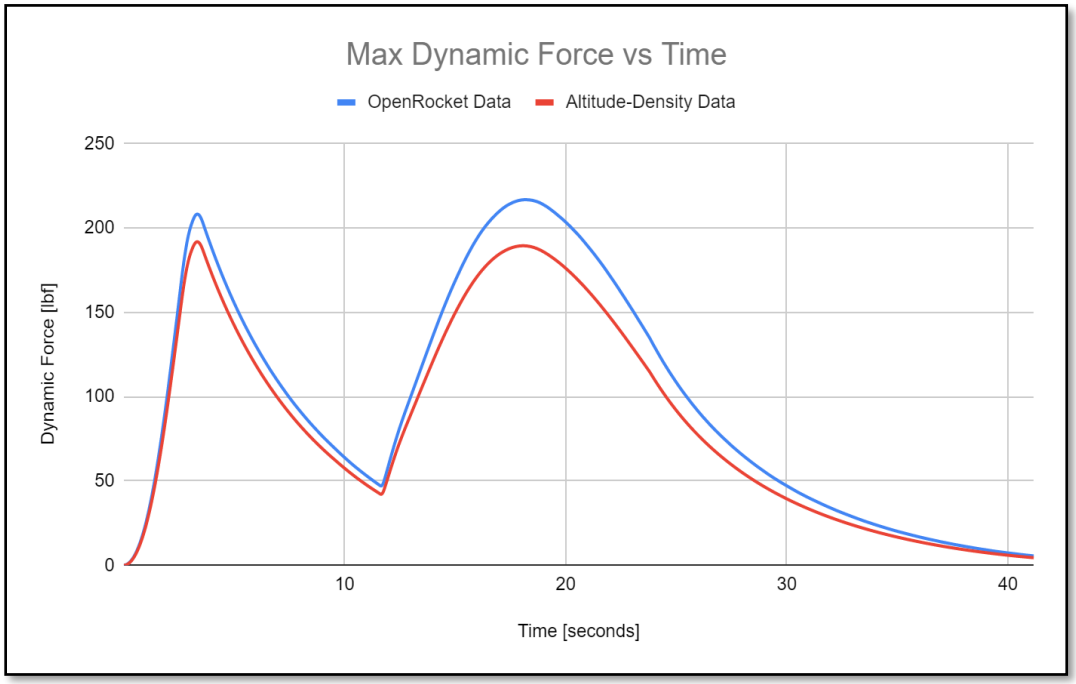

Figure 88 - Max Dynamic Force vs Time

Overall, both methods produced very similar graphs, with the dynamic force replicating the velocity curves through flight. It is evident when each motor burns out from the chart and both max dynamic forces occur at 2nd stage motor burnout. Although the final values varied slightly, both are well-within structural limits and the rocket should survive the point of max Q in flight. If the timing sequence or motors are adjusted in the future, the team can easily plug in OpenRocket flight data to reproduce the results in Excel.

There is one other method that was found which would require an extensive MATLAB or Excel calculation to develop a solution. It involves derivations for acceleration and density to calculate the dynamic force as a function of time. Again, given more time to focus specifically on these calculations, the team would be able to develop a higher confidence solution such as this, but the team is confident moving forward with the two developed solutions above which prove the structural integrity through max Q.

4.6. Parachute Deployment Methods and Layouts

Parachute deployment is another key feature in the rocket design. If the deployment methods do not function as expected, the rocket will return ballistically and result in a crash landing. All useful data obtained through flight, including the successfully flown rocket, will be

lost. For this reason, the team examined several deployment options. The addition of the 2nd stage rocket introduced several complexities into the recovery design, such as how and when to deploy the first stage drogue parachute, drogue and main parachute locations for both stages, and event sequences for both stages.

In a single stage rocket, the most common deployment method includes a drogue parachute, which is typically much smaller, being deployed at apogee. This is followed by a main parachute, typically much larger to control the descent, being deployed at a predetermined altitude during the descent phase. The drogue ensures that the rocket does not drift too far, while the main ensures that no components break upon landing due to a high kinetic energy.

It is typical for a single stage rocket to deploy each parachute from a separate compartment of the rocket as shown in the concept sketch below. This layout is referred to as “dual deployment” in recovery terminology.

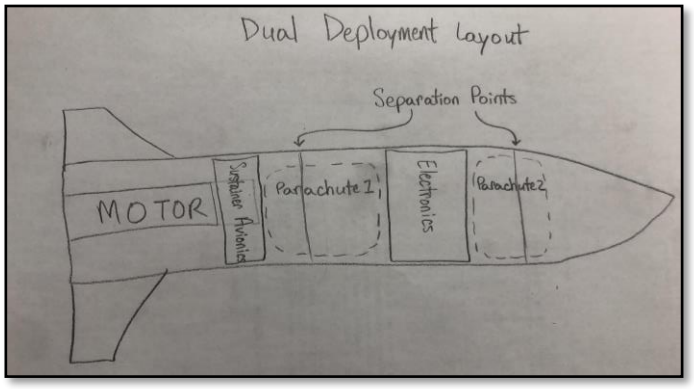

Figure 89 - Dual deployment concept sketch

The electronics system typically features an altimeter which can be programmed to ignite the black powder ejection charge with an electric match at a predetermined time or altitude. Placing the parachutes around the electronics system allows for ejection charges on both sides of the electronics and separation of the airframe pieces at the two separation points indicated in the figure. Due to familiarity with the system and rocket layout, the team believes this is the best option for sustainer parachute deployment. The sustainer motor section will also feature an avionics system for 2nd stage motor ignition between the motor and parachute, which is also depicted in the diagram. More details are included below for an analysis of the 1st stage parachute deployment.

Due to time constraints, the team did not focus on parachute design, but instead utilized the Akronauts Recovery subsystem members to correctly size the rocket’s parachutes based on IREC and team requirements for drift and kinetic energy at landing. The recovery team also developed the harness system to attach the parachutes within the rocket. The senior design team focused on the three options for deployment methods as listed in the following sections.

4.6.1. Tender Descender

A tender descender is one method of deploying both the drogue and main parachutes from the same compartment within the rocket. A photo of the tender descender wiring and layout is shown below [30]. This method includes a deployment bag for the main parachute to be secured between drogue ejection at apogee and main parachute deployment at the selected altitude. It is secured via a metal connecting component, the tender descender (shown in red),

between two quick links which keeps the cords from experiencing tension during drogue parachute deployment. This keeps the main parachute in the deployment bag until an altimeter sends a signal to the black powder charge in the tender descender (taped in blue) to separate the quick link connection and pull the bag off the main parachute at the desired altitude.

Figure 90 - Tender Descender layout and wiring

Benefits of the tender descender include reduced space for another parachute bay with shock cords. However, there is no redundancy in the tender descender unless a second one is placed in series, which doubles cost. The team's mentors have also mentioned that the tender descender is not always effective in deploying the main parachute from the deployment bag.

The Jolly Logic chute release is a similar mechanism for deploying two parachutes from the same compartment within the rocket. It features its own atmospheric pressure sensor and can be set to deploy at 100-foot increments from 100 to 1,000 feet above ground level (AGL) during descent. When it registers the selected altitude, it will unlatch a key and allow the main parachute to unravel and deploy. A picture of the assembled layout is shown below [8].

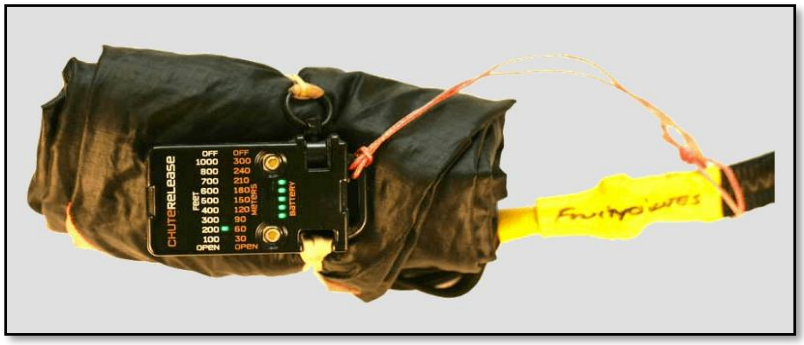

Figure 91 - Jolly Logic chute release assembled to a parachute

Benefits of the chute release system include the same reduced space as the tender descender and no additional altimeters or deployment charges. However, this design does not have a redundancy feature either, unless a second chute release is placed in series. Per the team's mentors, the chute release also works about 50% of the time, similar to the tender descender, with locking issues on the key prohibiting unraveling of the parachute.

4.6.3 Third Electronics Bay

The final potential solution the team examined was a third electronics bay for rocket separation. Utilizing just two electronics bays, one electronics bay on the 2nd stage rocket for dual deployment as indicated in the diagram above, along with one more for the first stage

rocket, would leave the design with two options: deploy the first stage drogue parachute at stage separation, when the booster stage is still traveling at nearly 600 ft/s which could tear the drogue apart, or incorporate one of the two previously mentioned main parachute delay systems to place both parachutes in the same compartment of the rocket which multiple rocket hobbyists have warned could be ineffective methods.

The final option is to include a third electronics bay in the rocket to incorporate a dual deployment layout in both stages, while still separating the two stages without deploying a parachute. A concept sketch of this layout is depicted below along with a sequence of events for the booster on the right side of the diagram.

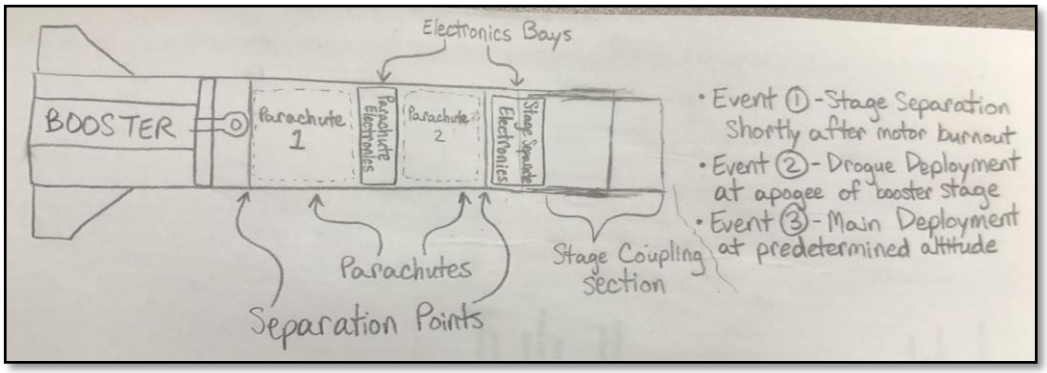

Figure 92 - Third electronics bay concept sketch with booster staging events

This design allows the team to utilize the conventional dual deployment parachute ejection method with a much higher reliability of parachute deployment than the other two options. Additionally, it can be ground tested prior to flying the rockets and risking the recovery. Adding two additional altimeters for $50 each is also a fraction of the $130 per unit of the tender descender and chute release systems. The negative to a third electronics bay is the added length and weight to the rocket, but the team believes this is a small price for a safe parachute deployment.

The first design iteration had the drogue parachute deploying at stage separation from within the stage coupling section and only including one electronics bay in the first stage. After realizing that the rocket was still traveling at a high velocity at stage separation, it was determined that the drogue parachute needed to be relocated. Based on this realization, the team dove into the pros and cons of the three deployment options listed above. A pros-cons list is outlined below as a reference for all three systems.

Parachute Deployment Methods & Layouts Pros & Cons

	Tender Descender	Jolly Logic	Third Electronics Bay
Pros	• Reduced space	• Most reduced space • No additional altimeters	• Conventional dual deployment • Team experience • Testable without a test flight • $50 per unit
Cons	• Works “50-50” per	• Works “50-50” per	• Additional Length

	team mentors • No redundant charges • $130 per unit	team mentors • No redundant charges • $130 per unit	• Added weight

Table 15 - Parachute deployment methods and layouts pros and cons

The sustainer ignition avionics must control the ignition of the second stage motor based on competition and team requirements. These requirements are extremely critical to the safety of the flight. The ability to adjust the timing of the ignition incrementally would increase the ability to optimize the altitude as mentioned in the Sustainer Separation & Ignition Timing section. The following sections outline the selection process for the components, the useful parameters of the selected components, additional features included to meet specific requirements, and the safety critical wiring solutions.

The tiltmeter is a critical component with regards to sustainer ignition and overall safety of the rocket over the course of flight, as it is used to determine the angle that the rocket is flying prior to igniting the second stage motor. The main characteristic that differentiates a tiltmeter from an altimeter is the addition of either an accelerometer or a gyroscope, which allows for the unit to account for the angle of the launch vehicle with respect to the calibrated vertical orientation. After researching available options, three units were compared to be used on the rocket: RocketTiltometer, TeleMega and EasyMega.

A RocketTiltometer was presented to the team by the team's mentor, Steve Eves, as he had successfully used the device for his multistage project. The device was reviewed with all available manuals but was not chosen because the manufacturer was no longer supporting the unit. The team had difficulties communicating with the unit due to lack of support online and the user manuals were not helpful to verify functionality. The unit is shown below.

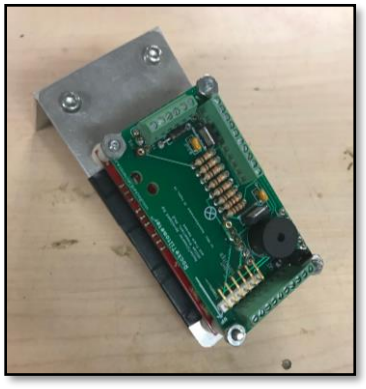

Figure 93 - Rocket Tiltometer

The TeleMega and EasyMega were found via Google search and are widely used both by NAR certified rocketeers and other university rocket design teams. Both are currently manufacturer supported by AltusMetrum. They can sense advanced parameters in flight such as a specific altitude, velocity, acceleration, or angle from vertical, as well as other settings.

Both have up to six pyro channels for different events: one for drogue parachute deployment at apogee, one for main parachute deployment at a specified altitude during descent, and four for independent events such as a sustainer motor ignition. They are nearly identical units with the only difference being that the TeleMega includes a GPS unit that requires ham radio certification for an additional $100. A photo of the $400 TeleMega is shown below.

Figure 94 - AltusMetrum TeleMega

The EasyMega costs $300 and does not include the GPS unit. Since the team already had a working GPS solution for both stages of the rocket, the team decided to dedicate the tiltmeter functionality to controlling second stage ignition by selecting the EasyMega tiltmeter. Keeping the GPS separate from the tiltmeter provides some separation of tasks between the electronic components. If the newly acquired tiltmeter were to malfunction, the currently functional GPS unit could still track the rocket through flight and recovery. A pro-con chart is shown below to summarize the three options that were reviewed.

Tiltmeter Pros & Cons

	RocketTiltometer	TeleMega	EasyMega
Pros	• Free to borrow • Mentor has experience with it	• Six pyro channels • Advanced parameter selection • Includes GPS unit	• Six pyro channels • Advanced parameter selection
Cons	• Manuals were difficult to interpret • No longer manufacturer supported	• $400 • GPS unit tied to tiltmeter functionality	• $300

Table 16 - Tiltmeter pros and cons

4.7.2. EasyMega Functionality

After selecting the AltusMetrum EasyMega tiltmeter for controlling the second stage ignition. The team looked to review the applicable settings and determine a set of constraints that would allow for a safe and successful flight.

The team was able to communicate with the unit using software provided by AltusMetrum online. The optional parameters include boundary conditions such as height above the pad, angle from vertical, time since launch, and vertical acceleration. The EasyMega has a built-in

software interface which allows for the boundary conditions to be entered into each cell corresponding to the given parameter. There is capacity for four pyro channels to be used, which allows for redundancy when firing the sustainer ignitors. An example of the pyro channel configuration showing all available parameters is shown below. All the selected parameters must be true for the igniter to fire.

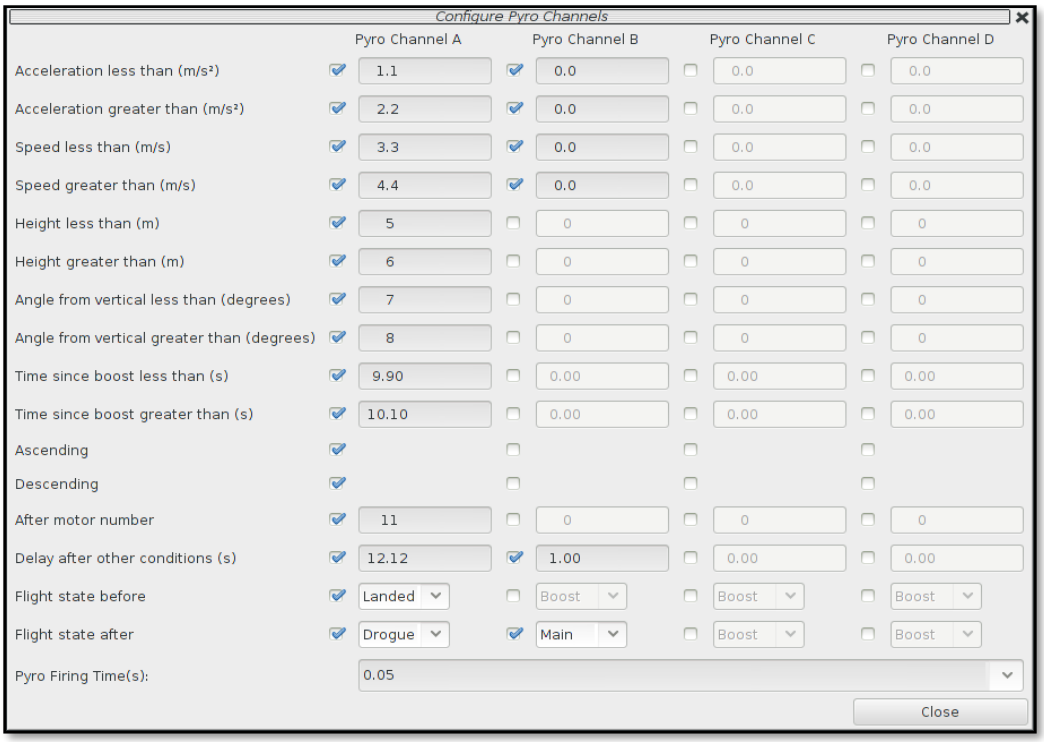

Figure 95 - Example pyro channel configuration

The EasyMega also has channels to fire a drogue and main parachute, at apogee and a specified altitude on descent, respectively. These could be used in place of an altimeter or in addition to an altimeter if desired. For simplicity, the team will focus on using the tiltmeter solely for second stage motor ignition. The team is hoping to utilize one or two of the four pyro channels for firing the second stage motor and wire them down to the base of the motor as mentioned in the Sustainer Avionics Wiring section below. A photo of the EasyMega tiltmeter is shown below.

Figure 96 - AltusMetrum EasyMega

Considering the optional parameters for sustainer ignition, the team identified four key parameters to meet competition and team requirements and ensure a safe and successful flight. These four parameters include “height greater than ‘z’”, “angle from vertical less than ‘a’”, “time since boost less than ‘y’”, and “time since boost greater than ‘x’”.

It should be noted that time since boost refers to the tiltmeter sensing the ignition of the first stage motor, so the delay times considered in the Sustainer Separation & Ignition Timing section should be added onto the first stage motor burn time to produce the values input into the tiltmeter. OpenRocket was only capable of inputting the delay times since motor burnout so the simulations were run with this base point for delays.

IREC requirements state that the flight computer controlling air-start ignition must be able to detect booster motor burnout and that the rocket has reached an altitude of at least 80% of the simulated altitude at the time when initiator firing is desired. This requirement will ensure that the motor does not fire prematurely and cause issues mid-flight. After speaking with IREC judges, the booster motor burnout requirement is met with the other configuration settings imposed, such as time since boost, since the team is accounting for the booster motor burn time. There is a specific setting to account for the phase of flight being after first stage motor burnout if that is desired in the future.

The 80% altitude requirement can be met by simulating the rocket’s flight with the desired delay times and finding the altitude at sustainer motor ignition in OpenRocket or RASAero II. Inputting 80% of this altitude into the “height greater than ‘z’” field will ensure the rocket is at least 80% of the simulated altitude for sustainer ignition. This height is about 1,578 m based on the most-recent simulations, but varies significantly based on the stage separation and sustainer ignition timing delays.

Next, the team has a self-imposed team requirement for angle from vertical being less than 20 degrees. This requirement will ensure the flight is stable prior to igniting the sustainer motor. If the angle were greater than 20 degrees, the rocket would veer off and fly very far away from the launch site, making it difficult to reach a scoring altitude range or even successfully recover.

Inputting 20 degrees into the “angle from vertical less than ‘a’” field will impose the angle requirement on the tiltmeter.

The final two requirements deal with time since boost. Together they should create a range of time during which the booster motor can fire if the other two conditions are also met. The requirement for “time since boost greater than ’x’” refers to the delay time simulations for sustainer ignition. This input field will detect the beginning of the range for acceptable ignition times, which the team found to be around 5-8 seconds after booster motor burnout. As previously mentioned, the burn time for the first stage motor will be added to this since the tiltmeter begins the timer at booster ignition, and the 2 second pressure build time for the CTI N1100 motor will be subtracted from this time to achieve ignition at the desired time per IREC judge recommendations. Launch day conditions will narrow down the exact ‘x’ value to input for the beginning of the time range.

Lastly, the end of the time range is controlled with the requirement for “time since boost less than ‘y’”. This parameter is imposed to close the window on the potential sustainer ignition for safety purposes. One can envision a scenario without this requirement, where the rocket is launched and is flying at an angle of around 21 degrees off vertical. Since the angle requirement is not met, the sustainer motor will not ignite. However, the rocket will separate as desired using the MiniTimers and once apogee is reached for the second stage, the parachute will be released, and the rocket will orient closer to vertical. Without this requirement for closing the time range, the sustainer motor will ignite with the drogue parachute deployed, which could lead to a catastrophic flight and loss of the motor section of the rocket when the shock cord is ripped off. For this reason, the end of the time range requirement was imposed. Originally, the team selected a time of 25 seconds to close the sustainer ignition window, since the sustainer stage was not expected to reach apogee until well after 25 seconds even if the sustainer motor did not ignite. After reviewing with IREC judges, a lower time around 8-10 seconds was suggested in case there was an unstable flight up to apogee that would cause the drogue to deploy prior to 25 seconds of flight time. The team would like to keep the window open as long as possible that does not hinder safety requirements. This would give the most time possible for the sustainer motor to ignite if there were any issues or inaccuracies in the predicted simulations, such as the 80% altitude. The team hopes to review the timing with IREC judges before the competition flight but is looking at closing the flight window around 10-15 seconds of flight time, if allowed. The suggested flight parameter configuration for the full-scale rocket is shown in the picture below. It is subject to change through manufacturing and launch day conditions.

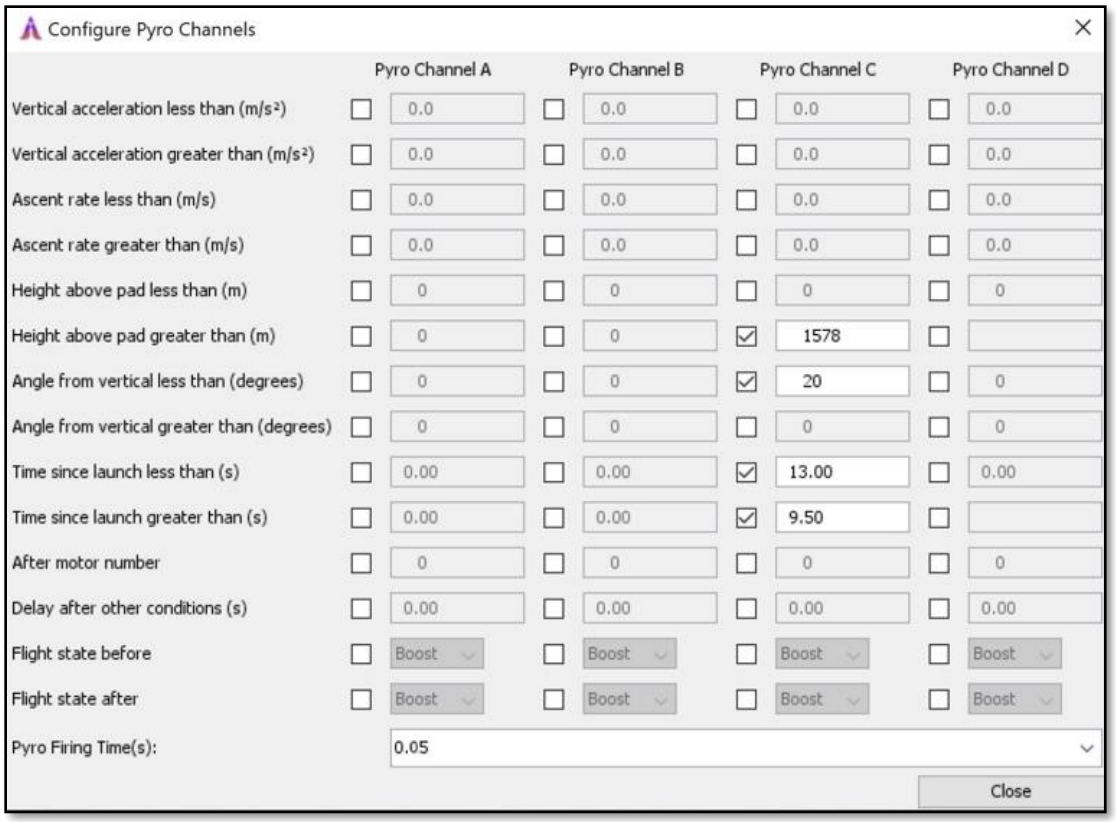

Figure 97 - Suggested full-scale pyro channel configuration (subject to change as the design develops)

Overall, the team was able to identify the key parameters for the tiltmeter and how to apply them in the software. The team successfully tested each setting individually to verify the intended functionality with the help of two rocket team members. The results of the testing are outlined in the Testing section of the report. These parameters will ensure a safe and successful flight of the rocket by following all team and competition requirements.

4.7.3 Sustainer Ignition Arming

IREC requirements also mandate that the sustainer igniter be capable of having an open circuit even after power on of the tiltmeter. There are two options for ensuring this requirement is met: a shunt system or an additional switch to arm the igniter. The cause for this concern stems from other two-stage rocket's sustainer motors firing while on the launch pad. The likely cause of early ignition is moving the rocket vertically on the pad after arming the electronics or using only a timer to fire the second stage. Once the accelerometer senses vertical acceleration, the timing sequence initiates and the sustainer motor fires once the input time has been reached, which could fire the sustainer motor while still on the launch pad with personnel in the area. This is another reason for the 80% altitude requirement mentioned above.

A shunt would act as an additional safety measure when arming the sustainer motor. It is designed to redirect current around an existing point in the circuit by introducing a low resistance path for the current to follow. The shunt would be implemented to redirect current from the sustainer ignitors to a current sink, which would prevent the sustainer motor from igniting until the wire or shunt is removed from the system. Placing it in the circuit would prevent the accelerometer from functioning until the shunt is pulled and the igniter receives current, thus

not allowing the sustainer motor to ignite until all other controls are in place. However, the team does not have experience with shunts and could not find a mechanical system to safely and effectively implement before it was realized that a switch would work as well.

The other option for opening the circuit is a two-pole rotary switch like those used for all switches in the rocket. A photo of the switch is shown in the Recovery Systems section. The team has experience using these switches and they meet the arming requirements for the competition. After speaking with IREC judges, they recommended one switch to turn on the tiltmeter and a separate switch to close the igniter circuit once the rocket is ready for launch. The team implemented this solution for the subscale model which is shown in detail in the Subscale Manufacturing section.

Due to the selection of a black powder separation system between the two stages, the 2nd stage motor igniters can be subject to a high amount of heat that could burn the wires if not protected. This could cause the second stage motor to not ignite at all or to ignite based on the stage separation, which would mean the tiltmeter safety restrictions are bypassed. Additionally, the wire management of the igniters from the tiltmeter located just above the motor to the base of the motor must be reviewed so that the assembly process is simple enough to complete in a short time.

Several options exist for heat-resistant wiring based on the wire size and expected temperatures. The black powder ejection temperature varies based on the amount of black powder present and the distance between the charges and the point of interest, so it can be difficult to determine. An easy solution would be a heat-resistant barrier or a heat sleeve for the wire. In the past, the team has used Kevlar to protect the parachutes from black powder heat which has burned holes through the chutes. Two common heat-resistant materials used commonly in aerospace wiring applications include Tefzel and Kapton. Tefzel wire [1] and Kapton tape [16] can be found for under $30 with temperature ratings of 300°F and 500°F, respectively, which should easily survive the expected temperatures. Photos of the Tefzel wire and Kapton tape are shown below.

Figure 98 - Example commercial tefzel wire

Figure 99 - Example commercial Kapton tape

Another thermally insulating option used commonly for thermocouples and general wire insulation is fire sleeve. It comes in tube insulation form or a silicone-based tape. The tape bonds to itself and can withstand 500°F [12]. The tubular insulation is made from fiberglass on the inside coated on the exterior with a silicone rubber [2]. This could be a valuable option for shock cord protection on the parachutes as well. A photo of this insulation material is shown below.

Figure 100 - Example commercial fire sleeve

The team also wants the igniter to be instantaneous in action, igniting as quickly as possible after reading the signal from the tiltmeter, since any unaccounted delay time will reduce the altitude achieved and possibly allow the rocket to tilt over the maximum allowable angle threshold. It is common in model rocketry to dip igniters in pyrogen for improved effectiveness, something the team's mentors have done in the past. Another potential igniter material is MTV (Magnesium Teflon Viton) which has high energy density and is sensitive to thermal ignition. This could be an issue of igniting the 2nd stage motor using the black powder separation charge, although the igniter should be packed a few feet into the 2nd stage motor, making this a very minimal concern. The nozzle of the motor will be taped off to prevent exposure to black powder as well. MTV igniters would also need to be custom-manufactured and manufacturing techniques have been limited via web search. Chris Pearson mentioned a mixture of magnesium, plasti-dip, zirconium, titanium, and potassium nitrate as an igniter solution that ignites instantaneously. The team will work with Chris as the competition date approaches to gather a better understanding of the igniters he uses.

For ease of assembly on launch day, the team would like to implement a wiring solution to avoid wiring the igniters from the bottom of the rocket, around the motor, through several centering rings, and into the avionics bay above the motor. A concept sketch of the initial setup is shown below.

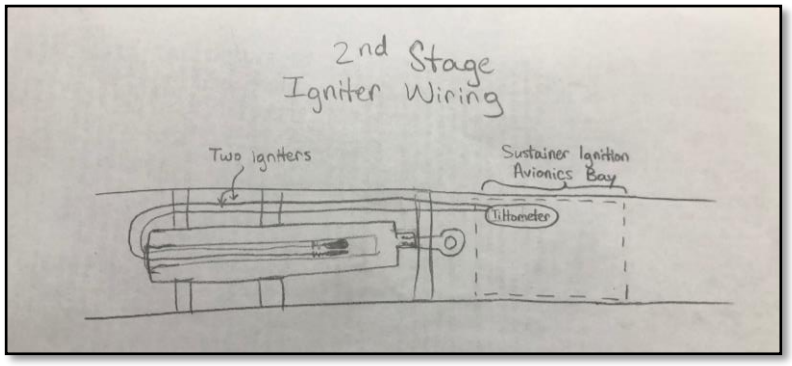

Figure 101 - Sustainer igniter wiring initial concept sketch

Potential solutions the team examined included cannon plugs, banana plugs or a similar plug in cable, and a terminal block. Placing a jointing feature near the bottom of the rocket would allow for ease of launch day assembly of the igniters on the launch pad. IREC does not allow igniter wiring until the rocket is on the launch pad, so a simpler solution was necessary. Based on familiarity and simplicity, the team is moving forward with a terminal block layout as depicted below. This allows the tiltmeter to wire to the terminal block permanently during initial assembly. On the launch pad, the team will be able to hook up the igniter wires through an access hole in the airframe or from the bottom of the 2nd stage before coupling them together.

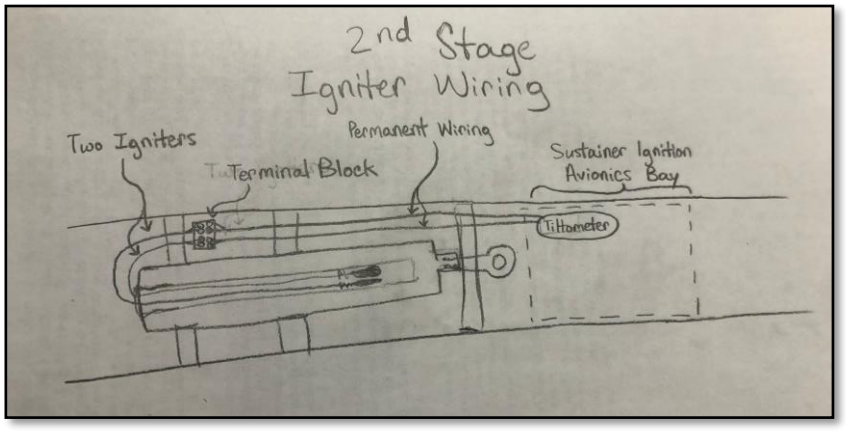

Figure 102 - Sustainer ease of assembly igniter wiring concept sketch

Lastly, the separation bay below the 2nd stage motor needs to be pressure-sealed to ensure stage separation. Electrical tape or plumbers' putty have been commonly used for sealing deployment bays in the past for the team. However, the bottom centering ring for the motor will need to be sealed in this bay as well. This could drive the fin attachment design to enable pressure sealing on the bottom surface without gaps or openings.

Overall, the team identified several wire management and wire protection solutions for safely wiring the sustainer igniters. In addition, the team discovered an igniter composition for a quick ignition for the second stage motor. These solutions will help ensure the safety of the sustainer motor wiring as well as the proper ignition of the motor itself.

5.1

Although the recovery systems were not the focus of the senior design project, the team acknowledged that these items needed to be selected to round out the entire vehicle design. The team focused on choosing items that have been used by the team frequently and/or that the team is confident will perform as expected. The recovery systems outlined in the following sections are all safety-critical and any non-functional element could correspond to a crashed rocket, so careful selection of items with high confidence of success was important. One additional feature examined for the recovery system is the ability to turn on the components at the launch pad for safety and battery life concerns.

5.1.1

Rocket altimeters are typically comprised of electrical components including a barometric sensor which converts pressure readings to altitude. They are mainly used for recording altitude during flight and initiating key events such as the deployment of parachutes. The team has used the PerfectFlite StrattologgerCF altimeter in the past with high success rate and feels comfortable using the altimeter for parachute deployment for the two-stage rocket. A photo of the altimeter is shown below [29].

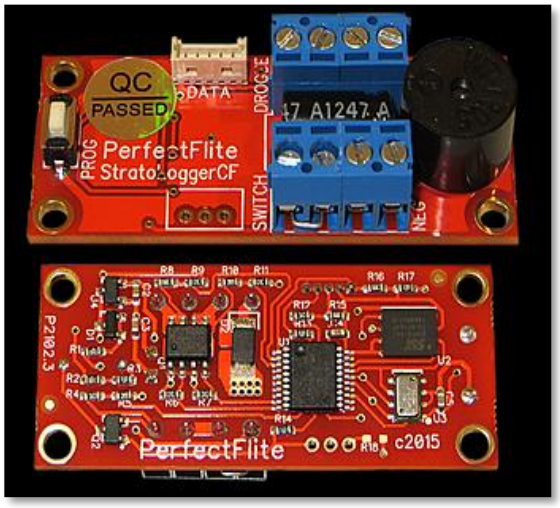

Figure 103 - PerfectFlite StrattologgerCF altimeters

The altimeters can be powered by a 9V battery for over 5 hours which is sufficient for turning them on at the launch pad and waiting for flight. IREC commonly refers to turning the altimeters on as “arming” them since they will eventually send a signal to ignite a small black powder explosion. The longest the team has had to wait between arming the altimeters on the pad and launching is about three hours, but it is usually within one hour.

To be able to turn the altimeters on at the launch pad, the team typically uses two pole rotary switches with a hole in the airframe to flip the switch with a small flathead screwdriver. This not only saves battery life compared to arming them during assembly, but also meets IREC safety requirements of arming the altimeters only when the rocket is on the launch pad. A photo of the two pole rotary switches is shown below [21].

Figure 104 - Commercial two-pole rotary switch

In the altimeter photo above, one can see the blue terminal blocks labeled for “SWITCH” and “NEG” which correspond to the switch and battery wiring, respectively. Only the battery wiring matters for polarity, so the negative wire will hook up to the block closest to the “NEG” label. The rotary switches have solder connections on the backside as shown. For simplicity, the team will stick with 22 AWG wire which is standard for all the rocket team’s electronics bays utilizing these components.

The StrattologgerCF altimeter has two additional terminal blocks opposite the switch and battery blocks. These correspond to the drogue and main parachute deployment wiring. Nonpolar electric matches can be inserted into these terminal blocks and wired to the black powder charges to deploy each parachute. The deployment altitudes and timings can be pre-programmed in the computer software before flight. For simplicity, the team will stick with deploying each drogue parachute at apogee of its corresponding stage and each main parachute between 500-1,000 feet above ground level during descent. The main parachute deployment altitudes will depend on wind conditions and drift for the parachutes on launch day. A simple, color-coded wiring diagram for the altimeter circuit is shown below.

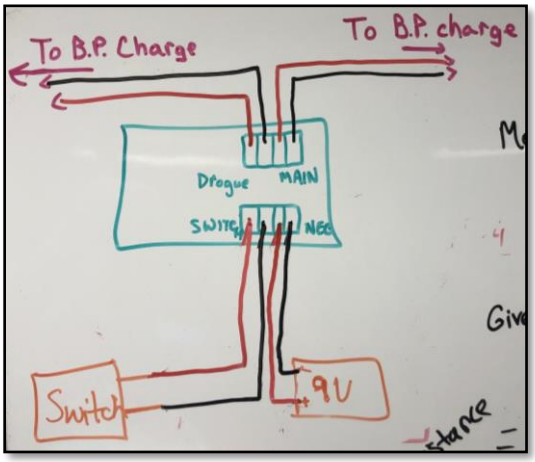

Figure 105 - Altimeter wiring diagram

Some additional important characteristics of the chosen altimeter are that it can record data up to 100,000 feet and it comes with a MachLock feature. The 100,000 feet is well-above the intended target altitude around 30,000 feet. The MachLock feature is an important safety feature that accounts for “Mach dips” corresponding to a sudden rise in pressure when the rocket reaches the speed of sound. This safety feature is intended to keep the drogue parachute from deploying early.

The team originally planned to use the same altimeters for stage separation. However, the altimeters can only be programmed to deploy at or around apogee for drogue parachute and at some predetermined altitude during descent for main parachute. For this reason, the team needed to investigate another deployment device for separating the two stages during the ascent phase of flight. Luckily, the altimeter manufacturer had another product that could fit the needs of stage separation: the MiniTimer4. A photo of this timer is shown below [20].

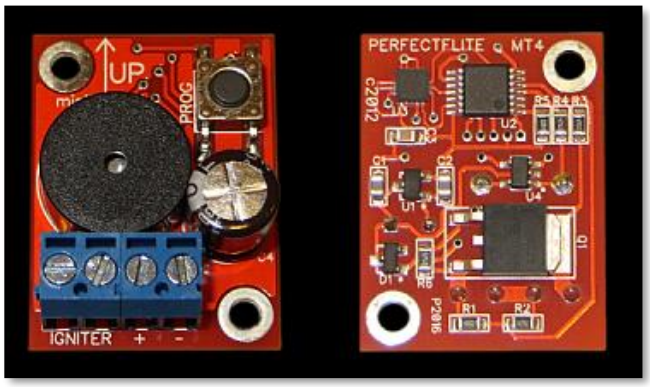

Figure 106 - PerfectFlite MiniTimer4s

This timer looks like a smaller version of the altimeter and must be mounted in this orientation in the rocket to align with the path of travel. The timers can be set to send a signal to an igniter at a predetermined time after sensing takeoff of the rocket. They can be set in increments of 0.01 seconds. This can allow the team to control the stage separation time of the rocket as outlined in the Sustainer Ignition Timing section. The igniter terminal block runs to the black powder charge to separate the two stages and the battery terminal block is wired to a switch and 9V battery as shown below. The same 9V battery should be sufficient for a similar battery life as the altimeters.

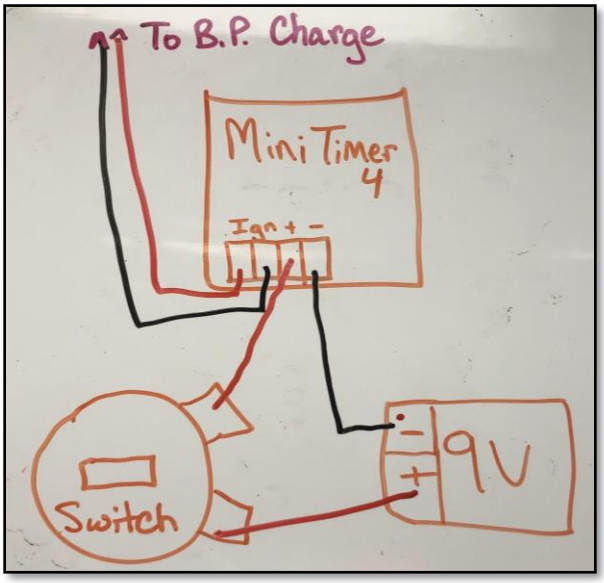

Figure 107 - MiniTimer4 wiring diagram

IREC requires that each stage of the rocket include a GPS unit for tracking it after it lands. The team has utilized the Featherweight GPS Tracker in the past with great success and will utilize it in this rocket design as well. It comes with its own 3.7V LiPo battery and can be wired to a two-pole rotary switch to arm it on the launch pad. This should have over 5 hours of battery life, as well. A photo of the Featherweight GPS is shown below [14].

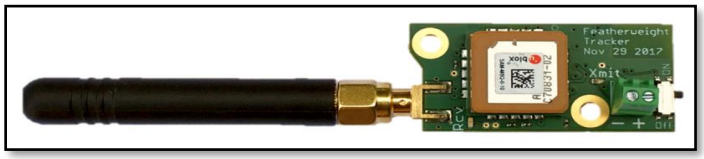

Figure 108 - Featherweight GPS

The senior design team utilized the rocket design team's recovery subsystem members to help size the parachutes for the rocket. They typically manufacture their own parachutes for exact sizing which have been used successfully in many previous rockets. The key characteristics for their parachute designs focused on descent velocity, drift distance under various wind speeds, and kinetic energy at landing to keep the rocket safe during the recovery phase. The final parachute sizes will depend on exact weights of the manufactured full-scale rocket, but estimates were derived from component weight estimates for simulation analysis.

5.5. Ejection Systems

The rocket team has utilized black powder ignited by electric matches for separating sections of the rocket almost exclusively throughout the years. It is simple and functions as expected if the amounts of black powder are ground tested prior to launch. One downside is that black powder can be corrosive to electronics, so the team must ensure it does not encounter any of the electronics throughout the assembly or flight. It is also critical that the deployment compartments in the rocket are pressure-sealed so the small explosion can build up the desired pressure to break the shear pins and separate the rocket. Shear pins are plastic screws to hold the rocket together at separating sections until the black powder charge in that compartment ignites and breaks them.

IREC has requirements for redundant recovery electronics as well, meaning there must be a backup system in place for every recovery event. This has been standard for all Akronauts competitions and the team has used two parallel altimeter circuits with separate 9V batteries, rotary switches, and black powder charges. The team will utilize a similar design for all recovery events and the stage separation event. Overall, the current design features four altimeters, two MiniTimer 4s, and two GPSs, along with the tiltmeter for sustainer motor ignition. All these items can be armed from the exterior of the rocket on the launch pad using a total of ten switches with two being dedicated to the tiltmeter.

6. Flight Predictions

The flight predictions included in the following sections were conducted with the most up-to-date simulations for accuracy. The importance of these flight predictions sections is to discuss the software configuration for simulating a flight, document the important flight characteristics between all three software in one location, and outline the stability margin of the rocket. Laying out the software configuration will help future readers understand the importance of the detailed simulation settings in producing a valid flight simulation. Additionally, having a simple breakdown of the flight characteristics is important to comparing the software based on the flight results. Finally, the stability margin has been referenced in several sections as a basis for design considerations. Generating an overview of the stability margin of the rocket and how it is calculated in the various software will help future readers understand its importance and explain its use as a driving factor in several design decisions.

6.1. Software Configuration

This section's purpose is to describe the team's flight settings specific to the two-stage rocket to be used at competition and outline how to adjust them in the different applications. The software configuration settings are important to a valid flight simulation. Ignoring any of the following settings or not considering the impact of them can produce an inaccurate depiction of the expected flight or give confidence to a faulty flight set up.

Overall, these software configuration settings are extremely important to a valid flight simulation, especially for a multistage rocket. Ignoring any of the settings mentioned below or not considering the impact of them can easily produce an inaccurate flight simulation which could result in a crashed rocket. They should be taken into consideration and reviewed thoroughly in the flight analysis leading up to competition.

6.1.1. OpenRocket Iteration

Firstly, the stage separation and sustainer ignition settings should be outlined since this is the team's first time using these conditions. Below is the OpenRocket display window within Motors & Configurations under the Stages tab which shows the various rocket motor configurations as well as the stage separation time for the booster stage. As shown, the current stage separation is set to booster stage motor burnout plus 6 seconds.

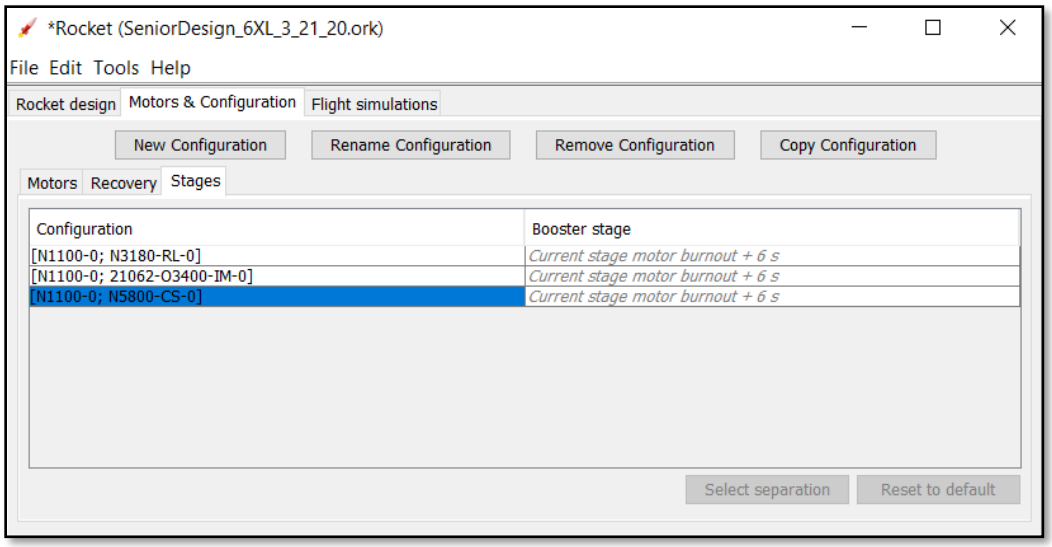

Figure 109 - OpenRocket Motors & Configuration tab

By clicking the button “Select separation” a window will appear as shown below to adjust the flight configuration with the delay time in increments of 0.01 seconds. The option also exists to vary the reference point for the time delay, but the team used the current stage motor burnout reference point as a standard to avoid factoring in the motor burn time.

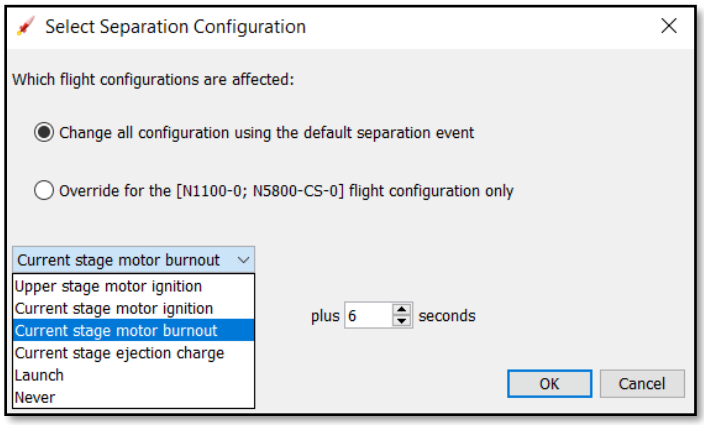

Figure 110 - OpenRocket Separation Configuration window

With the stage separation delay set, the next adjustment will be sustainer ignition delay time. Maneuvering to the Rocket design tab, selecting the Sustainer Body Tube, and maneuvering to the Motor tab will display the following window. Note that the Sustainer Body Tube is just the motor mount tube for the sustainer motor, which is set previously. In this window, the important new features are the delay time, which is currently set to plus 8 seconds and can be varied in increments of 0.01 seconds, and the reference point dropdown box for the ignition reference point. For consistency, the team used the first burnout of the previous stage, which is the booster stage in this case. With these settings configured correctly, the flight simulations are ready to be conducted.

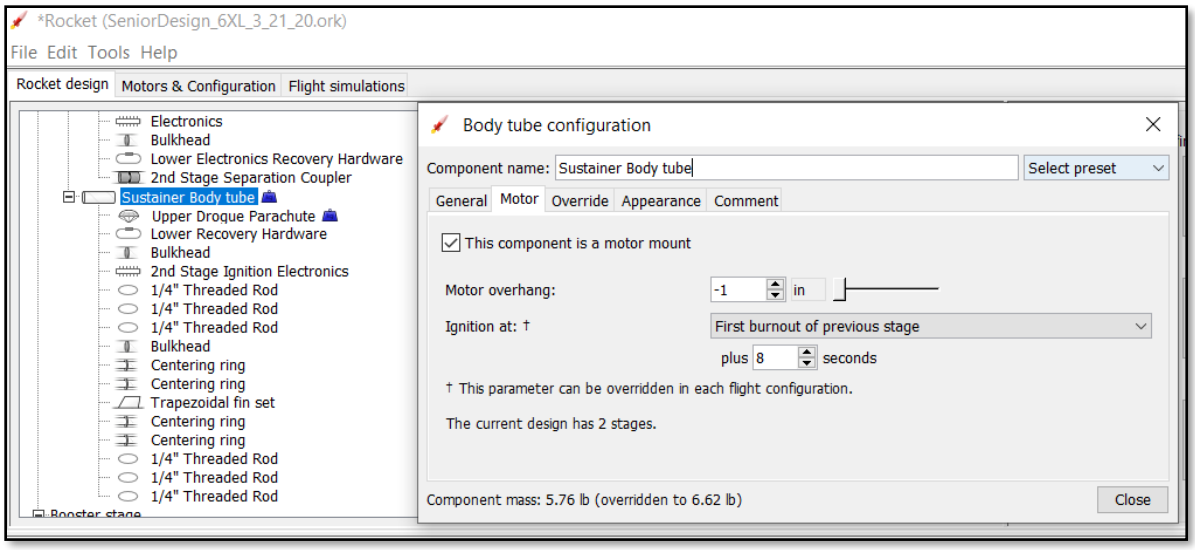

Figure 111 - OpenRocket Body tube configuration Motor tab

For all simulations, the team used a standardized set of conditions, shown below, to mimic a launch at Spaceport America for competition. These settings can be adjusted similarly in all three software. For several of the simulations, the average windspeed was varied between 0-20 mph, in increments of 5 mph, providing a range of projected maximum altitudes, drift distances, maximum velocities, etc. The following sections depict the flight for 10 mph wind speeds as a baseline. The launch rod length of 17 feet and the rail angle of 3 degrees from vertical are based on IREC requirements for multistage projects while the atmospheric conditions are estimates based on previous launches at the same location. The launch site specifications are based on the Spaceport America launch site near Las Cruces, New Mexico.

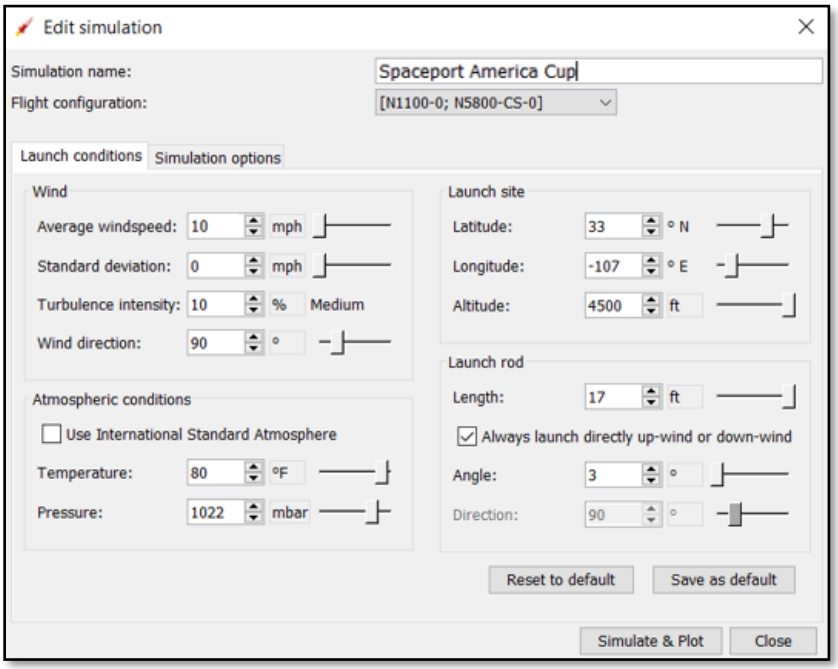

Figure 112 - OpenRocket Launch Conditions

After clicking the Simulate & Plot button, the following window will be opened. Within the Plot tab is a dropdown box for plot configurations that can show various plots through flight and can vary the x- and y-axis characteristics. In the dropdown box, the common plots the team considered for this project were Vertical motion vs. time, Ground track, and Angle of attack and orientation vs. time. These plots corresponded to producing the altitude, drift distance, and vertical orientation values that were used for the analysis of the stage separation and sustainer ignition delay times. Other common plot configurations the team uses frequently include Stability vs. time and Drag coefficients vs. Mach number. Values shown in the following sections were pulled from these graphs. As shown, there is also an Export data tab, which was used to export flight data to Excel for max dynamic force analysis.

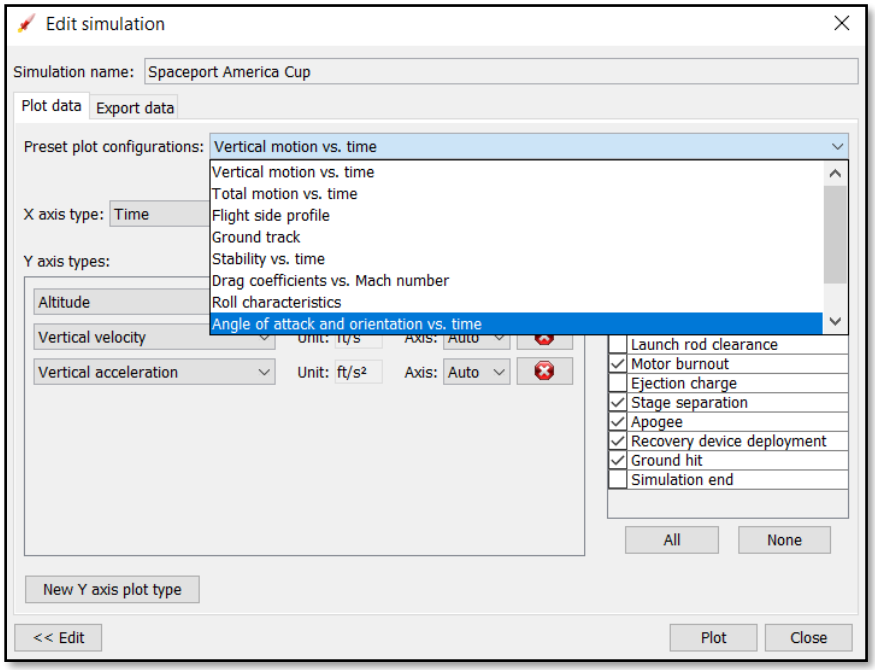

Figure 113 - OpenRocket Plot data tab

6.1.2. RASAero II Iteration

Like the OpenRocket configuration shown above, the stage separation and sustainer ignition settings and launch conditions for RASAero II are outlined below. The first window, shown below, is the “Flight” tab, which can be opened by selecting the “Flight Simulations” on the main page. The Flight tab displays all motor configurations as well as the max altitude, max velocity, and time to apogee. A nice feature of this tab is all simulations can be run simultaneously and output the three metrics mentioned previously in the same window. More detail about the data can be accessed by selecting the “View Data” button in the figure below.

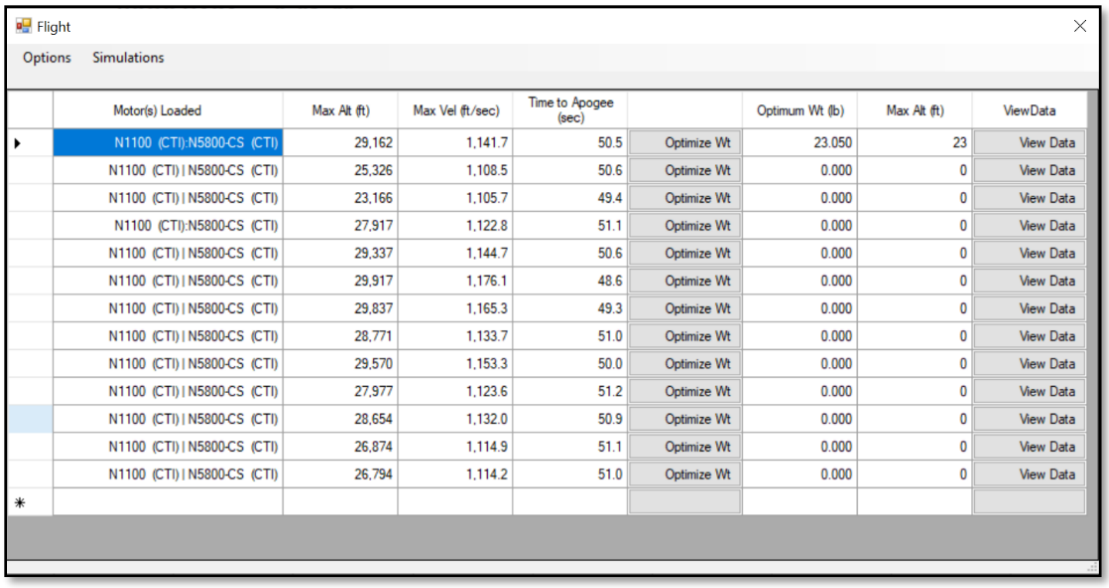

Figure 114 – RASAero II Motor Configuration tab

By double clicking on a configuration in the “Motor(s) Loaded” area shown in the “Flight” window above, the “Flight Data Entry” window shown below will open. In this tab, the booster and sustainer motor files can be selected. Be sure to check the “Include Booster” box. On the right, the weight and CG for both portions can be entered as well as any delay time for the stage separation and ignition delay. Once all configurations are set, be sure to save before exiting the window.

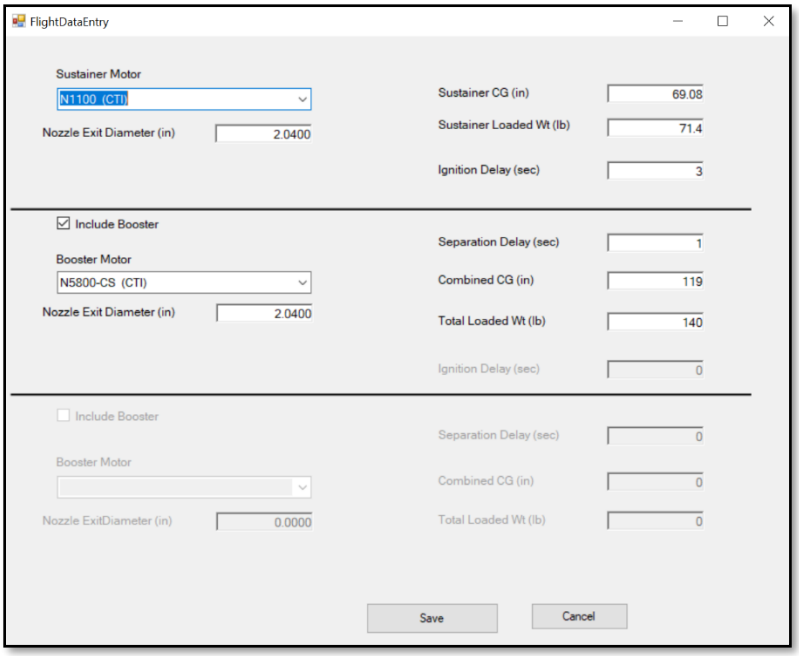

Figure 115 –RASAero II Motor Configuration

By clicking on the “View Data” button in the “Flight” window shown above with the listing of flight configurations, a graph for the selected scenario will be opened. The graphs shown below

are generated using the “Flight Data Entry” window shown above, which means stage separation time will be 1 second and ignition delay is 3 seconds. The first figure shown below is the display that opens after selecting “View Data”. Time is at zero and the “Stage” column shows “B” which signifies booster motor.

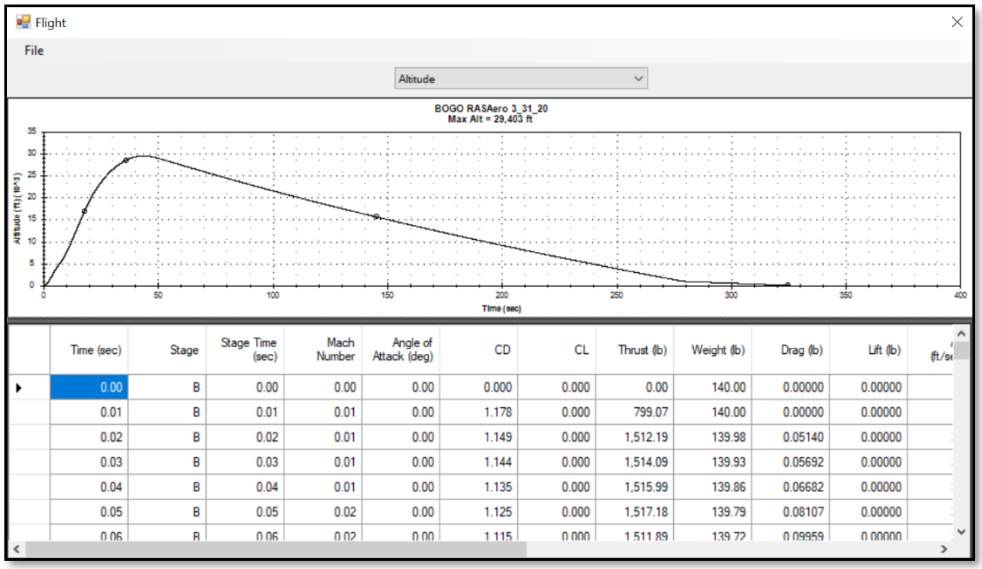

Time (sec)	Stage	Stage Time (sec)	Mach Number	Angle of Attack (deg)	CD	CL	Thrust (lb)	Weight (lb)	Drag (lb)	Lift (lb)
0.00	B	0.00	0.00	0.00	0.000	0.000	0.00	140.00	0.00000	0.00000
0.01	B	0.01	0.01	0.00	1.178	0.000	799.07	140.00	0.00000	0.00000
0.02	B	0.02	0.01	0.00	1.149	0.000	1,512.19	139.98	0.05140	0.00000
0.03	B	0.03	0.01	0.00	1.144	0.000	1,514.09	139.93	0.05692	0.00000
0.04	B	0.04	0.01	0.00	1.135	0.000	1,515.99	139.86	0.06682	0.00000
0.05	B	0.05	0.02	0.00	1.125	0.000	1,517.18	139.79	0.08107	0.00000
0.06	B	0.06	0.02	0.00	1.115	0.000	1,511.89	139.72	0.09959	0.00000

Figure 116 – RASAero II Flight Data

The figure shown below shows the stage separation. For reference, the burn time of the booster motor is 3.60 seconds, thus using a 1 second stage separation delay will cause the rocket to separate 4.60 seconds into flight. The “Stage Time” column then resets to 0 seconds.

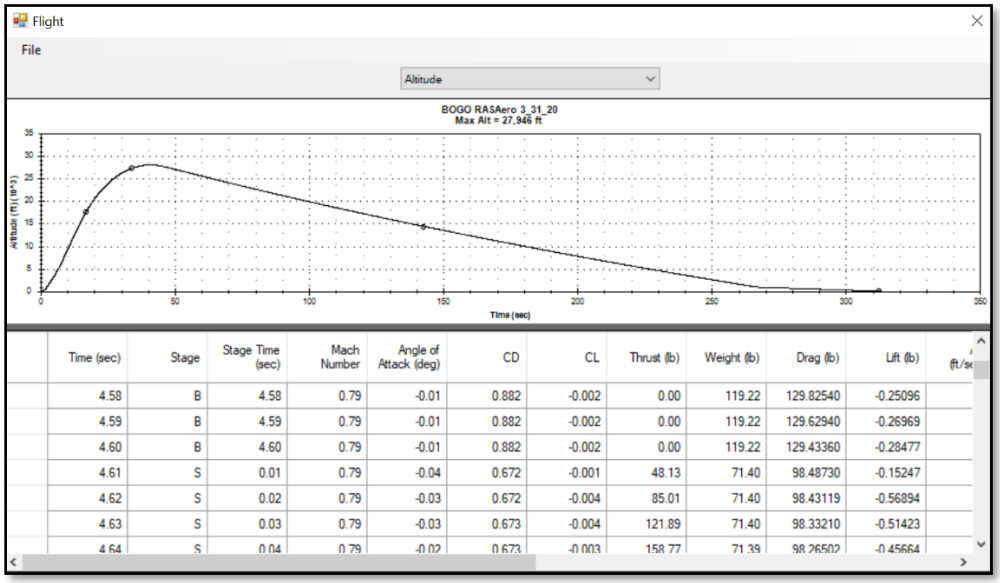

Time (sec)	Stage	Stage Time (sec)	Mach Number	Angle of Attack (deg)	CD	CL	Thrust (lb)	Weight (lb)	Drag (lb)	Lift (lb)
4.58	B	4.58	0.79	-0.01	0.882	-0.002	0.00	119.22	129.82540	-0.25096
4.59	B	4.59	0.79	-0.01	0.882	-0.002	0.00	119.22	129.62940	-0.26969
4.60	B	4.60	0.79	-0.01	0.882	-0.002	0.00	119.22	129.43360	-0.28477
4.61	S	0.01	0.79	-0.04	0.672	-0.001	48.13	71.40	98.48730	-0.15247
4.62	S	0.02	0.79	-0.03	0.672	-0.004	85.01	71.40	98.43119	-0.56894
4.63	S	0.03	0.79	-0.03	0.673	-0.004	121.89	71.40	98.33210	-0.51423
4.64	S	0.04	0.79	-0.02	0.673	-0.003	158.77	71.39	98.26502	-0.45664

Figure 117 – RASAero II Stage Separation

The figure shown below shows the ignition of the sustainer motor. With an ignition delay of 3 seconds, anything before 3.0 seconds should have zero thrust. Once the sustainer motor ignites

after the input delay time, the motor burn will be initiated and thrust will be applied again. In the data table, more information such as pitch attitude can be found by scrolling to the right.

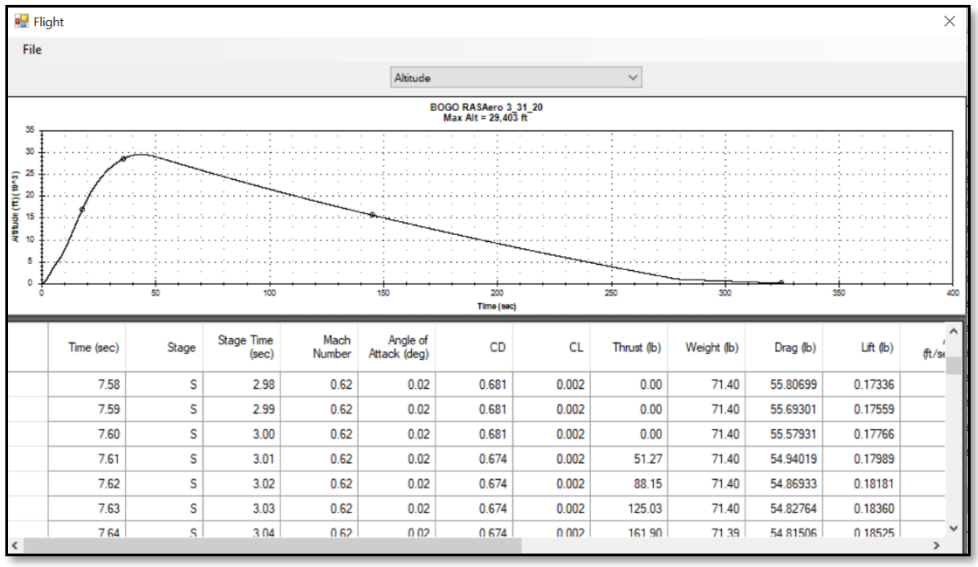

Time (sec)	Stage	Stage Time (sec)	Mach Number	Angle of Attack (deg)	CD	CL	Thrust (lb)	Weight (lb)	Drag (lb)	Lift (lb)
7.58	S	2.98	0.62	0.02	0.681	0.002	0.00	71.40	55.80699	0.17336
7.59	S	2.99	0.62	0.02	0.681	0.002	0.00	71.40	55.69301	0.17559
7.60	S	3.00	0.62	0.02	0.681	0.002	0.00	71.40	55.57931	0.17766
7.61	S	3.01	0.62	0.02	0.674	0.002	51.27	71.40	54.94019	0.17989
7.62	S	3.02	0.62	0.02	0.674	0.002	88.15	71.40	54.86933	0.18181
7.63	S	3.03	0.62	0.02	0.674	0.002	125.03	71.40	54.82764	0.18360
7.64	S	3.04	0.62	0.02	0.674	0.002	161.90	71.39	54.81506	0.18525

Figure 118 – RASAero II Sustainer Motor Ignition

A key difference between OpenRocket and RASAero II is the application of stage separation delay time and sustainer ignition delay time in both programs. In OpenRocket, both stage separation delay time and ignition delay time can be referenced from booster motor burnout. In RASAero II, only stage separation delay time references booster motor burnout and ignition delay time is based on stage separation. For example, say the optimal configuration was a 6 second stage separation delay without any ignition delay time. The OpenRocket configuration would be stage separation delay time of 6s and ignition delay time of 6s. The RASAero II configuration would be stage separation delay time of 6s and ignition delay time of 0s. This is an important factor for the RASAero II simulations.

The “Launch Site” tab can be accessed by selecting the “Options” tab in the Flight window. As mentioned in the Open Rocket section, launch site conditions must be accurate and consistent for the simulations to produce meaningful results. The same conditions are shown below for RASAero II.

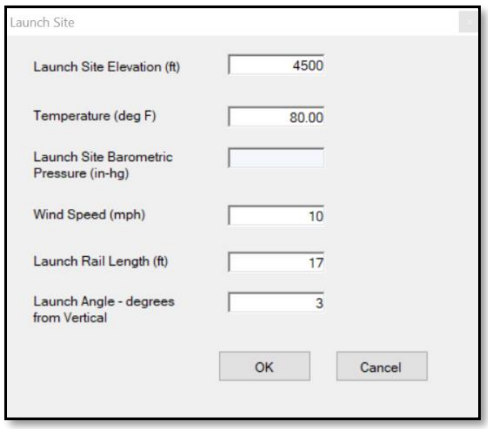

Figure 119 – RASAero II Launch Site Conditions

While the team is more experienced with using OpenRocket, they felt that utilizing multiple programs to verify the flight results would be more accurate. The team purchased licenses for RockSim, as it is renown in the model rocketry community.

From the team's experience, this software is much more user-friendly regarding motor layout and configuration. To select the motors for each stage, the user must go to the Prepare for Launch Tab.

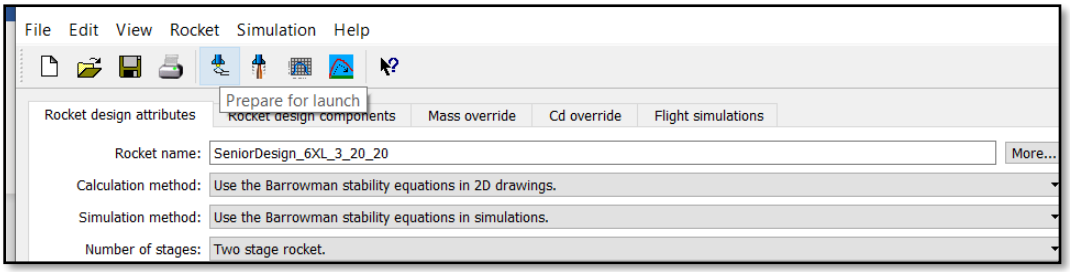

Figure 120 - RockSim Launch tab

Each motor can be selected and added to the desired stage, which is illustrated by a picture of the stage location. Each location is defined in the rocket during the layout process when the user checks a box determining if the tube is a motor tube or not. These are shown in the Launch Tab.

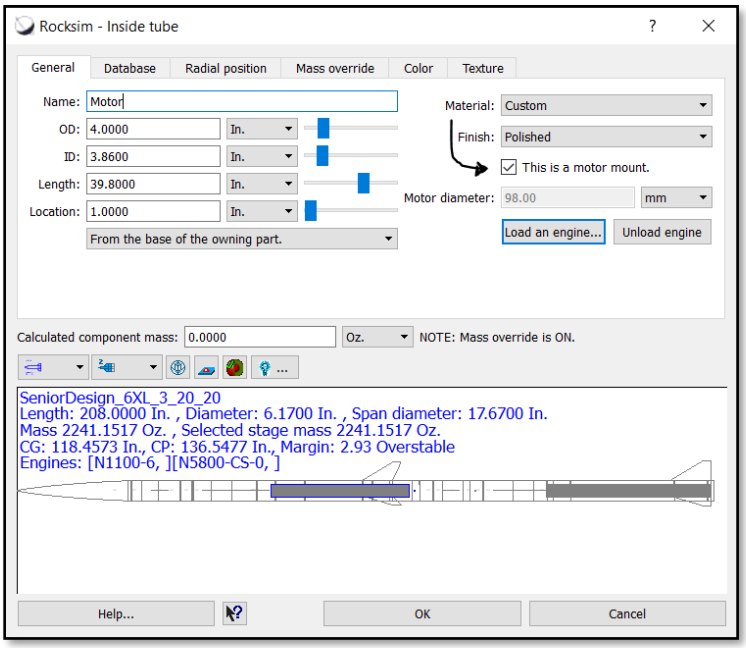

Figure 121 - RockSim Component Definitions

RockSim keeps all its motor controls in a single tab: Engine Selection. The Ejection Delay, the Ignition Delay, and the Motor Overhang are all on a single matrix to edit and can all be defined in increments of 0.01.

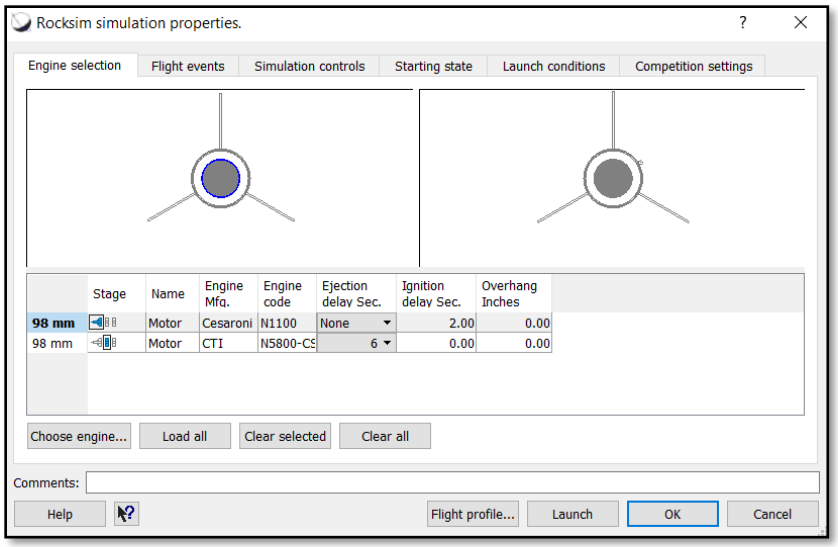

Figure 122 - RockSim Ejection selection tab

Note that the stage separation is dependent on the motor burnout and the sustainer ignition delay time is dependent on the stage separation. This is different than the OpenRocket software and the team must be aware of this or it could skew results, like with RASAero. This was discovered by using a mass tracking plot that showed the changing of mass during the flight. As the booster motor burns, the mass decreases to the dry mass of the 1st stage. Then, the mass stays the same during the 6 second ejection delay, where it then immediately drops to the wet mass of the 2nd stage. The mass only then decreases to the dry weight after the 2 second ignition delay.

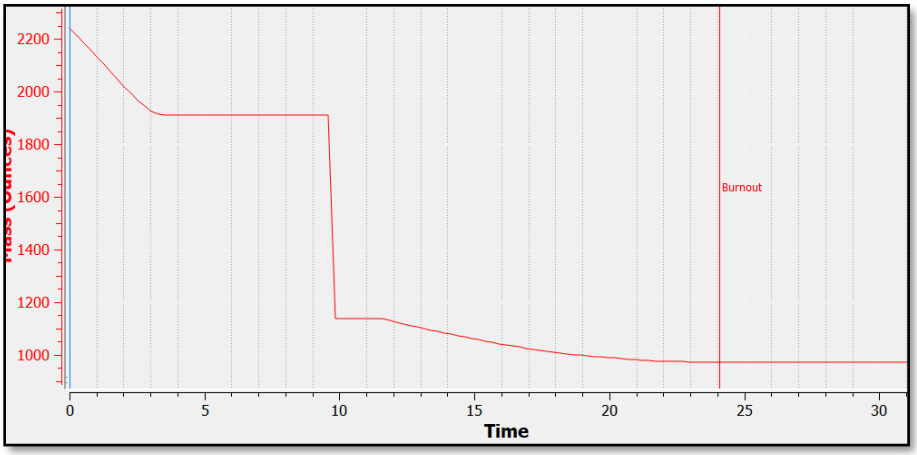

Figure 123 - RockSim Mass vs Time chart

The Flight Events tab can then be configured to determine when ejection charges will activate for the recovery system. Depending on the component, there are different event descriptions available to choose from. For example, the Upper Drogue Parachute can be activated at a multitude of opportunities like at the peak apogee of the rocket flight or even being completely cancelled. The Time tab can be utilized for events working on delays and the Altitude tab can be used for specific ejection points.

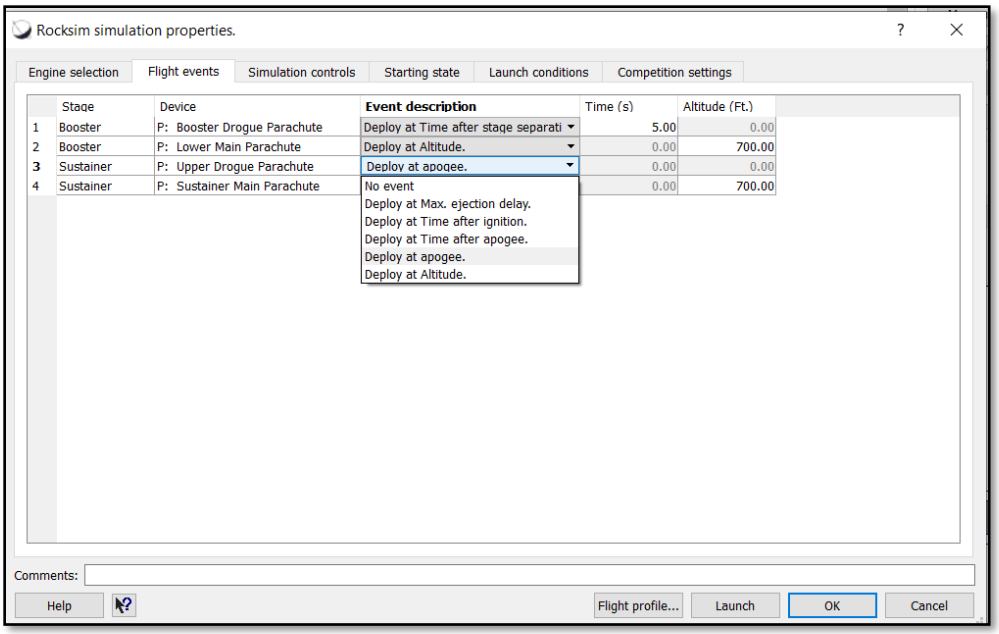

Figure 124 - RockSim Flight events tab

RockSim works on an iterative software using multiple input points. The Simulation control Tab allows for the tabulation of all the inputs from the profile and launch conditions and develops a final configuration of the data under the set amount of iterations.

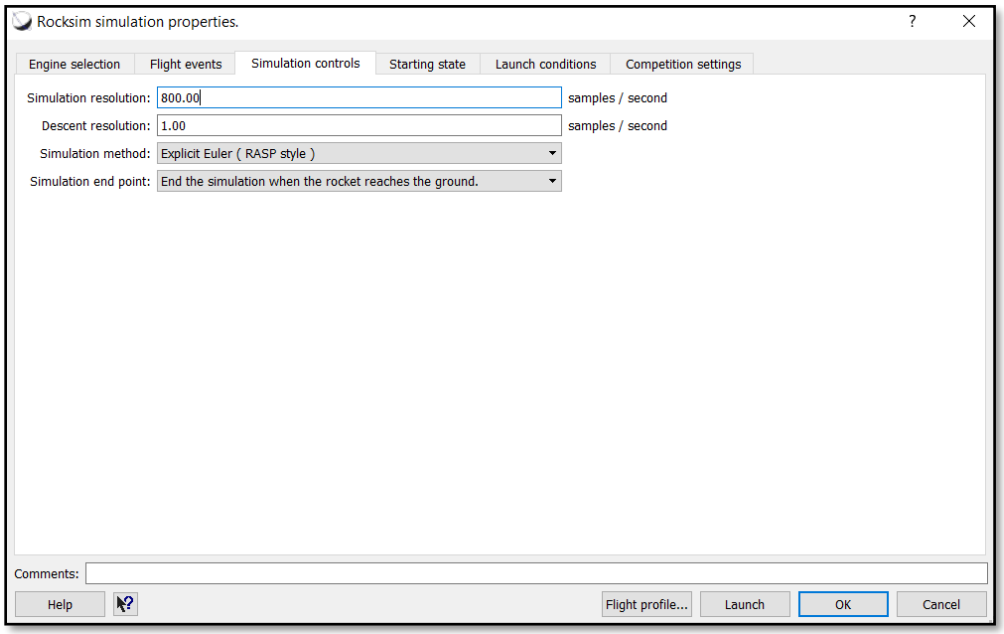

Figure 125 - RockSim Simulation controls tab

Lastly, the team can define all their launch conditions, from rail guide, to thermal diameter, to failure conditions. The next three tabs are where these are defined. Afterward the RockSim software can be launched and the users can filter through their desired results from altitude to flight time.

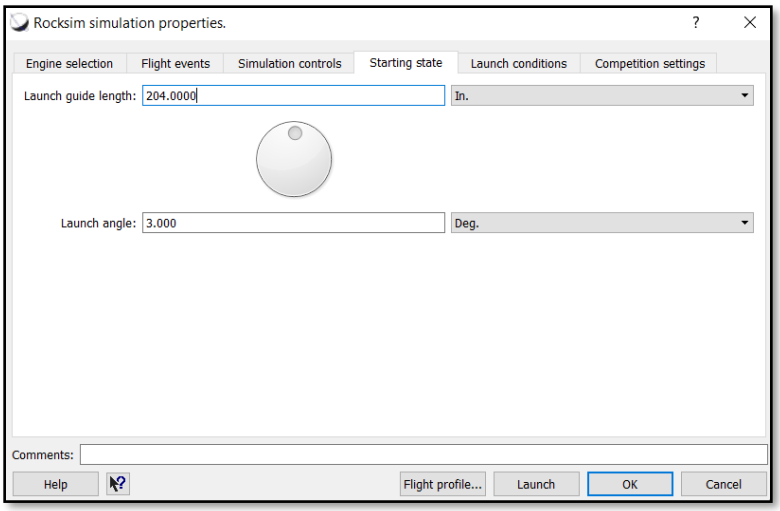

Figure 126 - RockSim Starting state tab

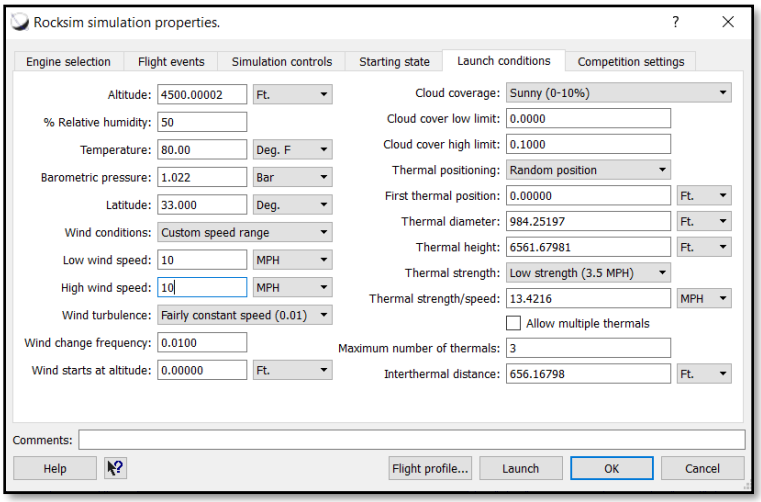

Figure 127 - RockSim Launch conditions tab

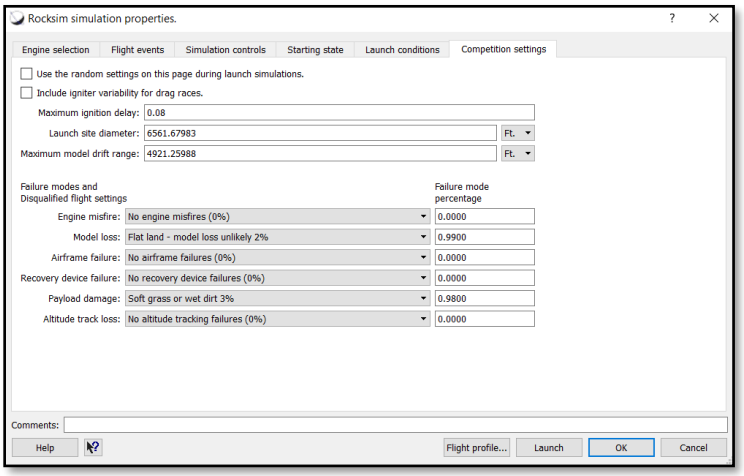

Figure 128 - RockSim Competition settings tab

These inputs are necessary for correct results for flight simulations and incorrect values can alter the flight like in OpenRocket and RASAero II. Diligence is key to using these flight software and comparing them between each other to ensure proper comparisons and valid simulations.

6.2. Flight Profile

Other sections utilized preliminary or nearly complete designs for the purpose of establishing an understanding of how certain factors affected the rocket. The previous simulations were used to consider design parameters such as the stage separation and sustainer ignition delay times, fin sweep angle and distance, launch lug placement on the airframe, altitude, vertical orientation, and drift distance. These sections are reserved for up to date flight profile information based on the simulations. The full-scale rocket has not been manufactured yet but will be upon completion of the subscale flight, which will lead to more accurate simulations. As mentioned previously in the report, the team used OpenRocket and RASAero II mainly, which are free software, to conduct various flight simulations throughout the design process of the launch vehicle. These sections will detail some use of RockSim as a third flight simulation software. The team is relatively unfamiliar with it but is hoping to learn more through the subscale flight. It is commonly used among other collegiate teams and the team's mentors and is like OpenRocket, but it is not free.

Overall, the team focused on OpenRocket while designing the rocket layout with incremental changes and updates. Once a solid design was established, RASAero II and RockSim models were replicated to mimic the design for comparison. The senior design team members were much more familiar with OpenRocket and it was easier to edit and adapt than the other two software, leading to it being the primary rocket development software. The OpenRocket flight profile that was replicated in RASAero II and RockSim is shown below.

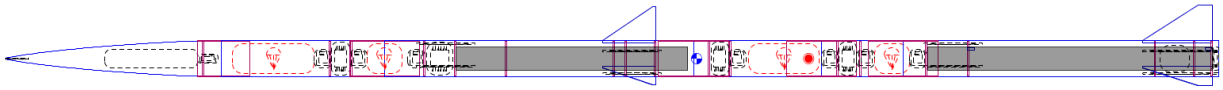

Figure 129 - OpenRocket Flight Profile for both stages

These flight profiles typically show the locations of all components and the center of pressure (red circle) and center of gravity (blue and white circle) locations. They offer a snapshot of the overall rocket layout and can be useful for quick analysis. Shown below is the OpenRocket flight profile for the sustainer stage.

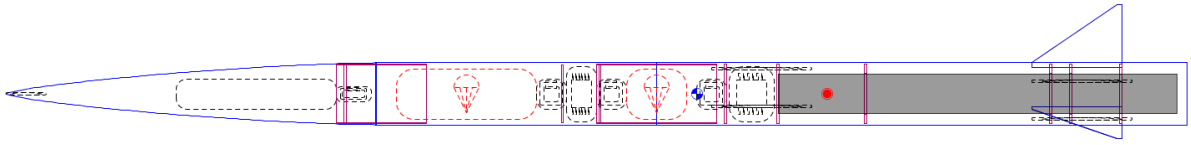

Figure 130 - OpenRocket Flight Profile for sustainer stage

Using the flight profiles and the software configurations mentioned previously, the team can compare and plot the key flight characteristics and the stability margins in all three software. Below is a table of key flight characteristics between the three software for both stages of the rocket together, including the thrust to weight ratio, maximum vertical velocity, drag coefficient at

maximum velocity, and rail exit velocity. The thrust to weight ratios and rail exit velocities are key to rocket stability at takeoff and all meet IREC requirements. The drag coefficients and maximum vertical velocities can be used for a quick comparison between the software. As shown, the RockSim drag coefficient is much lower which results in a larger final altitude in RockSim. It is currently unknown why the drag coefficient is much lower in this program, and the team cannot determine the actual drag coefficients until a flight is conducted. RockSim does offer a Drag Coefficient Override Tab, as shown below, but this would only be useful if the team knew the official coefficient of drag for each stage. Until then, the team must use what the software calculates and attribute it for a potentially real value.

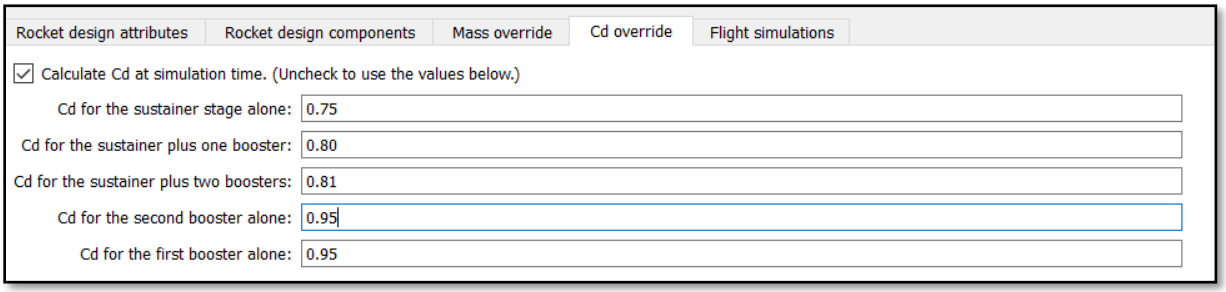

Figure 131 - RockSim Cd Override Tab

Flight Profile Calculations – Both Stages

Flight Profile Characteristic	OpenRocket	RASAero II	RockSim
Max Thrust to Weight Ratio	11.17	11.86	10.99
Maximum Vertical Velocity (ft/s)	951.95	960.70	989.05
Drag Coefficient at Max Velocity	0.908	0.837	0.437
Rail Exit Velocity (17 ft.) (ft/s)	103.45	102.20	103.46

Table 17 – Flight profile calculations for both stages

Below is a table of the same flight characteristics between the three software for the sustainer stages of the rocket only. The apogee achieved has been added in place of the rail exit velocity. These characteristics are equally important to ensure a safe flight on the sustainer stage. The thrust to weight ratios all meet IREC requirements. The drag coefficients and maximum vertical velocities are fairly similar between the three software, but RockSim has a significantly higher maximum vertical velocity. The higher maximum vertical velocity and lower drag coefficient for both stages resulted in a much higher final altitude. These flight characteristics will be useful to compare the accuracy of the three software for a multistage supersonic flight.

Flight Profile Calculations – Sustainer Stage

Flight Profile Characteristic	OpenRocket	RASAero II	RockSim
Max Thrust to Weight Ratio	8.58	8.89	8.51
Maximum Vertical Velocity (ft/s)	1,173	1,141	1,326
Drag Coefficient at Max Velocity	0.625	0.536	0.627

Apogee (ft)	29,202	29,162	37,838.58.02

Table 18 – Flight profile calculations for sustainer stage

The stability of a rocket is a key factor in the success of the overall flight and the ability to reach the expected altitude. The stability of the launch vehicle determines the rocket flight's susceptibility to exterior fluid forces. A high stability influences the rocket to fly into the airflow (direction of the wind) while a low stability has the opposite of this effect and could result in an unstable flight overall. This is illustrated in the RockSim flight path simulation below. The wind is blowing to the right, as shown by the drifting descent. As the rocket ascends, it directs its path into the wind.

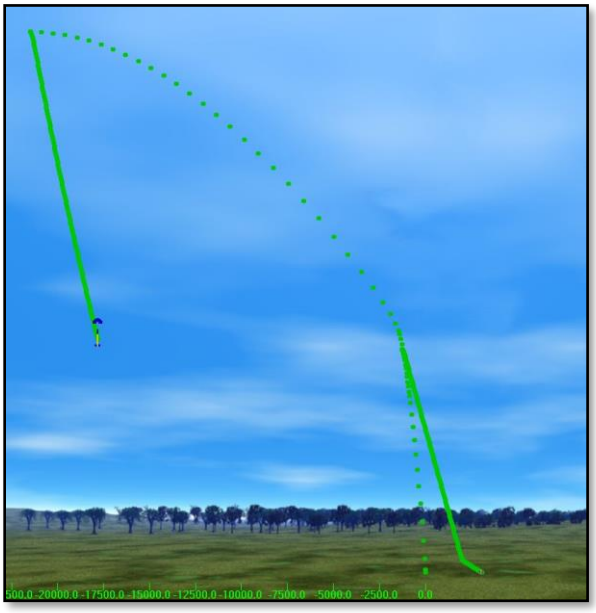

Figure 132 - Rocket Stability vs Wind Flight Path

The team aims to keep the launch pad stability margin between 1.75 and 3.50 for both stages and the sustainer stage. These values are based on successful previous rocket constructions and IREC requirements.

The stability margin is calculated as the distance between the Center of Pressure (CP) and the Center of Gravity (CG) divided by the airframe outer diameter, which is 6.17" for the team's rocket. The CP must be located aft of CG for a positive stability. This section details the basic calculation methods and values for the CP and CG of a rocket and the stability margin in all three software. The team will attempt to elaborate on minor differences which contribute to the varying flight predictions.

The airframe of a rocket has a defining influence on the overall stability of the flight. The Center of Pressure and Center of Gravity are the primary factors when determining stability. Depictions of CP and CG on a rocket are shown below, courtesy of NASA Glenn Research Center, specifically James Barrowman of the Sound Rocket Branch. These equations are drawn from the Rocket Mime website [7].

The Center of Pressure can be calculated using the equation shown below.

$$CP = \frac{(C_N)_N X_N + (C_N)_F X_F}{(C_N)_S}$$

Equation 19 - Center of Pressure

These values were defined by Barrowman using conical transition terms and fin terms that take in account the 2D geometry of the design.

$$(C_N)_T = 2\left[\left(\frac{d_R}{d}\right)^2 - \left(\frac{d_F}{d}\right)^2\right]$$

Equation 20 – Nose Cone Local Center of Pressure

$$X_T = X_P + \frac{L_T}{3}\left[1 + \frac{1 - \frac{d_F}{d_R}}{1 - \left(\frac{d_F}{d_R}\right)^2}\right]$$

Equation 21 – Nose Cone Center of Pressure Position

$$(C_N)_F = \left[1 + \frac{R}{S+R}\right]\left[\frac{4N\left(\frac{S}{d}\right)^2}{1 + \sqrt{1 + \left(\frac{2L_F}{C_R + C_T}\right)^2}}\right]$$

Equation 22 - Fin Local Center of Pressure

$$X_F = X_B + \frac{X_R}{3}\frac{(C_R + 2C_T)}{(C_R + C_T)} + \frac{1}{6}\left[(C_R + C_T) - \frac{(C_R C_T)}{(C_R + C_T)}\right]$$

Equation 23 - Fins Center of Pressure

L_N = length of nose
d = diameter at base of nose
d_F = diameter at front of transition
d_R = diameter at rear of transition
L_T = length of transition
X_P = distance from tip of nose to front of transition
C_R = fin root chord
C_T = fin tip chord
S = fin semispan

L_F = length of fin mid-chord line
R = radius of body at aft end
X_R = distance between fin root leading-edge and fin tip leading-edge parallel to body
X_B = distance from nose tip to fin root chord leading-edge
N = number of fins

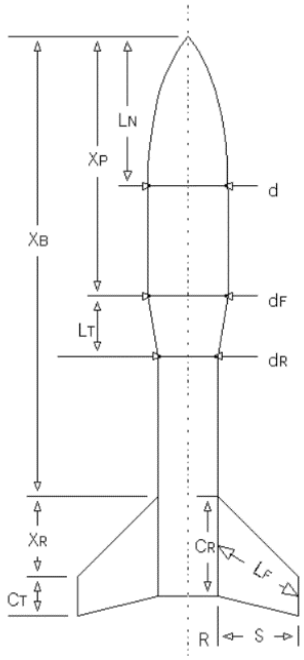

Figure 133 - Rocket Center of Pressure Diagram

The Center of Gravity can be calculated using the equation shown below.

$$CG = \frac{W_1 d_1 + W_2 d_2 + W_3 d_3 \ldots}{W}$$

Equation 24 - Center of Gravity

While the airframe size is heavily dependent on the interior loading, the fin dimensions are more easily adjustable. By adjusting their sizes, the CP distance from the nose cone can either be increased or decreased. This is due to Barrowman's equations using the 2D side profile to derive their values. This is especially influential, as the two-stage vehicle has two sets of fins. However, this also means that two different layouts, the two-stage model and the sustainer model, are influenced by the design. Due to this, the team was careful in their weight distribution and utilized the OpenRocket software to display their stability margin for each stage and each design iteration. In summary, the CP can most easily be influenced by the design of the fins, while the CG can be adjusted slightly with weight changes in certain locations. By leaving some margin for adjustment in these areas, the team can control the rocket stability margin. This is a key reason the final fin dimensions have not been selected at this point. They will be adjusted after all other components have been manufactured.

Below is a table outlining the stability calculations for both stages of the rocket together in all three software. The difference between the wet and dry calculation is that wet weight includes the fuel for that stage while the dry weight is the weight after all fuel is burned. This is helpful to ensure the rocket is stable after motor burnout as well. It is acceptable to have a slightly over stable rocket after motor burnout based on previous team and mentor experience. Overall, the stability margin in all three software meet team and competition requirements and the team is confident in the stability of the two-stage configuration.

Stability Calculations – Both Stages

Stability Characteristic	OpenRocket	RASAero II	RockSim
CP Wet (in)	138.04	137.59	137.55
CG Wet (in)	118.15	118.15	118.77
CG Post Burnout (in)	107.10	107.40	108.55
Stability Margin	3.22	3.15	3.04
Stability Margin Post Burnout	5.01	4.89	4.70

Table 19 – Stability calculations for both stages

Below is a table outlining the same stability calculations for the sustainer stage of the rocket only. The stability margin in all three software is slightly lower but it still meets team and competition requirements for the sustainer stage and the team is confident in the stability for the sustainer configuration.

Stability Calculations – Sustainer Stage

Stability Characteristic	OpenRocket	RASAero II	RockSim
CP Wet (in)	82.10	81.74	81.73
CG Wet (in)	68.90	69.08	69.23
CG Post Burnout (in)	64.30	61.20	64.50
Stability Margin	2.13	2.05	2.02
Stability Margin Post Burnout	2.88	3.33	2.79

Table 20 – Stability calculations for sustainer stage

7. Testing

The team performed subsystem testing with key launch vehicle components including airframe compression testing, shear testing, tiltmeter testing, and MiniTimer4 testing. These tests helped validate selected components and prove the functionality of certain electrical components. The compression and shear test results can be referenced for structural loads that the rocket is expected to endure throughout flight.

The original testing plan included additional tests such as wind tunnel tests, GPS tests, parachute drop tests, recovery component tensile tests, and ground separation tests which were all required to verify the functionality of the rocket before flight. However, the majority of these did not apply to the senior design project or were not conducted by senior design team members specifically, so they were not included. Wind tunnel tests could not be conducted since the University of Akron wind tunnel could not achieve dynamic similarity between a tested model and the full-scale version for the team's purposes (i.e. equivalent Reynolds numbers and Mach numbers). GPS tests, parachute drop tests, and recovery component tensile tests were completed for the NASA competition, but were outside the scope of the senior design project. Ground separation tests were delayed due to the COVID-19 epidemic. The sections below detail the testing sections that pertained to the senior design process and were completed.

7.1. Airframe Compression Test

The team conducted compression testing with a section of the 6" fiberglass airframe to verify the airframe could withstand the vertical forces of flight in compression for the two-stage rocket. This test was also used for verification of the rocket team's NASA competition rocket since it utilized the same airframe material.

The tube was cut to length and placed into the INSTRON UTM-HYD Compression Testing Machine. Characteristics of the tube were input into a computer program along with ramp rate. The top plate was lowered to the top of the tube to constrain it from above. The computer program initiated the test to apply an increasing load to the top of the tube until a drop off in loading was indicated. The ramp rate indicated the speed at which the load was applied, so to emulate the quick thrust of the motor, the highest ramp rate was selected at 20,000 lb/min. The drop off in loading near the end of the test indicated a fracture in the tube. After testing to failure, the team turned off the program before entering the testing area to assess the tube and clean up. A photo of the fiberglass body tube set up in the INSTRON machine is shown below.

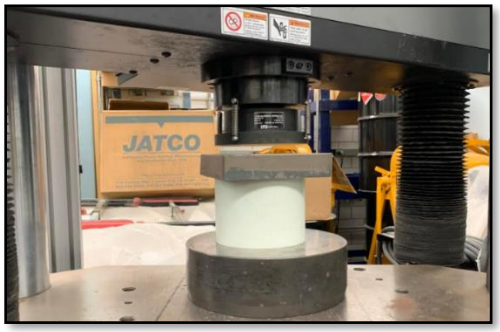

Figure 134 - Fiberglass body tube setup in INSTRON machine before compression test

The yield strength of the fiberglass airframe was approximately 30,486 lbf and compression strength was approximately 39,472 lbf. The factor of safety is just over 25 for the compression strength compared to the maximum thrust of the CTI N5800 motor. Photos of the compressed tube are shown below**.** The test validates the fiberglass body tube material will not fail during the flight of the two-stage rocket.

Figure 135 - Compressed tube in INSTRON machine post-test

A load force vs extension was plotted for the test and displayed below.

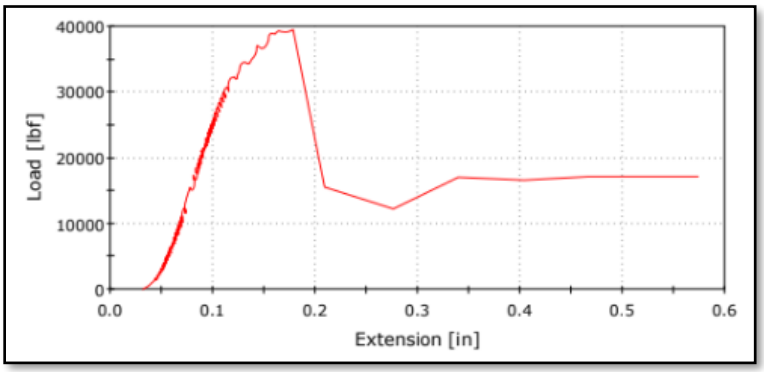

Figure 136 – Load Force vs Extension plot for fiberglass body tube compression test

7.2. Shear Tests

The team also conducted bulkhead shear tests to examine the shear stress on a bulkhead fastened into a body tube section with six 6-32 screws and six 4-40 screws, which is common practice for the rocket team. It was expected that the failure mode would be deformation or fracture of the screws in shearing, but the team wanted to verify the screws, bulkheads, and airframe met shear force strength requirements for the two-stage rocket. These tests were also conducted as part of the NASA competition objectives, but the team wanted to verify the strength for the full-scale as well. If the screws were not strong enough, another test with larger screws would be needed.

The tube was cut to length and a bulkhead was fastened into it at six locations along the outside diameter as shown in the figure below. The bulkhead was mounted flat in the tube to allow for an even distribution of force to the six screws. A large section of 5” aluminum round stock is placed above the bulkhead to distribute the force from the INSTRON UTM-HYD Compression Testing Machine.

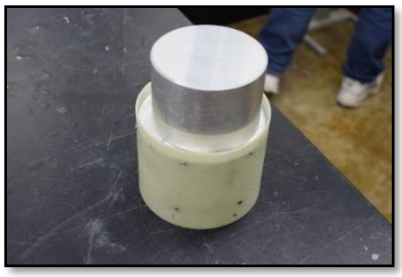

Figure 137 - Shear Test tube setup

The tube was placed into the compression machine with the aluminum stock on top of the bulkhead. Characteristics of the tube were input into the computer program along with the same ramp rate as the compression test. The top plate was lowered to the top of the aluminum stock to constrain the tube from above. The computer program initiated the test to apply an increasing load to the top of the round stock until a drop off in loading was indicated. The drop off in loading near the end of the test indicated a fracture in the tube. After testing to failure, the team turned off the program before entering the testing area to assess the tube and bulkhead and clean up. A photo of the set up in the INSTRON machine is shown below.

Figure 138 – Fiberglass body tube setup in INSTRON machine before shear test

The 6-32 screws failed in shearing at a force of 4,157 lbf after 12.5 seconds, while the 4-40 screws failed at a force of 2,514 lbf after 7 seconds. The factors of safety are 2.64 for the 6-32 screws and 1.60 for the 4-40 screws compared to the maximum thrust of the N5800 motor. An example photo of a sheared bulkhead through the fiberglass body tube is shown in the figure below.

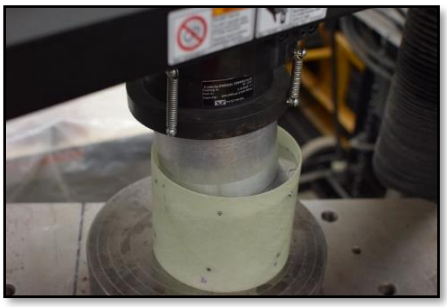

Figure 139 - Sheared bulkhead through fiberglass airframe

While both the 4-40 and 6-32 screws can withstand the thrust of the motor, the team will move forward with the 6-32 screws due to the added safety factor. Force vs Extension graphs for both the 4-40 and 6-32 screws are shown below.

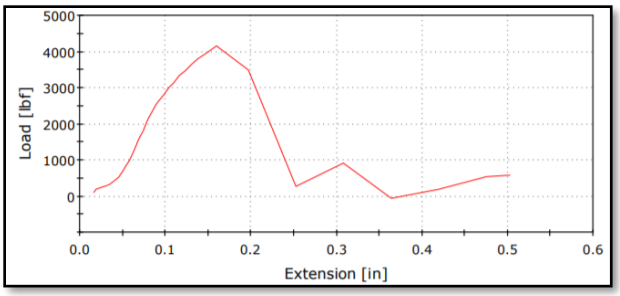

Figure 140 - Force vs Extension plot for 6-32 Shear Test

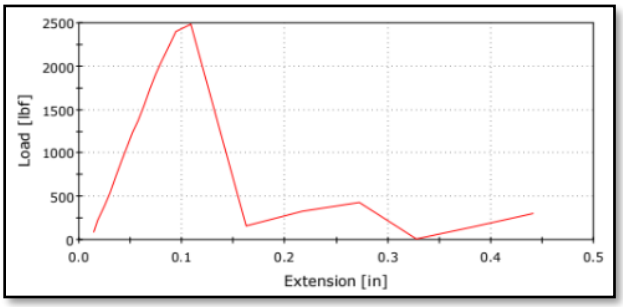

Figure 141 - Force vs Extension plot for 4-40 Shear Test

7.3. EasyMega Tests

The EasyMega, which is the second stage motor ignition device, has a multitude of features that allow for multiple layers of safety when igniting the second stage motor. The electronic chip features barometric sensors, two accelerometers, and a tiltmeter. The system needed to be tested to verify that the team's selected settings would function as expected since the motor ignition is a safety-critical event. Each setting was tested individually to ensure that they would all perform as expected. The team performed the testing along with two rocket design team members so that they could learn the process and understand the tiltmeter for future two-stage rockets. The four settings tested include minimum altitude, maximum angle from vertical, and minimum and maximum time delay after boost.

The system was tested to verify the functionality of the timing aspect by programming arbitrary time points $T_{min} = 6$ seconds and $T_{max} = 10$ seconds (initiated on launch) and setting up the electrical system within a 6" long test airframe with a swing handle. The physical test airframe set up is shown below.

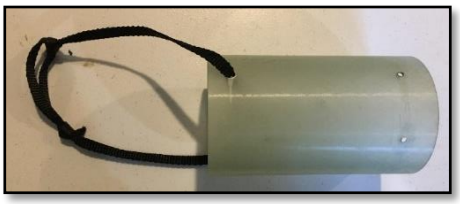

Figure 142 - Swing test airframe setup

An igniter was attached to pyro terminal D on the chip. To initiate the test, the EasyMega tiltmeter senses launch by using one of its accelerometers to verify liftoff by registering a large

change in acceleration. This is achieved by turning the EasyMega system on and spinning it rapidly in a circle, which the chip registers as a launch. The EasyMega's test frame was halted prior to $T_{min} = 6$ seconds. The chip will not allow for the charge to go off until it is between the time frame of 6-10 seconds based on the outlined settings for the test. Stopping the airframe before $T_{min} = 6$ seconds and having the pyro charge not ignite before that time verified that the system was functional. The EasyMega was also tested by spinning the system to sense a launch and continuing to spin it until long after the programmed $T_{max} = 10$ seconds time. The pyro charge did not ignite, verifying that the motor will not ignite while the first stage motor is still burning. The system was brought to a rest after $T_{max} = 10$ seconds and the charge did not ignite, verifying the maximum time condition worked. A photo of the airframe swung during timing tests is shown below.

Figure 143 - EasyMega time delay testing

The EasyMega's angle-based settings were tested in a similar manner. The EasyMega was first programmed to activate the pyro channel if the angle from vertical is less than 20 degrees. A time-based setting was also configured to allow for the unit to be oriented as needed before the EasyMega activated the pyro channel. The sled was then mounted inside the test airframe and swung to initiate a simulated flight reading. Once the simulated flight was recognized, the unit was brought to a stop and oriented within 20-degrees from vertical. The pyro charge fired as expected.

To verify functionality further, the EasyMega was subjected to the same test a second time with a final orientation of near 90 degrees from vertical. The pyro charge was not fired when the unit was in this orientation proving that an angle greater than the specified angle would be recognized by the unit.

One final test to verify the angle-based settings was performed. In this test, the unit was oriented at an angle greater than the 20-degree window after the simulated flight was detected. The unit was then slowly rotated towards a vertical orientation. Upon reaching the 20-degree threshold, the unit fired the pyro charge verifying an accurate angular reading is possible with the EasyMega. Photos of the angle-based testing are shown below.

Figure 144 - EasyMega angle testing within 20-degrees (left) and outside of 20-degrees (right)

Finally, the EasyMega's altitude programming feature was tested in the same way as previous tests, but a constant ascent was required. An arbitrary altitude was programmed at 20 meters AGL (Above Ground Level) which could be attained by climbing stairs. Once initiating the launch by swinging the test airframe, a team member ran up a flight of stairs as fast as possible to simulate continuous altitude rise and continued until the pyro charge on channel D ignited. This test was challenging due to the continuous altitude ascent, but it was successful.

7.4. MiniTimer4 Test

The MiniTimer4s that control the stage separation event were tested to verify functionality. They can be programmed in increments of 0.1 seconds up to 99.9 seconds. The user manual describes a swing test procedure like the test for the tiltmeter shown above. The MiniTimer4s register launch in the same way and begin a timer that sends a current to the pyro charges to ignite the black powder at the predetermined time. Both MiniTimer4s were tested by setting the delay times to 10.0 and 12.5 seconds, respectively. They were mounted in the same test airframe as the tiltmeter tests and swung rapidly to initiate the timer start. Both electric matches ignited successfully on the first attempt. A photo of the electric matches igniting during the test is shown below.

Figure 145 - MiniTimer4 testing

8. Subscale Manufacturing

The senior design team constructed a subscale version of the competition rocket by the original senior design project due date and hoped to test fly it prior to the completion of the project. Due to the COVID-19 epidemic, the launch was postponed. However, the team was able to manufacture the rocket and the following sections detail the manufacturing and assembly of key sections that were highlighted through the team's research and design.

The subscale two-stage launch vehicle was designed to reach an altitude of around 10,000 feet, so it could be flown at a local Ohio launch field or in a nearby state. Springfield, Ohio, has a launch field that could support the team's flight up to around 17,000 feet and is the leading candidate thus far. The team attempted to utilize the same design decisions from the full-scale rocket in the design of the subscale launch vehicle to flush out any potential issues in manufacturing or assembly and possibly find better alternatives if problems are encountered. The rocket was reviewed with the team's mentor, Chris Pearson, who would be providing approval to launch in Springfield, Ohio later. His comments and suggestions are included in applicable sections. If the full-scale rocket could not be constructed, the subscale rocket was designed such that it would meet all IREC requirements and could be flown in its place at competition in the 10,000 feet altitude scoring division.

8.1. Structural Design

Although the subscale model will not fly at supersonic speeds, the team tried to keep structural designs the same to verify functionality. The subscale rocket was constructed with most of the same materials to the full-scale version, including 4" diameter fiberglass for the airframe and aluminum for bulkheads and centering rings. The fins were not manufactured by the project due date due to time constraints and limited access to a machine shop near the end of the project. The following sections detail the application of the structural design decisions for the subscale rocket.

8.1.1. Nose Cone

The nose cone is a scaled-down version of the commercial Von Karman design. It has a 5.5:1 fineness ratio, though, since that was all that was available commercially. It is also translucent, so drilling airframe holes would be relatively easy. The subscale nose cone is shown below for clarity.

Figure 146 - Subscale 5.5:1 fiberglass Von Karman nose cone

8.1.2. Fin Design

The fins were designed to be clipped delta fins for both stages of the rocket like the full-scale version. There will be three fins on each stage, and they will be 3/16” thick aluminum which is identical to the full-scale design. Since the rocket will be traveling slower for the subscale rocket, the fins will not experience fin flutter on the subscale. The leading-edge of the fins is swept back about 47 degrees for the subscale rocket, which was necessary for stability of both stages. Although the sweep angle was not optimized for drag, the stability margins will ensure a safe flight for the subscale rocket. Overall, the team is confident the subscale fin designs will keep the rocket stable through flight and will not flutter.

8.1.3. Fin Retention

The fin retention system that the team designed for the full-scale rocket was implemented on the subscale model and some minor assembly issues were encountered. The team found that the tolerance on the L bracket slots was very small and it was difficult to slide the fins into their location. However, the smaller 4” airframe made it difficult to expand the L bracket spacing for the fins. This issue should be easier to deal with on the full-scale rocket since the 6” airframe will offer more space around the motor. For the subscale rocket, the fins were buffed at the edges that slid between the L brackets to reduce the interference. Below is a photo of the mounted L brackets on a subscale centering ring.

Figure 147 - Subscale assembled centering ring for fin retention

Another change was the decision to use two rings instead of three to hold the fins. Two rings slightly reduced the interference issues mentioned above and are more than strong enough to hold the subscale fins. The full-scale version can implement two or three rings.

The assembly process for mounting the fins is difficult since the fins must be slid in through the fin slots rather than mounting them to the centering rings prior to mounting them into the rocket. The fin slots could not be cut to the end of the airframe because of pressure-sealing concerns and added friction on the coupler as mentioned in the Stage Separation section. Because of this, the fins must be mounted after the centering rings are in place.

The team drilled 0.5” holes in the airframe to slide the screws in to attach to the L brackets. Only one side of the L brackets that constrain the fins is tapped to accept and tighten the ¼” screws. The other L bracket has a through hole to accept the screws. Bill Wenzel, the Senior Research Technician in the machine shop at the University of Akron, recommended only tapping the last connecting bracket unless they could all be tapped as an assembly. The other option was to have a nut on the backside of the L bracket, but the team cannot reach a wrench into this location to tighten the nut due to space constraints. Shown below is the assembled centering rings with a test fin piece in place. The fiberglass test fin pieces were used as place holders until the fins were manufactured.

Figure 148 - Subscale assembled fin retention system

Overall, the team is confident with the fin retention system heading into the subscale flight. Chris Pearson said the design was impressive and should be fine for full-scale flight as well. The seniors had some minor concerns regarding the large 0.5” holes to fit the screws in from the exterior of the airframe, but Chris said it should not be an issue in flight for either the subscale or the full-scale.

8.1.4 Bulkheads & Centering Rings

The bulkheads and centering rings for the subscale rocket were all manufactured by the senior design team or using the CNC available in the machine shop. Although they were not the focus of the senior design project, the team gained valuable machine shop experience using the manual lathe, end mill, and bandsaw to machine these components from aluminum 6061 round stock. The lathe and bandsaw were used to manufacture the plates for the bulkheads and the mill was used to drill all the face holes and tapped holes on the outside diameter of the bulkheads. Chris Pearson said the bulkheads and centering rings were very well-done, although he does not use as much metal in his rocket designs. The team is confident the bulkheads and centering rings will function as expected for the subscale flight. Shown below is a team member using the manual lathe to manufacture the plates.

Figure 149 - Senior design team member manufacturing bulkheads with a manual lathe in the machine shop

8.1.5. Motor Retention

The two motors for the subscale model were retained using the same methods as the full-scale design to verify functionality and flush out any assembly issues. The booster motor was retained with a 54mm Aeropack motor retainer as shown below. This retainer cap was fastened to the lower fin retention centering ring. Due to the smaller diameter, alignment of the six retention cap holes was critical to avoid the L bracket holes. The holes in the centering ring were tapped for ease of assembly. Shown below is the assembled Aeropack retainer holding the first stage motor.

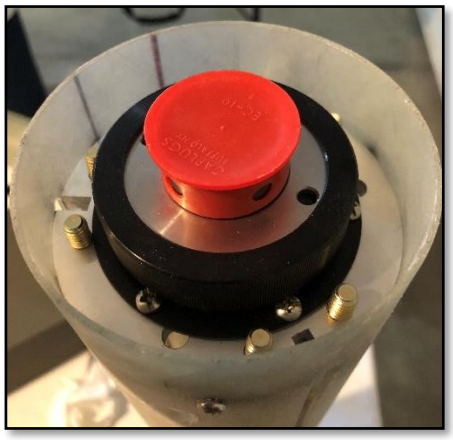

Figure 150 - Subscale booster motor retention with Aeropack

The sustainer motor was retained using the forward closure with an eye bolt. However, the 54mm motor forward closure utilized a 1/4”-20 eye bolt while the 98mm motors for the full-scale will contain a 3/8”-16 thread. The 1/4” eye bolt length of 6” was longer than required, but the team utilized washers to keep the thread from bottoming out in the motor while still maintaining sufficient thread engagement. A photo of the sustainer motor retained with an eye bolt is shown below.

Figure 151 - Subscale sustainer motor retention with eyebolt

Overall, the team is confident in both motor retention methods after manufacturing them and reviewed them with Chris Pearson who provided his approval. He mentioned that the black part of the sustainer forward closure could be a phenolic material, but the threaded insert inside is aluminum and is strong enough to retain the motor through flight.

8.1.6. Rail Buttons

The two rail buttons were mounted with 8-32 tapped holes in the lower fin retention ring and a bulkhead on the first stage of the subscale model. The buttons are about two feet apart per IREC judge recommendations and the lower button is located as low as possible on the airframe to maximize rail exit velocity. There were no issues with the rail button mounting for the subscale rocket, so it will be used on the full-scale as well. Extra 8-32 tapped holes can be tapped in various bulkheads and centering rings to mount the rail buttons in different locations if desired. The assembled rail buttons are shown below for the subscale launch vehicle.

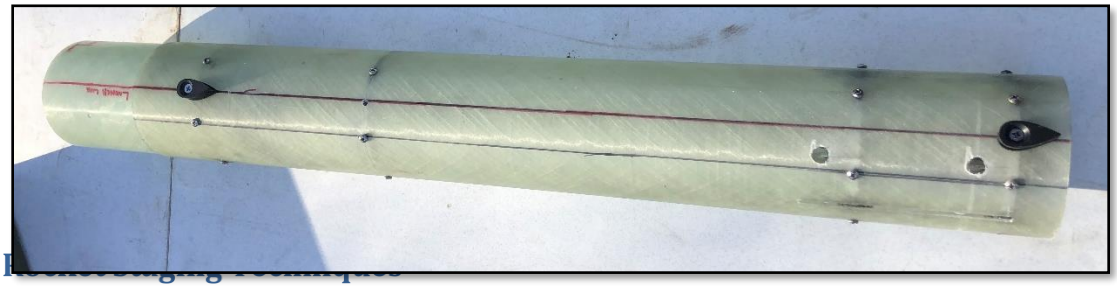

8.2. [illegible]

Figure 152 - Subscale booster airframe with assembled rail buttons

Key aspects of the team's research for staging techniques were implemented for the subscale rocket where applicable. Some aspects were not investigated deeply for the subscale since the concern was greatly reduced by flying to a lower maximum altitude at subsonic speeds. Drift analysis and max dynamic force calculations were considered negligible for the senior design team's subscale development. By using similar strength components and allowing the rocket team's members to design the parachutes, the focus on these topics was reduced.

This allowed the seniors to direct their attention to the implementation and functionality of the staging research and design. More important aspects were reviewed in detail in the following sections.

The subscale model will implement the constant diameter, forced stage separation system mentioned for the full-scale design. It will have a black powder stage separation at a predetermined time. Shown below is the rocket layout with the airframe assembled. The separation point is between the wooden rocket stands, just below the second set of fins.

8.2.1. Stage Separation

Figure 153 - Subscale rocket airframe layout

The team identified a potential fin attachment issue that would have caused interference on the coupler and a lack of pressure-sealing in the separation bay prior to manufacturing. The solution to slot the fins up to a certain distance along the airframe was implemented for the subscale rocket with no issues. The coupler slides into the airframe smoothly and the bay can be pressure sealed. A photo of the second stage fin slots is shown below with 5” to the bottom of the airframe left uncut.

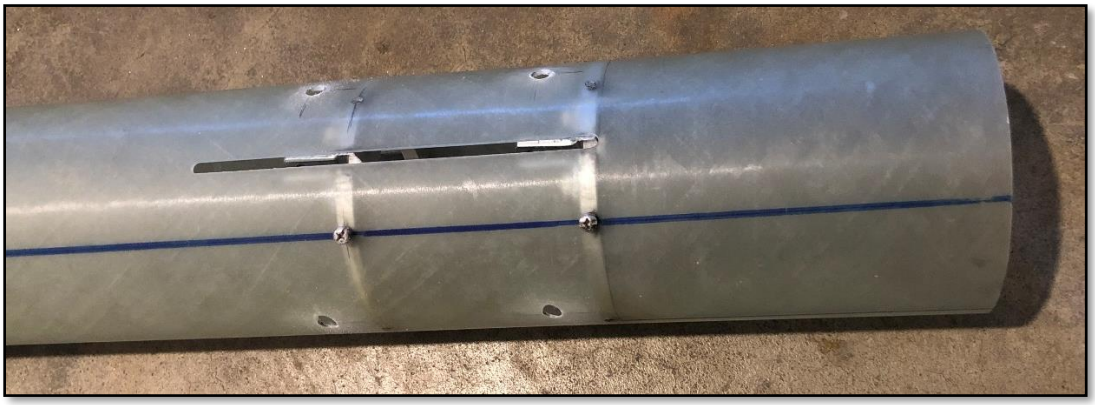

Figure 154 - Subscale sustainer fin slots with assembled centering rings

The fin slots were manufactured using the end mill in the machine shop. This gave the team experience setting up an uncommon manufacturing application in a machine shop setting. The tube was leveled with spacers on the opposite end of the chuck and a team member applied pressure to that end to constrain it. A locator tool helped find the center and starting locations on the tube and a 3/16” end mill cut the slots to the required lengths. The chuck was rotated 120 degrees to the next slot location since there were three evenly spaced fins. A photo of the first stage fin slots cut on the end mill in the machine shop is shown below.

Figure 155 - Subscale booster fin slot manufacturing with an end mill in the machine shop

8.2.2. Motor Selection

The two commercial motors selected for the subscale rocket reflected similar decisions for the full-scale rocket. The first stage motor is a CTI K1440 with a maximum thrust of 386 lbf and a quick burn time of 1.7 seconds. Based on the most up-to-date weight estimates of around 39.5 lb for the total subscale rocket weight, the thrust to weight ratio is 9.77 which would meet competition requirements of 8:1 for the booster stage. The thrust curve for the CTI K1440 motor is shown below.

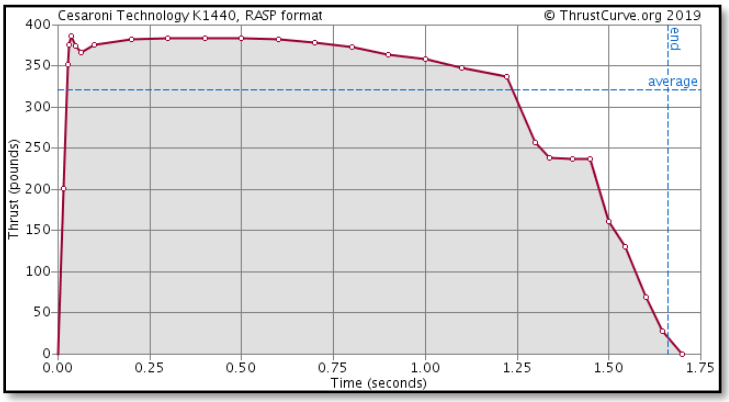

Figure 156 - CTI K1440 thrust curve

The sustainer motor was selected as a long-burning motor and will be the CTI K260. It has a maximum thrust of 97 lbf and a burn time of 8.5 seconds. With the sustainer stage weighing 18.6 lb, the second stage thrust to weight ratio is 5.22 which would meet competition requirements of 3:1. The thrust curve for the CTI K260 motor is shown below.

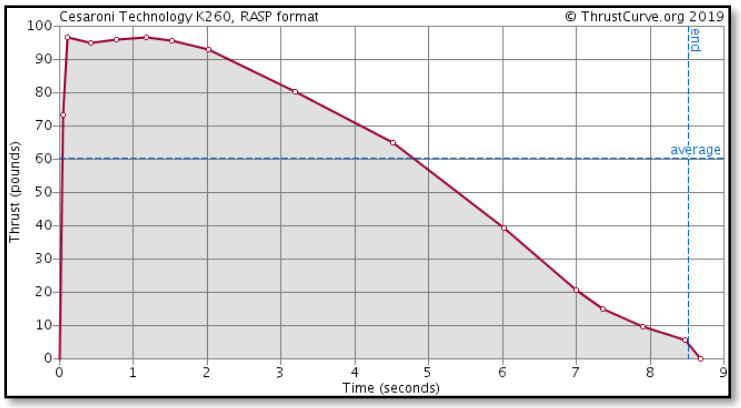

Figure 157 - CTI K260 thrust curve

The team examined the stage separation and ignition timing over a smaller range of 0 to 5 seconds for the subscale rocket. The nearby launch fields might impose altitude restrictions even though the Springfield site can support launches up to 17,000 feet, so maximizing altitude was not the key factor in the team's analysis. However, the team would like to try to utilize some delay times, if possible, to replicate the separation and ignition sequence of the full-scale rocket. The simulations were conducted with the most up-to-date weight estimates and potential launch day conditions to get the best estimate possible. The sections below briefly analyze the results for altitude and vertical orientation.

8.2.3.1. Altitude Analysis

The team simulated altitude while using varying the stage separation and sustainer ignition delays. The predicted altitudes all fall within a range of 10,000-12,000 feet. For the subscale launch, the altitude limitation depends on the flight ceiling constraints of the launch site. There are several launch sites with 12,000 ft capable flight ceilings the team is reaching out to for a potential test flight, but Springfield remains the most likely site. After simulating up to a 5 second sustainer ignition delay, the team noticed that altitude dropped off significantly after 3 seconds. Like the full-scale simulations, the altitude dropped with wind speed for all delay values simulated. A sample plot for the 10 mph wind speed scenario is shown below for OpenRocket.

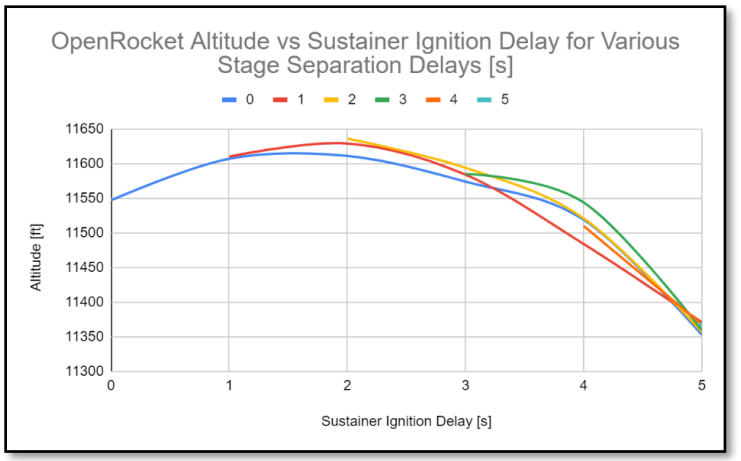

Figure 158 - Subscale OpenRocket Altitude vs Sustainer Ignition Delay for Various Stage Separation Delays

RASAero II was then used to create a plot for altitude to be compared to the OpenRocket plot under the same conditions as described above. The simulations conducted in RASAero II yielded the expected altitude to be somewhere between 7,900-8,400 feet, which is much lower than what is predicted by OpenRocket. Both OpenRocket and RASAero II produced very similar results for the full-scale altitude simulations, although the altitudes drop off more quickly on the subscale rocket. The team suggests looking into possible causes for the inconsistency in altitude between the two software for future readers.

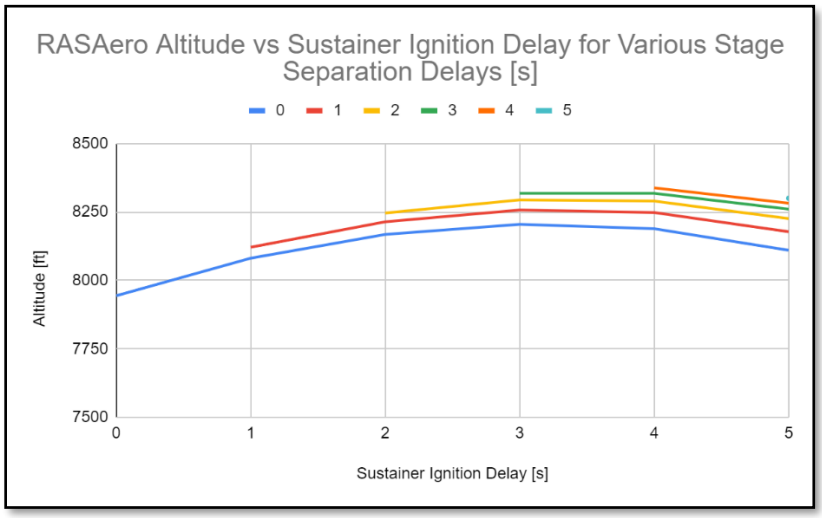

Figure 151 - Subscale RASAero II Altitude vs Sustainer Ignition Delay for Various Stage Separation Delays

Finally, the team simulated the flight using RockSim and developed an array from 13,500-14,700 ft. This exceeds both the OpenRocket and RASAero II simulations, and the team believes this to the due to RockSim user lower drag coefficients than the other two software. These results are like the full-scale simulations, as RockSim seemed to produce much higher altitudes than OpenRocket and RASAero II. These discrepancies further encourage a test flight to verify the simulations, while they also provide the team with a solid range for their results. Overall, the team is relying on OpenRocket for the most accurate altitude predictions due to experience and familiarity with the software.

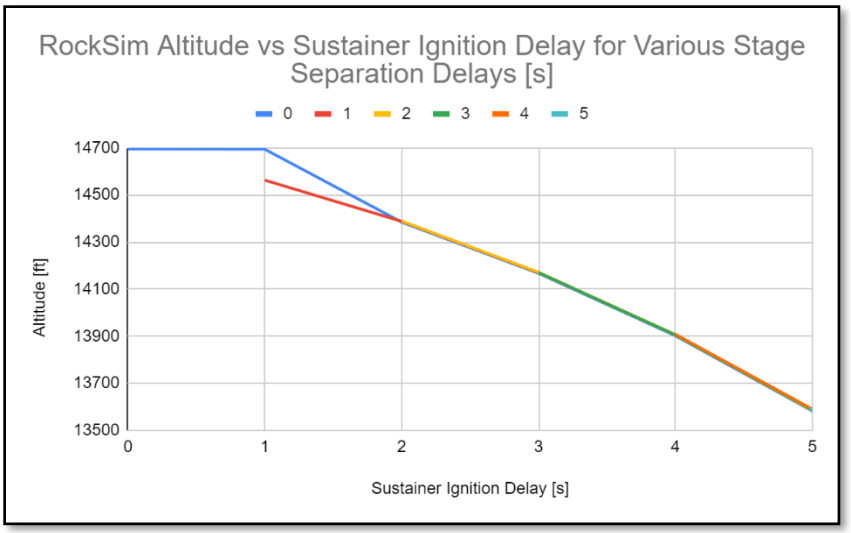

Figure 159 - Subscale RockSim Altitude vs Sustainer Ignition Delay for Various Stage Separation Delays

The team also analyzed the vertical orientation regarding stage separation and sustainer ignition delay. The purpose of these simulations was to verify that the launch vehicle will be within the team requirement of 20-degrees from vertical to ensure the sustainer motor will ignite and the rocket will not fly excessively far from the launch site.

The team analyzed vertical orientation plots for wind speeds of 10 mph by varying only the stage separation delay and sustainer motor ignition delay like the simulations above. In this case, 90 degrees is vertical. To emulate subscale launch conditions, simulations were conducted at a 0-degree launch rail angle since the test flight rail angle can be selected by the team. If there are requirements imposed by the launch field, the team will simulate the flight with updated conditions. Like the full-scale simulations, the plot below shows that vertical orientation is more dependent on sustainer ignition delay, with stage separation delay not being a large factor. At the worst-case scenario of 5 second delay and 20 mph winds, simulations predict the rocket will be approximately 17 degrees off the vertical axis, which satisfies team requirements. Below is the OpenRocket plot for vertical orientations at 10 mph wind speeds as a reference. Overall, the simulations show that the drop off in vertical orientation is quicker for the subscale rocket, so smaller delay times will be required.

The team analyzed vertical orientation plots for wind speeds of 10 mph by varying only the stage separation delay and sustainer motor ignition delay like the simulations above. In this case, 90 degrees is vertical. To emulate subscale launch conditions, simulations were conducted at a 0-degree launch rail angle since the test flight rail angle can be selected by the team. If there are requirements imposed by the launch field, the team will simulate the flight with updated conditions.

Like the full-scale simulations, the plot below shows that vertical orientation is more dependent on sustainer ignition delay, with stage separation delay not being a large factor. At the worst-case scenario of 5 second delay and 20 mph winds, OpenRocket simulations predict the rocket will be approximately 17 degrees off the vertical axis, which satisfies team requirements. Below is the OpenRocket plot for vertical orientations at 10-mph wind speeds as

a reference. Overall, the simulations show that the drop off in vertical orientation is quicker for the subscale rocket, so smaller delay times will be required.

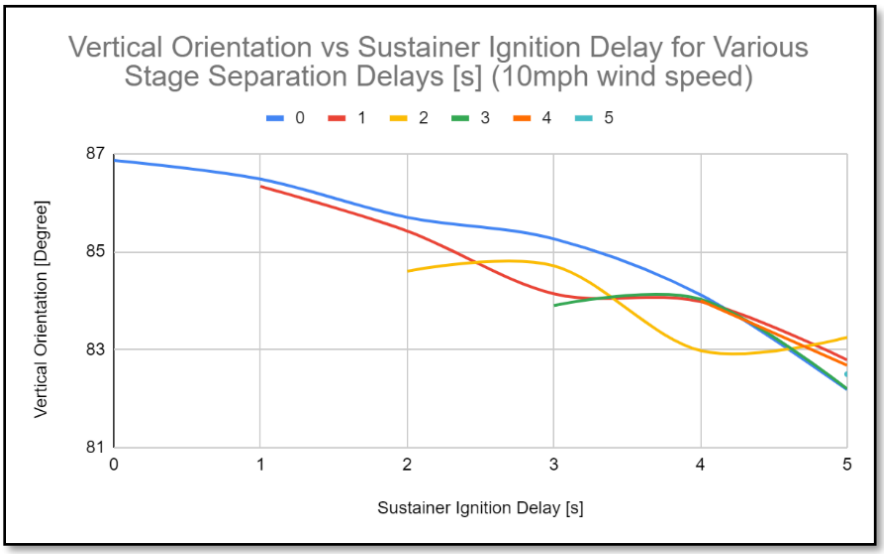

Figure 160 - Subscale OpenRocket Vertical Orientation vs Sustainer Ignition Delay for Various Stage Separation Delays (10 mph wind speed)

RASAero II was then used to create a plot for vertical orientation to be compared to the OpenRocket plot under the same conditions as described above. At the worst-case scenario of 5 second delay and 20 mph wind speeds, RASAero simulations predict the rocket will be approximately 15 degrees off the vertical axis, which is within team requirements. Below is the RASAero II plot for vertical orientations at 10 mph wind speeds. For the 10 mph wind scenario, at a 5 second delay the rocket will be approximately 8 degrees off the vertical axis. Overall, the results from RASAero II and OpenRocket are very comparable and the angular displacement of the launch vehicle is not expected to inhibit sustainer ignition.

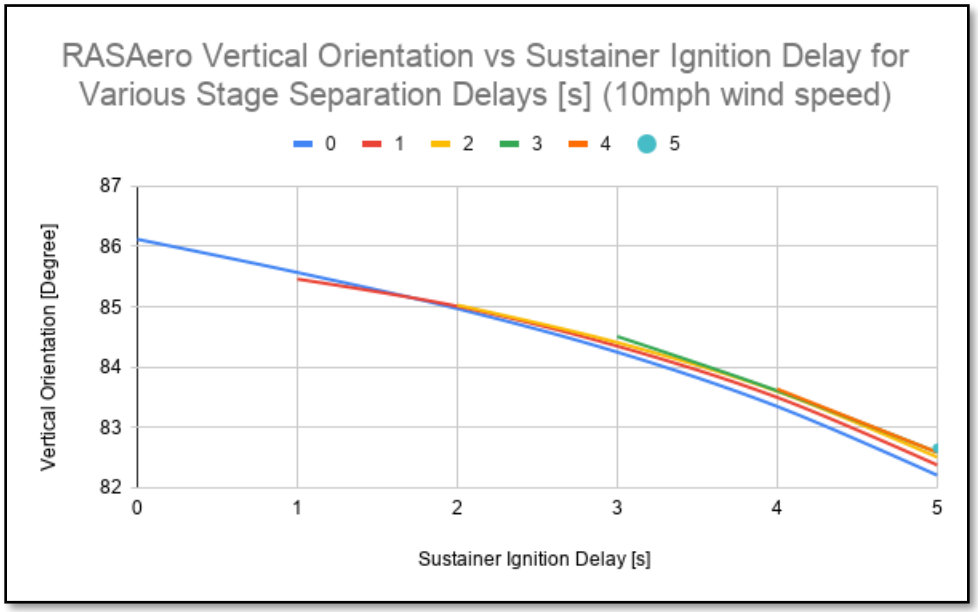

Figure 161 - Subscale RASAero II Vertical Orientation vs Sustainer Ignition Delay for Various Stage Separation Delays (10 mph wind speed)

Lastly, the team looked at the RockSim software to cover the higher altitude simulations. At 20 mph winds with delay times of 5 seconds for stage separation and sustainer ignition, the vertical orientation at sustainer ignition is 74.5 degrees (15.5 degrees off vertical). This is well still the allotted range of 20-degrees for a safe ignition and would likely be safe for the flight, but would not be ideal. The team is safe under the worst case conditions. Under more likely 10 mph winds, 5 second delays result in 82.3 degrees off vertical, and uses less than half the allotted angle within the team's safety restrictions. The team will take the subscale launch in order to compare the results with the three software to find the most accurate. Shown below is a chart depicting RockSim's vertical orientation vs the sustainer ignition delay under 10 mph wind speeds.

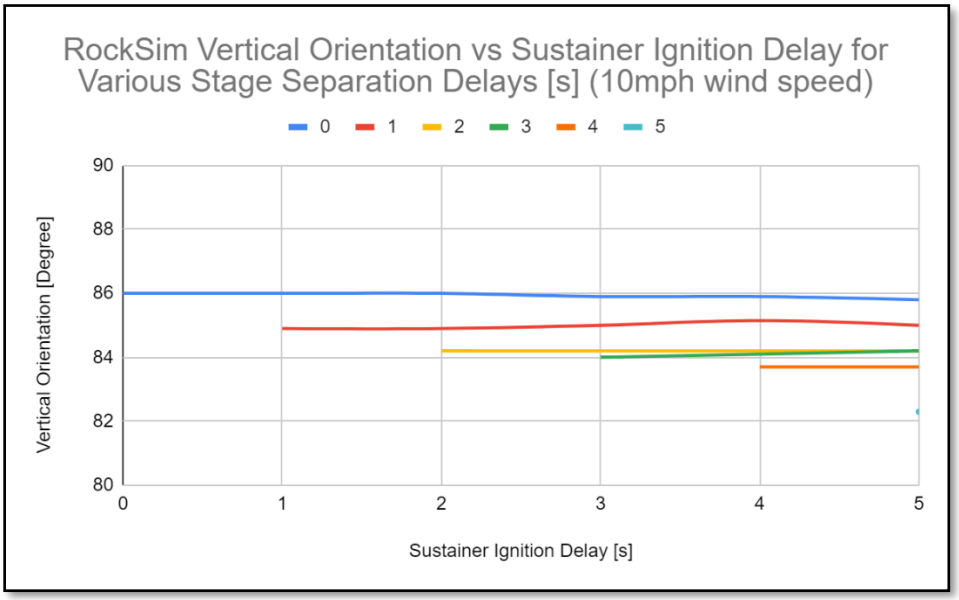

Figure 162 - Subscale RockSim Vertical Orientation vs Sustainer Ignition Delay for Various Stage Separation Delays (10 mph wind speed)

8.2.4. Parachute Deployment Layout

The parachute deployment layout featured the third electronics bay for dual deployment on both stages as previously described in the design section. This allows a separate electronics bay to control the parachute deployment for the first stage. A portion of the OpenRocket layout is shown below in the booster stage parachute area to verify that there are two electronics bays in this stage: one for stage separation and one for parachute deployment.

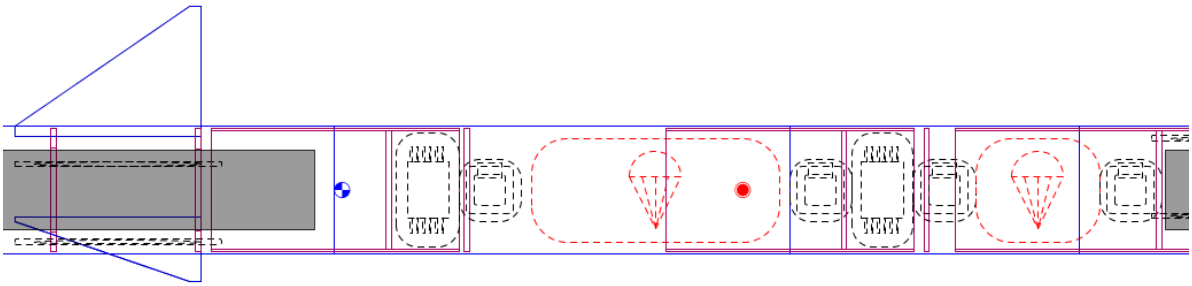

Figure 163 - Subscale OpenRocket booster stage separation layout

The sustainer ignition avionics system design was implemented on the subscale model to verify functionality and ease of assembly of the components. The assembly was reviewed with Chris Pearson in person for additional suggestions. Some improvements were made to the assembly as a result. The following sections detail the electronics bay controlling sustainer motor ignition and the wiring solutions in place.

8.2.5.1 Tiltmeter Bay & Wiring

The tiltmeter bay was designed by the senior design team and printed at the University of Akron 3D printing lab with PLA filament. It features a square extrusion for mounting components on each side while allowing the eye bolt for sustainer motor retention to pass through the center. The tiltmeter bay is constrained on threaded rods between two bulkheads like the other electronics bay designs. The components required to control and power the EasyMega tiltmeter include a 3.7V LiPo battery, two switches, and two terminal blocks for ease of wiring. The assembled tiltmeter bay is shown in the four photos below.

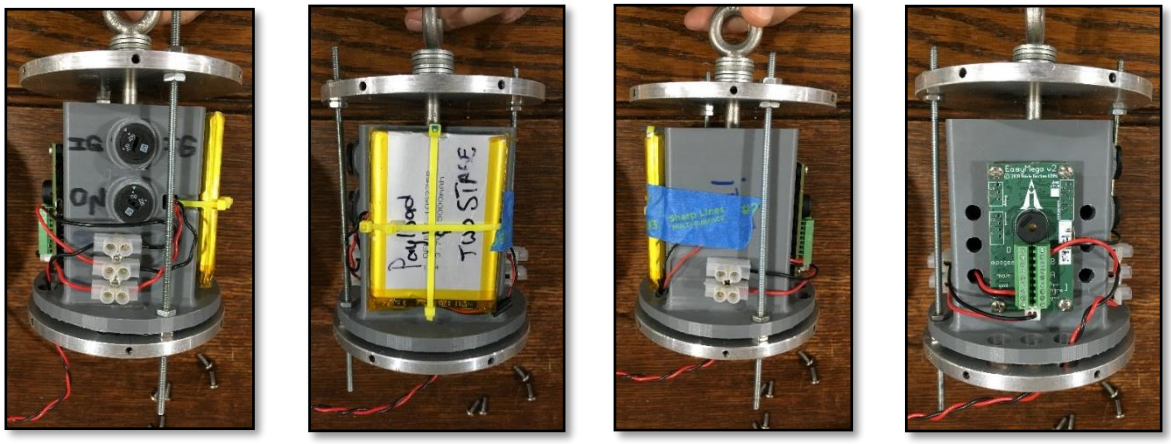

Figure 164 – Subscale EasyMega tiltmeter electronics bay in various orientations

From left to right in the photos above, the switches were both mounted on the same side and opposite the launch rail so they could be reached on the launch pad. The terminal block below them was implemented to verify continuity of the igniter-specific switch. Since this switch will not activate a buzzer or light to verify it is on, the team will check continuity on the terminal block with a multimeter prior to launch. This switch and terminal block were implemented to meet IREC requirements that mandate the sustainer igniter be capable of having an open circuit even after power on of the tiltmeter.

The second photo shows the 3.7V LiPo battery zip tied in place to avoid dislodging during flight. It will be wired to the terminal block in the third photo to power the EasyMega tiltmeter. The fourth photo shows the tiltmeter with wiring from the LiPo battery to its left, wiring from the switch through the hole in the bottom left of the panel, and wiring to the igniter from pyro channel C which is closest to the igniter terminal block on the right. The igniter wiring continues down through the bulkhead and will wire to a terminal block near the base of the sustainer motor. The wiring to this terminal block is shown below looking up from the bottom of the sustainer stage.

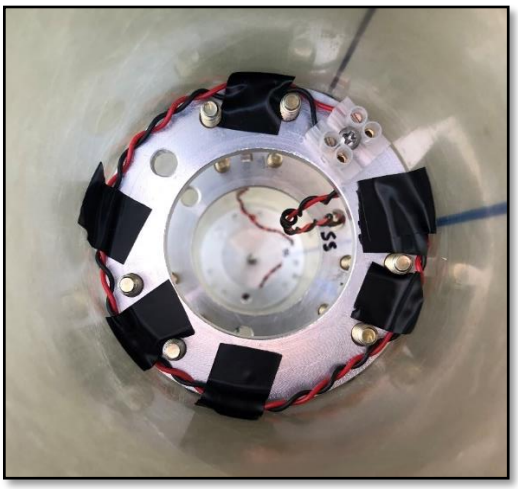

Figure 165 - Subscale sustainer igniter wiring

The excess wire at the base of the terminal block was necessary for assembling the tiltmeter bay from outside the rocket, but it was managed and strain-relieved by wiring around the L bracket screws. This wire is heat resistant Tefzel wire to protect against burning from the black powder separation. Kapton tape or another heat-resistant tape can be used to pressure-seal the bay. The opposite side of the terminal block will wire to the motor igniter for ignition of the sustainer. The igniter should be heat-protected as well to avoid burning or singeing and the motor should be covered with painter's tape or a plastic cap to avoid FOD (foreign object debris) in the motor.

The terminal block was originally designed to be mounted on the top side of the lowest sustainer stage centering ring and accessed through a hole in the airframe. Upon assembling the system, it was determined that it would be easier to access the terminal block through the bottom of the airframe, so it was placed on the bottom side. This can be implemented for the full-scale as well for easier access.

Chris Pearson suggested including two igniters on the sustainer motor for redundancy, which the team was considering as well and will be tested prior to flight without the motor in place. Both can be wired to the same terminal block shown in the photo above. He also suggested taping or gluing the igniters to a motor grain approximately two thirds of the distance up the sustainer motor for longer burning motors as a rule of thumb for an effective burn. Due to his experience with igniters and rocket motors, the team will adhere to these recommendations for the subscale rocket.

6.2.3.2. EasyMega Functionality

Overall, the team is confident in the sustainer igniter wiring and the tiltmeter avionics bay. After reviewing the layout with Chris, the systems are ready for ground separation testing and igniter testing prior to subscale flight.

The four parameters controlling sustainer motor ignition were adjusted for the subscale flight, but the controls are the same. Results from the simulations with estimated launch day conditions for altitude analysis and vertical orientation, along with the altitude limit on the launch field of around 10,000 feet were key factors in the selection of these parameters. Advice from

Chris Pearson was another key factor in the decision making process. The “angle from vertical less than” parameter was kept at 20 degrees, the same as the full-scale rocket.

Based on the simulations for the subscale rocket, the team determined that the sustainer ignition delay time would be 3 seconds after first stage motor burnout. Adding this to the burn time for the first stage motor of 1.7 seconds results in a total delay time of 4.7 seconds. After speaking with Chris Pearson, he recommended talking to the motor manufacturer or the IREC judges to find the delay time for pressure build up in the sustainer motor since he had not flown the CTI K260 before. IREC judges mentioned a delay time of approximately 0.5 seconds for pressure build up. So, the final value for “time since boost greater than” is 4.2 seconds. The “height greater than” parameter was set to 1,220 feet (372 meters), which is 80% of the simulated altitude at sustainer ignition from OpenRocket. This would meet the IREC requirement for a condition indicating 80% of the simulated altitude at sustainer ignition. Finally, the team consulted with Chris with regards to the “time since boost less than” parameter. The seniors recommended setting the parameter to 8 seconds to close the window on sustainer ignition time, which Chris said he was comfortable with. By simulating the flight with an 8 second sustainer ignition delay, the vertical orientation is around 79 degrees, which is still within the team’s 20-degree window and is not too close to apogee for the sustainer stage.

8.3. Recovery Systems

The recovery systems were not the focus of the senior design project, but the team selected key components to round out the entire vehicle design as well as designing simple 3D printed housing units for the components. As previously mentioned, the recovery systems are all safety-critical and any non-functional element could correspond to a crashed rocket, so the team will take care to verify functionality of all components prior to flight. The rocket design team was a key resource to help with assembly and verification of the electronics functionality. The seniors worked closely with the electronics and recovery subsystem leads to ensure the systems functioned as expected. The following sections detail the 3D printed electronics bays that were designed by the seniors with their selected components.

8.3.1. Parachute Electronics Bays

The two parachute electronics bays were 3D printed in red and green PLA filament for the booster and sustainer, respectively, so that they could be visibly differentiated from each other and other electronics systems. Other than color, they are identical to each other since they house all the same components. Each 3D printed sled is constrained along two 6-32 threaded rods to two bulkheads which are fastened to the airframe to keep the electronics secured throughout flight.

Both electronics bays include two StrattologgerCF altimeters, one Featherweight GPS, one 3.7V LiPo battery for the GPS, two 9V batteries for the altimeters, a terminal block for GPS wiring and three switches to arm the electronics from the exterior of the rocket on the launch pad. The electronics bays are shown in the four photos below. The 9V batteries are not pictured for the green electronics bay because the battery holders were not in stock at the time. After reviewing the electronics bays with the electronics subsystem leads, there were no issues identified, other than assembling the 9V batteries. Both systems will be ready for flight.

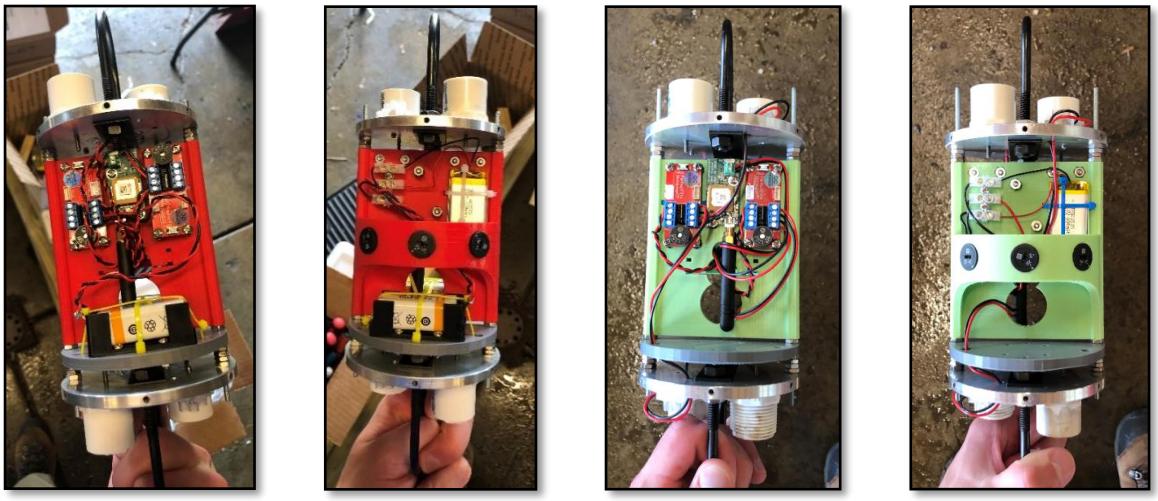

Figure 166 - Subscale parachute electronics bays for the booster (left two) and sustainer (right two)

8.3.2. Stage Separation Electronics Bay

The stage separation electronics bay was designed by the seniors and 3D printed in yellow PLA filament to distinguish it from other electronics systems. It houses two MiniTimer4s, two 9V batteries, and two switches. It is mounted into the rocket like the other electronics bays, using two 6-32 threaded rods and two bulkheads. Each MiniTimer4 controls one ejection charge, so there are two total ejection charges on the top of the bay directed toward the sustainer. The opposite side has a U-bolt to attach to the parachute below the bay, but the parachute deployment electronics bays will control their deployment as previously mentioned. The stage separation bay is shown in the two photos below. The MiniTimer4s were tested and function as expected. The system shown is ready for flight.

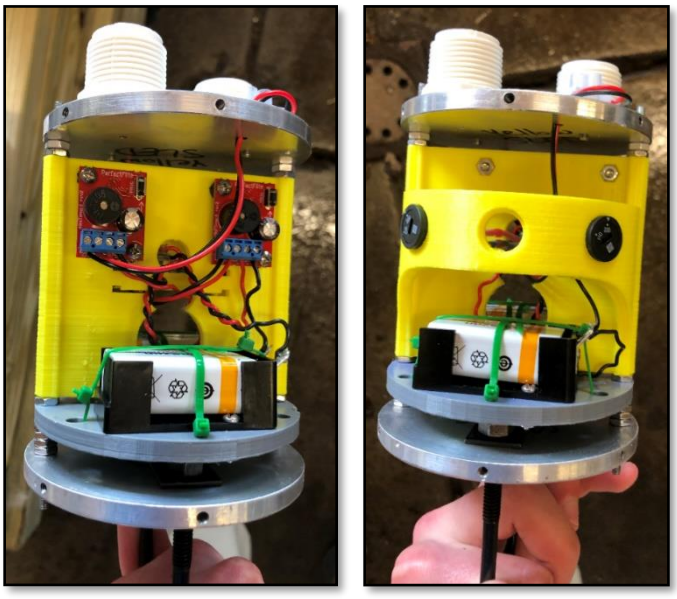

Figure 167 - Subscale stage separation electronics bay

8.4. Flight Predictions

The flight predictions included in the following sections were conducted with the most up-to-date simulations for accuracy. Like the flight predictions section for the full-scale rocket, this section details the flight profile and stability characteristics for the manufactured subscale rocket. The simulations were all conducted using a two second stage separation time delay and a three second sustainer ignition time delay for comparison. These values were based on the analysis conducted for the subscale rocket for altitude and vertical orientation. The estimated launch conditions are shown below for the Springfield, Ohio launch site and were replicated for each software with the stage separation and sustainer ignition time delays.

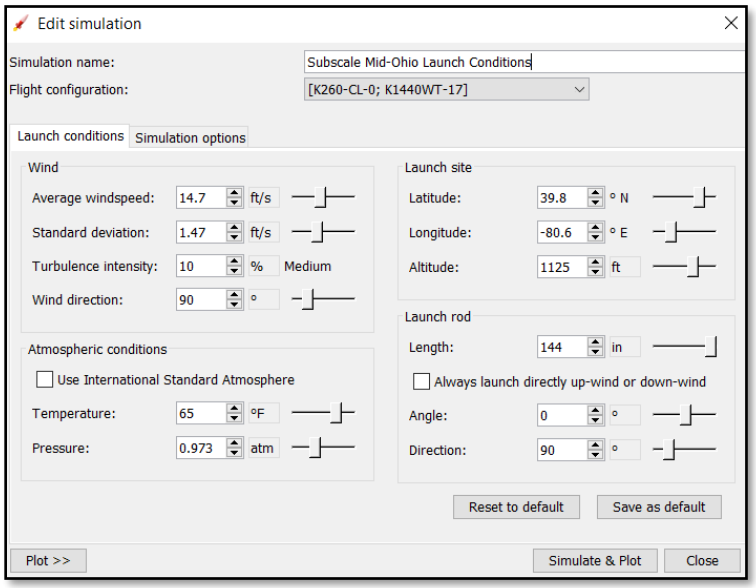

Figure 168 - Subscale Mid-Ohio Launch Conditions

8.4.1. Flight Profile

The OpenRocket flight profile that was replicated in RASAero II and RockSim is shown below for both stages together and the sustainer alone. The main difference other than airframe size is that there is no payload in the nose cone on the subscale rocket.

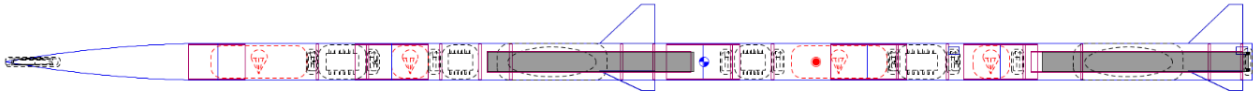

Figure 124 – Subscale OpenRocket Flight Profile for both stages

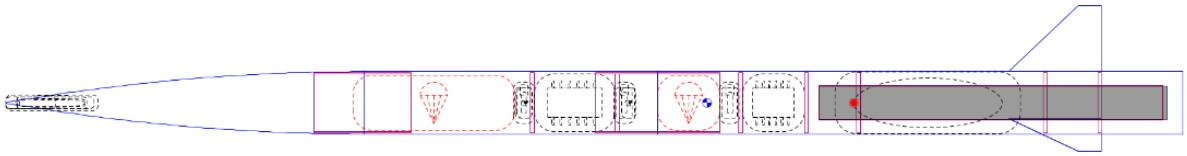

Figure 125 – Subscale OpenRocket Flight Profile for sustainer stage

Using the flight profiles and the software configurations, the team compared and plotted the same key flight characteristics and the stability margins in all three software, like the full-scale

rocket. Below is a table of key flight characteristics between the three software for both stages of the rocket together. The thrust to weight ratios and rail exit velocities all meet IREC requirements for the subscale rocket. The drag coefficients and maximum vertical velocities can be used for a quick comparison between the software. Unlike the full-scale rocket, the RockSim drag coefficient is much closer to the other two software, but it is still lower. All other flight characteristics are similar between the three software.

Subscale Flight Profile Calculations – Both Stages

Flight Profile Characteristic	OpenRocket	RASAero II	RockSim
Maximum Thrust to Weight Ratio	13.14	13.59	11.24
Maximum Vertical Velocity (ft/s)	431.3	424.1	430.5
Drag Coefficient at Max Velocity	0.751	0.692	0.565
Rail Exit Velocity (12 ft.) (ft/s)	87.8	87.5	88.3

Table 13 – Subscale flight profile calculations for both stages

Below is a table of the same flight characteristics between the three software for the sustainer stages of the rocket only, with apogee achieved instead of the rail exit velocity. The thrust to weight ratios all meet IREC requirements for the subscale rocket. The apogee achieved for RASAero is much lower than the other two software and RockSim appears to be closer to OpenRocket, although it is still higher. This leads the team to believe that the drag coefficients are the leading causes of the different values. The drag coefficient for RASAero is highest, while the RockSim drag coefficient is much lower, like the full-scale rocket. These flight characteristics will be useful to compare the accuracy of the three software for a multistage flight. Then the full-scale launch will help validate which software is more accurate for supersonic flight.

Subscale Flight Profile Calculations – Sustainer Stage

Flight Profile Characteristic	OpenRocket	RASAero II	RockSim
Maximum Thrust to Weight Ratio	5.37	5.40	5.21
Maximum Vertical Velocity (ft/s)	766.85	611.11	827.08
Drag Coefficient at Max Velocity	0.525	0.625	0.299
Apogee (ft)	11,635	7,929	13,655

Table 14 – Subscale flight profile calculations for sustainer stage

8.4.2. Stability

The team attempted to keep the stability margins like the full-scale rocket for both configurations to prove the stability. Below is a table outlining the subscale stability calculations for both stages of the rocket together in all three software. Overall, the stability margin in all three software meet team and competition requirements, are close to the full-scale rocket values, and the team is confident in the stability of the two-stage configuration.

Subscale Stability Calculations – Both Stages

Stability Characteristic	OpenRocket	RASAero II	RockSim

CP Wet (in)	88.61	88.44	89.01
CG Wet (in)	76.36	76.36	76.30
CG Post Burnout (in)	72.66	72.64	73.59
Stability Margin	3.04	3.09	3.14
Stability Margin Post Burnout	3.83	3.92	3.95

Table 15 – Subscale stability calculations for both stages

Below is a table outlining the same stability calculations for the sustainer stage of the rocket only. The subscale stability margin in all three software of around 2.40 is slightly higher than the full-scale sustainer stability margin of around 2.05, but it still meets team and competition requirements for the sustainer stage and the team is confident in the stability for the sustainer configuration.

Subscale Stability Calculations – Sustainer Stage

Stability Characteristic	OpenRocket	RASAero II	RockSim
CP Wet (in)	54.96	54.98	55.35
CG Wet (in)	45.44	45.44	45.61
CG Post Burnout (in)	42.23	42.04	42.35
Stability Margin	2.36	2.37	2.42
Stability Margin Post Burnout	3.29	3.21	3.33

Table 16 – Subscale stability calculations for sustainer stage

9. Project BOGO was an outstanding senior design project to apply existing knowledge and research further to learn more about rocketry, specifically multistage and supersonic rockets. This document serves as a guide of the thought process of the senior design team and a record of all design decisions, analytical and simulation results, and the manufacturing and assembly results of the subscale two-stage rocket.

The team used various software packages such as Solidworks for CAD applications, ANSYS for analysis of the rocket to verify the design would withstand various forces of flight, and Excel to calculate and plot various trends or results. Additionally, the team gained much more experience using common flight simulation software such as OpenRocket, RASAero II, and RockSim, specifically for two-stage flight.

Beyond the software experience, the team gained mechanical and aerospace design experience through comparing concept ideas and commercial options that were reviewed, as well as developing pros and cons to compare the options for specific scenarios. The team found research articles and discussed with team mentors in the rocketry community to gather a knowledgebase of supersonic and multistage rocket information which has been documented in the report. Specific focus areas included nose cone and fin design, motor selection and retention, stage separation, parachute deployment, and sustainer ignition avionics. Using the team's own intuition, additional research was conducted with the software packages previously mentioned.

Due to the unique challenges and requirements of a supersonic multistage rocket, the team had to develop creative solutions and learn how to use components for the first time. The team conceptualized and designed several new fin retention assemblies that are optimized for retention strength while not interfering with stage separation. The team also gained experience with new avionic components, including the MiniTimer4 and EasyMega, which are used for stage separation and sustainer motor ignition, respectively. As mentioned above, the team also gained experience with flight simulation software, specifically using multistage rockets, and optimizing flight based on launch conditions and stage separation and sustainer ignition time delays.

Additionally, the team conducted several tests and manufactured a subscale version of the two-stage rocket. The goals of the tests were to verify structural strength of the team's components and to verify functionality of the new electrical components. These subsystem tests were detailed so that they can be repeated by future team members. The subscale two-stage rocket was built as a scaled-down version of the supersonic rocket based on similar design ideas. It does not replicate all aspects of the full-scale, such as reaching supersonic speed, but it can be used to verify the functionality of the stage separation mechanics and narrow down the accuracy of the three simulation software in regards to multi-staging. The subscale rocket helped flush out manufacturing issues for the first two-stage rocket the team has built and helped identify issues that can be solved on the full-scale rocket.

In conclusion, the team is grateful for the opportunity to work on and learn through an independent research and design project at the University of Akron. The four senior design team members had control of the project from the outset and were able to shape it and find their own direction as desired. This is a very underappreciated aspect of the team's project. Without

having a guide to follow for the design, the four team members gained valuable project management experience and efficient decision making skills on shortened timelines that will be useful in their future careers. Overall, the senior design project was a success as it exemplified the students' mechanical and aerospace engineering abilities and the skills that were learned through the engineering curriculums at the University of Akron.

10 Appendix

10.1 Timeline Breakdown

The senior design team began the two-stage launch vehicle project in the middle of the summer of 2019, much earlier than the required start date by the University. The team engaged in the difficult challenge of successfully designing and manufacturing a functional multistage rocket for the first time in the rocket team's history. From the outset, the four seniors developed an all-encompassing timeline for all subsystems of the project in Microsoft Project, along with documentation that would be required for the Spaceport America Cup. All four team members had experience leading projects and developing timelines for single stage rockets and subsystem-specific projects. However, the two-stage project included new research and design components that were difficult to account for in the timeline and new topics to review that the team did not anticipate when considering the architectural design for the launch vehicle. Realizing this, the senior design team narrowed the project's scope from the entire rocket design to the aerostructure-related components along with some electrical and propulsion components, which still includes a large majority of the rocket design. The remaining components were designed by rocket design team members while working with the senior design group for interfacing requirements, specifically for the payload and recovery subsystems.

The senior design project objectives also changed rapidly throughout the project. The team decided a few months into research that they wanted to build the first supersonic rocket in Akronauts' history. On top of this, the group felt a subscale rocket should be built and tested to verify system functionality. In early spring, the COVID-19 epidemic arrived, leaving subscale manufacturing at a standstill for a few weeks. These unforeseen events and changes, specifically the COVID-19 epidemic, delayed the project timeline to the point that a test flight could not be conducted by the University's senior design project due date. However, the team was able to nearly finish manufacturing the subscale version of the rocket and plans to fly it soon. Although the Spaceport America Cup competition was canceled near the end of March 2020, the rocket design team would like to still pursue manufacturing the full-scale version of the two-stage rocket and launch it in the summer or early fall, if possible.

Below is the project timeline that the senior design team members created at the beginning of the year. This will give future readers a glimpse of the process the team attempted to go through over the course of the year. It also displays the project management skills and rocket understanding of the senior design members to create an extensive timeline to encompass a difficult research project of this scale. The four seniors hope that the timeline as well as the research and design the team has conducted will guide the Akronauts Rocket Design Team and other engineers as they seek to understand the team's thought process for the multistage launch vehicle.

Senior Design Project Timeline

Task Name	Duration	Start	Finish
Senior Design Project 2019-2020	**196 days**	**Mon 7/1/19**	**Mon 3/30/20**
Two-Stage Launch Vehicle Development	**196 days**	**Mon 7/1/19**	**Mon 3/30/20**
Aerostructure	**196 days**	**Mon 7/1/19**	**Mon 3/30/20**
Launch Vehicle Summary	**141 days**	**Mon 7/1/19**	**Mon 1/13/20**
Estimated Sizes and Masses for all Components	11 days	Mon 7/1/19	Mon 7/15/19
Final Sizes and Masses for all Components	36 days	Mon 11/25/19	Mon 1/13/20
Rail Size	11 days	Mon 7/29/19	Mon 8/12/19
Launch Vehicle Design	**196 days**	**Mon 7/1/19**	**Mon 3/30/20**
Design Options	**51 days**	**Mon 7/1/19**	**Mon 9/9/19**
Body Tubes & Couplers	36 days	Mon 7/1/19	Mon 8/19/19
Nose Cone	11 days	Mon 8/5/19	Mon 8/19/19
Fin Attachment	21 days	Mon 7/29/19	Mon 8/26/19
Fins	16 days	Mon 8/5/19	Mon 8/26/19
Centering Rings & Bulkheads	16 days	Mon 8/5/19	Mon 8/26/19
Motor Options	31 days	Mon 7/8/19	Mon 8/19/19
Motor Mounting & Retention	41 days	Mon 7/15/19	Mon 9/9/19
Separation System	41 days	Mon 7/15/19	Mon 9/9/19
Material Choices	51 days	Mon 7/1/19	Mon 9/9/19
3D Models	**171 days**	**Mon 8/5/19**	**Mon 3/30/20**
Nose Cone	6 days	Mon 9/9/19	Mon 9/16/19
Body Tubes and Couplers	6 days	Mon 9/9/19	Mon 9/16/19
Centering Ring & Bulkheads	31 days	Mon 8/5/19	Mon 9/16/19
Motor Mount Systems	11 days	Mon 9/9/19	Mon 9/23/19
Fins	6 days	Mon 9/9/19	Mon 9/16/19
Fin Mounting	36 days	Mon 8/5/19	Mon 9/23/19
Stability Ballast(s)	11 days	Mon 9/9/19	Mon 9/23/19
Full Assembly	11 days	Mon 3/9/20	Mon 3/23/20
CAD Drawings of Final Launch Vehicle	16 days	Mon 3/9/20	Mon 3/30/20
Flight Integrity	**146 days**	**Mon 7/1/19**	**Mon 1/20/20**
Suitablity of Fin and Attachment Design	31 days	Mon 8/5/19	Mon 9/16/19
Sufficient Motor Mounting and Retention	11 days	Mon 9/9/19	Mon 9/23/19
Separation System Mechanics	56 days	Mon 7/22/19	Mon 10/7/19
2nd Stage Ignition Mechanics	56 days	Mon 7/29/19	Mon 10/14/19
Stability Margin	146 days	Mon 7/1/19	Mon 1/20/20
Fin Flutter	11 days	Mon 8/19/19	Mon 9/2/19
Nose Cone Temperature	11 days	Mon 8/19/19	Mon 9/2/19
Rail Attachment and Hardware	16 days	Mon 8/19/19	Mon 9/9/19
Mission Performance Predictions	**171 days**	**Mon 7/1/19**	**Mon 2/24/20**
OpenRocket Model	46 days	Mon 7/1/19	Mon 9/2/19

RASAero II Model	11 days	Mon 9/2/19	Mon 9/16/19
Simulation Estimates	**26 days**	**Mon 9/2/19**	**Mon 10/7/19**
Thrust to Weight Ratio	26 days	Mon 9/2/19	Mon 10/7/19
Rail Exit Velocity	26 days	Mon 9/2/19	Mon 10/7/19
Altitude Predictions	26 days	Mon 9/2/19	Mon 10/7/19
Stability Margin	26 days	Mon 9/2/19	Mon 10/7/19
Simulated CP/CG Locations	26 days	Mon 9/2/19	Mon 10/7/19
As-Built Predictions	**31 days**	**Mon 1/13/20**	**Mon 2/24/20**
Thrust to Weight Ratio	31 days	Mon 1/13/20	Mon 2/24/20
Rail Exit Velocity	31 days	Mon 1/13/20	Mon 2/24/20
Altitude Predictions	31 days	Mon 1/13/20	Mon 2/24/20
Stability Margin	31 days	Mon 1/13/20	Mon 2/24/20
Simulated CP/CG Locations	31 days	Mon 1/13/20	Mon 2/24/20
Flight Profile	**31 days**	**Mon 1/13/20**	**Mon 2/24/20**
Vertical Motion vs. Time	31 days	Mon 1/13/20	Mon 2/24/20
Stability vs. Time	31 days	Mon 1/13/20	Mon 2/24/20
Manufacturing	**91 days**	**Mon 11/11/19**	**Mon 3/16/20**
Outline of Construction Process	11 days	Mon 11/25/19	Mon 12/9/19
Outline of Assembly Process	21 days	Mon 2/17/20	Mon 3/16/20
Build	**56 days**	**Mon 11/11/19**	**Mon 1/27/20**
Nose Cone	31 days	Mon 12/2/19	Mon 1/13/20
Body Tubes and Couplers	31 days	Mon 12/2/19	Mon 1/13/20
Centering Ring & Bulkheads	46 days	Mon 11/11/19	Mon 1/13/20
Motor Mount Systems	31 days	Mon 12/2/19	Mon 1/13/20
Fins	31 days	Mon 12/2/19	Mon 1/13/20
Fin Mounting	46 days	Mon 11/11/19	Mon 1/13/20
Stability Ballast(s)	46 days	Mon 11/11/19	Mon 1/13/20
Independent Sections	26 days	Mon 12/23/19	Mon 1/27/20
Recovery	**151 days**	**Mon 7/29/19**	**Mon 2/24/20**
Recovery Design	**46 days**	**Mon 7/29/19**	**Mon 9/30/19**
Canopy Designs	21 days	Mon 7/29/19	Mon 8/26/19
Material Selection	21 days	Mon 7/29/19	Mon 8/26/19
Parachute Placement	21 days	Mon 7/29/19	Mon 8/26/19
Number of Devices and Events	26 days	Mon 7/29/19	Mon 9/2/19
Ejection Methods	26 days	Mon 7/29/19	Mon 9/2/19
Hardware	**26 days**	**Mon 8/26/19**	**Mon 9/30/19**
U-bolts/Eyebolts	26 days	Mon 8/26/19	Mon 9/30/19
Quick Links	26 days	Mon 8/26/19	Mon 9/30/19
Harness/Shock Cords/Ropes	26 days	Mon 8/26/19	Mon 9/30/19
Shear Pins	26 days	Mon 8/26/19	Mon 9/30/19
Mission Performance Predictions	**126 days**	**Mon 9/2/19**	**Mon 2/24/20**
Simulation Estimates	**26 days**	**Mon 9/2/19**	**Mon 10/7/19**
Parachute Sizing for Safe Descent	26 days	Mon 9/2/19	Mon 10/7/19

Descent Times	26 days	Mon 9/2/19	Mon 10/7/19
Drift Calculations	26 days	Mon 9/2/19	Mon 10/7/19
Snatch Force Calculation	26 days	Mon 9/2/19	Mon 10/7/19
Load Ratings and Expected Loads	26 days	Mon 9/2/19	Mon 10/7/19
Ejection Charge Amounts	26 days	Mon 9/2/19	Mon 10/7/19
Kinetic Energy During Key Phases	26 days	Mon 9/2/19	Mon 10/7/19
Shear Pin Calculations	26 days	Mon 9/2/19	Mon 10/7/19
As-Built Predictions	**31 days**	**Mon 1/13/20**	**Mon 2/24/20**
Parachute Sizing for Safe Descent	31 days	Mon 1/13/20	Mon 2/24/20
Descent Times	31 days	Mon 1/13/20	Mon 2/24/20
Drift Calculations	31 days	Mon 1/13/20	Mon 2/24/20
Snatch Force Calculation	31 days	Mon 1/13/20	Mon 2/24/20
Load Ratings and Expected Loads	31 days	Mon 1/13/20	Mon 2/24/20
Ejection Charge Amounts	31 days	Mon 1/13/20	Mon 2/24/20
Kinetic Energy During Key Phases	31 days	Mon 1/13/20	Mon 2/24/20
Shear Pin Calculations	31 days	Mon 1/13/20	Mon 2/24/20
Flight Integrity	**21 days**	**Mon 12/2/19**	**Mon 12/30/19**
Drag Coefficient Solidworks Simulations	21 days	Mon 12/2/19	Mon 12/30/19
Recovery Harness and Connection Diagram	21 days	Mon 12/2/19	Mon 12/30/19
ConOps for Key Events	21 days	Mon 12/2/19	Mon 12/30/19
Manufacturing	**26 days**	**Mon 12/2/19**	**Mon 1/6/20**
Outline of Recovery Assembly Process	26 days	Mon 12/2/19	Mon 1/6/20
Manufacture Parachute(s)	26 days	Mon 12/2/19	Mon 1/6/20
Assemble Hardware, Rope, Shock Cords	26 days	Mon 12/2/19	Mon 1/6/20
Electronics	**131 days**	**Mon 7/22/19**	**Mon 1/20/20**
Electronics Bay Designs	**61 days**	**Mon 7/22/19**	**Mon 10/14/19**
1st Stage Parachute Deployment Electronics	**56 days**	**Mon 7/29/19**	**Mon 10/14/19**
Altimeters	16 days	Mon 7/29/19	Mon 8/19/19
GPS	41 days	Mon 7/29/19	Mon 9/23/19
Batteries	16 days	Mon 7/29/19	Mon 8/19/19
Switches	16 days	Mon 7/29/19	Mon 8/19/19
External Charging Capability (if applicable)	41 days	Mon 7/29/19	Mon 9/23/19
Block & Wiring Diagrams	26 days	Mon 9/9/19	Mon 10/14/19
Sled Design	41 days	Mon 7/29/19	Mon 9/23/19
Assembly Drawing	26 days	Mon 9/9/19	Mon 10/14/19
2nd Stage Parachute Deployment Electronics	**56 days**	**Mon 7/29/19**	**Mon 10/14/19**
Altimeters	16 days	Mon 7/29/19	Mon 8/19/19
GPS	41 days	Mon 7/29/19	Mon 9/23/19
Batteries	16 days	Mon 7/29/19	Mon 8/19/19

Switches	16 days	Mon 7/29/19	Mon 8/19/19
External Charging Capability (if applicable)	41 days	Mon 7/29/19	Mon 9/23/19
Block & Wiring Diagrams	26 days	Mon 9/9/19	Mon 10/14/19
Sled Design	41 days	Mon 7/29/19	Mon 9/23/19
Assembly Drawing	26 days	Mon 9/9/19	Mon 10/14/19
2nd Stage Ignition Electronics	**61 days**	**Mon 7/22/19**	**Mon 10/14/19**
Deployment Electronics (Tiltmeter or equivalent)	56 days	Mon 7/22/19	Mon 10/7/19
Batteries	46 days	Mon 7/29/19	Mon 9/30/19
Switches	21 days	Mon 7/29/19	Mon 8/26/19
External Charging Capability (if applicable)	46 days	Mon 7/29/19	Mon 9/30/19
Block & Wiring Diagrams	26 days	Mon 9/9/19	Mon 10/14/19
Sled Design	26 days	Mon 9/9/19	Mon 10/14/19
Assembly Drawing	26 days	Mon 9/9/19	Mon 10/14/19
Flight Integrity	**41 days**	**Mon 9/9/19**	**Mon 11/4/19**
Operating Frequencies	41 days	Mon 9/9/19	Mon 11/4/19
Power Requirements and Battery Life	26 days	Mon 9/9/19	Mon 10/14/19
Range Capability	26 days	Mon 9/9/19	Mon 10/14/19
System Redundancy	11 days	Mon 9/9/19	Mon 9/23/19
Sled Design Mechanical Retention and Space Efficiency	26 days	Mon 9/9/19	Mon 10/14/19
Recovery Systems sensitivity to Transmitters	41 days	Mon 9/9/19	Mon 11/4/19
Pressure Equalization for Altimeters	11 days	Mon 9/9/19	Mon 9/23/19
Manufacturing	**51 days**	**Mon 11/11/19**	**Mon 1/20/20**
Outline of Assembly Processes for Electronics Bays	**11 days**	**Mon 1/6/20**	**Mon 1/20/20**
1st Stage Parachute Deployment Electronics	11 days	Mon 1/6/20	Mon 1/20/20
2nd Stage Parachute Deployment Electronics	11 days	Mon 1/6/20	Mon 1/20/20
2nd Stage Ignition Electronics	11 days	Mon 1/6/20	Mon 1/20/20
Build	**41 days**	**Mon 11/11/19**	**Mon 1/6/20**
1st Stage Parachute Deployment Electronics	**26 days**	**Mon 11/11/19**	**Mon 12/16/19**
Mounting System	26 days	Mon 11/11/19	Mon 12/16/19
Altimeters	26 days	Mon 11/11/19	Mon 12/16/19
GPS	26 days	Mon 11/11/19	Mon 12/16/19
Batteries	26 days	Mon 11/11/19	Mon 12/16/19
Switches	26 days	Mon 11/11/19	Mon 12/16/19
External Charging Capability (if applicable)	26 days	Mon 11/11/19	Mon 12/16/19

2nd Stage Parachute Deployment Electronics	**26 days**	**Mon 11/11/19**	**Mon 12/16/19**
Mounting System	26 days	Mon 11/11/19	Mon 12/16/19
Altimeters	26 days	Mon 11/11/19	Mon 12/16/19
GPS	26 days	Mon 11/11/19	Mon 12/16/19
Batteries	26 days	Mon 11/11/19	Mon 12/16/19
Switches	26 days	Mon 11/11/19	Mon 12/16/19
External Charging Capability (if applicable)	26 days	Mon 11/11/19	Mon 12/16/19
2nd Stage Ignition Electronics	**21 days**	**Mon 12/9/19**	**Mon 1/6/20**
Mounting System	21 days	Mon 12/9/19	Mon 1/6/20
Deployment Electronics (Tiltmeter or equivalent)	21 days	Mon 12/9/19	Mon 1/6/20
Batteries	21 days	Mon 12/9/19	Mon 1/6/20
Switches	21 days	Mon 12/9/19	Mon 1/6/20
External Charging Capability (if applicable)	21 days	Mon 12/9/19	Mon 1/6/20
Propulsion	**161 days**	**Mon 7/15/19**	**Mon 2/24/20**
Preliminary Motor Choices	21 days	Mon 7/15/19	Mon 8/12/19
Final Motor Choices	46 days	Mon 12/23/19	Mon 2/24/20
Thrust Curves for Motors	46 days	Mon 12/23/19	Mon 2/24/20
Igniter Wiring Diagrams	41 days	Mon 12/16/19	Mon 2/10/20
3D Models & Drawings of Motors	41 days	Mon 12/16/19	Mon 2/10/20
Ground Launch Support Equipment Identified & Obtained	41 days	Mon 12/16/19	Mon 2/10/20
Payload (if applicable)	**96 days**	**Mon 10/7/19**	**Mon 2/17/20**
Payload Summary	**16 days**	**Mon 10/7/19**	**Mon 10/28/19**
Success Criteria	16 days	Mon 10/7/19	Mon 10/28/19
Experiment Description	16 days	Mon 10/7/19	Mon 10/28/19
Payload Design	**61 days**	**Mon 10/14/19**	**Mon 1/6/20**
Experiment Functionality	11 days	Mon 10/14/19	Mon 10/28/19
3D Models and CAD Drawings	41 days	Mon 11/11/19	Mon 1/6/20
Wiring and Block Diagrams (if applicable)	41 days	Mon 11/11/19	Mon 1/6/20
Payload Integration into Launch Vehicle	**46 days**	**Mon 10/28/19**	**Mon 12/30/19**
Retention System	46 days	Mon 10/28/19	Mon 12/30/19
Deployment System (if applicable)	46 days	Mon 10/28/19	Mon 12/30/19
Manufacturing	**41 days**	**Mon 12/23/19**	**Mon 2/17/20**
Outline of Assembly Process	41 days	Mon 12/23/19	Mon 2/17/20
Build and Assemble Payload	41 days	Mon 12/23/19	Mon 2/17/20
Launch Vehicle Integration and Testing	**96 days**	**Mon 11/18/19**	**Mon 3/30/20**
Identify all test objectives, success criteria, test variables, and methods	31 days	Mon 11/18/19	Mon 12/30/19
Discuss Results and Effects on Vehicle Design	56 days	Mon 11/18/19	Mon 2/3/20

Subsystem Testing	**81 days**	**Mon 11/18/19**	**Mon 3/9/20**
Wind Tunnel Tests with rocket and parachutes	29.77 days	Mon 11/18/19	Mon 12/30/19
Body Tube Compression Test	31 days	Mon 11/18/19	Mon 12/30/19
Screw Shear Tests with Bulkhead	31 days	Mon 11/18/19	Mon 12/30/19
Recovery Hardware Tensile Tests	31 days	Mon 11/18/19	Mon 12/30/19
Ground Separation Tests	81 days	Mon 11/18/19	Mon 3/9/20
Parachute Drop Tests	31 days	Mon 11/18/19	Mon 12/30/19
GPS Tests	31 days	Mon 11/18/19	Mon 12/30/19
2nd Stage Ignition Electronics Tests	41 days	Mon 11/18/19	Mon 1/13/20
Full Scale Test Flight (if applicable)	**26 days**	**Mon 2/24/20**	**Mon 3/30/20**
Summary with Error Discussion	26 days	Mon 2/24/20	Mon 3/30/20
Altitude Achieved along with other Flight Data	26 days	Mon 2/24/20	Mon 3/30/20
Drag Coefficient and Post-Flight Simulation	26 days	Mon 2/24/20	Mon 3/30/20
Discuss Similarities and Differences between test flight and future competition flight	26 days	Mon 2/24/20	Mon 3/30/20
Safety	**116 days**	**Mon 10/7/19**	**Mon 3/16/20**
Procedures	**61 days**	**Mon 12/16/19**	**Mon 3/9/20**
Launch Vehicle Assembly	21 days	Mon 1/27/20	Mon 2/24/20
Recovery Preparation	**21 days**	**Mon 1/27/20**	**Mon 2/24/20**
Ejection System Preparation	21 days	Mon 1/27/20	Mon 2/24/20
Parachute Preparation	21 days	Mon 1/27/20	Mon 2/24/20
Motor Preparation	21 days	Mon 12/16/19	Mon 1/13/20
Igniter Installation	21 days	Mon 1/27/20	Mon 2/24/20
Electronics Preparation & Assembly	**36 days**	**Mon 12/16/19**	**Mon 2/3/20**
GPS Preparation	21 days	Mon 12/16/19	Mon 1/13/20
Altimeter Preparation	21 days	Mon 12/16/19	Mon 1/13/20
2nd Stage Ignition Electronics Preparation	36 days	Mon 12/16/19	Mon 2/3/20
Electronics Sled Assembly	36 days	Mon 12/16/19	Mon 2/3/20
Payload Preparation and Assembly (if applicable)	31 days	Mon 1/13/20	Mon 2/24/20
Setup on Launch Pad	16 days	Mon 12/16/19	Mon 1/6/20
Launch	16 days	Mon 12/16/19	Mon 1/6/20
Troubleshooting	21 days	Mon 2/10/20	Mon 3/9/20
Hazard Analysis	**116 days**	**Mon 10/7/19**	**Mon 3/16/20**
Failure Modes and Effects Analysis	**116 days**	**Mon 10/7/19**	**Mon 3/16/20**
Aerostructure	116 days	Mon 10/7/19	Mon 3/16/20
Recovery	116 days	Mon 10/7/19	Mon 3/16/20
Electronics	116 days	Mon 10/7/19	Mon 3/16/20
Propulsion	116 days	Mon 10/7/19	Mon 3/16/20
Payload (if applicable)	116 days	Mon 10/7/19	Mon 3/16/20

Personal Hazard Analysis	76 days	Mon 10/7/19	Mon 1/20/20
Environmental Hazard Analysis	76 days	Mon 10/7/19	Mon 1/20/20
Derivation Requirements	**161 days**	**Mon 8/5/19**	**Mon 3/16/20**
Derive Project Requirements	**26 days**	**Mon 8/5/19**	**Mon 9/9/19**
Launch Vehicle	26 days	Mon 8/5/19	Mon 9/9/19
Recovery	26 days	Mon 8/5/19	Mon 9/9/19
Payload	26 days	Mon 8/5/19	Mon 9/9/19
Validate Project Requirements	**81 days**	**Mon 11/25/19**	**Mon 3/16/20**
Launch Vehicle	81 days	Mon 11/25/19	Mon 3/16/20
Recovery	81 days	Mon 11/25/19	Mon 3/16/20
Payload	81 days	Mon 11/25/19	Mon 3/16/20
Budget	**71 days**	**Mon 8/12/19**	**Mon 11/18/19**
Aerostructure	61 days	Mon 8/19/19	Mon 11/11/19
Recovery	61 days	Mon 8/19/19	Mon 11/11/19
Electronics	61 days	Mon 8/19/19	Mon 11/11/19
Propulsion	61 days	Mon 8/19/19	Mon 11/11/19
Payload	61 days	Mon 8/19/19	Mon 11/11/19
Administrative	61 days	Mon 8/19/19	Mon 11/11/19
Travel	61 days	Mon 8/19/19	Mon 11/11/19
Funding Sources	71 days	Mon 8/12/19	Mon 11/18/19

Table 21 – Senior Design Project timeline

10.2. Acknowledgements

The team would not have been able to complete this project without assistance from several parties. First, the team wants to thank Dr. Francis Loth for advising this project, attending weekly meetings, and providing guidance throughout the process. Next, the team thanks Dr. Ajay Mahajan and Dr. Scott Sawyer who have offered their time to read and critique the report. The team thanks the Akronauts Rocket Design Team advisors, Chris Pearson and Steve Eves, for offering advice on several aspects of the project and helping to coordinate the subscale launch. The team thanks Bill Wenzel and Ian Wilcox for assisting with the machining of several rocket components and providing manufacturing advice in various areas. The team thanks David Hirt for his help with supersonic Fluent modeling. The team thanks Blake Bowser and Emily Armbrust of the Akronauts Rocket Design Team for providing manufacturing and assembly assistance, as well as storing the rocket components during the COVID-19 quarantine. The team thanks Grace Phillips and Ronnie Wallingford of the Akronauts Rocket Design Team for their assistance and expertise in parachute dimensioning and fabrication. The team thanks Jonathan Davis of the Akronauts Rocket Design Team for his help with the electronics systems development. The team would also like to thank the entire Akronauts Rocket Design Team for assistance with systems of the rocket outside of the project scope (parachutes, electronics, payload, and assembly), as well as providing an outstanding extracurricular experience. Finally, each member of the team would like to thank the University of Akron for providing an excellent education in both Mechanical Engineering and Aerospace Systems Engineering, as well as a unique undergraduate experience.

10.3. Nomenclature

π	Pi
Θ	Theta
γ	Gamma
λ	Lambda
α	Alpha
ρ	Rho

10.4. Acronyms

AGL	Above Ground Level
ANSYS	Analysis System
BOGO	Buy One, Get One
CAD	Computer Aided Design
CFD	Computational Fluid Dynamics
CG	Center of Gravity
CNC	Computer Numerical Control
COTS	Commercial Off the Shelf
COVID-19	Coronavirus Disease of 2019
CP	Center of Pressure
CTI	Cesaroni Technology Incorporated
ESRA	Experimental Sounding Rocket Association
FAR	Friends of Amateur Rocketry
FEA	Finite Element Analysis
FOD	Foreign Object Debris
FOS	Factor of Safety
ICEM	Advanced Geometry/Mesh Preparation Software
IREC	Intercollegiate Rocket Engineering Competition
ISO	International Organization for Standardization
MATLAB	Matrix Laboratory
MTV	Magnesium Teflon Viton
NACA	National Advisory Committee for Aeronautics
NAR	National Association of Rocketry
NASA	National Aeronautics and Space Administration
ORFN	Region Not Contained within a Geometry
PLA	Polylactic Acid
RSO	Range Safety Officer
SRAD	Student Researched and Designed
TRA	Tripoli Rocketry Association

10.5. References

1. “22 AWG M22759/32 Tefzel Wire (Red w/ Stripe).” *Race Spec*, 2020, racespeconline.com/products/22-awg-m22759-32-tefzel-wire-others-w-stripe?variant=35117832577.

2. "Aerospace Firesleeve." *Fire Sleeve*, 2020, www.firesleeve.com/product/aerospace-firesleeve/.
3. Black, M. Dean. "Finless Rockets Using Engine-Driven Gas-Dynamic Stabilization." *Apogee Rockets*, 2 Dec. 2014, www.apogeerockets.com/education/downloads/Newsletter379.pdf .
4. Budynas, Richard G., et al. *Shigley's Mechanical Engineering Design*. McGraw-Hill Education, 2020.
5. Black, M. Dean. "Finless Rockets Using Engine-Driven Gas-Dynamic Stabilization." *Apogee Rockets*, 2 Dec. 2014, www.apogeerockets.com/education/downloads/Newsletter379.pdf .
6. Bhaskaran, Rajesh. "Supersonic Flow Over a Wedge." *Confluence: Cornell University*, 21 February, 2019, https://confluence.cornell.edu/pages/viewpage.action?pageId=170201582.
7. "Bulkhead Motor Retainers for Minimum Diameter Rockets." *Aero Pack Incorporated*, aeropack.net/min_dia_retainers.asp.
8. "Chute Release." *Jolly Logic*, 2017, www.jollylogic.com/products/chuterelease/.
9. Culp, Randy. "Rocket Equations." *Rocket Equations*, 22 Mar. 2019, www.rocketmime.com/rockets/rckt_eqn.html#Method.
10. Dielectric Manufacturing. "Material Properties of ABS - Acrylonitrile-Butadlene-Styrene." *Dielectric Manufacturing*, Dielectric Manufacturing, 24 Mar. 2020, dielectricmfg.com/knowledge-base/abs/.
11. Dunbar, Jonathan. "A Study into Reducing the Thrust of Black Powder Propellant Motors ." N*ational Association of Rocketry*, nar.org/member-only-reports/rd/NARAM_54_Reports_TCR25/Krushnic%20Effect%20on%20Reducing%20BP%20Motor%20Thrust%20(J.%20Dunbar,%20NARAM%2054,%202012).pdf .
12. "End Seal Wrap - Red." *Fire Sleeve*, 2020, www.firesleeve.com/product/end-seal-wrap-red/.
13. Engineers Edge, LLC. "Minimum Thread Engagement Equation and Calculator ISO." *Engineers Edge*, www.engineersedge.com/thread_strength/thread_minimum_length_engagement.htm.
14. "Featherweight GPS Tracker." *Featherweight Altimeters*, www.featherweightaltimeters.com/store/p14/GPS_Tracker.html.html.
15. Howard, Zachary. "How to Calculate Fin Flutter Speed." *Apogeerockets.com*, 19 July 2011, www.apogeerockets.com/education/downloads/Newsletter291.pdf
16. "Insulating Kapton Tape." *ThorLabs*, 2020, www.thorlabs.com/newgrouppage9.cfm?objectgroup_ID=6809.
17. Jackson, H. Herbert. "Free-Flight Measurements of the Zero-Lift Drag of Several Wings at Mach Numbers from 1.4 to 3.8." *Nasa*, 22 June 1956, ntrs.nasa.gov/archive/nasa/casi.ntrs.nasa.gov/19930089113.pdf.
18. Mandell, Gordon K. "The Krushnik Effect." *Ninfinger*, Nov. 1969, www.ninfinger.org/rockets/ModelRocketry/Model_Rocketry_v02n02_11-69.pdf.

19. Mastrocola, N. “Effect of Number of Fins on the Drag of a Pointed Body of Revolution at Low Supersonic Velocities.” *Nasa*, 7 Apr. 1947, ntrs.nasa.gov/archive/nasa/casi.ntrs.nasa.gov/19930085604.pdf.
20. “miniTimer4.” *Perfectflite*, 25 Nov. 2019, www.perfectflite.com/MT4.html.
21. “Missile Works Corporation.” *Missile Works*, www.missileworks.com/store/.
22. “Motor Staging Information.” *Motor Staging Information*, 2014, www.spaceportrocketry.org/Motor%20Staging.html.
23. Perkins, Edward W., et al. “Investigation of the Drag of Various Axially Symmetric Nose Shapes of Fineness Ratio 3 for Mach Numbers from 1.24 to 7.4.” *Nasa*, 1958, ntrs.nasa.gov/archive/nasa/casi.ntrs.nasa.gov/19930091022.pdf.
24. *Pro98 Gen2 Motor Hardware Dimensions*. 11 Oct. 2014.
25. Sanders, E. Claude. “Damping in Roll of Models with 45°, 60°, and 70° Delta Wings Determined at High Subsonic, Transonic, and Supersonic Speeds with Rocket-Powered Models.” *Nasa.gov*, 25 June 1952, ntrs.nasa.gov/archive/nasa/casi.ntrs.nasa.gov/19930087208.pdf.
26. “Sonic Boom.” *U.S. Air Force*, 25 Apr. 2003, www.af.mil/About-Us/Fact-Sheets/Display/Article/104540/sonic-boom/.
27. “Spaceport America Cup Intercollegiate Rocket Engineering Competition Rules & Requirements Document.” *Sounding Rocket*, 2019, www.soundingrocket.org/uploads/9/0/6/4/9064598/sa_cup_irec_rules___requirements_document_20191118__rev_d_final_.pdf .
28. Stoney, William E. “Transonic Drag Measurements of Eight Body-Nose Shapes.” *Nasa*, 5 Feb. 1954, ntrs.nasa.gov/archive/nasa/casi.ntrs.nasa.gov/19930087953.pdf.
29. “StratoLoggerCF Altimeter.” *Perfectflite*, 25 Nov. 2019, www.perfectflite.com/SLCF.html.
30. “Tender Descender.” *Fruity Chutes*, fruitychutes.com/Recovery_Tether_Manual.pdf.
31. Trenkle, F., and M. Reinhardt. “In-Flight Temperature Measurements.” *Spaceagecontrol.com*, spaceagecontrol.com/AD-InFlightTemperatureMeasurement.pdf
32. “U.S. Standard Atmosphere.” *Engineering ToolBox*, 2003, www.engineeringtoolbox.com/standard-atmosphere-d_604.html.